Enhancing Genetic and Epigenetic Sample Preparation with Microfluidics

Rachelle Ashley Turiello
Charlottesville, Virginia

B.A. Interdisciplinary Studies, University of Maryland Baltimore County, 2014
M.S. Forensic Science, Towson University, 2017

A Dissertation presented to the Graduate Faculty of the University of Virginia in Candidacy for the Degree of Doctor of Philosophy

Department of Chemistry

University of Virginia

August 2024

_____

_____

_____

_____

Abstract

Since the completion of the Human Genome Project in 2003, the nucleic acid (NA) code has continually been leveraged to provide actionable information to patients for personalized care and to enable statistically irrefutable *matches* for forensic human identification (HID). As such, the research and development focused on the miniaturization and automation of tools for NA analysis has increased year after year. Regardless of the application, the methods associated with the preparation of genetic material for downstream analysis are arguably the most vital. Briefly, the ability to recover and conserve NAs from sample enrichment, DNA extraction, or epigenetic conversion will ultimately be outcome determinative of any associated assay. And yet, many of these aforementioned benchtop techniques are considered labor-intensive, time-consuming, and difficult to automate due to the harsh associated reagents, lengthy incubations, and multitude of required pipetting steps. Furthermore, the performance of each process is inconsistent from analyst-to-analyst and resulting in variable NA loss. This body of work describes multiple microfluidic approaches aimed to streamline and enhance genetic and epigenetic sample preparation methods, including bisulfite conversion, DNA extraction, and virion enrichment.

As an alternative to forensic genetic identification by short tandem repeats (STRs), probing epigenetic variation can provide information related to HID. In particular, examining the methylation of cytosine at targeted locations along the genome has provided mechanisms to differentiate between monozygotic twins, predict smoking habits, and estimate chronological age within ~1 year of accuracy, to name a few. Unlike conventional testing by STR analysis, methylation interrogation requires an extensive, multi-step sample preparation process resulting

in a magnitude of DNA loss. In particular, the bisulfite conversion (BSC) technique, which chemically modifies all cytosine residues not containing a methyl tag to uracil, is known to result in the loss of more than 50% of DNA. Chapter 2 describes the development of a rotationally-driven microfluidic method for dynamic solid phase-BSC (dSP-BSC) that automates the sample preparation process for up to four samples in parallel. By leveraging the microfluidic format and reduced reaction volumes, incubation intervals were shortened by ~40% overall with maintained DNA recovery and conversion efficiency compared to the conventional approach.

Chapter 3 focuses on the integration of DNA extraction by enzymatic lysis upstream from BSC to enhance DNA recovery and couple the sample preparation workflow from extraction to conversion. While gold-standard methods for DNA extraction involve cellular lysis followed by silica-assisted purification of NAs, this work incorporates an alternative method for DNA extraction based upon the introduction of a highly thermostable neutral protease from *Bacillus* sp. strain EA1. Extraction by the EA1 enzyme permits NA preparation in a single tube and eliminates the need for pro K, SDS, harsh chemicals, and silica purification altogether. Herein, compatibility between EA1 and downstream BSC is established for the first time. Performance is evaluated with standards, K-562 samples, and blood samples. Toward a fully integrated approach to epigenetic sample preparation, a rotationally-driven device design in proposed and assessed using colorimetric dye studies and preliminary testing with venous blood samples.

Utilizing similar microfluidic design features as those proposed in Chapters 2 – 3, Chapter 4 presents a method for the sample preparation of severe acute respiratory syndrome coronavirus 2 (SARS-CoV-2) aimed for diagnostic testing via downstream RT-PCR. This work was completed in response to the 2020 global pandemic and with support from the National Institutes

of Health (NIH) Rapid Acceleration of Diagnostics (RADx) initiative to enhance viral surveillance and containment efforts. Once again, two sample preparation processes were coupled via a rotationally-driven microfluidic interface. These included the enrichment of SARS-CoV-2 virions by affinity-capture, magnetic nanoparticles and extraction by the EA1 enzyme. With the integrated device, sample preparation was possible in under 15 minutes and for a total of up to six samples in parallel. Performance of the device was comparable to a gold-standard method for sample preparation and evaluated using standards, patient nasopharyngeal swabs, and contrived saliva samples.

Chapter 5 highlights the ongoing studies and future work toward the microfluidic integration of epigenetic sample preparation from extraction to conversion and discusses persistent challenges associated with pyrosequencing and material-related fluid loss and inhibition. Considering much of the work detailed in this dissertation was focused on the development of a microfluidic tool for forensic genetic integration, the remaining focus of Chapter 5 highlights multiple trade-offs faced in the forensic landscape as it relates to the adaptation of new scientific methods. Opportunity zones for microfluidic research and development within the bounds of HID and criminal investigation are posited that might increase laboratory efficiency and expand the capacity of forensic science services in the future.

Acknowledgements

I have been steadfast and resounding in my belief that luck does not exist. I have believed that a sense of belonging, accomplishment, or purpose is earned from hard work, discipline, and self-reflection. But as I reflect now, I can only think about how lucky I am to have found the support of numerous mentors and loved ones. My *luck* is that I encountered each one of them at just the right time so that they might help to shape the trajectory of my life. With the completion of this dissertation and my graduate work at UVA, I can say that I feel as if I belong, I am proud of my accomplishments, and I have found my purpose; while I did work very hard, I attribute much of this to the circle of people I hold around me and my luck at having found them.

To Dr. James Landers – I am so lucky to have met you at that AAFS conference six years ago. How lucky is it that we happened to stand alongside one another in that ballroom? Thank you for indulging me as I talked all things epigenetics that evening. Little did you know, I'd keep talking your ear off about it all these years later. I can't thank you enough for so graciously inviting me into your group, trusting in my potential, and supporting my growth every step of the way. I appreciate the latitude you have afforded me as I have navigated research and life; it is this trust that has endowed me with the confidence to lead projects and others today. You have pushed to send me around the world, participate in unique and cutting-edge research, and stand on stages with so many brilliant scientists. You set a high bar and have the highest of expectations for your people, and I thank you eternally for giving me the opportunity to rise to the occasion.

To all of those mentors and collaborators who have shaped this journey and the path that led here, I thank you. My interests in forensic genetics and the human phenotype were nurtured with so much care by Patricia LaNoue and Stephen McAlpine in the Interdisciplinary Studies

program at UMBC. In this impactful time of my life, you both shared so much kindness and wisdom. To Mark Profili, thank you giving me a home at Towson and my first opportunity to indulge in research and teaching. With you, I went to my first conference and met so many of the scientists who inspired my interests then and now. Today, I have you to thank for my huge forensic network and any of my street cred. In my moments of doubt, I often hear your voice in my head saying 'you're goin' places girl.' To Dr. Cynthia Zeller, thank you for introducing me to epigenetics and to research in your lab. You spent so much time and attention breaking down the fundamentals to me, grabbing blank sheet after sheet from your printer to work out the math or explain a workflow. I strive to be this thorough and patient when I explain a new concept to incoming students. I would also like to thank my dissertation committee members Dr. Rebecca Pompano, Dr. Charles Grisham, Dr. Cliff Stains, and Dr. Kathryn Laughon for your time and guidance during this incredible undertaking.

To the talented and inspiring scientists I have worked with along the way, thank you for extending your kindness, patience, and brilliance with me. Thank you to my collaborators and notable co-authors including Jeff Hickey, Dr. Anchi Scott, Dr. Charlie Clark, Dr. Robin Cotton, and Dr. Francine Garrett-Bakelman. I am especially grateful to Dr. Renna Nouwairi, Dr. Leah Dignan, and Larissa Cunha. Each of you have been instrumental in not only my success in this program, but also my personal happiness in these last five years. Cheers to many more inside jokes and momentous occasions ahead.

To my family, thank you for all of your support along the way and for instilling in me that education is the most important investment one can make. Mom, you have been my loudest cheerleader for the longest time. I am this self-assured, confrontational, and direct because of

you; because of you, I am a leader. To Dr. Michael Epstein, my dad and uncle, thank you for taking me in when I needed it most. Without you, my life looks much different. To my little sister Brooke, I love that you are part of this Charlottesville story and that we now call this place home together. Thank you for your sharing all of your sweetness with me when I could use it the most, I have so much to learn from you. To the family that I am so lucky to now call my own, the Turiellos – I adore each of you so much. I can't say enough how much I appreciate your support, love, and care for myself and Violette. To my husband Michael – I am the most lucky to have met you. The dedication you have to me and the growth of our family has carried us these last five years. I never imagined something like this for myself, I didn't know what it could look like. You never had any doubt that I could do this, even when I did. Thank you for all of the sacrifices you made so that I might live out this dream. I love you.

Dedication

To my husband Michael, I dedicate all of this to you. Thank you for your unwavering support and love. Cheers to a lifetime together.

“Anything worth doing is worth overdoing.”

Dissertation Contents

List of Figures

List of Tables

Chapter 1. Taking the Microfluidic Approach to Nucleic Acid Analysis in Forensics

Publication(s) included in Chapter 1:

- **Turiello, R.**; Nouwairi, R.; Landers, J. P. Taking the Microfluidic Approach to Nucleic Acid Analysis in Forensics: Review and Perspectives. *Forensic Science International: Genetics*, 2022, 63. doi: 10.1016/j.fsigen.2022.102824
- *Clark, C.; ***Turiello, R.**; Cotton, R.; Landers, J. P. Analytical Approaches to Differential Extraction for Sexual Assault Evidence. *Analytica Chimica Acta*, 2021, 1141, 230 - 245. doi: 10.1016/j.aca.2020.07.059
- Nouwairi, R.; Cunha, L. L.; **Turiello, R.**; Scott, O.; Hickey, J.; Thompson, S.; Knowles, S.; Chapman, J. D.; Landers, J. P. Ultra-Rapid Real-Time Microfluidic RT-PCR Instrument for Nucleic Acid Analysis, *Lab on a Chip*, 2022, 18, 3424 - 3435. doi: 10.1039/D2LC00495J

*Both contributed equally to this manuscript as co-first authors

1.1. Introduction

Research proposing the miniaturization and automation of analytical tools for nucleic acid (NA) analysis has boomed in recent years, with developers producing several clever techniques with transformative potential in both clinical and forensic settings.[1] For forensic investigation, and particularly human identification (HID), microfluidic methods have been proposed to expedite the existing laborious and highly manual methods in specific use-cases, including DNA extraction and short tandem repeat (STR) detection and analysis.[2] In some instances, completely automated 'sample-to-answer' systems have been designed to eliminate analyst intervention altogether,

ostensibly mitigating the variation associated with interoperability and reducing the likelihood for contamination.[3,4] This investigative arena has been identified as one that would benefit greatly from microfluidic intervention for a number of reasons. From the perspective of the forensic practitioners working in largely overburdened laboratories with limited resources, tools that facilitate automation and limit contamination in concert with increasingly sensitive chemistries and minimized perceived bias are a welcomed potential source of relief.[5,6] For academics and those looking to commercialize new technology, the applied nature of the work is both exciting and rewarding. Furthermore, the implementation landscape is not as stringent or expensive as other sectors (e.g., clinical), which often require approval from the Food and Drug Administration (FDA); thus, the utilization of devices is driven largely by a perceived need within the community itself and its successful validation with forensically-relevant samples.

Reports from the National Institute of Justice (NIJ), dating back to the early 2000s, predict an increasing trend toward automation and miniaturization, anticipating DNA analysis at the crime scene with portable and handheld microchips by 2010.[7] Similar sentiments are echoed by other organizations responsible for the oversight of forensic DNA analysis, including the National Institute of Standards and Technology (NIST) and the International Criminal Police Organization (INTERPOL), acknowledging the utility of 'swab in - profile out' systems for use at police booking stations, border crossings, embassies, and traditional forensic laboratories.[8] Two decades later, few microfluidic DNA technologies are commercially available and their adoption by agencies interested in identification has been limited. From the author's perspective, the forensic community expected that microfluidics developers would produce a rapid, inexpensive, and automated instrument that successfully and seamlessly miniaturized the sample preparation and

analysis steps associated with forensic DNA typing.[9] In reality, while Rapid DNA methods are automated and do enable faster turnaround times, testing is significantly more expensive and not comparable to conventional workflows in terms of sensitivity, reproducibility, and multiplex capacity.[10] It has been suggested that several major challenges have contributed to this outcome; namely, the expectation that each step of the forensic DNA process could be simply miniaturized and integrated into an automated device that produced an end-result comparable to a case working laboratory.[9]

This introductory chapter aims to confer the relationship between microfluidics and forensic HID, and the limited implementation of miniaturized tools for this small and niche market.[11] To this end, an abridged overview of microfluidic technology from a historical perspective is provided, as well as an accounting of some of the miniaturized methods developed for use with the genetic laboratory workflow as it relates to HID. Likewise, the unique advantages and practical limitations associated with microfluidic integration of the HID workflow are also considered. In fact, it was these unique advantages and practical limitations as it relates to the forensic genetic market, that motivated the preponderance of research and development (R&D) described in this dissertation. Briefly, much of this work involved a microfluidic mode designed to streamline *epigenetic* sample preparation, a type of genetic analysis that is only recently translating from academia to industry despite hundreds of research articles suggesting the relationships between epigenetic information and HID.[12,13] Instead of developing a tool meant to displace an existing benchtop approach already in routine use, the microfluidic method designed and evaluated through R&D sought to make epigenetic analysis more accessible for forensic laboratories. In this vein, this introductory chapter closes with a discussion of the role of

epigenomics in forensic HID and the associated issues that led to its limited routine use. Additionally, a description of the limited microfluidic methods proposed to mitigate issues with sample preparation is provided.

1.2. A Brief Primer on Microfluidics

Microfluidics can be defined as involving precise manipulation of small (micro- to nano-liter) fluid volumes within designed architectures featuring dimensions on the nano- or micrometer scale; however, the discipline is more aptly described in terms of functional capacity rather than by size restrictions.[14] Microdevices, including 'lab-on-a-chip'[15] and 'lab-on-a-Disc'[16] formats, aim to integrate multiple analytical processes on a single interface, typically consuming smaller reagent volumes and offering rapid analysis times with minimal to no manual intervention. Early innovation indicated the promise that micro-total analysis systems (μTAS) held for changing lab-based and field-deployable analyses; as a result, interest was intense, and excitement and potential end-user expectations were high[17]. Over the course of three decades, fabrication techniques and requisite assay performance improved remarkably, but this shifted the burden to process integration and hardware challenges that required more improvement to minimize the trade-offs associated with adoption. For NA analysis in particular, the development of techniques for processes such as DNA extraction, amplification, and separation have not been simple to microscale.

1.2.1. An Abridged History of Microfluidic Technology. When viewed at a high level, the history of microfluidics in the context of forensic HID follows the Gartner Hype Cycle Model[18] fairly well,

including the five key phases in a technology life cycle of: a technology trigger, a peak of inflated expectations, a trough of disillusionment, a slope of enlightenment, and finally, a plateau of productivity (**Fig. 1-1**). It can be argued that the Innovation Trigger for microfluidics occurred in the early 1990s, leveraging 20+ years of development in the microelectronics industry, where the photolithographic processing of silicon set the stage for etching silica substrates.[19] Manz et al. were the first to coin the term "micro-total analysis systems", inciting an Era of Innovation in the field, and the development of research-based devices.[20] Initial techniques were focused on clinical applications and the analysis of clinically-relevant analytes via microchip

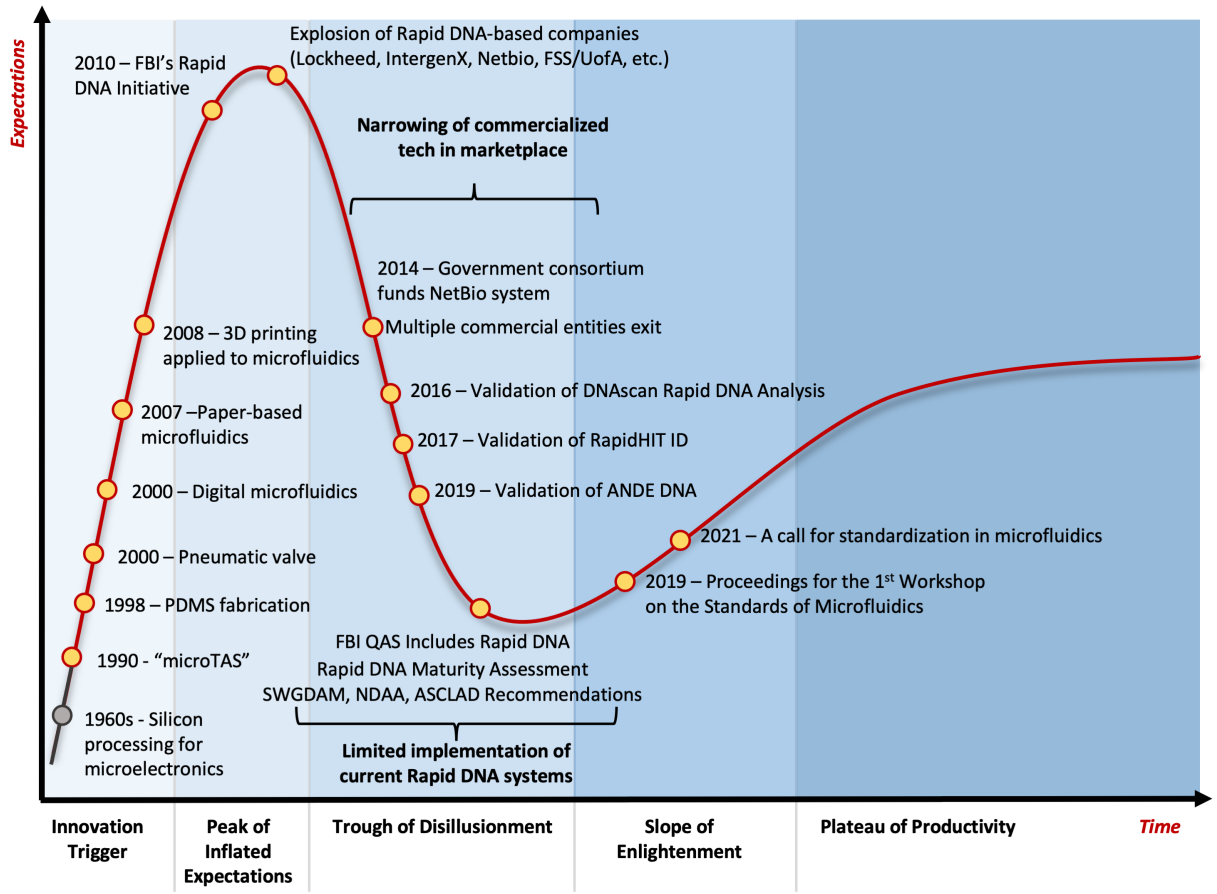

Figure 1-1. Timeline of milestones. Demonstrating progress toward integrated microdevices for forensic human identification relating to the Gartner Hype Plot. Figure adapted from Turiello et al. 2023.[11]

electrophoresis.[21] In parallel, microscale electrophoresis gave the Human Genome Project a much-needed boost when rapid, sensitive, high-throughput and high-resolution separation methods for NA analysis were desperately needed.[22] The advantages of capillary electrophoresis (CE) spilled over into clinical chemistry labs, as a means of expediting micro separations. However, it became clear that translating to glass or silicon microdevices would ultimately require integration of the sample preparation processes. The cost of these materials emphasized the need for technological innovation toward the development of microdevices amenable to rapid prototyping and ultimately point of need (PON) utilization.

1.2.2. General Approaches to Fluidics at the Microscale. The development of analytical tools at the microscale requires careful consideration of the multiple processes, often orthogonal in nature, that must be effectively interfaced to form a fully-integrated system. The mode(s) of fluid transport must be judiciously selected, and the desired substrate must be compatible with those processes, yet manufacturable and cost-effective. With regard to fluid flow control, microdevices

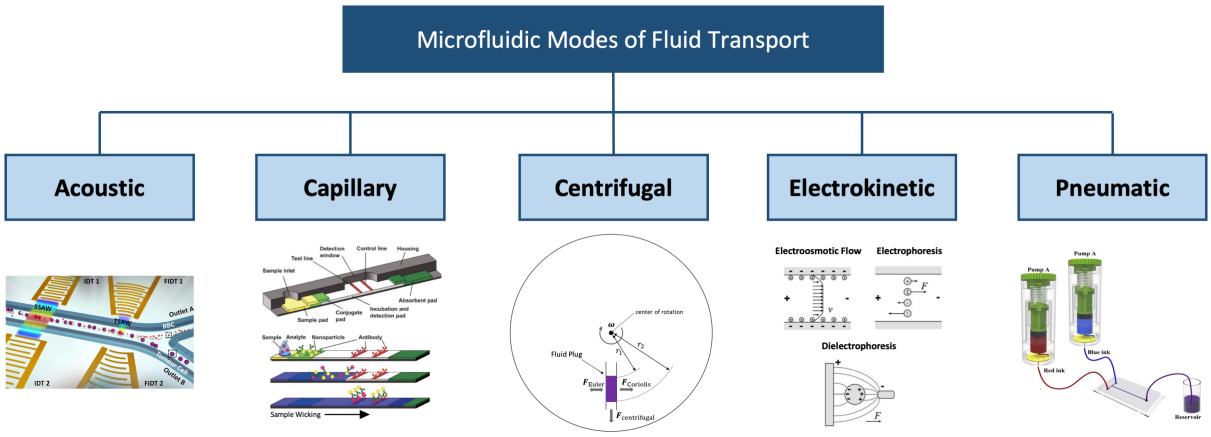

Figure 1-2. Microfluidic approaches to fluid transport. Diagram demonstrating the five primary mechanisms for fluid transport. Figures representing fluid flow for acoustic, capillary, centrifugal, electrokinetic, and pneumatic adapted from Turiello et al. 2023.[11]

can be divided into five general categories based on method(s) utilized, which include acoustic-,[23] capillary-,[15] centrifugal-,[24] electrokinetic-,[15] and pneumatic[25] action (**Fig. 1-2**). Similarly, selection of the substrate for creating microdevices plays into the final 'cost per test'. For example, cyclic olefin copolymer (COC) can be orders of magnitude more expensive than polymethylmethacrylate (PMMA), impacting the overall cost, assay performance, and ease of device fabrication. More recent development has focused on polymeric substrates, including elastomers, such as poly(dimethylsiloxane) (PDMS), glassy polymers, such as PMMA, and thermoplastics, like polycarbonate (PC), polyethylene terephthalate (PET), and COC. Polymeric materials are compatible with simpler manufacturing processes, such as soft lithography, embossing, injection molding, and laser ablation – techniques that can be used for cost-effective development.[26,27,28] Overall, the goal is to stitch together a series of processes that 'mimic' conventional, manual workflows, including fluidic mixing, metering, valving, heating, reacting, and separating, but in a closed, automated microsystem. This is where some of the other attributes of microfluidics not discussed here come into play. Flow at the microscale involves 'laminar' or smooth 'plug' flow smooth, unlike the 'turbulent' flow observed with larger scale features, and this is ideal for processes like electrophoresis, where high resolution DNA separation may be desired.[29] However, one of the most trivial bench processes, mixing, can be challenging due to the laminar flow, but 'micromixing' strategies have been developed to address this.[29] Also important is the fact that in microfluidic architecture, the surface area (SA) that fluid is exposed to in channels is large, relative to the volume of fluid (V) those channels contain. In fact, the microscale SA:V ratio may be orders of magnitude larger in microfluidics than its benchtop counterparts (e.g., 200x for CE versus ME). This is advantageous when there is a need to dissipate

Joule heat from processes that generate it and it is for this reason that application of high voltage is not detrimental to ultrafast electrophoretic DNA separations.[30] However, the large SA:V also provides a vast surface for adsorption of analytes, leading to a potential for loss of sample/reagent that is never even considered when using polypropylene tubes. Taking all of this into account, researchers have successfully demonstrated large scale integration is possible for complex biochemical assays, with a growing toolkit of independent 'unit operations' available to generate both proof-of-concept and commercializable microdevices.[1] It is the author's perspective that this contributed to the inflated expectations of researchers and practitioners that microfluidic systems would become ubiquitous in the near future.

1.2.3. Current State of Microfluidics in Forensics. As researchers perfected the ability to mimic CE in a planar glass substrate, it became clear that the μTAS that Manz described would require integration of several standard NA analysis processes, and this was not trivial. Ultimately, an analysis of the collective literature reveals that this stalled the progress of microfluidics, whereby sample processing was seamlessly interfaced with the analytical step. Complete integration required careful consideration of valving strategy, providing robust mechanisms to simultaneously isolate different domains on the chip, while physically and fluidically connecting them at will.[31,32] Not only did the advent of valving strategies allow for fluidic connections between different parts of the microfluidic architecture, it permitted large scale integration, leading to complex, integrated sample-to-answer systems that set the stage for Rapid DNA.[33] Of course, research in Rapid DNA microtechnology promoted widespread enthusiasm for an integrated microfluidic system that could carry out HID, in an automated manner.[9] The FBI's 2010

Rapid DNA Initiative laid out the expectations for microfluidic systems to integrate multiple existing workflows into one rapid, automated instrument for HID.[34] This program was established to direct the development and implementation of Rapid DNA systems for swab in-profile out STR analysis performed by untrained users in 1-2 hours. Participating research institutions were provided with a list of expected performance criteria that included both "threshold" and "goal" target deliverables; this list contained four categories of requirements, dealing with the systems themselves, extraction and purification, amplification and separation/detection, and output/analysis. Each category highlighted features such as cost per sample, post-extraction sample purity, target multiplex capacity, and CODIS compatibility, to name only a few. **Table 1-1** highlights many of these performance criteria and the expected output anticipated to be met by microfluidics R&D teams. Ultimately, projects required more trade-offs than originally anticipated, and interest and funding appeared to diminish as the projected timelines to completion came and went.[7] To make adoption possible, the endeavor has required additional R&D, more time to mature, and an acknowledgement from funding institutions and end-users that there would be tangible trade-offs associated with the microfluidic approach, most likely in the form of cost, sensitivity, speed, and/or throughput.

After a modest investment from industry and government agencies, some Rapid DNA technologies were commercialized and trade-offs materialized into limitations, including decreased sensitivity compared to macroscale methods, and higher costs than originally anticipated for both the instrument and sample analysis. End-point user acknowledgement of these trade-offs meant narrowing use-cases to buccal reference and arrestee samples for whatever technology was available at the time; this ensured fair treatment of those presumed

Rapid DNA System Performance Criteria			
Category	**Attribute**	**Threshold**	**Goal**
System Requirements	**Sample-to-Profile Analysis Time**	1 hr	45 min
	Channels/Sample per Analysis	8	≥16
	Sample Types	Buccal swab	Buccal swab, blood, standards, touch/trace
	Reference Samples	Yes	Yes
	Trace Performance	-	Full profile with ≤50 pg DNA
	Size	29" x 16" x 21"	25" x 15" x 20"
	Weight	≤ 110 lb	≤ 100 lb
	Portable/Ruggedized	Yes	Yes
	Reagent Storage Time Limit	3 months	6 months
	Reagent Storage Temperature Limit	20°C - 30°C	-10°C - 40°C
	Disposable, Preloaded Consumables	Yes	Yes
	Cost per Instrument	≤ $275K	≤ $75K
	Cost per Sample	≤ $75	≤ $20
	Set-Up Time	< 15 min	< 10 min
Extraction/Purification Requirements	**Compatibility with Fresh and Dried Buccal Samples**	Yes	Yes
	Automated Extraction/Purification	Yes	Yes
	Quantitation	No	No
	Purity Equivalent to Gold-Standard	Yes	Yes
Amplification & Separation/Detection Requirements	**Rapid Amplification (≤ 16 Loci)**	≤ 30 min	≤ 10 min
	5-Color Detection	Yes	Yes
	Detection Resolution	Single bp	Single bp
	COTS Reagent Compatibility	Yes	Yes
	Full STR Profile Detection	Yes (≤ 16 loci)	Yes (≤ 16 loci)
	Acceptable Signal Strength, Peak-Height Ratio, Stutter, and Inter-Loci Balance	Yes	Yes
Output/Analysis Requirements	**CODIS Compatible Format**	Yes	Yes
	Standard Expert Systems Compatibility	Yes	Yes
	Raw Data Output Available	Yes	Yes
	Privacy/Security Capabilities	Yes	Yes
	Unique Sample Identifier	Yes	Yes
	External Profile Communication	Yes	Yes

Table 1-1. Threshold and goal performance criteria for Rapid DNA tools. Table adapted from Turiello et al. 2023.[11]

innocent and entered into DNA databases and conserved finite crime scene materials. With the Rapid DNA Act of 2017 and the requisite update to the FBI Quality Assurance Standards (QAS),[35,36] end-users have had the opportunity to engage with microfluidic technology and have a better understanding that miniaturizing existing workflows on these fully-automated systems was not inconsequential. As Rapid DNA technology has slowly become more robust from continued, targeted development and the inclusion of more compatible use-cases through published validations, we consider the possibility that forensic microfluidic techniques are trending toward enlightenment. At present, these technologies are used in limited capacity for reference profiles and at booking stations, however, guidelines for use with crime scene samples for non-CODIS cases and corresponding considerations for court have been shared with law enforcement agencies.[37] Likewise, the FBI has established a separate database, the DNA Index of Special Concern (DISC), that includes generated profiles from crime scenes originating from select unsolved homicides, sexual assaults, and kidnapping and terrorism cases for arrestee matching. A trend toward enlightenment is also supported by the institutional standardization of microfluidic methods for device prototyping, manufacturing, and analysis and an acknowledgment from funding agencies that while the use of these instruments are limited now, further R&D will enable applications to casework.[37,38,39,40]

1.3. Microfluidic Technology for Forensic Human Identification

Motivation for developing microfluidic forensic HID systems is discussed more thoroughly in Chapter 5; but generally, researchers and commercial entities view forensics as exciting and application-driven, and, at least in theory, involving fewer barriers to market entry compared with

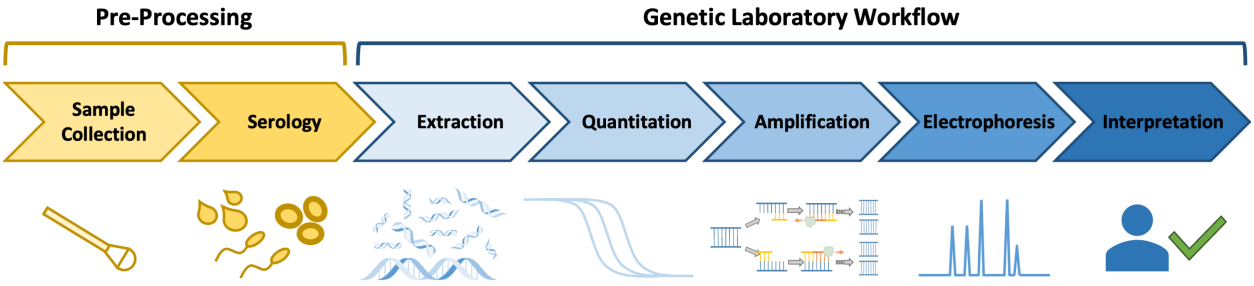

Figure 1-3. The typical forensic DNA workflow. Sample pre-processing includes collection, either from the crime scene or an item of evidence, and serology. The genetic laboratory workflow begins with DNA extraction, and further includes quantification, amplification, CE, and interpretation. Figure adapted from Turiello et al. 2023.[11]

drug discovery or clinical diagnostic microsystems. Thus, prior to and in concert with, the development of fully-integrated instruments for forensic genetic analysis, researchers explored the ways in which components of the DNA workflow could be adapted to the microscale, with numerous publications spanning several years.[1,2,24] The typical forensic procedure (**Fig. 1-3**) begins at the crime scene: pre-processing includes sample collection, followed by serological analysis to identify forensically-relevant body fluids and define probative items suitable for downstream NA analysis. Sample preparation, including cell lysis and NA purification, marks the beginning of the genetic laboratory workflow and may include a method for differential cell lysis with suspected sperm contributions. An intermediate concentration determination step via real-time quantitative PCR (qPCR) enables quantification of genetic contributions to normalize input concentrations prior to multiplexed amplification and separation via CE. Finally, resultant electrophoretic profiles are interpreted by highly trained personnel for comparison to reference profiles and/or database searching. From a microfluidics perspective, development of micro-processes to 'mimic' each traditionally laborious step required clever, strategic considerations of principles spanning multiple disciplines. The following sections details some of these considerations and the progress made by microfluidic researchers and commercial entities

toward the automation of this workflow, beginning with NA extraction. Descriptions below are not intended to act as a comprehensive review of the literature, as plenty of these exist already; instead, this chapter serves to provide some insight into the difficulties, breakthroughs, and progress made toward adaptation.

1.3.1. Nucleic Acid Lysis and Purification. The extraction of genetic material from purported forensic stains is arguably the most vital part of the forensic identification process chain. Downstream amplification and detection by either separation techniques (e.g., STR analysis) or sequencing, rely on the complete lysis and isolation of NAs from other cellular material and

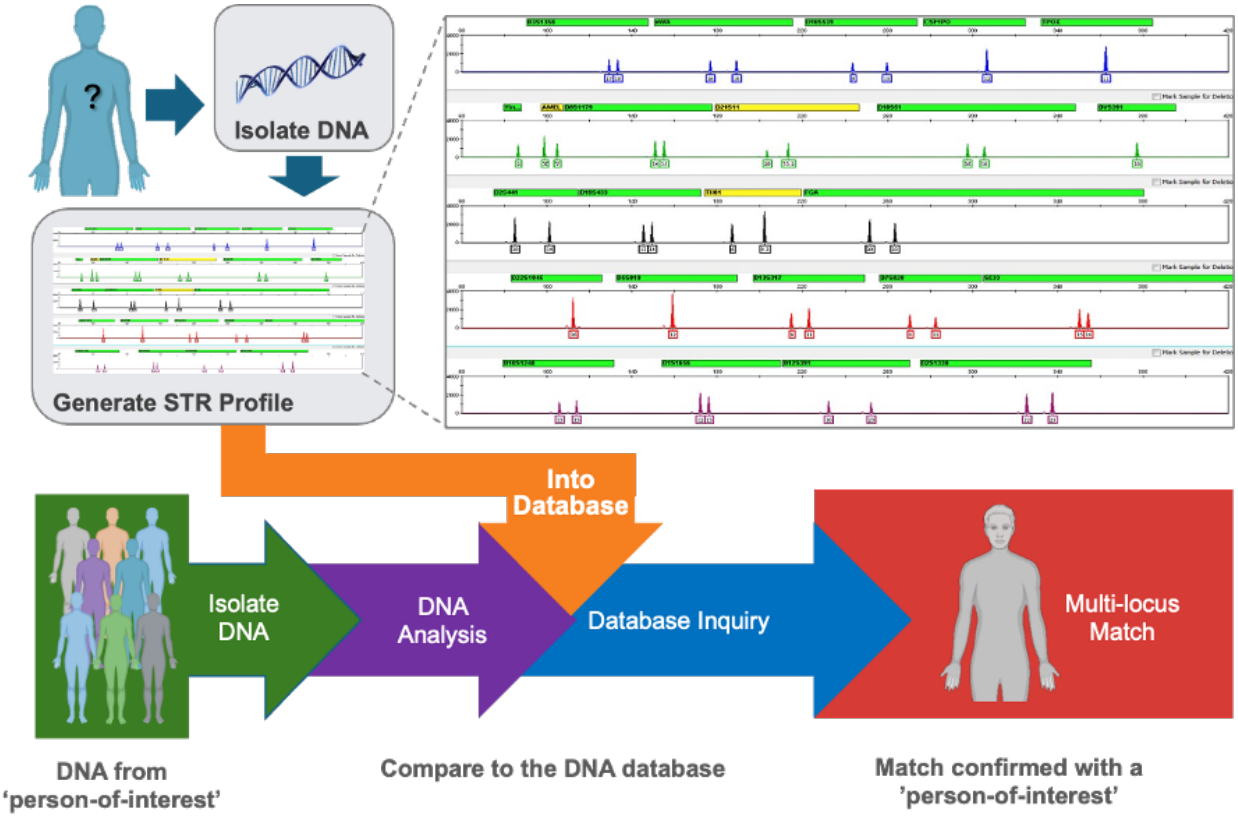

Figure 1-4. STR profiling for forensic human identification. Genetic material is isolated from unknown persons, amplified, and separated to develop an STR profile for database or reference matching. Figure adapted from Clark and Turiello et al. 2020.[41]

inhibitors.[9] The ability to 'match' STR profiles, either to references from known persons or database entries is largely depended upon this step (**Fig. 1-4**).[41] Cell lysis occurs with the introduction of mechanical, chemical, and/or thermal energy; processes that are ostensibly amenable to integration with a variety of microdevices.[42] Cellular lysis and the isolation of genetic material via a solid phase (e.g., silica) or functionalized particle was adapted for the microscale successfully;[43,44] however, the development of an extraction protocol for forensic samples is exceptionally complicated, as the process must be compatible with a wide variety of raw sample types and capable of removing pervasive environmental contaminants known to inhibit PCR, including dyes from denim and tannins.[45] At present, sample-to-answer commercial systems for rapid forensic identification that incorporate NA preparation are available and approved for database searching from reference samples in the United States, however, they require further development to reproducibly deal with complex samples, low NA concentrations, and non-swab substrates.[34] Work is underway to expand the use of these systems in terms of input sample, with multiple published applications and validations for non-swab substrates, including post-mortem bloodstains, body fluids, and bone samples.[46,47,48] The extraction processes associated with these technologies have been detailed elsewhere; notably, each system utilizes completely different strategies for preparation, with purification being omitted entirely in some instances.[46] Multiple reviews detailing proposed strategies for NA lysis or purification at the microscale and their potential for automation and integration with downstream techniques date back to 2000.[42,44,45,49]

Further complicating NA sample preparation, forensic laboratories are also faced with a multitude of evidence from sexual assault cases, often containing cellular mixtures from both the victim and the alleged perpetrator. In these cases, differential extraction (DE) is required to

increase the likelihood of obtaining a DNA profile more amenable to mixture deconvolution. This particular method, in which the chemical lysis of epithelial cells is completed prior to the multistep treatment of a sperm pellet (**Fig. 1-5**), has been identified as one that would benefit greatly from microfluidic automation, provided it has remained largely manual despite the development of liquid handling systems.[41,50] In the interest of cell sorting at the microfluidic scale for the treatment of sexual assault evidence, several groups have elected to omit centrifugation entirely, instead relying on separation methods that exploit the different cellular characteristics of sperm and non-sperm contributions. For instance, by leveraging the sperm cell's affinity for the Sialyl-Lewisx (SLEX) molecule found on the surface of female oocytes, microfluidic affinity-based sorting has resulted in high sperm capture rates (52 - 88%) post-lysis.[51] Taking advantage of the size and density differences, some techniques have used hydrodynamic sorting, either relying on sedimentation with controlled flow rates or upon the laminar flow observed at the microscale.[52,53] Acoustic differential extraction

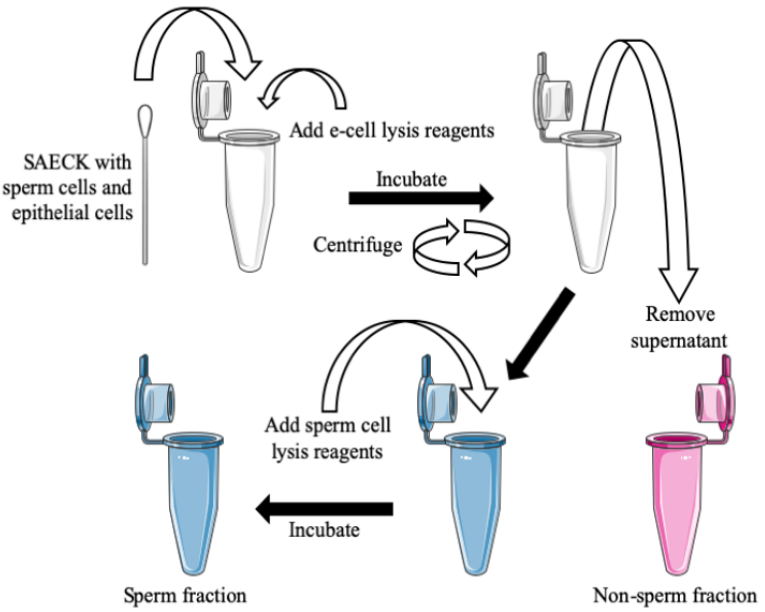

Figure 1-5. Conventional workflow for differential extraction. For mixed cell type DNA extraction for forensic HID, a cutting of the sample is combined with lysis reagents for epithelial cell contributions to liberate non-sperm DNA. Sperm cells are pelleted via centrifugation and manually removed by pipette from the bottom of the microcentrifuge tube, where they are subsequently lysed by a reducing agent. This process results in a 'sperm' and 'non-sperm' lysate for purification and downstream STR analysis. Figure adapted from Clark and Turiello et al. 2020.[41]

leverages particle size, density, and compressibility to “trap” sperm cells at a low pressure node in a standing acoustic wave on hybrid PDMS/glass microchips.[54,55] Similarly, optical trapping has also been applied to cell sorting on a microfluidic interface to enable sperm cell isolation via a high-density focused laser beam.[56] Finally, dielectrophoresis has been exploited as an elegant mode for isolation of cells by subjecting them to a tuned, nonuniform electric field for cell capture and downstream lysis, as with the DEPArray system.[57] Unfortunately, current techniques aimed to provide ease of sample preparation in this area echo the shortcomings of liquid handling systems: most are not currently capable of full integration and some level of manual intervention is required.[45]

1.3.2. DNA Amplification and Quantitation. Compared to other parts of the forensic DNA workflow, DNA amplification is one area in which the advantages of microfluidics are clear and thoroughly characterized in the literature.[58,59,60,61,62] PCR amplification requires repeated heating and cooling to drive enzymatic and chemical processes that generate hundreds of millions of copies of genetic transcripts for analysis; at the macroscale and on the surface, this step is limited by diffusion and heat transfer in (relatively) large reaction volumes, and the interfacing rapid temperature ramping ability of the system. With microfluidics, smaller reaction volumes and higher SA:V ratios in microchambers enable rapid heat transfer and shorter distances reduce diffusion limits between reagents and DNA transcripts.[63] Microfluidic thermal cycling can be enabled by resistive heaters, infrared energy, microwave energy, and thermoelectric devices; all can provide rapid and localized heating, but require feedback controls to ensure reaction volumes are reaching the intended temperatures.[61] The transition of a sample through the temperatures

required to promote the denaturation, annealing, and extension phases of the reaction, can be accomplished by two primary modes involving either flow through a microchannel or stationary heating in a microchamber.[63] Flow-through, or 'space domain PCR', methods involve the continuous flow of the reaction through distinct temperature zones via serpentine, spiral, circular, or oscillating microchannels.[63,64] While this a clever exploitation of microfluidics for PCR, the 'stationary' method dominates by far, wherein thermal cycling is accomplished in a stationary fluid situated in a PCR chamber and is time-dependent. 'Time domain PCR' modes offer more flexibility for reaction heating and cooling profiles, and are more amenable to integration with sample preparation and/or detection on a microdevice.[63,65] With these methods, total PCR

A

Protocol #	Protocol Type	Color	Ramp Rate (°C/s)	Initial Denaturation Dwell Time (s)	Cycling Denaturation Dwell Time (s)	Annealing Dwell Time (s)	Time to complete 40 cycles (min)
1	Manufacturer		4	120	5	20	52
2	Optimized		8	1	1	10	15
3	Rapid		12 up, 10 down	1	1	1	8

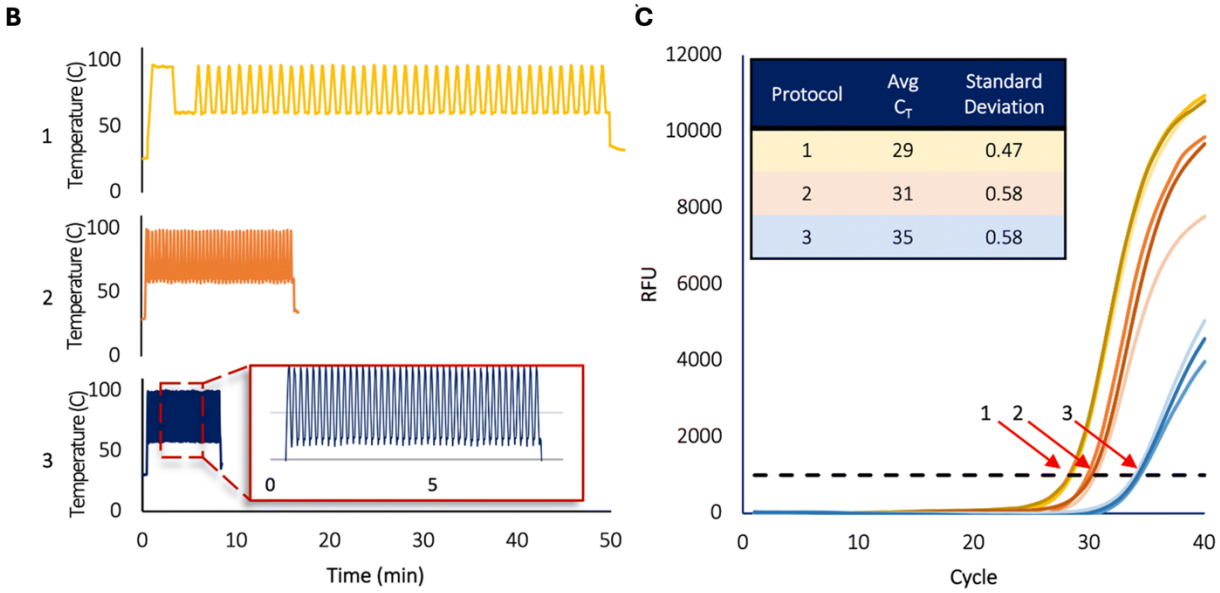

Figure 1-6. Amplification of human genomic DNA (hgDNA) using an in-house instrument for rapid amplification and detection. (A) Table detailing the amplification details for three different protocols and their resultant **(B)** thermal cycling and **(C)** amplification profiles for each condition. Figure adapted from Nouwairi et al. 2022.[69]

reaction times may can be minimized while maintaining PCR efficiency by hitting the desired temperatures through extremely fast ramp rates (heating and cooling), reduction of dwell times, and an increase in primer and polymerase concentrations.[66,67] While forensic HID systems have done a remarkable job compressing the total forensic workflow into a sub-90 minute analytical time (e.g., expedited PCR completed in 20 minutes), this may not represent the full potential of microfluidics. For example, microfluidic DNA amplification has been demonstrated to be extremely rapid; 30 cycles of PCR 240 s,[68] and 45 cycles in 8.75 minutes (**Fig. 1-6**).[69] However, this last point necessitates that commercial multiplexed forensic HID kit chemistries intended for conventional volumes and thermocycling speeds, will require adjustment prior to being adapted to the microscale. With regard to PCR, there are chemical, physical, and biological aspects of this analytical step that require consideration; with microfluidics, we can overcome the physical limitations, but not necessarily the chemical (e.g., primers and salts) or biological (e.g., polymerases). Thus, an important caveat is that the longer dwell times associated with conventional thermocycling parameters are optimized for their ability to maintain efficiency across all targets in a multiplex reaction and encourage peak height balance across the genetic profile. In other words, forensic STR multiplex kits are developed with the chemical and biological aspects of the reaction in mind over speed.[70] It follows that a loss in sensitivity and/or specificity of a heavily multiplexed reaction with rapid, microfluidic HID is possible and could dictate redesign of primers or use of more efficient polymerases, to name a few. Additionally, fluidic microchips and/or cartridges designed to avoid cold-chain storage, may require further modification of buffer/salt concentrations for the rehydration of lyophilized or dehydrated reagents.

Quantitative real-time PCR (qPCR) involves intermittent measurement of a fluorescent signal during thermocycling. This is important within the context of the conventional DNA workflow, where the quantification of human autosomal and Y-chromosome DNA precedes multiplexed amplification for HID to ensure an optimized mass of input DNA is utilized.[35] Here, quantification is based upon the dilution of similarly amplified standards and the cycle threshold (C_t) values they produce; sample DNA concentration is obtained by comparison to a standard curve.[9] Despite great success with microfluidic amplification and the development of multicapillary detection systems to make fluorescent monitoring possible, most devices do not incorporate quantification.[2] This is likely due to domination of the PCR market by clinical diagnostics, where larger sample volumes are available. From a demand-based standpoint, incorporating qPCR with further downstream analysis by CE or sequencing is not traditionally necessary for clinical applications, in which input concentrations are less stochastic and variable than those experienced with forensic samples. From a microengineering perspective, while qPCR has been accomplished with microsystems, avoidance is ideal, especially if integrated downstream analysis is required, as simultaneous heating and fluorescence monitoring gets complicated. Most commonly, heating is accomplished with non-contact systems, such as lamps and lasers, or contact thermoelectric modules (TEM).[65] Non-contact heating is great from a detection perspective, since the chamber is not obscured and available for monitoring throughout the reaction from all sides; however, preferential compatibility with non-polymeric substrates (e.g., glass) increases the cost per chip and complexity associated with device fabrication[71]. Alternatively, efficient contact heating that requires coverage from two sides to eliminate the possibility of temperature non-uniformity obscures the reaction chamber from

detection.[69] Notably, as it pertains to forensic quantification: if the conventional method were to simply be miniaturized for forensic Rapid HID, microsystems would require the incorporation of additional chambers and channels to facilitate the amplification and detection of known concentration standards and some method for feedback to inform downstream procedures. In essence, overcoming the complications associated with micro-quantification in fully-integrated systems would require alternative strategies, such as metering from more standard inputs or incorporating solid phase materials with known binding capacity.[72]

1.3.3. STR Analysis by Microchip Electrophoresis. Capillary electrophoresis is the principal technique for separation and fluorescence detection of STR alleles.[9] At its core, CE involves electrokinetic injection of amplicons and a voltage-driven, size-based separation through a long (30-60 cm), circular silica capillary. As fluorescently-tagged amplicons traverse across a detection window they are excited via laser-induced fluorescence, monitored by an on-board detection system, and analyzed with automated software to produce an electropherogram.[29] Commercially available instruments must be able to spatially resolve amplicons down to single nucleotides, spectrally resolve multiple fluorescent dyes, and precisely size DNA fragments for accurate STR typing.

The earliest and most common examples of miniaturization were applied to the electrophoresis of clinically-relevant analytes, given that the relative simplicity of capillaries and mechanisms that generate separation translate well to microfluidics.[29] Early iterations of microchip electrophoresis (ME) consisted of circular channels that were reminiscent of small-bore capillaries and fabricated with glass. Glass devices recreated a separation environment akin to

conventional CE but with significantly shorter channel lengths enabling rapid separations 10-100 times faster than conventional instrumentation.[9] Following the development of microchannels in glass, researchers developed cost-effective polymeric-based devices for ME using optically-clear materials compatible with fluorescence detection.[21] However, despite the reduced cost and time associated with these technologies, the single-base pair resolution required for STR analysis and sequencing was challenging to achieve relative to conventional options. In devices that demonstrated single-base resolution – as was the case with Mathies' elegant, disc-shaped 96-lane microcapillary array[73] – upstream sample preparation was still required off-chip. Incorporation of ME with other workflows is often omitted as this requires integration of complex hardware, including fluorescent detectors for separation, electrodes for voltage application, and heating elements for amplification. Despite the fact that this particular portion of the NA analysis workflow has received the majority of funding and time, fully integrated Rapid DNA systems still make use of a modified capillary for STR analysis, similar to commercial benchtop genetic analyzers.

1.3.4. Sample-to-Answer Systems. The greatest advantage of microfluidic devices for NA analysis the ability to seamlessly integrate sample preparation with the analytical (read-out) step, thus enabling the automation of workflows and decreasing the analysis time, labor, and cost associated with traditional sample processing.[74] Yet, for forensic DNA analysis, few sample-to-answer systems have garnered enough traction and funding for commercialization despite early predictions that portable, integrated microdevices would be available for use with case work

samples by 2020.[7] Following the 2010 Rapid DNA Initiative, multiple groups worked to develop fully-integrated systems for forensic DNA analysis.[9]

The University of Arizona in concert with the Forensic Science Service (UK) developed an integrated sample-to-answer system that produced a DNA profile in less than 4 hours and with resolution of 1.2 base pairs (bps).[75] Simultaneously, Lockheed Martin, in collaboration with ZyGEM, MicroLab Diagnostics, and the Landers group at the University of Virginia, developed a 4-sample microchip system that incorporated liquid NA extraction, multiplexed amplification, and microchip electrophoresis in approximately 2 hours with single bp resolution and a much smaller chip size.[76,77,78] Later, the Landers group secured federal funding to further decrease the device footprint with the development of an alternative microCD method for analysis from buccal swabs that produced limited loci (10) single-source profiles in under an hour.[79] Earlier, LGC Forensics brought to market a Taqman-based, non-electrophoretic, limited loci STR profiling rapid instrument intended for crime scene use; the ParaDNA Intelligence Test typed a total of 5 markers for HID in 75 minutes.[80] IntegenX and Mathies' research group at the University of California-Berkeley also developed a fully-automated prototype device that could provide results in three hours with enhanced limits of detection (LOD = 2.5 ng DNA input) resulting from integrated post-PCR clean-up and a pre-CE streptavidin-based enrichment strategy.[81] Network Biosystems (NetBio) and the Whitehead Institute of the Massachusetts Institute of Technology (MIT) incrementally worked toward a fully-integrated system with the Genebench-FX, which enabled the rapid, microfluidic separation and detection of STRs, mini-STRs, and mitochondrial DNA sequences.[82]

Eventually, the latter two technologies advanced adequately for government testing. The IntegenX system was a microfluidic/capillary electrophoresis hybrid, 'multi-sample-to-answer' platform (late 2012), and announced a UK-based partnership with Key Forensic Services and publishing several developmental and internal validations with multiple collaborating agencies for years after.[77,83,84] Acquisition of IntegenX by Thermo Fisher Scientific in 2018 launched a significantly-modified, single-sample version of the technology into the commercial sector, and years of R&D culminated into the RapidHIT device portfolio. Contemporaneously, NetBio was exclusively funded for further development by a government-based consortium composed of the Federal Bureau of Investigation (FBI), the Department of Defense (DoD), and the Department of Homeland Security (DHS). Today, the Accelerated Nuclear DNA Equipment (ANDE) 6C Rapid DNA ID System is commercially-available in the form of a ruggedized platform marketed for PON DNA analysis. The specifications that make each system unique are collated in **Table 1-2** for ease of comparison.[47,84] A maturity assessment of these technologies was completed by the NIST in 2018 to demonstrate success with single-source samples[85] and it was around this time that multiple agencies published their position statements in support of limiting the use of Rapid DNA technologies in terms of accessing DNA databases.[86,87,88] Beyond limiting the use, a consortium of forensic oversight bodies responded to the assessment highlighting five major areas of concern that require further evaluation before certain use-case scenarios could be expanded beyond reference profile generation.[10] Recommendations focused on transparency (i.e., the provision of raw data and well-defined developmental validations), standardization via the integration of internal positive controls, fully-automated on-board expert systems, and improved performance

Rapid DNA System Comparison		RapidHIT ID System	ANDE 6C Rapid DNA System
			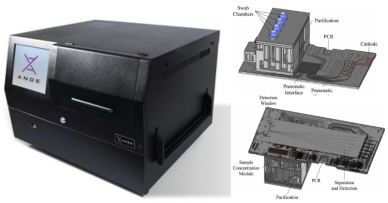
Cost	System Cost	~150 – 200 k	~250 k
	Cost per Sample	~$150/sample	~$250/sample
Investigative Time	Analysis time	90 mins	90 mins
	Hands-On Time	~1 minute	~1 minute
Practical Implementation	System Size (L x W x H)	19 x 10.5 x 21 inches 62.6 lbs	17.7 x 29.5 x 23.6 inches 117 lbs
	Cold Storage	Required	Not Required
	Throughput	1 sample per run	4 – 5 samples per run
	NDIS Approval	✓	✓

Table 1-2. Comparison of current commercially-available rapid DNA instrumentation. The table compares each in terms of cost, investigative time, and practical implementation for use at the PON. Figures adapted from Turiello et al. 2023.[11]

for low quantity and mixed samples.[10] Likewise, the microfluidics community is working to standardize microfluidic-based devices for more robust performance and ease of commercialization;[40] in 2017, the first Workshop on Standards for Microfluidics was hosted by NIST, supporting better communication, and standardizing testing and manufacturing practices.[39]

1.4. Microfluidics in the Forensic DNA Laboratory

The application of microfluidic technology to forensic NA processing and analysis is desirable for a number of reasons. Laboratories are largely overburdened, with the demand for services greatly outpacing resources and creating a steadily increasing backlog that ultimately impacts investigative and prosecutorial efforts.[5] Technology with the capacity to disrupt this cycle should be rapid, automated, cost-effective, and permit facile integration with the existing infrastructure. Microfluidic modes of analysis offer several of these advantages, but are perceived as lacking in sensitivity and suitability to be used at the PON when compared to their conventional counterparts.[86,87,88] Beyond trade-offs, discussed further in Chapter 5 of this manuscript, it is this author's perspective that the cultural landscape for implementation of these new techniques is complex and has led to the limited use of commercialized sample-to-answer platforms.

1.4.1. Unique Advantages Offered by Microfluidics. Regardless of the approach to fluid flow control, microfluidic modes of analysis are advantageous for a number of pertinent reasons. At a foundational level, miniaturized interfaces support the use of reduced reagent volumes as well as architectural features with increased SA:V ratios compared with traditional reaction tubes and spin-columns. These features alone set them apart from conventional methods by enabling fast analysis times, increased sensitivity, smaller footprints, and lower costs at scale. A list of microfluidic devices for point-of-care (POC) diagnostics that realize these benefits in the form of commercialized devices has recently been published.[89] In leveraging the physics of fluid flow, molecular motion and heat transfer, rapid heating and mixing are possible at the microscale, thus, decreasing overall reaction times compared to traditional workflows. Moreover, all of the

characteristics that make microfluidics advantageous can, in combination, lead to enhanced assay sensitivity, particularly by minimizing processes in the workflow where exposure to harsh conditions is detrimental.[90,91] The reduction in scale inherent with microfluidic technology presents a tangible potential for instruments with a smaller footprint, which would not only benefit laboratories with limited bench space, but allow for a smaller instrument size that would be critical for direct analysis at the crime scene.[75] Consequently, by reducing reagent volumes and decreasing instrument size and complexity, the cost of the system is in theory reduced. In addition to the clear benefits afforded by an expedited approach to executing NA analysis, microfluidic systems are ideally designed by multidisciplinary teams with the end-user in mind. In this pursuit, the development of both microdevices and the associated instruments, requires blurring of the lines between chemistry, materials science engineering, mechatronics and physics, in order to create practical solutions for use in the real world.[92] Given the advances in molecular diagnostics with microfluidic systems, it follows that approaches could be developed for use with HID. For the end-user, microfluidic tools for forensic NA analysis should reduce risks associated with contamination and analyst-to-analyst variation. Additionally, a sample-to-result system that is automated should enhance efficiency in the lab, by limiting intervention and freeing analysts to tackle case backlog reduction, complete data interpretation, and provide alternative investigative services.

1.4.2. Practical Limitations to Overcome with Microfluidic Methods. While the promise that microfluidic technology presented in the early 1990s was vast, the reality is that few commercial products have been delivered.[93] In fact, only very recently have microfluidic devices

experienced exponential success, with a compound annual growth rate of 22% as of 2017.[40] It may be surmised that the attenuation of growth early on can been attributed to several factors, including a disconnect between academics and professionals in target markets, the general scarcity of functional, manufacturable, fully-integrated systems, and a lack of standardization in the field.

A cursory search of the literature in any niche microfluidic application finds a series of proof-of-concept microsystems purporting to outperform existing methods in terms of speed, sensitivity, and cost, to name a few. Thus far, a negligible percentage of applications realize their full potential, for a variety of reasons including that they were not designed with commercialization in mind and/or researchers did not consider compatibility with existing laboratory infrastructures.[93] Compatibility issues can be avoided by integrating the entire workflow into a single μTAS; however, some processes are less amenable to microminiaturization and integration and, hence, require some level of off-chip pretreatment or downstream analysis.[94] For those processes that are integratable, the difficulties are the following: 1) committing to a mode of liquid transport that is compatible with all of the processes in a multi-step workflow, 2) the selection of a versatile, affordable fabrication material (e.g., silica, COC, PDMS, etc.), 3) successful incorporation with modular components, and 4) interfacing with a supporting instrument. For example, a μTAS for NA analysis may employ pneumatic pumping in a polymeric substrate for extraction and amplification, but require electrokinetic injection to drive resultant analytes through a microchannel; the integration of these ostensibly closed channel modular components and their interfacing pumps, heating elements, electrodes, and detectors is not trivial. A suggestion to decrease the complexity associated with microdevice development

and enhance system reproducibility is to focus the path by implementing professional standards, a process that is still largely underway, as previously mentioned.[38,39,40]

Generally, analytical microsystems that automate one or several steps of the forensic DNA typing workflow, possess some inherent limitations that end-users should be aware of. First, the microliter volumes that are touted as part of the value proposition for microfluidics, can be problematic with sampling-related reduction in assay sensitivities. For example, when a swab or swab cutting is inserted into a microchip for NA extraction, a comparatively 'large' volume of liquid is required to saturate the swab, likely exceeding what is ideal for effective microfluidic lysis/extraction. Another example involves washing of the outer surface of a condom to collect genetic material; several milliliters of 'wash' could result, and this volume is enormous by microfluidic standards. Within the microfluidics community, this phenomenon is referred to as the 'macro-to-micro interface' challenge.[95] This issue can be mitigated with the clever use of enrichment techniques that may exploit additional solid phases upstream of extraction, or employ modular components that increase the capacity for larger on-board fluid volumes. Largely, these issues can be resolved through integration of the known processes from an ever-increasing microfluidic toolkit and, together with improvements to commercial forensic kit chemistries designed to mitigate the stochastic effects typically encountered with heavily degraded forensic stains and touch DNA samples. With the Rapid DNA technologies that exist today, lower sensitivity is generally observed relative to their macroscale counterparts, and, as discussed, this has sparked debate regarding their ultimate suitability for use with evidence samples at the crime scene.[96]

Other criticisms involving the use of Rapid DNA systems at the PON involve the lack of integrated DNA quantification.[85] The conventional DNA typing workflow includes amplification-based quantitation to assess the concentration of unknown genetic contributions so that reaction volumes may be adjusted for normalized analysis and the deconvolution of DNA mixtures. 'Miniaturizing' this portion of the workflow in an integrated format would require dividing the eluate following extraction and completing qPCR along with a set of internal standards of known concentrations to define the volume of the remaining extract for multiplexed amplification. Given the complexity of incorporating a multistep workflow that requires feedback mid-analysis and the fact that current Rapid instruments were designed for reference buccal swabs, quantitation was not built into these systems. At present, this precludes them from searching and storing DNA profiles originating from crime scenes in CODIS. Furthermore, a lack of quantification and subsequent input concentration normalization in currently available instruments may result in less than ideal electrophoretic results, leading to complications with the typing and analysis of DNA mixtures. Given that the majority of crime scene stains contain genetic material from multiple contributors, a number of system capabilities need to be addressed before they can be exploited reproducibly at the crime scene or in the laboratory for probative items with mixed cellular contributions. This would include providing the raw data for analyst interpretation, further balancing electrophoretic peak heights between and among alleles, and incorporating an on-board expert system to remove artifacts and differentiate multi-source profiles.[10] A combination of these factors likely contribute to the limited adoption of integrated, microfluidic systems for Rapid DNA analysis; that is, according to the Federal Bureau of Investigation QAS,

Rapid DNA technology is only to be used in conjunction with the CODIS database searching and storage of single-source reference DNA profiles originating from buccal swabs at this time.[35,36]

1.5. The Epigenome and Forensic HID

As an alternative to matching in CODIS or with reference profiles via the STR identification system, investigation of the human epigenome has been suggested for a variety of forensic applications related to forensic DNA phenotyping (FDP).[97] Here, epigenetic 'marks' are correlated with phenotypic traits that may confer information related human sex,[98] monozygotic twin differentiation,[99] body fluid identification,[100] lifestyle habits (e.g., smoking, alcohol consumption, etc.),[101] and chronological age determination,[102] to name a few. In particular, the majority of this research correlates locus-specific *DNA methylation* patterns with phenotypic information.[103] DNA methylation refers, most commonly, to the modification of the 5' position of cytosine (C) bases in CpG dinucleotides by a methyl (CH_3) group.[103] Methylation is a normal biochemical process involved in the regulatory activity of DNA expression via the promoter region, whereby high levels are commonly associated with transcriptional silencing.[103] As it relates to forensic HID, the presence or absence of methylated DNA at certain positions may assist with the derivation of phenotypic information in the absence of a comparative STR profile, originating from a known victim of suspect.[104] If there are no investigative leads to generate a DNA 'match' from using the conventional approach, epigenetic information may be used to provide phenotypic information and a produce *biological witness*.[97]

1.5.1. Age Approximation by Epigenetic Testing. As epigenetics relates to forensic HID, determination of human chronological age has produced the most research studies proposing predictive panels. In this area, over 300 research studies and systematic reviews have been printed, with more than 30 posited strategies for predicting age from epigenetic data, published between 2014 and 2019 alone.[105] Epigenetic age prediction models have been developed with forensically-relevant tissues including blood,[106,107,108,109,110] saliva,[111,112,113] buccal swabs,[114,115] semen,[116,117] and teeth,[118] and predictive capabilities are purported to be as high as ± 0.94 years[119] from an age range of 0 – 95 years.[120] The progression in the appearance of these chemical signatures at particular loci have been positively associated with human aging to establish what has been coined an *epigenetic clock.*[121] While age determination is, by and large, polygenic, there are models which have developed strong correlations using only one locus;[122] although many models use a combination of five or so CpG sites in their prediction models.[13] Interestingly, this appears to be one application wherein the addition of more genetic loci does not necessarily increase prediction accuracy.

1.5.2. Issues Associated with the Epigenetic Analysis of Forensic DNA. For most workflows, determination of methylation status at a genetic locus requires modification of the sequence by bisulfite conversion (BSC) to differentiate between methylated and unmethylated cytosines. With extracted DNA, this process preferentially deaminates unmethylated cytosines to uracil while leaving methylated cytosines intact; enabling base differentiation following downstream amplification and analysis. Following DNA extraction and BSC, methylation detection is most commonly accomplished with either real-time PCR (RT-PCR) by a specialized assay (e.g., methyl-

light, methylation-specific PCR, etc.) or downstream sequencing by pyro- or next generation sequencing (NGS). Given the genetic workflow is roughly the same as with STR typing, besides the additional BSC sample preparation step, one might assume that methylation-based age prediction would be readily adopted by case-working scientists. This is especially in light of the fact that relevant research data has been subject to scientific scrutiny for over 10 years, and DNA-based testing is regarded as the gold-standard for forensic analysis.[104] However, this has not been the case for epigenetic-based testing, primarily because of the added BSC step. Not only is epigenetic conversion a time-consuming and labor-intensive process with multiple open-tube steps that can lead to contamination and inter-operability induced variation, it also results in a significant amount of DNA loss.[123] In fact, it is for this reason that kit chemistries for methylation-based analysis recommend starting with a significant amount of genetic material (>1 μg).[124] Unfortunately, forensic DNA is often limited and fragmented for a variety of reasons, largely having to do with its deposition in unfavorable environments,[125] but also as a result of DNA isolation during the extraction/purification process.[126] To summarize, case working forensic analysts are likely hesitant to risk precious, probative genetic material to a variable, time-consuming workflow that may result in poor quality results given the limited sample available.

1.5.3. Microfluidic Methods for Epigenetic Sample Preparation. Miniaturized methods for epigenetic sample preparation by bisulfite conversion are limited, likely because of the long, heated incubations and the sequential addition and removal of reagents that the workflow necessitates. Briefly, the complexity of a multi-step process like BSC dictates careful consideration of materials and fabrication method, flow strategy, and the approach to administering sequential

unit operations (e.g., valving, magnetic actuation, etc.). One such technology originating from the Wang Laboratory at Johns Hopkins University leverages a polydimethylsiloxane (PDMS) cartridge consisting of a linear array of chambers containing BSC buffer droplets that are combined and traversed through via magnetic actuation of DNA-containing silica beads (**Fig. 7-A**).[127,128] The primary benefit of this BSC method is automation and the parallel processing of up to three samples on one device; additionally, they developed an enhanced approach coupling lysis by proteinase K and downstream detection by RT-PCR (**Fig. 7-B**).[128] However, there is no exploration of reduced incubation intervals or measurement of conversion efficiency besides what can be gleaned from amplification results.[127] A system was also developed by Yoon et al. (**Fig. 7C**), wherein a conversion module is coupled with a detection platform employing isothermal solid-phase amplification; while the integration of components is impressive, the method requires input of pre-extracted DNA.[129]

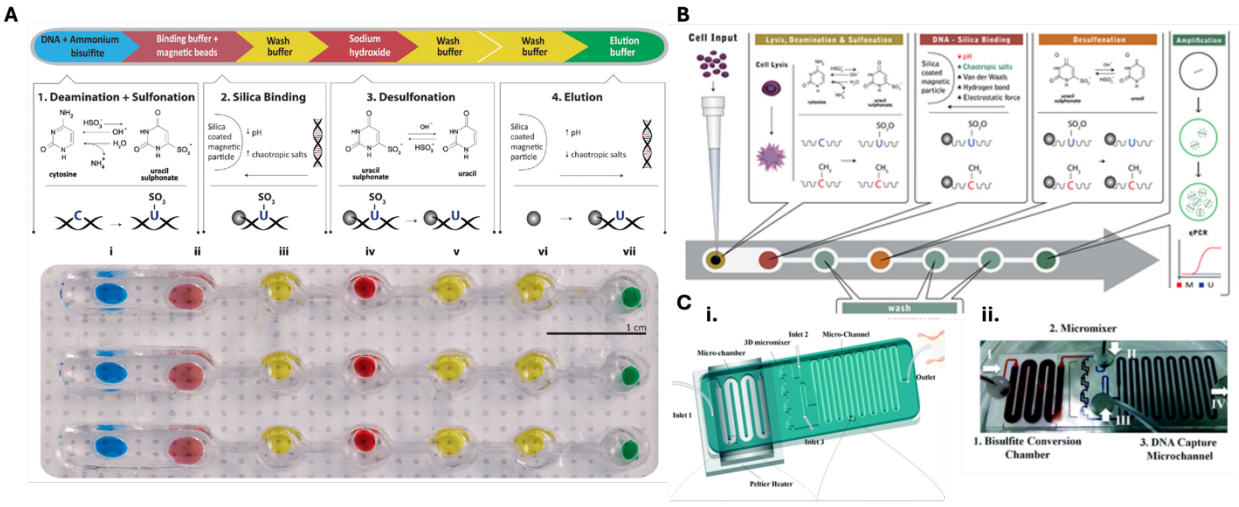

Figure 1-7. Microfluidic methods for bisulfite conversion. (A - B) Wang Laboratory 'magnetofluidic' chip, adapted from Stark et al. 2016[127] and Stark et al. 2018.[128] **(C)** Shin Laboratory single-channel bisulfite conversion module for integrated methylation preparation and analysis, adapted from Yoon et al. 2015.[129]

1.6. Research Goals and Concluding Remarks

This dissertation is focused on the development of integrated sample preparation workflows for NA analysis, using a rotationally-driven, microfluidic interface for ease of use at the benchtop, and with the potential for integration in PON analytical systems. The primary focus is detailed in **Chapters 2 and 3**, which describe a method that automates forensic epigenetic sample preparation, specifically as it relates to the prediction of human chronological age. **Chapter 2** details the design and testing of a technique for epigenetic conversion by ammonium bisulfite (BSC). Here, the approach was tested with forensically-relevant concentrations of DNA and reaction intervals were shortened with the goal of microfluidic integration and the conservation of genetic material for downstream analysis. In the interest of streamlining the entire epigenetic sample preparation workflow, **Chapter 3** describes the incorporation of an enzymatic lysis method upstream of microfluidic BSC. In this chapter, the compatibility of BSC with an enzyme-based, purification-free DNA extraction method by EA1 is reported for the first time and coupled via a microfluidic regime. Coupling these processes significantly reduced analytical time and issues associated with analyst interoperability, while permitting parallel reactions of up to five samples on one disc.

For relevance beyond forensic HID, **Chapter 4** utilizes the same enzymatic extraction chemistry detailed in **Chapter 3** for the preparation of patient samples containing severe acute respiratory syndrome coronavirus 2 (SARS-CoV-2), once again employing a centrifugally-driven microfluidic interface. Upstream of RNA extraction, the microfluidic method utilizes affinity-capture, magnetic nanoparticles for enrichment and supernatant removal, all incorporated into a

single device for NA analysis. With the integrated device, sample preparation is possible in under 15 minutes and for a total of up to six samples in parallel. **Chapter 4** also describes preliminary research toward integration of this method with a sample-to-answer platform situated for use at the PON.

In summary, the following chapters highlight the progress made toward the development and validation of multiple microfluidic modes aimed to provide real-world solutions to both forensic and clinical problems at the benchtop. As the preponderance of work focuses on a solution aimed for forensic epigenetic sample preparation, **Chapter 5** provides concluding remarks considering all research and development described in this dissertation. Ongoing work, future work, and persistent challenges are also discussed. The latter portion of the chapter describes the intricate forensic climate, commenting on the limited implementation of microfluidic tools developed for forensic HID. Looking to the future, I consider the possibility that microfluidic technologies would have a higher impact potential if they were developed to solve new problems or facilitate the use of emerging techniques that have not yet been widely utilized beyond proof-of-principle research. In this vein, multiple opportunity zones for microfluidic integration within HID and criminal investigation are proposed to increase laboratory efficiency and expand the capacity of forensic science services in the future. Furthermore, I discuss the potential for the integration of the existing commercial systems for Rapid DNA analysis and expedited HID.

1.7. References

(1) Niculescu, A.-G.; Chircov, C.; Bîrcă, A. C.; Grumezescu, A. M. Fabrication and Applications of Microfluidic Devices: A Review. *IJMS* **2021**, *22* (4), 2011. https://doi.org/10.3390/ijms22042011.

(2) Bruijns, B.; van Asten, A.; Tiggelaar, R.; Gardeniers, H. Microfluidic Devices for Forensic DNA Analysis: A Review. *Biosensors* **2016**, *6* (3), 41. https://doi.org/10.3390/bios6030041.

(3) Carney, C.; Whitney, S.; Vaidyanathan, J.; Persick, R.; Noel, F.; Vallone, P. M.; Romsos, E. L.; Tan, E.; Grover, R.; Turingan, R. S.; French, J. L.; Selden, R. F. Developmental Validation of the ANDE™ Rapid DNA System with FlexPlex™ Assay for Arrestee and Reference Buccal Swab Processing and Database Searching. *Forensic Science International: Genetics* **2019**, *40*, 120–130. https://doi.org/10.1016/j.fsigen.2019.02.016.

(4) Buscaino, J.; Barican, A.; Farrales, L.; Goldman, B.; Klevenberg, J.; Kuhn, M.; Lin, F.; Nguyen, P.; Salceda, S.; Schueren, R.; Smith, C.; Troup, C.; Tsou, D.; Vangbo, M.; King, D. Evaluation of a Rapid DNA Process with the RapidHIT® ID System Using a Specialized Cartridge for Extracted and Quantified Human DNA. *Forensic Science International: Genetics* **2018**, *34*, 116–127. https://doi.org/10.1016/j.fsigen.2018.02.010.

(5) Kobus, H.; Houck, M.; Speaker, P.; Riley, R.; Witt, T. Managing Performance in the Forensic Sciences: Expectations in Light of Limited Budgets. *Forensic Science Policy & Management: An International Journal* **2011**, *2* (1), 36–43. https://doi.org/10.1080/19409044.2011.564271.

(6) Dror, I. E. Practical Solutions to Cognitive and Human Factor Challenges in Forensic Science. *Forensic Science Policy & Management: An International Journal* **2013**, *4* (3–4), 105–113. https://doi.org/10.1080/19409044.2014.901437.

(7) *Future of Forensic DNA Testing: Predictions of the Research and Development Working Group*; NIJ Issues and Practices in Criminal Justice 183697; National Institute of Justice, 2000. https://nij.ojp.gov/library/publications/future-forensic-dna-testing-predictions-research-and-development-working-group.

(8) Butler, J. M.; Willis, S. Interpol Review of Forensic Biology and Forensic DNA Typing 2016-2019. *Forensic Science International: Synergy* **2020**, *2*, 352–367. https://doi.org/10.1016/j.fsisyn.2019.12.002.

(9) Butler, J. M. *Advanced Topics in Forensic DNA Typing: Methodology*; Elsevier/Academic Press: Walthan, MA, 2012.

(10) Hares, D. R.; Kneppers, A.; Onorato, A. J.; Kahn, S. Rapid DNA for Crime Scene Use: Enhancements and Data Needed to Consider Use on Forensic Evidence for State and National DNA Databasing – An Agreed Position Statement by ENFSI, SWGDAM and the Rapid DNA Crime Scene Technology Advancement Task Group. *Forensic Science International: Genetics* **2020**, *48*, 102349. https://doi.org/10.1016/j.fsigen.2020.102349.

(11) Turiello, R.; Nouwairi, R. L.; Landers, J. P. Taking the Microfluidic Approach to Nucleic Acid Analysis in Forensics: Review and Perspectives. *Forensic Science International: Genetics* **2023**, *63*, 102824. https://doi.org/10.1016/j.fsigen.2022.102824.

(12) Vidaki, A.; Kayser, M. Recent Progress, Methods and Perspectives in Forensic Epigenetics. *Forensic Science International: Genetics* **2018**, *37*, 180–195. https://doi.org/10.1016/j.fsigen.2018.08.008.

(13) Kampmann, M.-L.; Fleckhaus, J.; Børsting, C.; Jurtikova, H.; Piters, A.; Papin, J.; Gauthier, Q.; Ghemrawi, M.; Doutremepuich, C.; McCord, B.; Schneider, P. M.; Drabek, J.; Morling, N. Collaborative Exercise: Analysis of Age Estimation Using a QIAGEN Protocol and the PyroMark Q48 Platform. *Forensic Sciences Research* **2024**, *9* (1), owad055. https://doi.org/10.1093/fsr/owad055.

(14) Chiu, D. T.; deMello, A. J.; Di Carlo, D.; Doyle, P. S.; Hansen, C.; Maceiczyk, R. M.; Wootton, R. C. R. Small but Perfectly Formed? Successes, Challenges, and Opportunities for Microfluidics in the Chemical and Biological Sciences. *Chem* **2017**, *2* (2), 201–223. https://doi.org/10.1016/j.chempr.2017.01.009.

(15) Haeberle, S.; Zengerle, R. Microfluidic Platforms for Lab-on-a-Chip Applications. *Lab Chip* **2007**, *7* (9), 1094. https://doi.org/10.1039/b706364b.

(16) Kellner, M. J.; Ross, J. J.; Schnabl, J.; Dekens, M. P. S.; Heinen, R.; Grishkovskaya, I.; Bauer, B.; Stadlmann, J.; Menéndez-Arias, L.; Fritsche-Polanz, R.; Traugott, M.; Seitz, T.; Zoufaly, A.; Födinger, M.; Wenisch, C.; Zuber, J.; Vienna Covid-19 Diagnostics Initiative (VCDI); Pauli, A.; Brennecke, J. *A Rapid, Highly Sensitive and Open-Access SARS-CoV-2 Detection Assay for Laboratory and Home Testing*; preprint; Molecular Biology, 2020. https://doi.org/10.1101/2020.06.23.166397.

(17) Mukhopadhyay, R. Microfluidics: On the Slope of Enlightenment. *Anal. Chem.* **2009**, *81* (11), 4169–4173. https://doi.org/10.1021/ac900638w.

(18) Dedehayir, O.; Steinert, M. The Hype Cycle Model: A Review and Future Directions. *Technological Forecasting and Social Change* **2016**, *108*, 28–41. https://doi.org/10.1016/j.techfore.2016.04.005.

(19) Manz, A.; Harrison, D. J.; Verpoorte, E. M. J.; Fettinger, James. C.; Paulus, A.; Lüdi, H.; Widmer, H. M. Planar Chips Technology for Miniaturization and Integration of Separation Techniques into Monitoring Systems. *Journal of Chromatography A* **1992**, *593* (1–2), 253–258. https://doi.org/10.1016/0021-9673(92)80293-4.

(20) Manz, A.; Verpoorte, E.; Raymond, D. E.; Effenhauser, C. S.; Burggraf, N.; Widmer, H. M. M-TAS: Miniaturized Total Chemical Analysis Systems. In *Micro Total Analysis Systems*; Van den Berg, A., Bergveld, P., Eds.; Springer Netherlands: Dordrecht, 1995; pp 5–27. https://doi.org/10.1007/978-94-011-0161-5_2.

(21) Nouwairi, R. L.; O'Connell, K. C.; Gunnoe, L. M.; Landers, J. P. Microchip Electrophoresis for Fluorescence-Based Measurement of Polynucleic Acids: Recent Developments. *Anal. Chem.* **2021**, *93* (1), 367–387. https://doi.org/10.1021/acs.analchem.0c04596.

(22) Whitesides, G. M. The Origins and the Future of Microfluidics. *Nature* **2006**, *442* (7101), 368–373. https://doi.org/10.1038/nature05058.

(23) Zhang, P.; Bachman, H.; Ozcelik, A.; Huang, T. J. Acoustic Microfluidics. *Annual Rev. Anal. Chem.* **2020**, *13* (1), 17–43. https://doi.org/10.1146/annurev-anchem-090919-102205.

(24) Strohmeier, O.; Keller, M.; Schwemmer, F.; Zehnle, S.; Mark, D.; von Stetten, F.; Zengerle, R.; Paust, N. Centrifugal Microfluidic Platforms: Advanced Unit Operations and Applications. *Chem. Soc. Rev.* **2015**, *44* (17), 6187–6229. https://doi.org/10.1039/C4CS00371C.

(25) Zhang, X.; Xia, K.; Ji, A. A Portable Plug-and-Play Syringe Pump Using Passive Valves for Microfluidic Applications. *Sensors and Actuators B: Chemical* **2020**, *304*, 127331. https://doi.org/10.1016/j.snb.2019.127331.

(26) Duffy, D. C.; McDonald, J. C.; Schueller, O. J. A.; Whitesides, G. M. Rapid Prototyping of Microfluidic Systems in Poly(Dimethylsiloxane). *Anal. Chem.* **1998**, *70* (23), 4974–4984. https://doi.org/10.1021/ac980656z.

(27) Liu, K.; Fan, Z. H. Thermoplastic Microfluidic Devices and Their Applications in Protein and DNA Analysis. *Analyst* **2011**, *136* (7), 1288. https://doi.org/10.1039/c0an00969e.

(28) Faustino, V.; Catarino, S. O.; Lima, R.; Minas, G. Biomedical Microfluidic Devices by Using Low-Cost Fabrication Techniques: A Review. *Journal of Biomechanics* **2016**, *49* (11), 2280–2292. https://doi.org/10.1016/j.jbiomech.2015.11.031.

(29) *Handbook of Capillary and Microchip Electrophoresis and Associated Microtechniques*, 3rd ed.; Landers, J. P., Ed.; CRC Press: Boca Raton, 2008.

(30) Emrich, C. A.; Tian, H.; Medintz, I. L.; Mathies, R. A. Microfabricated 384-Lane Capillary Array Electrophoresis Bioanalyzer for Ultrahigh-Throughput Genetic Analysis. *Anal. Chem.* **2002**, *74* (19), 5076–5083. https://doi.org/10.1021/ac020236g.

(31) Unger, M. A.; Chou, H.-P.; Thorsen, T.; Scherer, A.; Quake, S. R. Monolithic Microfabricated Valves and Pumps by Multilayer Soft Lithography. *Science* **2000**, *288* (5463), 113–116. https://doi.org/10.1126/science.288.5463.113.

(32) Grover, W. H.; Ivester, R. H. C.; Jensen, E. C.; Mathies, R. A. Development and Multiplexed Control of Latching Pneumatic Valves Using Microfluidic Logical Structures. *Lab Chip* **2006**, *6* (5), 623. https://doi.org/10.1039/b518362f.

(33) Thorsen, T.; Maerkl, S. J.; Quake, S. R. Microfluidic Large-Scale Integration. *Science* **2002**, *298* (5593), 580–584. https://doi.org/10.1126/science.1076996.

(34) Laboratory Division Biometrics Analysis Section. *Guide to All Things Rapid DNA*; U. S. Department of Justice Federal Bureau of Investigation Science and Technology Branch, 2022. http://www.lsp.org/pdf/FBI_Guide_to_All_Things_Rapid_DNA_01_27_2022.pdf.

(35) *Quality Assurance Standards for Forensic DNA Testing Laboratories*; Federal Bureau of Investigation, 2011. https://ucr.fbi.gov/lab/biometric-analysis/codis/quality-assurance-standards-for-forensic-dna-testing-laboratories.

(36) James F. Sensenbrenner Jr. *Rapid DNA Act of 2017*; 2017. https://www.congress.gov/bill/115th-congress/house-bill/510.

(37) *Non-CODIS Rapid DNA Considerations and Best Practices for Law Enforcement Use*; Law Enforcement Resources; Federal Bureau of Investigation, Non-CODIS Rpaid DNA Best Practices/Outreach and Courtroom Considerrations Task Group, 2019. https://le.fbi.gov/file-repository/non-codis-rapid-dna-best-practices-092419.pdf/view.

(38) Klapperich, C. M. Microfluidic Diagnostics: Time for Industry Standards. *Expert Review of Medical Devices* **2009**, *6* (3), 211–213. https://doi.org/10.1586/erd.09.11.

(39) Reyes, D. R.; van Heeren, H. Proceedings of the First Workshop on Standards for Microfluidics. *J. RES. NATL. INST. STAN.* **2019**, *124*, 124001. https://doi.org/10.6028/jres.124.001.

(40) Reyes, D. R.; van Heeren, H.; Guha, S.; Herbertson, L.; Tzannis, A. P.; Ducrée, J.; Bissig, H.; Becker, H. Accelerating Innovation and Commercialization through Standardization of

Microfluidic-Based Medical Devices. *Lab Chip* **2021**, *21* (1), 9–21. https://doi.org/10.1039/D0LC00963F.

(41) Clark, C.; Turiello, R.; Cotton, R.; Landers, J. P. Analytical Approaches to Differential Extraction for Sexual Assault Evidence. *Analytica Chimica Acta* **2020**, S0003267020307972. https://doi.org/10.1016/j.aca.2020.07.059.

(42) Kim, J.; Johnson, M.; Hill, P.; Gale, B. K. Microfluidic Sample Preparation: Cell Lysis and Nucleic Acid Purification. *Integr. Biol.* **2009**, *1* (10), 574. https://doi.org/10.1039/b905844c.

(43) Dineva, M. A.; Mahilum-Tapay, L.; Lee, H. Sample Preparation: A Challenge in the Development of Point-of-Care Nucleic Acid-Based Assays for Resource-Limited Settings. *Analyst* **2007**, *132* (12), 1193. https://doi.org/10.1039/b705672a.

(44) Wen, J.; Legendre, L. A.; Bienvenue, J. M.; Landers, J. P. Purification of Nucleic Acids in Microfluidic Devices. *Anal. Chem.* **2008**, *80* (17), 6472–6479. https://doi.org/10.1021/ac8014998.

(45) Chong, K. W. Y.; Thong, Z.; Syn, C. K. Recent Trends and Developments in Forensic DNA Extraction. *WIREs Forensic Sci* **2021**, *3* (2). https://doi.org/10.1002/wfs2.1395.

(46) Gin, K.; Tovar, J.; Bartelink, E. J.; Kendell, A.; Milligan, C.; Willey, P.; Wood, J.; Tan, E.; Turingan, R. S.; Selden, R. F. The 2018 California Wildfires: Integration of Rapid DNA to Dramatically Accelerate Victim Identification. *J Forensic Sci* **2020**, *65* (3), 791–799. https://doi.org/10.1111/1556-4029.14284.

(47) Turingan, R. S.; Tan, E.; Jiang, H.; Brown, J.; Estari, Y.; Krautz-Peterson, G.; Selden, R. F. Developmental Validation of the ANDE 6C System for Rapid DNA Analysis of Forensic

Casework and DVI Samples. *J Forensic Sci* **2020**, *65* (4), 1056–1071. https://doi.org/10.1111/1556-4029.14286.

(48) Murakami, C.; Irie, W.; Sasaki, C.; Nakamaru, N.; Sakamoto, M.; Nagato, J.; Satoh, F. Individual Identification Using the RapidHIT™ ID System for Forensic Samples. *Legal Medicine* **2020**, *47*, 101776. https://doi.org/10.1016/j.legalmed.2020.101776.

(49) Kutter, J. P.; Jacobson, S. C.; Ramsey, J. M. Solid Phase Extraction on Microfluidic Devices. *J. Micro. Sep.* **2000**, *12* (2), 93–97. https://doi.org/10.1002/(SICI)1520-667X(2000)12:2<93::AID-MCS5>3.0.CO;2-P.

(50) Vuichard, S.; Borer, U.; Bottinelli, M.; Cossu, C.; Malik, N.; Meier, V.; Gehrig, C.; Sulzer, A.; Morerod, M.-L.; Castella, V. Differential DNA Extraction of Challenging Simulated Sexual-Assault Samples: A Swiss Collaborative Study. *Investig Genet* **2011**, *2* (1), 11. https://doi.org/10.1186/2041-2223-2-11.

(51) Inci, F.; Ozen, M. O.; Saylan, Y.; Miansari, M.; Cimen, D.; Dhara, R.; Chinnasamy, T.; Yuksekkaya, M.; Filippini, C.; Kumar, D. K.; Calamak, S.; Yesil, Y.; Durmus, N. G.; Duncan, G.; Klevan, L.; Demirci, U. A Novel On-Chip Method for Differential Extraction of Sperm in Forensic Cases. *Adv. Sci.* **2018**, *5* (9), 1800121. https://doi.org/10.1002/advs.201800121.

(52) Horsman, K. M.; Barker, S. L. R.; Ferrance, J. P.; Forrest, K. A.; Koen, K. A.; Landers, J. P. Separation of Sperm and Epithelial Cells in a Microfabricated Device: Potential Application to Forensic Analysis of Sexual Assault Evidence. *Anal. Chem.* **2005**, *77* (3), 742–749. https://doi.org/10.1021/ac0486239.

(53) Liu, W.; Chen, W.; Liu, R.; Ou, Y.; Liu, H.; Xie, L.; Lu, Y.; Li, C.; Li, B.; Cheng, J. Separation of Sperm and Epithelial Cells Based on the Hydrodynamic Effect for Forensic Analysis. *Biomicrofluidics* **2015**, *9* (4), 044127. https://doi.org/10.1063/1.4928453.

(54) Norris, J. V.; Evander, M.; Horsman-Hall, K. M.; Nilsson, J.; Laurell, T.; Landers, J. P. Acoustic Differential Extraction for Forensic Analysis of Sexual Assault Evidence. *Anal. Chem.* **2009**, *81* (15), 6089–6095. https://doi.org/10.1021/ac900439b.

(55) Clark, C. P.; Xu, K.; Scott, O.; Hickey, J.; Tsuei, A.-C.; Jackson, K.; Landers, J. P. Acoustic Trapping of Sperm Cells from Mock Sexual Assault Samples. *Forensic Science International: Genetics* **2019**, *41*, 42–49. https://doi.org/10.1016/j.fsigen.2019.03.012.

(56) Auka, N.; Valle, M.; Cox, B. D.; Wilkerson, P. D.; Dawson Cruz, T.; Reiner, J. E.; Seashols-Williams, S. J. Optical Tweezers as an Effective Tool for Spermatozoa Isolation from Mixed Forensic Samples. *PLoS ONE* **2019**, *14* (2), e0211810. https://doi.org/10.1371/journal.pone.0211810.

(57) Williamson, V. R.; Laris, T. M.; Romano, R.; Marciano, M. A. Enhanced DNA Mixture Deconvolution of Sexual Offense Samples Using the DEPArray™ System. *Forensic Science International: Genetics* **2018**, *34*, 265–276. https://doi.org/10.1016/j.fsigen.2018.03.001.

(58) Roper, M. G.; Easley, C. J.; Landers, J. P. Advances in Polymerase Chain Reaction on Microfluidic Chips. *Anal. Chem.* **2005**, *77* (12), 3887–3894. https://doi.org/10.1021/ac050756m.

(59) Zhang, C.; Xu, J.; Ma, W.; Zheng, W. PCR Microfluidic Devices for DNA Amplification. *Biotechnology Advances* **2006**, *24* (3), 243–284. https://doi.org/10.1016/j.biotechadv.2005.10.002.

(60) Zhang, Y.; Ozdemir, P. Microfluidic DNA Amplification—A Review. *Analytica Chimica Acta* **2009**, *638* (2), 115–125. https://doi.org/10.1016/j.aca.2009.02.038.

(61) Chang, C.-M.; Chang, W.-H.; Wang, C.-H.; Wang, J.-H.; Mai, J. D.; Lee, G.-B. Nucleic Acid Amplification Using Microfluidic Systems. *Lab Chip* **2013**, *13* (7), 1225. https://doi.org/10.1039/c3lc41097h.

(62) Gorgannezhad, L.; Stratton, H.; Nguyen, N.-T. Microfluidic-Based Nucleic Acid Amplification Systems in Microbiology. *Micromachines* **2019**, *10* (6), 408. https://doi.org/10.3390/mi10060408.

(63) Ahrberg, C. D.; Manz, A.; Chung, B. G. Polymerase Chain Reaction in Microfluidic Devices. *Lab Chip* **2016**, *16* (20), 3866–3884. https://doi.org/10.1039/C6LC00984K.

(64) Kulkarni, M. B.; Goel, S. Advances in Continuous-Flow Based Microfluidic PCR Devices—a Review. *Eng. Res. Express* **2020**, *2* (4), 042001. https://doi.org/10.1088/2631-8695/abd287.

(65) Yin, J.; Suo, Y.; Zou, Z.; Sun, J.; Zhang, S.; Wang, B.; Xu, Y.; Darland, D.; Zhao, J. X.; Mu, Y. Integrated Microfluidic Systems with Sample Preparation and Nucleic Acid Amplification. *Lab Chip* **2019**, *19* (17), 2769–2785. https://doi.org/10.1039/C9LC00389D.

(66) Wittwer, C. T.; Garling, D. J. Rapid Cycle DNA Amplification: Time and Temperature Optimization. *Biotechniques* **1991**, *10* (1), 76–83.

(67) Farrar, J. S.; Wittwer, C. T. Extreme PCR: Efficient and Specific DNA Amplification in 15–60 Seconds. *Clinical Chemistry* **2015**, *61* (1), 145–153. https://doi.org/10.1373/clinchem.2014.228304.

(68) Giordano, B. C.; Ferrance, J.; Swedberg, S.; Hühmer, A. F. R.; Landers, J. P. Polymerase Chain Reaction in Polymeric Microchips: DNA Amplification in Less Than 240 Seconds. *Analytical Biochemistry* **2001**, *291* (1), 124–132. https://doi.org/10.1006/abio.2000.4974.

(69) Nouwairi, R. L.; Cunha, L. L.; Turiello, R.; Scott, O.; Hickey, J.; Thomson, S.; Knowles, S.; Chapman, J. D.; Landers, J. P. Ultra-Rapid Real-Time Microfluidic RT-PCR Instrument for Nucleic Acid Analysis. *Lab Chip* **2022**, 10.1039.D2LC00495J. https://doi.org/10.1039/D2LC00495J.

(70) Romsos, E. L.; Vallone, P. M. Rapid PCR of STR Markers: Applications to Human Identification. *Forensic Science International: Genetics* **2015**, *18*, 90–99. https://doi.org/10.1016/j.fsigen.2015.04.008.

(71) Miralles, V.; Huerre, A.; Malloggi, F.; Jullien, M.-C. A Review of Heating and Temperature Control in Microfluidic Systems: Techniques and Applications. *Diagnostics* **2013**, *3* (1), 33–67. https://doi.org/10.3390/diagnostics3010033.

(72) Tan, E.; Turingan, R. S.; Hogan, C.; Vasantgadkar, S.; Palombo, L.; Schumm, J. W.; Selden, R. F. Fully Integrated, Fully Automated Generation of Short Tandem Repeat Profiles. *Investig Genet* **2013**, *4* (1), 16. https://doi.org/10.1186/2041-2223-4-16.

(73) Paegel, B. M.; Emrich, C. A.; Wedemayer, G. J.; Scherer, J. R.; Mathies, R. A. High Throughput DNA Sequencing with a Microfabricated 96-Lane Capillary Array Electrophoresis Bioprocessor. *Proc. Natl. Acad. Sci. U.S.A.* **2002**, *99* (2), 574–579. https://doi.org/10.1073/pnas.012608699.

(74) Horsman, K. M.; Bienvenue, J. M.; Blasier, K. R.; Landers, J. P. Forensic DNA Analysis on Microfluidic Devices: A Review. *J Forensic Sci* **2007**, *52* (4), 784–799. https://doi.org/10.1111/j.1556-4029.2007.00468.x.

(75) Hopwood, A. J.; Hurth, C.; Yang, J.; Cai, Z.; Moran, N.; Lee-Edghill, J. G.; Nordquist, A.; Lenigk, R.; Estes, M. D.; Haley, J. P.; McAlister, C. R.; Chen, X.; Brooks, C.; Smith, S.; Elliott, K.; Koumi, P.; Zenhausern, F.; Tully, G. Integrated Microfluidic System for Rapid Forensic DNA Analysis: Sample Collection to DNA Profile. *Anal. Chem.* **2010**, *82* (16), 6991–6999. https://doi.org/10.1021/ac101355r.

(76) Le Roux, D.; Root, B. E.; Hickey, J. A.; Scott, O. N.; Tsuei, A.; Li, J.; Saul, D. J.; Chassagne, L.; Landers, J. P.; de Mazancourt, P. An Integrated Sample-in-Answer-out Microfluidic Chip for Rapid Human Identification by STR Analysis. *Lab Chip* **2014**, *14* (22), 4415–4425. https://doi.org/10.1039/C4LC00685B.

(77) Smith, C.; Strauss, S.; DeFrancesco, L. DNA Goes to Court. *Nat Biotechnol* **2012**, *30* (11), 1047–1053. https://doi.org/10.1038/nbt.2408.

(78) Le Roux, D.; Root, B. E.; Reedy, C. R.; Hickey, J. A.; Scott, O. N.; Bienvenue, J. M.; Landers, J. P.; Chassagne, L.; de Mazancourt, P. DNA Analysis Using an Integrated Microchip for Multiplex PCR Amplification and Electrophoresis for Reference Samples. *Anal. Chem.* **2014**, *86* (16), 8192–8199. https://doi.org/10.1021/ac501666b.

(79) Easley, C. J.; Karlinsey, J. M.; Bienvenue, J. M.; Legendre, L. A.; Roper, M. G.; Feldman, S. H.; Hughes, M. A.; Hewlett, E. L.; Merkel, T. J.; Ferrance, J. P.; Landers, J. P. A Fully Integrated Microfluidic Genetic Analysis System with Sample-in–Answer-out Capability. *Proc. Natl. Acad. Sci. U.S.A.* **2006**, *103* (51), 19272–19277. https://doi.org/10.1073/pnas.0604663103.

(80) Ball, G.; Dawnay, N.; Stafford-Allen, B.; Panasiuk, M.; Rendell, P.; Blackman, S.; Duxbury, N.; Wells, S. Concordance Study between the ParaDNA ® Intelligence Test, a Rapid DNA Profiling Assay, and a Conventional STR Typing Kit (AmpFlSTR ® SGM Plus ®). *Forensic Science International: Genetics* **2015**, *16*, 48–51. https://doi.org/10.1016/j.fsigen.2014.12.006.

(81) Liu, P.; Li, X.; Greenspoon, S. A.; Scherer, J. R.; Mathies, R. A. Integrated DNA Purification, PCR, Sample Cleanup, and Capillary Electrophoresis Microchip for Forensic Human Identification. *Lab Chip* **2011**, *11* (6), 1041. https://doi.org/10.1039/c0lc00533a.

(82) Read, T. D.; Turingan, R. S.; Cook, C.; Giese, H.; Thomann, U. H.; Hogan, C. C.; Tan, E.; Selden, R. F. Rapid Multi-Locus Sequence Typing Using Microfluidic Biochips. *PLoS ONE* **2010**, *5* (5), e10595. https://doi.org/10.1371/journal.pone.0010595.

(83) Hennessy, L. K.; Mehendale, N.; Chear, K.; Jovanovich, S.; Williams, S.; Park, C.; Gangano, S. Developmental Validation of the GlobalFiler® Express Kit, a 24-Marker STR Assay, on the RapidHIT® System. *Forensic Science International: Genetics* **2014**, *13*, 247–258. https://doi.org/10.1016/j.fsigen.2014.08.011.

(84) Wiley, R.; Sage, K.; LaRue, B.; Budowle, B. Internal Validation of the RapidHIT ® ID System. *Forensic Science International: Genetics* **2017**, *31*, 180–188. https://doi.org/10.1016/j.fsigen.2017.09.011.

(85) Romsos, E. L.; French, J. L.; Smith, M.; Figarelli, V.; Harran, F.; Vandegrift, G.; Moreno, L. I.; Callaghan, T. F.; Brocato, J.; Vaidyanathan, J.; Pedroso, J. C.; Amy, A.; Stoiloff, S.; Morillo, V. H.; Czetyrko, K.; Johnson, E. D.; Tagyos, J.; Murray, A.; Vallone, P. M. Results of the 2018

Rapid DNA Maturity Assessment. *J Forensic Sci* **2020**, *65* (3), 953–959. https://doi.org/10.1111/1556-4029.14267.

(86) *Scientific Working Group on DNA Analysis Methods Position Statement on Rapid DNA Analysis*; Scientific Working Group DNA Analysis Methods (SWGDAM), 2017. https://docs.wixstatic.com/ugd/4344b0_f84df0465a2243218757fac1a1ccffea.pdf.

(87) *ASCLD Position Statement*; American Society of Crime Laboratory Directors (ASCLD), 2017. https://www.ascld.org/wp-content/uploads/2017/11/ASCLD-Position-Statement-RAPID-DNA.pdf.

(88) *NDAA Position Statement on Use of Rapid DNA Technology*; National District Attorneys Association, 2018. https://dps.alaska.gov/getmedia/fb933229-8e52-4cf8-8fe0-cb72d5e039e3/NDAA-Statement-on-Use-of-Rapid-DNA-Technology-2018.pdf.

(89) *Advanced Microfluidics Based Point-of-Care Diagnostics: A Bridge between Microfluidics and Biomedical Applications*, First edition.; Khan, R., Dhand, C., Sanghi, S. K., Shabi, T. S., Mishra, A. B. P., Eds.; CRC Press, Taylor & Francis Group: Boca Raton, 2022.

(90) Konry, T.; Bale, S. S.; Bhushan, A.; Shen, K.; Seker, E.; Polyak, B.; Yarmush, M. Particles and Microfluidics Merged: Perspectives of Highly Sensitive Diagnostic Detection. *Microchim Acta* **2012**, *176* (3–4), 251–269. https://doi.org/10.1007/s00604-011-0705-1.

(91) Wittwer, C. T.; Herrmann, M. G. Rapid Thermal Cycling and PCR Kinetics. In *PCR Applications*; Elsevier, 1999; pp 211–229. https://doi.org/10.1016/B978-012372185-3/50015-8.

(92) Repko, A. F.; Szostak, R. *Interdisciplinary Research: Process and Theory*, Fourth edition.; SAGE: Los Angeles, 2021.

(93) Chin, C. D.; Linder, V.; Sia, S. K. Commercialization of Microfluidic Point-of-Care Diagnostic Devices. *Lab Chip* **2012**, *12* (12), 2118–2134. https://doi.org/10.1039/C2LC21204H.

(94) Li, Z.; Bai, Y.; You, M.; Hu, J.; Yao, C.; Cao, L.; Xu, F. Fully Integrated Microfluidic Devices for Qualitative, Quantitative and Digital Nucleic Acids Testing at Point of Care. *Biosensors and Bioelectronics* **2021**, *177*, 112952. https://doi.org/10.1016/j.bios.2020.112952.

(95) Fredrickson, C. K.; Fan, Z. H. Macro-to-Micro Interfaces for Microfluidic Devices. *Lab Chip* **2004**, *4* (6), 526. https://doi.org/10.1039/b410720a.

(96) Mapes, A. A.; Stoel, R. D.; de Poot, C. J.; Vergeer, P.; Huyck, M. Decision Support for Using Mobile Rapid DNA Analysis at the Crime Scene. *Science & Justice* **2019**, *59* (1), 29–45. https://doi.org/10.1016/j.scijus.2018.05.003.

(97) Kayser, M. Forensic DNA Phenotyping: Predicting Human Appearance from Crime Scene Material for Investigative Purposes. *Forensic Science International: Genetics* **2015**, *18*, 33–48. https://doi.org/10.1016/j.fsigen.2015.02.003.

(98) Naito, E.; Dewa, K.; Yamanouchi, H.; Takagi, S.; Kominami, R. Sex Determination Using the Hypomethylation of a Human Macro-Satellite DXZ4 in Female Cells. *Nucl Acids Res* **1993**, *21* (10), 2533–2534. https://doi.org/10.1093/nar/21.10.2533.

(99) Li, C.; Zhang, S.; Que, T.; Li, L.; Zhao, S. Identical but Not the Same: The Value of DNA Methylation Profiling in Forensic Discrimination within Monozygotic Twins. *Forensic Science International: Genetics Supplement Series* **2011**, *3* (1), e337–e338. https://doi.org/10.1016/j.fsigss.2011.09.031.

(100) Frumkin, D.; Wasserstrom, A.; Budowle, B.; Davidson, A. DNA Methylation-Based Forensic Tissue Identification. *Forensic Science International: Genetics* **2011**, *5* (5), 517–524. https://doi.org/10.1016/j.fsigen.2010.12.001.

(101) Kaur, G.; Begum, R.; Thota, S.; Batra, S. A Systematic Review of Smoking-Related Epigenetic Alterations. *Arch Toxicol* **2019**, *93* (10), 2715–2740. https://doi.org/10.1007/s00204-019-02562-y.

(102) Bocklandt, S.; Lin, W.; Sehl, M. E.; Sánchez, F. J.; Sinsheimer, J. S.; Horvath, S.; Vilain, E. Epigenetic Predictor of Age. *PLoS ONE* **2011**, *6* (6), e14821. https://doi.org/10.1371/journal.pone.0014821.

(103) Moore, L. D.; Le, T.; Fan, G. DNA Methylation and Its Basic Function. *Neuropsychopharmacol* **2013**, *38* (1), 23–38. https://doi.org/10.1038/npp.2012.112.

(104) Vidaki, A.; Daniel, B.; Court, D. S. Forensic DNA Methylation Profiling—Potential Opportunities and Challenges. *Forensic Science International: Genetics* **2013**, *7* (5), 499–507. https://doi.org/10.1016/j.fsigen.2013.05.004.

(105) Maulani, C.; Auerkari, E. I. Age Estimation Using DNA Methylation Technique in Forensics: A Systematic Review. *Egypt J Forensic Sci* **2020**, *10* (1), 38. https://doi.org/10.1186/s41935-020-00214-2.

(106) Zbieć-Piekarska, R.; Spólnicka, M.; Kupiec, T.; Parys-Proszek, A.; Makowska, Ż.; Pałeczka, A.; Kucharczyk, K.; Płoski, R.; Branicki, W. Development of a Forensically Useful Age Prediction Method Based on DNA Methylation Analysis. *Forensic Science International: Genetics* **2015**, *17*, 173–179. https://doi.org/10.1016/j.fsigen.2015.05.001.

(107) Freire-Aradas, A.; Phillips, C.; Mosquera-Miguel, A.; Girón-Santamaría, L.; Gómez-Tato, A.; Casares de Cal, M.; Álvarez-Dios, J.; Ansede-Bermejo, J.; Torres-Español, M.; Schneider, P. M.; Pośpiech, E.; Branicki, W.; Carracedo, Á.; Lareu, M. V. Development of a Methylation Marker Set for Forensic Age Estimation Using Analysis of Public Methylation Data and the Agena Bioscience EpiTYPER System. *Forensic Science International: Genetics* **2016**, *24*, 65–74. https://doi.org/10.1016/j.fsigen.2016.06.005.

(108) Park, J.-L.; Kim, J. H.; Seo, E.; Bae, D. H.; Kim, S.-Y.; Lee, H.-C.; Woo, K.-M.; Kim, Y. S. Identification and Evaluation of Age-Correlated DNA Methylation Markers for Forensic Use. *Forensic Science International: Genetics* **2016**, *23*, 64–70. https://doi.org/10.1016/j.fsigen.2016.03.005.

(109) Naue, J.; Hoefsloot, H. C. J.; Mook, O. R. F.; Rijlaarsdam-Hoekstra, L.; van der Zwalm, M. C. H.; Henneman, P.; Kloosterman, A. D.; Verschure, P. J. Chronological Age Prediction Based on DNA Methylation: Massive Parallel Sequencing and Random Forest Regression. *Forensic Science International: Genetics* **2017**, *31*, 19–28. https://doi.org/10.1016/j.fsigen.2017.07.015.

(110) Feng, L.; Peng, F.; Li, S.; Jiang, L.; Sun, H.; Ji, A.; Zeng, C.; Li, C.; Liu, F. Systematic Feature Selection Improves Accuracy of Methylation-Based Forensic Age Estimation in Han Chinese Males. *Forensic Science International: Genetics* **2018**, *35*, 38–45. https://doi.org/10.1016/j.fsigen.2018.03.009.

(111) Hong, S. R.; Jung, S.-E.; Lee, E. H.; Shin, K.-J.; Yang, W. I.; Lee, H. Y. DNA Methylation-Based Age Prediction from Saliva: High Age Predictability by Combination of 7 CpG Markers.

Forensic Science International: Genetics **2017**, *29*, 118–125. https://doi.org/10.1016/j.fsigen.2017.04.006.

(112) Hong, S. R.; Shin, K.-J.; Jung, S.-E.; Lee, E. H.; Lee, H. Y. Platform-Independent Models for Age Prediction Using DNA Methylation Data. *Forensic Science International: Genetics* **2019**, *38*, 39–47. https://doi.org/10.1016/j.fsigen.2018.10.005.

(113) Jung, S.-E.; Lim, S. M.; Hong, S. R.; Lee, E. H.; Shin, K.-J.; Lee, H. Y. DNA Methylation of the ELOVL2, FHL2, KLF14, C1orf132/MIR29B2C, and TRIM59 Genes for Age Prediction from Blood, Saliva, and Buccal Swab Samples. *Forensic Science International: Genetics* **2019**, *38*, 1–8. https://doi.org/10.1016/j.fsigen.2018.09.010.

(114) Eipel, M.; Mayer, F.; Arent, T.; Ferreira, M. R. P.; Birkhofer, C.; Gerstenmaier, U.; Costa, I. G.; Ritz-Timme, S.; Wagner, W. Epigenetic Age Predictions Based on Buccal Swabs Are More Precise in Combination with Cell Type-Specific DNA Methylation Signatures. *Aging* **2016**, *8* (5), 1034–1048. https://doi.org/10.18632/aging.100972.

(115) Bekaert, B.; Kamalandua, A.; Zapico, S. C.; Van de Voorde, W.; Decorte, R. A Selective Set of DNA-Methylation Markers for Age Determination of Blood, Teeth and Buccal Samples. *Forensic Science International: Genetics Supplement Series* **2015**, *5*, e144–e145. https://doi.org/10.1016/j.fsigss.2015.09.058.

(116) Lee, H. Y.; Jung, S.-E.; Oh, Y. N.; Choi, A.; Yang, W. I.; Shin, K.-J. Epigenetic Age Signatures in the Forensically Relevant Body Fluid of Semen: A Preliminary Study. *Forensic Science International: Genetics* **2015**, *19*, 28–34. https://doi.org/10.1016/j.fsigen.2015.05.014.

(117) Li, L.; Song, F.; Huang, Y.; Zhu, H.; Hou, Y. Age-Associated DNA Methylation Determination of Semen by Pyrosequencing in Chinese Han Population. *Forensic Science International:*

Genetics Supplement Series **2017**, *6*, e99–e100. https://doi.org/10.1016/j.fsigss.2017.09.042.

(118) Giuliani, C.; Cilli, E.; Bacalini, M. G.; Pirazzini, C.; Sazzini, M.; Gruppioni, G.; Franceschi, C.; Garagnani, P.; Luiselli, D. Inferring Chronological Age from DNA Methylation Patterns of Human Teeth: INFERRING AGE FROM DNA METHYLATION OF HUMAN TEETH. *Am. J. Phys. Anthropol.* **2016**, *159* (4), 585–595. https://doi.org/10.1002/ajpa.22921.

(119) Freire-Aradas, A.; Phillips, C.; Lareu, M. V. Forensic Individual Age Estimation with DNA: From Initial Approaches to Methylation Tests. *Forensic Sci Rev* **2017**, *29* (2), 121–144.

(120) Hamano, Y.; Manabe, S.; Morimoto, C.; Fujimoto, S.; Tamaki, K. Forensic Age Prediction for Saliva Samples Using Methylation-Sensitive High Resolution Melting: Exploratory Application for Cigarette Butts. *Sci Rep* **2017**, *7* (1), 10444. https://doi.org/10.1038/s41598-017-10752-w.

(121) Bell, C. G.; Lowe, R.; Adams, P. D.; Baccarelli, A. A.; Beck, S.; Bell, J. T.; Christensen, B. C.; Gladyshev, V. N.; Heijmans, B. T.; Horvath, S.; Ideker, T.; Issa, J.-P. J.; Kelsey, K. T.; Marioni, R. E.; Reik, W.; Relton, C. L.; Schalkwyk, L. C.; Teschendorff, A. E.; Wagner, W.; Zhang, K.; Rakyan, V. K. DNA Methylation Aging Clocks: Challenges and Recommendations. *Genome Biol* **2019**, *20* (1), 249. https://doi.org/10.1186/s13059-019-1824-y.

(122) Zbieć-Piekarska, R.; Spólnicka, M.; Kupiec, T.; Makowska, Ż.; Spas, A.; Parys-Proszek, A.; Kucharczyk, K.; Płoski, R.; Branicki, W. Examination of DNA Methylation Status of the ELOVL2 Marker May Be Useful for Human Age Prediction in Forensic Science. *Forensic Science International: Genetics* **2015**, *14*, 161–167. https://doi.org/10.1016/j.fsigen.2014.10.002.

(123) Leontiou, C. A.; Hadjidaniel, M. D.; Mina, P.; Antoniou, P.; Ioannides, M.; Patsalis, P. C. Bisulfite Conversion of DNA: Performance Comparison of Different Kits and Methylation Quantitation of Epigenetic Biomarkers That Have the Potential to Be Used in Non-Invasive Prenatal Testing. *PLoS ONE* **2015**, *10* (8), e0135058. https://doi.org/10.1371/journal.pone.0135058.

(124) Sabeeha; Hasnain, S. E. Forensic Epigenetic Analysis: The Path Ahead. *Med Princ Pract* **2019**, *28* (4), 301–308. https://doi.org/10.1159/000499496.

(125) Bhoyar, L.; Mehar, P.; Chavali, K. An Overview of DNA Degradation and Its Implications in Forensic Caseworks. *Egypt J Forensic Sci* **2024**, *14* (1), 15. https://doi.org/10.1186/s41935-024-00389-y.

(126) Katevatis, C.; Fan, A.; Klapperich, C. M. Low Concentration DNA Extraction and Recovery Using a Silica Solid Phase. *PLoS ONE* **2017**, *12* (5), e0176848. https://doi.org/10.1371/journal.pone.0176848.

(127) Stark, A.; Shin, D. J.; Pisanic, T.; Hsieh, K.; Wang, T.-H. A Parallelized Microfluidic DNA Bisulfite Conversion Module for Streamlined Methylation Analysis. *Biomed Microdevices* **2016**, *18* (1), 5. https://doi.org/10.1007/s10544-015-0029-8.

(128) Stark, A.; Shin, D. J.; Wang, T.-H. A Sample-to-Answer Droplet Magnetofluidic Assay Platform for Quantitative Methylation-Specific PCR. *Biomed Microdevices* **2018**, *20* (2), 31. https://doi.org/10.1007/s10544-018-0276-6.

(129) Yoon, J.; Park, M. K.; Lee, T. Y.; Yoon, Y.-J.; Shin, Y. LoMA-B: A Simple and Versatile Lab-on-a-Chip System Based on Single-Channel Bisulfite Conversion for DNA Methylation Analysis. *Lab Chip* **2015**, *15* (17), 3530–3539. https://doi.org/10.1039/C5LC00458F.

Chapter 2. A Streamlined Method for the Deamination of Cytosines by Bisulfite Conversion

Publication(s) included in Chapter 2:

- **Turiello, R.**; Nouwairi, R.; Keller, J.; Cunha, L. L.; Dignan, L. M.; Landers, J. P. A Rotationally-Driven Dynamic Solid Phase Sodium Bisulfite Conversion Disc for Forensic Epigenetic Sample Preparation. *Lab on a Chip*, 2023, 24 (1), 97 - 112. doi: 10.1039/d3lc00867c

2.1. Introduction

Current approaches to human identification (HID) of unknown persons remain largely comparative in nature, whereby short tandem repeat (STR) profiles from unknown evidence samples are compared with known reference materials/database profiles.[1] Alternatively, unidentified human remains are morphologically categorized by visual interpretation by an anthropologist, as compared to discrete, published standards.[2] Despite the statistical success of producing a *match* via STR analysis, many genetic profiles are generated from crime scenes, human remains, and sexual assault and evidence collection kits (SAECKs) that do not have a genetic reference material for comparison and do not produce a database *hit*. Further, the precision with which any trait is discerned via anthropological assessment for identification has been determined to be dependent upon the completeness of the remains and the anthropologist's prior experience.[3] For these types of cases, the human epigenome has been suggested as a reservoir of information for sex typing[4], monozygotic twin individualization[5], body fluid identification[6], behavioral traits[7], and DNA phenotyping (FDP) by estimation of human chronological age.[8] In particular, over the past 15 years more than 300 research studies and

review articles have been published suggesting the utility of epigenetic methylation status at specified genetic loci for approximation of human age.[9] Studies have demonstrated predictive success within 0.94 years[10] from forensically-relevant body fluids including, but not limited to, blood[11,12,13,14,15,16], saliva[17,18,19], semen[20,21], and teeth[22]. However, despite great research success and the forensic community's high regard for DNA-based testing, epigenetic age prediction has not been adapted into the forensic DNA analysis workflow or even used as a routine investigative technique by law enforcement personnel.

If adopted, the forensic epigenetic workflow would require an additional step during sample preparation, referred to as bisulfite conversion (BSC), a method that has remained largely steadfast in its approach since its inception. Through a series of chemical modifications, the BSC process preferentially deaminates all unmethylated cytosines in the DNA transcript to yield uracil residues, leaving those cytosines containing a methyl group (e.g., 5-methylcytosines) intact and distinguishable for downstream analysis by methylation-specific real-time polymerase chain reaction (RT-PCR) or sequencing. Unfortunately, these techniques are characterized by extensive DNA loss; in fact, a 2015 study by Leontiou and co-workers comparing four of the most widely used BSC kits determined that the recovery from 200 ng of input DNA averaged as low as 33.2% and only as high as 55%. Further, these methods require time-consuming, labor-intensive workflows with a high propensity for contamination due to the multitude of open-tube pipetting steps. I have concluded that adaptation of the epigenetic analysis workflow by the forensic community has stalled given the current requirement for large amounts of input DNA and the constraint that implementation of the associated laborious processes are not optimal for integration into the existing forensic DNA workflow.

I describe a microfluidic solution for forensic epigenetic sample preparation that leverages centrifugal force to enable rapid, efficient conversion of forensically-relevant DNA input masses in an automated microCD (μCD) format. Shortened conversion intervals are possible with the use of reduced reagent and sample volumes in chambers with an enhanced surface-area-to-volume ratio when compared with the conventional, in-tube BSC method; diffusion theories associated with miniaturization dictate that a system $1/10^{th}$ of the original reaction chamber size will result in 100-fold reduction in time, thus minimizing the need for long incubations.[23, 24] The proposed work varies from those in literature on a number of fronts, but namely I sought to develop a method more amenable to low template DNA. Additionally, my method employs centrifugal force as the mechanism for fluid movement, which is advantageous for forensics applications for three primary reasons. First, this ensures that only a single mechanism is required for propulsion, eliminating the need for bulky external hardware (e.g., syringe pumps, electronics, tubing, etc.) that hinder portability and take up valuable bench space. Second, the mechanism permits automation in a fully closed system to mitigate contamination risk. Third, the forces controlling fluid movement through channels and into reaction chambers for precise chemistries are easily controlled by simply adjusting rotational speed, an aspect that may be coded for automation via a corresponding graphical user interface (GUI). With regard to automation specifically, the μCD approach is fully programmable via custom, external systems capable of heating, imparting rotational and magnetic forces at specified frequencies, and laser valving to open and close fluidic channels. For this application, the use of a silica dynamic solid phase (dSP) enables magnetically-actuated, bead-based conversion; together with careful consideration of fluidic architecture and valving strategy, this permits the completion of several sequential unit operations on-board.

Conversion discs were designed to accommodate approximately 1/10th of the fluid volumes required by conventional BSC methods and with a view of multiplexing in mind: that is, each µCD is capable of converting up to four samples per disc.

Microfluidic integration was assessed with standards and multiple downstream analytical processes, including RT-PCR, high resolution melting (HRM), and electrophoresis. Early phase goals of this project included testing the chemistry at the microfluidic scale, adjusting the parameters of the reaction steps associated with DNA loss, optimizing microfluidic architecture, and comparing µCD converted eluates with those originating from an in-tube, gold-standard method for conversion. For proof-of-concept, assay characterization was completed with primers targeting FHL2, a locus associated with age determination. Results suggest the increased surface-area-to-volume ratio at the microscale enabled reduction of incubation intervals, thereby decreasing the total assay time, with some evidence of increased DNA recovery and comparable conversion efficiency to a gold-standard method. Finally, I compared this method to an alternative, enzymatic method for cytosine conversion.

2.2. Materials and Methods

2.2.1. Sample Materials. Preliminary testing of the in-tube and µCD dSP-BSC methods was accomplished with the Human Methylated & Non-Methylated DNA Set (Zymo Research, Irvine, CA, USA) at an initial concentration of 250 ng/µL to assess relative DNA recovery and BSC efficiency without potential variability resulting from DNA extraction. Universal Methylation Human DNA Standard (Zymo Research, Irvine, CA, USA) at a starting concentration of 20 ng/µL was used as a positive control for amplification; here, the positive control is fully methylated at

all cytosine positions and bisulfite converted by the manufacturer. Negative controls were included during the BSC process, whereby human sample was substituted for nuclease free water and otherwise handled as if containing human genetic material. No template controls consisting of nuclease free water in place of the BSC eluate were included in all amplification and HRM detection modes.

2.2.2. In-Tube ds-BSC. For comparison with a gold-standard method, the dSP-BSC process was completed with the EZ-96 DNA Methylation-Lightning MagPrep (Zymo Research, Irvine, CA, USA) kit, according to the manufacturer recommended protocol, adapted for lower sample throughput (e.g., replacing the 96-well plate format with individual tubes and a magnet stand). For in-tube microfluidic reactions, volumes corresponding to the microdevice chamber capacities were used. Here, 2.5 µL DNA standard was added to 12.5 µL of Lightning Conversion Reagent (Zymo Research, Irvine, CA, USA) in a 0.2 mL tube; the 15 µL reaction mixture was heated on the Veriti thermal cycler (Thermo Fisher Scientific, Waltham, MA, USA) at 95°C for 1 min and 54°C 45 min for sulphonation and hydrolytic deamination. In separate 1.5 mL tubes, 40 µL of M-Binding Buffer and 10 µL MagBinding Beads were combined with the partially-converted DNA. Samples were mixed by vortexing, incubated at room temperature for 1 min, and placed on a magnetic stand before the supernatant was removed and discarded. The beads were then resuspended in 40 µL M-Wash Buffer, mixed by vortexing, and placed on the magnet stand for supernatant removal. Beads were then mixed with 40 µL L-Desulphonation Buffer, mixed by vortexing, and incubated at room temperature for 20 min Following Desulphonation, a second wash step was completed, as before, and the tubes were subsequently placed on a dry bath set to 55°C for 1 min to remove

residual M-Wash Buffer. Finally, the beads were resuspended in 25 µL of M-Elution Buffer, heated to 55°C for 4 min and placed back on the magnetic stand. The BSC eluate was separated from the bead fraction by pipette and added to a 0.2 mL tube, which was then retained and stored at -20°C until further analysis. For downstream detection via RT-PCR and HRM, a 5 µL volume of the BSC eluate was used, corresponding to a final PCR concentration of 5 ng/µL, except for the bead volume optimization study, wherein the final PCR concentration was 2 ng/µL. All in-tube BSC conversions were completed in technical replicates of 3 and PCR/HRM was also run in replicates of 3.

2.2.3. Real-Time Polymerase Chain Reaction and High Resolution Melting. Amplification and detection of BSC eluates and corresponding controls was accomplished using the ZymoTaq™ DNA Polymerase (Zymo Research, Irvine, CA, USA) chemistry. Detection was made possible with the inclusion of an intercalating LAMP Fluorescent Dye (New England Biolabs, Ipswich, MA, USA). Forward and Reverse primers for the FHL2 region were designed according to specifications published previously.[25] For conservation of reagents, half-reactions totaling 25 µL were used, including 12.5 µL 2x Reaction Buffer (1x), 0.25 µL dNTP mix (0.25 mM), 0.625 µL of 10 µM forward and reverse primers (0.4 µM) (Integrated DNA Technologies, Coralville, Iowa, USA), 0.2 µL ZymoTaq™ DNA Polymerase (2 U/50 µL), 1.25 µL LAMP Fluorescent Dye (2.5 µM), 4.55 µL PCR-grade water, and 5 µL of BSC eluate, positive control, or nuclease-free water. All samples were run in triplicate on the QuantStudio 5 Real-Time PCR System with detection in the FAM channel (Thermo Fisher Scientific, Waltham, MA, USA). Thermal conditions included initial denaturation (95°C, 600 s), 45 cycles of denaturation (95°C, 30 s), annealing (50°C, 45 s), and extension (72°C,

60 s), and a final extension step (72°C, 420 s). For data analysis, eluates and controls were considered positive if they crossed the instrument-defined threshold, producing a C_t value. HRM was accomplished immediately following amplification on the QuantStudio 5 System and included thermal conditions whereby the reaction was denatured at 95°C for 1 s, subsequently cooled to 50°C and held for 20 s, before being incrementally heated to 95°C at a rate of 0.1°C/s, with data acquisition occurring at each interval. The T_m of each sample was determined via the instrument's own algorithm. For visual clarity, some RT-PCR and HRM plots were recreated in excel using raw fluorescence values extracted from the QuantStudio 5 system. To show the threshold line, baseline subtraction was calculated from cycles 3 through 15 and the threshold was plotted at three times the standard deviation of the mean baseline, as before.[26]

2.2.4. Operation of Mechatronic Systems. Spin systems to impart centrifugal force, enable laser-based valving to open and close fluidic channels, perform magnetic mixing, and on-disc heating were all designed in-house, as described previously.[27, 28, 29] These systems are controlled by 8-core microcontrollers (Propeller P8X32A-M44; Propeller, Inc., Rockland, CA, USA) and corresponding, custom programs written in *Spin* and run from an external laptop. Rotational fluid propulsion and laser-based valving was accomplished with the Power, Time, and Z-Height Adjustable (PrTZAL) system.[29] Here, valves were opened to permit flow into a new fluidic layer and into the corresponding chamber using laser power settings of 500 mW for an actuation time of 500 ms, and positioned 15 mm above the surface of the disc,[30] Similarly, fluidic channels were closed by the same 638 nm laser diode to prevent backflow into the system using power, time, and z-height settings of 700 mW, 2500 ms, and 26 mm, respectively.[29] Here, automation is

enabled through use of the GUI code, instructing the PrTZAL system when to stop rotation and position the disc under the valve for each valving event. A separate dynamic Solid-Phase Extraction (dSPE) platform was used to impart external magnetic control over the silica solid phase for efficient mixing of both DNA for capture and reagents for effective conversion, using settings optimized by Dignan et al.[27] On-disc heating was accomplished with a dual-clamped Peltier system.[31]

2.2.5. Microdevice Design and Fabrication. Iterative and final μCD prototyping was accomplished with AutoCAD software (Autodesk, Inc., Mill Valley, CA, USA). Designs were laser ablated into thermoplastic substrates and corresponding adhesives via a CO_2 laser (VLS 3.50, Universal Laser Systems, Scottsdale, AZ, USA). The core device contains five primary poly(ethylene terephthalate) (PeT) layers (Film Source, Inc., Maryland Heights, MO, USA); whereby primary fluidic layers (layers 2 and 4) are encapsulated with heat-sensitive adhesive (HSA) (EL-7970-39, Adhesives Research, Inc., Glen Rock, PA, USA). At the center of the μCD, a black PeT (bPeT) (Lumirror X30, Toray Industries, Inc., Chuo-ku, Tokyo, Japan) layer enables laser-based valving and provides a barrier between the two primary fluidic layers.[30, 29] Following alignment of the 5-layer device, layers were heat-bonded using a commercial-off-the-shelf laminator (UltraLam 250B, Akiles Products, Inc., Mira Loma, CA, USA) according to the "print, cut, laminate" method, described elsewhere.[32] Multiple accessory pieces were added to the device via pressure-sensitive adhesive (PSA) transfer tape (MSX-7388, 3M, Saint Paul, MN, USA). Poly-(methyl methacrylate) (PMMA) (1.5 mm thickness, McMaster Carr, Elmhurst, IL, USA) capped with PeT was added to all chambers, not including the bisulfite conversion chamber, to increase chamber volume capacity.

Polytetrafluoroethylene (PTFE) hydrophobic membranes (0.2 µm, Sterlitech, Auburn, WA, USA) were added to the vents of the bisulfite conversion and magnetic manipulation chambers to permit gas exchange during heated incubations on-board. Fluidic channels enabling flow from one chamber to another upon device rotation were designed to be approximately 100 µm deep and have widths between 400 and 500 µm.

2.2.6. Fluidic Dye Studies and Corresponding Image Analysis. For early optimization of fluidic architecture, blue and yellow aqueous dye solutions were used to visually represent sample reagents. Following each workflow step (e.g., sulphonation and deamination), scanned images of the µCD were captured using an Epson Perfection V100 Photo desktop scanner (Seiko Epson Corporation, Suwa, Nagano Prefecture, Japan). Characterization of fluidic loss during the initial heating steps of the reaction was completed with 0.1 M Allura red dye solution (Sigma-Aldrich, St. Louis, MO, USA) diluted in 1x Tris-EDTA Buffer, pH 7.5 (Sigma-Aldrich, St. Louis, MO, USA). Fiji Image J Freeware was used to evaluate fluid loss via 'The Crop-Threshold-and-Go' method of analysis.[33] Briefly, cropped chamber images from digital scans were analyzed via the ImageJ color thresholding module to overlay a mask denoting the region of interest (ROI) from any background and providing a number of pixels associated with that mask. To build the calibration curve and measure fluid loss pre- and post-heating, a total of 5 technical replicates were measured for each parameter.

2.2.7. Microdevice Dynamic Solid Phase Bisulfite Conversion. The complete µCD dSP-BSC process can be followed in the dye study, described below. The reaction begins with reagent and

sample loading, wherein C1 is loaded with 13 µL Lightning Conversion Reagent and 2 µL of DNA sample. The neighboring C2 is loaded with a mixture of 40 µL Bead Binding Buffer and 10 µL Magnetic Beads. Chambers 4 and 8 are loaded with 40 µL of Wash Buffer and C6 is loaded with 40 µL of Desulphonation Buffer, while C10 is loaded with 25 µL of Elution Buffer. V1 is closed and C1 is positioned within the dual-clamped heating system for the following temperature intervals: 95°C for 1 min and 54°C for 45 min to complete the denaturation, sulphonation, and deamination steps. Following incubation, V2 is opened and the disc is spun (2000 rpm, 30 s) to introduce the partially converted DNA to C2 for bead binding. V3 is closed and the mixture is magnetically agitated on the dSPE system for 1 min Beads are subsequently pelleted (2000 rpm, 30 s), V4 is opened, and the disc is spun (1500 rpm, 30 s) to remove waste to C3, and V5 is closed. Wash #1 begins with the opening of V6 and disc rotation (1500 rpm, 15 s) to introduce Wash Buffer to C2. Following magnetic mixing (1 min), beads are pelleted once again (2000 rpm, 30 s), V7 is opened, and the disc is spun (1500 rpm, 30 s) to remove supernatant to C5 before V8 is closed. To begin the desulphonation step, V9 is opened and the disc is spun (1500 rpm, 15 s) to introduce Desulphonation Buffer from C6 to C2. The cocktail is magnetically mixed (1 min) and held at room temperature for 20 min to complete conversion. Desulphonation waste is removed following bead pelleting (2000 rpm, 30 s), the opening of V10, a spin step (1500 rpm, 30 s), and the closing of V11. The final wash occurs when V12 is opened and the disc is spun (1500 rpm, 15 s), introducing Wash Buffer into C2. The mixture is magnetically mixed (1 min), beads are pelleted (2000 rpm, 30 s), V13 is opened, the disc is spun again (1500 rpm, 30 s), and V14 is closed off to the upstream architecture. C2 is then placed between the dual-clamping Peltier system at a temperature of 55°C for 5 min for Wash Buffer evaporation, prior to DNA elution. Elution is

initiated when V15 is opened and the disc is rotated (1500 rpm, 30 s) to introduce Elution Buffer to C2 and the beads. V16 is closed and C2 is once again placed under the clamping system and heated to 55°C, except for only 4 min Once the DNA has been released from the beads, they are once again pelleted (2000 rpm, 30 s), V17 is opened, and the disc is spun to move the eluate from C2 to C11 for pipette removal.

2.2.8. Electrophoresis. Electrophoresis was completed with the 2100 Bioanalyzer Instrument (Agilent Technologies, Santa Clara, CA, USA). The Agilent DNA 1000 Kit (Agilent) was used according to manufacturer recommendations, whereby 9 μL of Gel Dye Matrix, 5 μL of DNA 1000 Marker, 1 μL of DNA 1000 Ladder, and 1 μL of converted DNA eluate was added to the requisite wells in the microfluidic chip. Analysis was completed with the 2100 Expert Software (Agilent).

2.2.9. Degradation Study. Degradation associated with the on-disc sample preparation method was assessed with the Quantifiler Trio Quantification Kit (Thermo Fisher Scientific, Waltham, MA, USA) according to the manufacturer recommendations and using the QuantStudio 5 Real-Time PCR System. Degradation indices were calculated by the HID Real-Time PCR Analysis Software (Thermo Fisher Scientific, Waltham, MA, USA) and were based upon the C_t values of diluted standards for large and small autosomal targets from 50 – 0.005 ng/μL according to manufacturer recommendations. Non-Methylated DNA standards were bisulfite converted using the on-disc μCD approach at a final concentration of 25 ng/μL in technical replicates of 3 and exactly 1 μL of converted eluate was used from each conversion replicate for evaluation of resultant degradation, equating to 1.25 ng/μL in each Quantifiler Trio reaction.

2.2.10. Enzymatic Methyl-Seq (EM) Conversion. A total of 13 µL Human Non-Methylated control DNA (Zymo Research, Irvine, CA, USA) was added to 117 µL 10 mM Tris-EDTA Buffer (Sigma-Aldrich, St. Louis, MO, USA), pH 8.0, for DNA fragmentation at a final concentration of 25 ng/µL. Shearing was completed using an S2 Ultrasonicator (Covaris, Woburn, MA, USA) with the 6 x 16 mm AFA Fiber microTubes (Covaris, Woburn, MA, USA) and settings associated with mean fragment sizes of 1.5 kilobases (kb) for a downstream application in RT-PCR and HRM, per manufacturer recommendations. The requisite volumes of sheared DNA were mixed with 10 mM Tris-EDTA Buffer to a total volume of 28 µL to begin conversion and amplify converted product to a final DNA input amount of 100, 10, and 1 ng of total input DNA in technical replicates of 2. The NEBNext® Enzymatic Methyl-Seq Conversion Module (New England Biolabs, Ipswitch, MA, USA) was used for enzymatic conversion according to the manufacturer's protocol and with Hi-Di Formamide (Applied Biosystems, Waltham, MA, USA) for denaturation and NEBNExt® Sample Purification Beads (New England Biolabs, Ipswitch, MA, USA) for purification. Subsequent amplification and HRM of converted eluates was completed as described here previously for the FHL2 target in replicates of 3.

2.2.11. Statistics and Reproducibility. All statistical calculations related to significance testing were completed with GraphPad Prism Software (San Jose, CA, USA). C_t and T_m values were described as the mean $\pm$ standard deviations for all technical BSC replicates and/or amplification replicates. All described t-tests are two-tailed, using unpaired comparison parameters, and with

a significance (α) of 0.05 (e.g., 95% confidence interval). Any analysis of variance (ANOVA) used a one-way framework and with a the same 95% confidence interval parameters.

2.3. Experimental

The development and characterization of a rotationally-driven microfluidic device for the dynamic solid phase bisulfite conversion (dSP-BSC) of differentially-methylated human DNA is described. Preliminary characterization of the chemical workflow was accomplished in-tube and all iterative changes to the method were tested by comparing resultant eluates to those produced from the manufacturer recommended protocol to a corresponding 'in-tube microfluidic' protocol using reduced reagent volumes and incubation parameters. Likewise, BSC eluates produced following sample preparation via the 'on-disc' μCD approach were compared with those using the previously described in-tube approach. The selected target for early characterization is in the promoter region of FHL2, and is one associated with forensic human age prediction across multiple tissues.[12, 19, 22, 34] The primer sequences were adapted from Hamano et al.,[25] wherein the assay was used for age prediction using PCR amplification and HRM and have thus been previously vetted for PCR bias, function, and relevance to human age approximations.

2.3.1. Dynamic Solid Phase Bisulfite Conversion Workflow. The conventional, 'gold-standard' BSC workflow was developed according to the manufacturer's protocol but modified for in-tube sample preparation (**Fig. 2-1A**). During the initial incubation, samples are heated to facilitate complete denaturation and subsequent progression of unmethylated cytosines through two

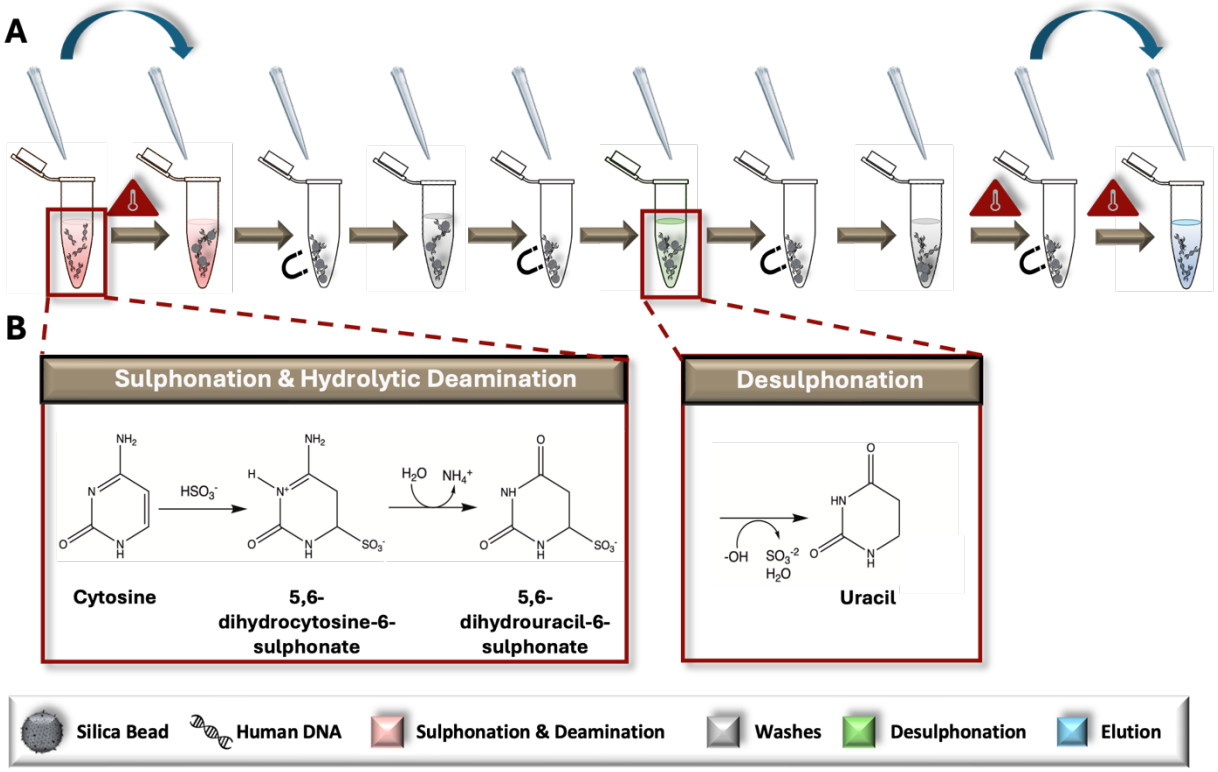

Figure. 2-1 Adapted dSP-BSC workflow. (A – B) The in-tube gold-standard method for bead-based conversion; sulphonation and deamination of unmethylated cytosine residues begins when the dsDNA is denatured and incubated with ammonium bisulfite at elevated temperatures. Genomic material with partially converted bases is affixed to a silica dSP and washed prior to final desulphonation. A second wash step is completed, and the beads are heated in an open tube to evaporate residual ethanol before the DNA is eluted and removed for downstream analysis. Blue arrows indicate tube transfers. Figure adapted from Turiello et al. 2023.[49]

intermediate structures, including 5,6-dihydrocytosine-6-sulphate and 5,6-dihydrouracil-6-sulphonate via ammonium bisulfite; this phase is referred to collectively as *sulphonation and hydrolytic deamination* (**Fig. 2-1B**). Following a bead wash and immobilization step, *desulphonation* occurs, forming uracil residues via incubation in a sodium hydroxide solution. Elution of the chemically converted DNA from the dynamic solid phase is completed following another bead wash (**Fig. 2-1B**). Following the reaction, only unmethylated cytosines are converted to uracil; methylated cytosines remain intact, as the addition of a methyl group to the

ring contributes to stabilization of the structure and a lack of conversion due to steric hindrance and electrostatic repulsion.

2.3.2. Downstream Analysis Strategy by RT-PCR and HRM. To assess the analytical performance of the upstream sample preparation method, multiple techniques were used to measure relative DNA recovery and conversion efficiency. Relative DNA recovery was evaluated via RT-PCR, whereby resultant cycle threshold (C_t) values were compared. Because these values are representative of starting concentration, it follows that samples prepared with optimal BSC conditions for DNA preservation would produce more rapid amplification (e.g., lower C_t values). Here, the ZymoTaq™ DNA Polymerase chemistry was used, as it was specifically designed for the amplification of bisulfite-treated DNA; however, the protocol was modified for reagent conservation and to enable real-time detection by utilizing only half-reactions and adding an intercalating Syto 9 dye, respectively. For verification of this detection method, methylated and non-methylated DNA standards were bisulfite converted in triplicate along with BSC negative controls and using the manufacturer's adapted protocol described above (**Fig. 2-1**). Resultant eluates were successfully amplified along with methylated positive controls (previously converted by the manufacturer) and no template controls (**Fig. 2-2**); non-methylated standards produced C_t values of ~33.9 (± 0.60) and methylated standards and converted

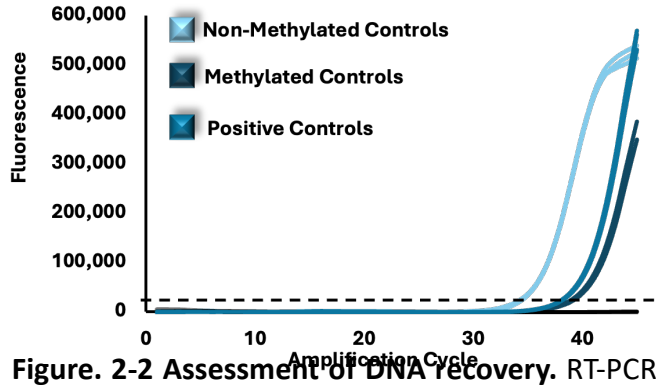

Figure. 2-2 Assessment of DNA recovery. RT-PCR results, originating from methylation standards, bisulfite converted with the gold-standard approach. Figure adapted from Turiello et al. 2023.[49]

positive controls produced values of ~38.99 (± 0.54) and ~38.33 (± 0.13), respectively. Noticeably, there was no statistical difference detected between the methylated standard converted in-house and with the modified in-tube approach and the positive control previously modified by the manufacturer (unpaired t-test, α = 0.05, p-value = 0.7446). While this may not signify that the modified 'gold-standard' method performs comparably in terms of conversion, since this is a fully methylated standard and conversion is not taking place, this does indicate that the methods are comparable in recovery (e.g., degradation). In addition, all samples were amplified with an initial concentration of 5 ng/µL per reaction; however, there is a reproducible shift in C_t units between the non-methylated and methylated samples. This shift may be explained by PCR bias, whereby the GC content of the methylated template is higher than that of the non-methylated sample post-conversion, leading to a comparatively diminished amplification product.[35]

Likewise, relative conversion efficiency was demonstrated with HRM analysis, whereby the T_m of non-methylated and methylated control samples post-conversion was determined, and the corresponding differences were associated with a shift in GC content. Assuming 99 - 100% conversion efficiency with the gold-standard method, as is alleged, would dictate that all unmethylated cytosines are converted to uracil and then to thymine following PCR, thus, these transcripts should consistently exhibit a much lower T_m than their

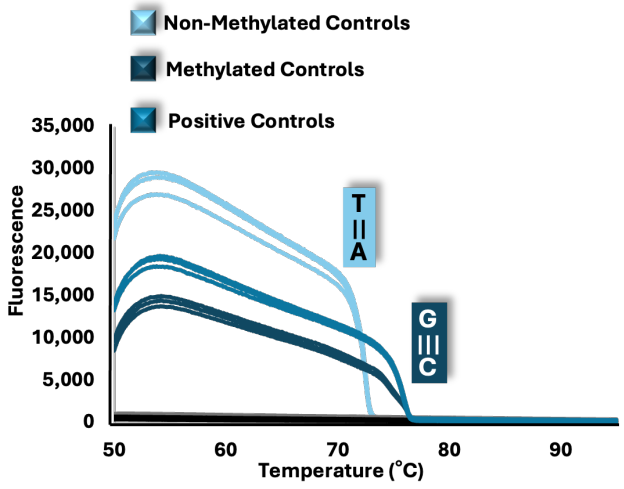

Figure 2-3. Assessment of conversion efficiency. HRM results, originating from methylation standards, bisulfite converted with the gold-standard approach. Figure adapted from Turiello et al. 2023.[49]

methylated counterparts. However, if BSC conditions are such that conversion efficiency becomes diminished, the T_m of unmethylated amplicons will undoubtedly shift upward, approaching that of the methylated sequences with higher GC content. As a baseline, non-methylated and methylated amplicons melted at temperatures of ~72.39°C (± 0.16°C) and ~76.51°C (± 0.11°C), respectively (**Fig. 2-3**), indicating that, post conversion, non-methylated standards will have a lowered GC content compared with that of methylated standards, due to the overall reduction in hydrogen bonds in the template. For additional confirmation of the HRM method, methylated positive controls, previously converted by the manufacturer, also showed reproducible melt temperatures at ~76.08 (± 0.23°C). Moving forward, if a statistically significant difference is detected for those non-methylated transcripts that have been bisulfite converted, it may be assumed that conversion efficiency has be altered. However, it is important to note here that HRM is only a measure of relative conversion efficiency and cannot be used to calculate the precise percentage (0 – 100%) typically associated with this metric.

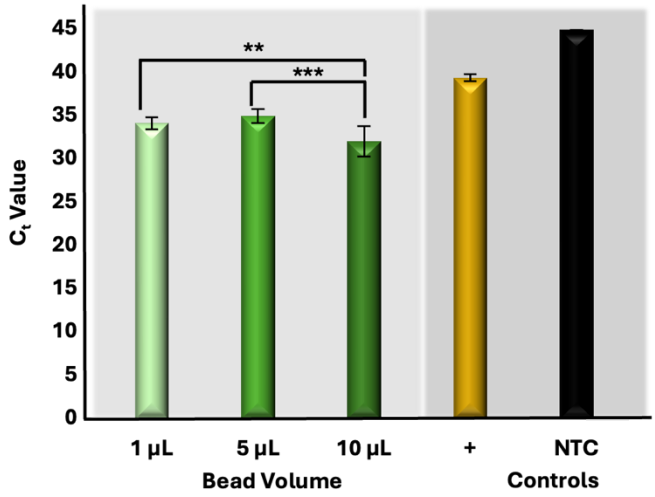

Figure 2-4. Reduced bead volumes in the BSC reaction. RT-PCR results comparing non-methylated control DNA standards, converted with reduced bead volumes. Figure adapted from Turiello et al. 2023.[49]

2.3.3. In-Tube Optimization of the Microfluidic Method. The conventional, gold-standard dSP-BSC process is a multi-step workflow requiring several sequential tube transfers, vortexing steps, incubations (both heated and at room temperature), and magnetic manipulations. Given the complexity, in-

tube studies were completed prior to microdevice adaptation to isolate each variable for optimal performance at the microfluidic scale. First, samples were prepared with decreased BSC reagent volumes, approximately 1/10th of the manufacturer recommended amount; however, the concentration of silica beads remained consistent, as a reduction in the volume of beads resulted in diminished DNA recovery (**Fig. 2-4**). C_t values originating from samples with decreasing volumes of silica bead solutions from 10 µL to 5 µL and 1 µL show statistical differences overall (one-way ANOVA, α = 0.05, p-value = 0.0002), with the lowest C_t values demonstrated with preparation using 10 µL volumes (32.09 $\pm$ 1.76) (**Fig. 2-4**). Likewise, the elution volume was kept consistent to ensure a large enough volume for downstream testing. Regarding remaining BSC reagents, unpaired t-tests comparing C_t values originating from samples bisulfite converted with full and microfluidic volumes show no statistical differences for non-methylated and methylated control samples (α = 0.05, p-values = 0.3803 and 0.1016, respectively), indicating similar recovery (**Fig. 2-5**). Likewise, non-methylated control samples, for which all cytosines would ostensibly be converted to uracil, produced statistically similar HRM values (unpaired t-test, α = 0.05, p-value = 0.248) and were consistent with the known T_m for that locus (**Fig. 2-6**), indicating comparable

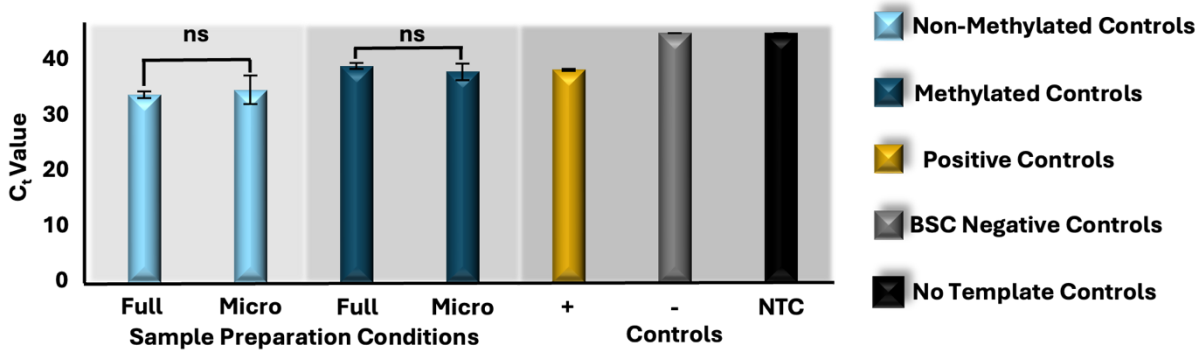

Figure 2-5. Estimated comparative recovery with microfluidic dSP-BSC reaction optimization. RT-PCR results, comparing methylation standards converted with either the manufacturer recommended 'full' volume or the decreased 'micro' volumes. Figure adapted from Turiello et al. 2023.[49]

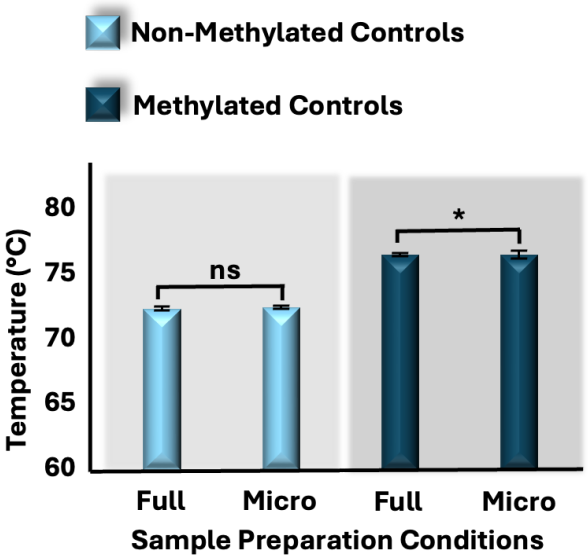

Figure 2-6. Estimated comparative conversion efficiency with microfluidic dSP-BSC reaction optimization. HRM results, comparing methylation standards converted with either the manufacturer recommended 'full' volume or the decreased 'micro' volumes. Figure adapted from Turiello et al. 2023.[49]

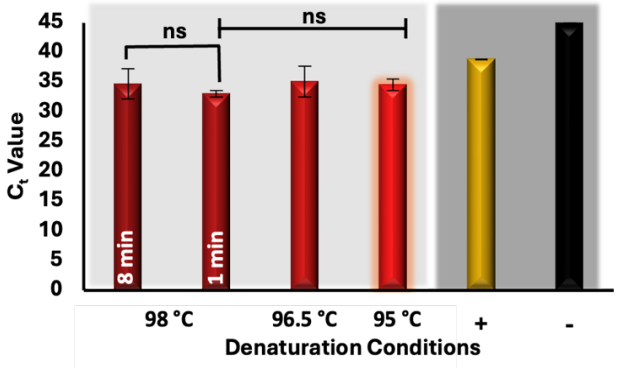

Figure 2-7. RT-PCR results following reduced incubation intervals and temperature for the initial denaturation step. C_t values demonstrating relative recovery from altered denaturation parameters. Figure adapted from Turiello et al. 2023.[49]

conversion efficiency. Dissimilarly, a comparison of the T_m values for the methylated controls converted with different conditions showed statistical differences (unpaired t-test, α = 0.05, p-value = 0.0265); however, the difference between means was only calculated to be ~0.266°C (± 0.11°C) (**Fig. 2-6**). These results were considered acceptable and further in-tube optimization to decrease dwell temperatures and intervals was completed with microfluidic volumes.

Three incubation parameters were optimized at the microfluidic scale to increase adaptability of the protocol to the microfluidic system and reduce total analytical time, including 1) *denaturation*, 2) *sulphonation and deamination*, and 3) *desulphonation*. Conventional denaturation parameters necessitated an 8 min incubation at 98°C; this parameter was reduced first from 8 min to 1 min with no difference in estimated recovery (unpaired t-test, α = 0.05, p-value = 0.0972) (**Fig. 2-7**). Dwell temperature

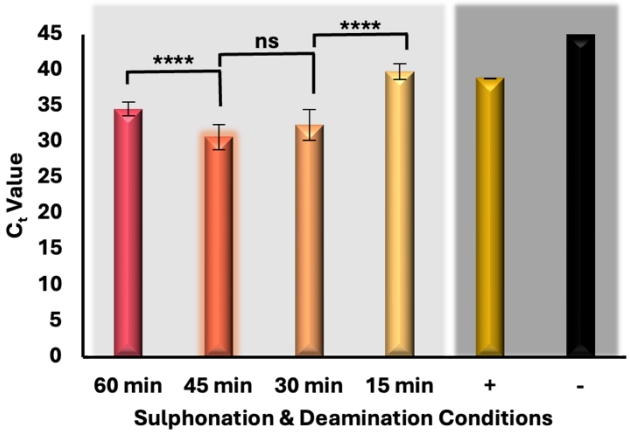

Figure 2-8. RT-PCR results following reduced incubation time for the sulphonation and deamination reaction. C_t values demonstrating relative recovery indicated with reduced dwell times from 60 min to 15 min. Figure adapted from Turiello et al. 2023.[49]

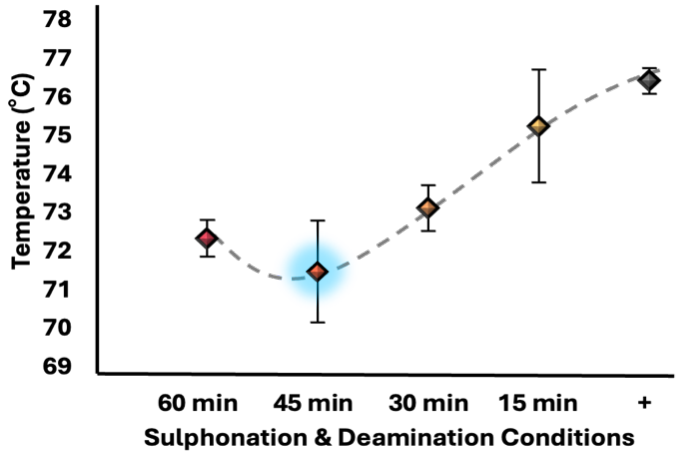

Figure 2-9. HRM results following reduced incubation intervals for the sulphonation and deamination reaction. T_m values results demonstrating relative conversion efficiency indicated with reduced dwell times from 60 min to 15 min. Figure adapted from Turiello et al. 2023.[49]

was subsequently decreased from 98°C to 96.5°C and 95°C for 1 min; likewise, one-way ANOVA results indicated no statistical differences between eluates produced with decreasing dwell temperature overall (α = 0.05, p-value = 0.0511) (**Fig. 2-7**). For successive studies, samples were converted at 95°C for 1 min, parameters much more amenable to microfluidic integration. For optimization of the next incubation step, sulphonation and deamination intervals were reduced from 60 min to 45, 30, and 15 minutes; interestingly, samples prepared via the conventional protocol (e.g., 60 min incubation) showed higher C_t values (34.60 ± 0.98) than those incubated for only 45 min (30.67 ± 1.75), indicating recovery was enhanced by reducing the incubation time (**Fig. 2-8**). This trend was reversed when samples were only incubated for 30 or 15 min, likely as a result of incomplete conversion and corresponding primer mismatch during amplification. In fact, **Figure 2-9** shows the corresponding T_m values,

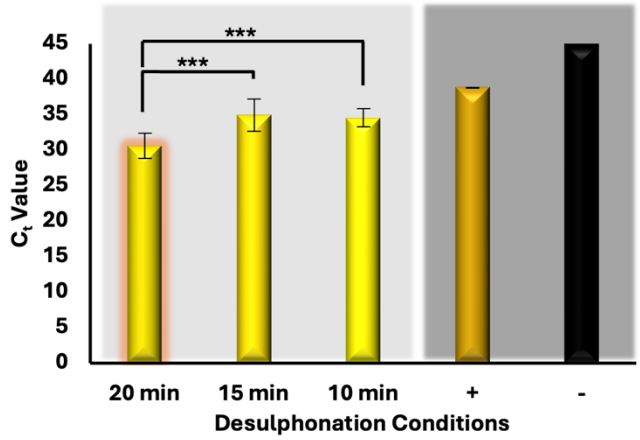

Figure 2-10. RT-PCR results following reduced incubation time for the desulphonation reaction. C_t values demonstrating relative recovery indicated with reduced dwell times from 20 min to 10 min. Figure adapted from Turiello et al. 2023.[49]

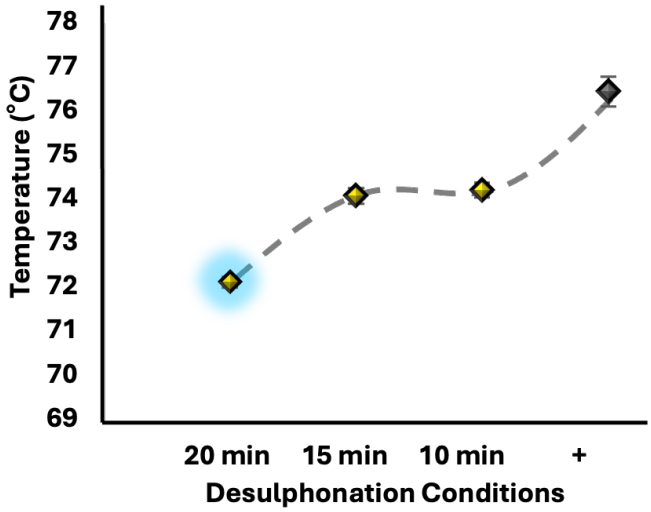

Figure 2-11. HRM results following reduced incubation intervals for the deamination reaction. T_m values results demonstrating relative conversion efficiency indicated with reduced dwell times from 20 min to 10 min. Figure adapted from Turiello et al. 2023.[49]

providing evidence of incomplete conversion as incubation time decreased lower than a 45 min interval. Also evident from this figure is a statistical difference between T_m values undergoing sulphonation and deamination for 60 or 45 min (α = 0.05, p-value = 0.027), with 45 min incubated samples providing lower T_m values, indicating potentially increased conversion efficiency. Notably, samples undergoing sulphonation and deamination for less than 45 minutes showed either reduced recovery (**Fig. 2-8**) or conversion efficiency (**Fig. 2-9**). Thus, to test the optimal conversion time of the final reaction interval, desulphonation, a 45 min sulphonation and deamination was used. For desulphonation, the ideal interval in terms of both recovery and conversion efficiency was determined to be the conventional one of 20 min, producing eluates with the lowest C_t (**Fig. 2-10**) and T_m values (**Fig. 2-11**). The final elution time was decreased as well, from 4 min to 1 min,

Procedural Step	Gold-Standard (min)	On-Disc (min)
Initial Denaturation	8	1
Sulphonation & Deamination	60	45
Desulphonation	20	20
Ethanol Evaporation	20	1
DNA Elution	4	0.5
Total time (min)	112	**67.5**

Table 2-1. Comparison of gold-standard versus on-disc microfluidic conversion incubation intervals. Reaction incubation times are collectively reduced by 41 minutes using the on-disc method when compared to the gold-standard. Intervals that have been altered are highlight in red. Table adapted from Turiello et al. 2023.[49]

following similar testing indicating negligible differences between C_t and T_m values following a stepwise reduction of incubation times including 240 s, 120 s, 60 s, and 30 s (data not shown). In summary, the BSC parameters have been adapted for microfluidic integration, with decreased reagent volumes (e.g., 1/10th of the standard workflow, not including silica beads), and reduced incubation intervals, with denaturation occurring at 95°C for 1 min and sulphonation and deamination shortened to 45 min total. Moving forward, the on-disc workflow incorporated all optimized parameters discussed above; additionally, wash evaporation time was reduced from 20 min to 1 min, as no wash buffer was visibly detected with on-disc evaporation at 55°C for the shortened interval, reducing the entire workflow by ~39.73% compared to the gold-standard method **(Table 2-1)**.

2.3.4. Microdevice Design. The rotationally-driven µCD was designed for multiplexed analysis of up to four samples in parallel (**Fig. 2-12A, 2-12B**). Each domain includes all the necessary architectural features to support the sequential unit operations associated with the dSP-BSC workflow, wherein all of the architecture situated towards the center of rotation from the magnetic manipulation chamber houses the aqueous reagents, and the chambers closer to the edge of the disc accommodate reaction waste and the final BSC eluate (**Fig. 2-12C**). Initial

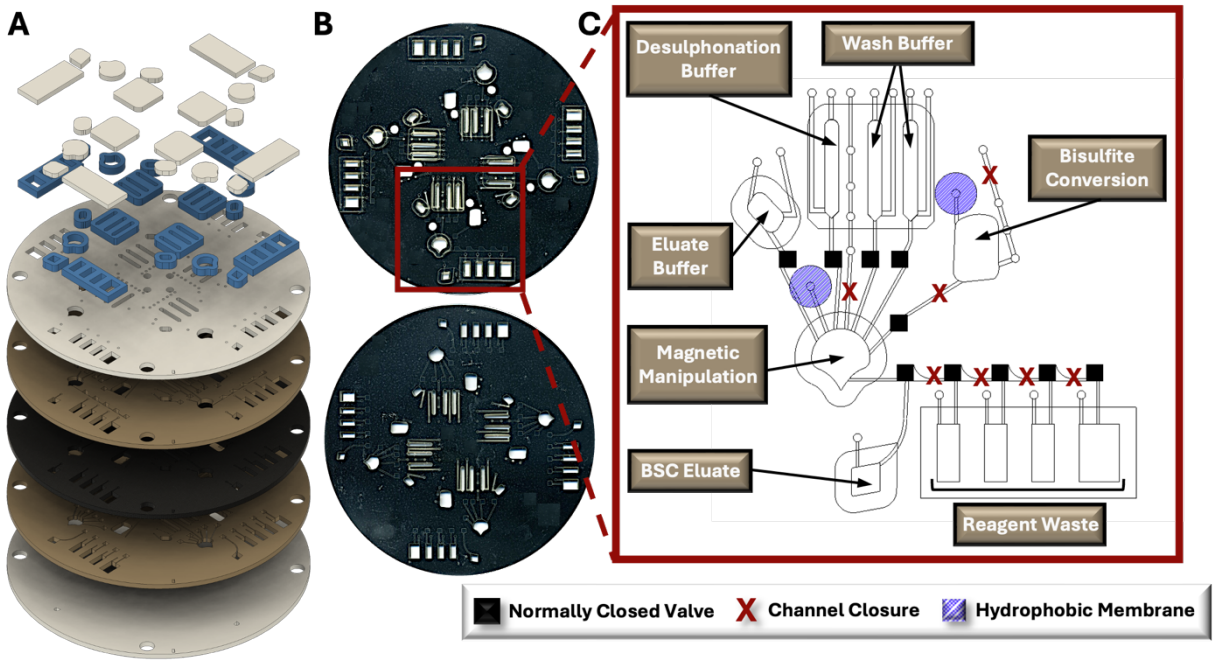

Figure 2-12. Rotationally-driven microfluidic device for automated bisulfite conversion. (A) Exploded rendering of the core, 5-layer polymeric disc and corresponding accessory pieces that increase reagent volume capacities. (B) Digital scans of the front and back of a fabricated µCD. (C) One labeled domain from the 4-plex µCD depicting the positions of reagent chambers, fluidic channels, pressure vents, sacrificial valve locations, reagent loading ports, and hydrophobic membrane patches. Figure adapted from Turiello et al. 2023.[49]

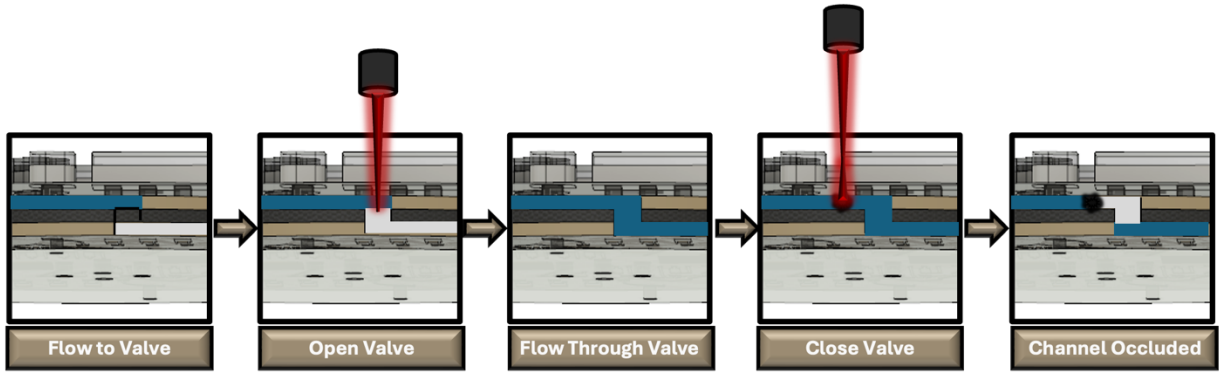

Figure 2-13. Valving mechanism. Schematic representation of the sacrificial valving process to enable sequential unit operations and prevent backflow of potentially inhibiting reagents. Figure adapted from Turiello et al. 2023.[49]

conversion steps, including denaturation and sulphonation and deamination, are completed in the bisulfite conversion chamber. Following these steps, the partially converted material and aqueous buffer is spun into the magnetic manipulation chamber featuring the dynamic solid

phase and a chaotropic solution to promote DNA-silica bead interactions. Note that the concave-shaped magnetic manipulation chamber was designed to retain magnetic beads during waste removal and was previously optimized elsewhere (**Fig. 2-12C**).[27, 28] Both the bisulfite conversion and magnetic manipulation chambers undergo heated incubations that may cause thermal pumping and subsequent fluid loss; thus, each of these chambers feature a hydrophobic membrane composed of polytetrafluoroethylene (PTFE) on the vent and a 'closed' loading arm channel. The device makes use of sacrificial valves to enable sequential unit operations, making each device single-use and preventing the potential for contamination and device failure from repeated use. The valving strategy is depicted in the schematic shown in **Figure 2-13**. Briefly, this approach was adapted from one described by Garcia-Cordero et al.[30] and makes use of an optically-dense intermediate layer at the center of the disc that is thermally ablated by an external laser to form a pinhole, permitting fluid to flow from layer 2 to layer 4. To subsequently close channels and prevent backflow, the laser is positioned upstream from the opened valve, and laser

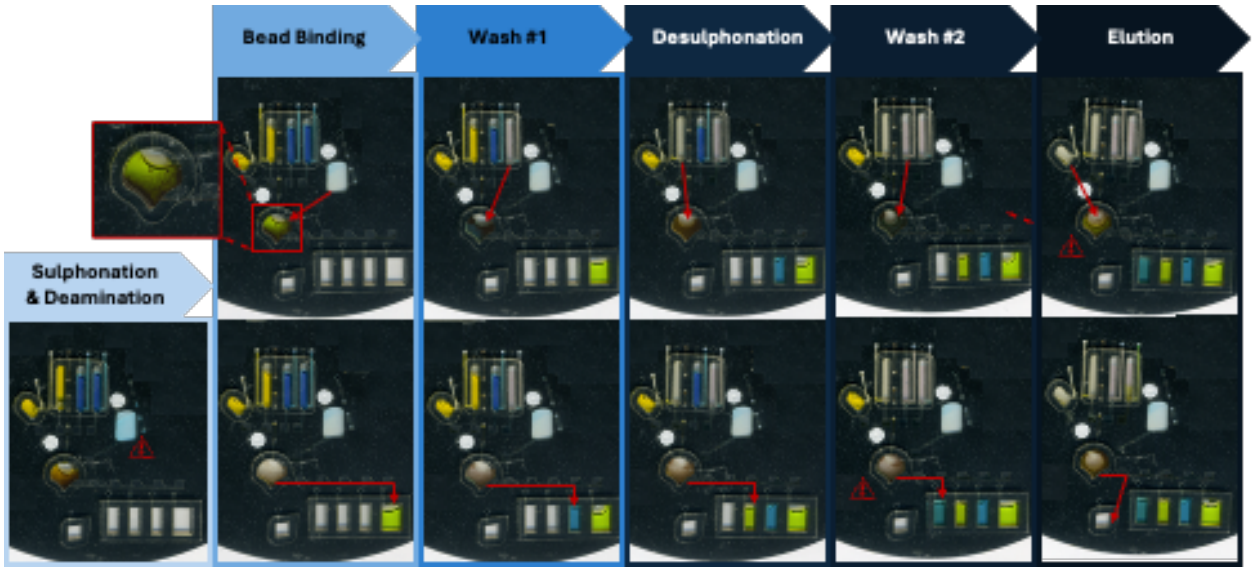

Figure 2-14. Fluidic dye studies. Digital scans showing one representative dye study. Figure adapted from Turiello et al. 2023.[49]

parameters, including output power, contact time, and height from the surface of the disc, are altered to thermally deform and occlude flow. This method was developed in-house[29] and the precise parameters for both valve opening and channel or 'valve' closing are detailed in the methods section.

2.3.5. Fluidic Control Testing and Characterization. Reliability of the microfluidic BSC method is based upon the reproducibility of the fully-integrated µCD. To assess the architectural features

A

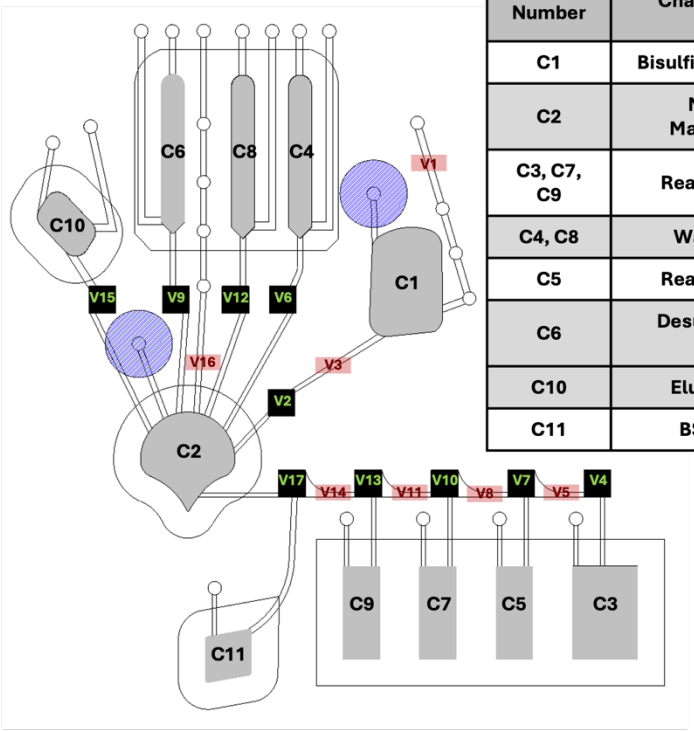

B

Chamber Number	Chamber Name
C1	Bisulfite Conversion
C2	Magnetic Manipulation
C3, C7, C9	Reagent Waste
C4, C8	Wash Buffer
C5	Reagent Waste
C6	Desulphonation Buffer
C10	Eluate Buffer
C11	BSC Eluate

C

Valve Number	Radial Position (mm)
Valve #1	19.0
Valve #2	33.7
Valve #3	33.3
Valve #4	46.9
Valve #5	46.8
Valve #6	28.9
Valve #7	44.8
Valve #8	44.9
Valve #9	30.9
Valve #10	43.4
Valve #11	43.7
Valve #12	29.4
Valve #13	42.5
Valve #14	43.3
Valve #15	33.2
Valve #16	33.7
Valve #17	42.4

Figure 2-15. Details from one µCD domain. (A) One domain with numbered chambers and positions of valves. (B) Associated key. (C) The radial positions of each valve; green corresponds to 'normally closed valves' that are opened and red corresponds to 'channel closures.' Figure adapted from Turiello et al. 2023.[49]

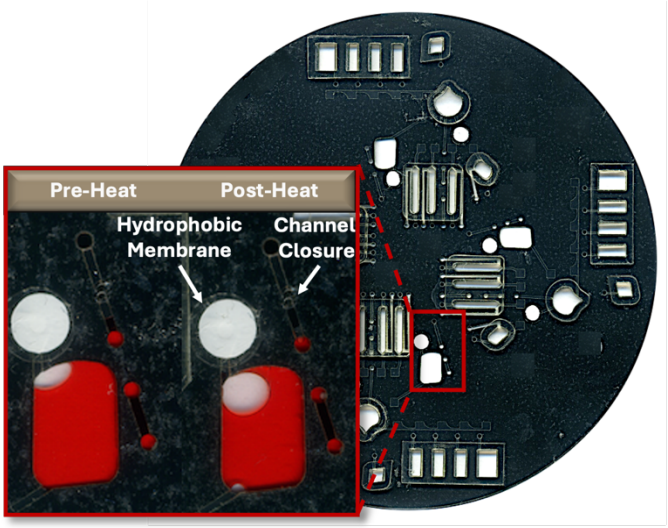

Figure 2-16. Observed fluid volume reduction. Digital scans of the bisulfite conversion chamber pre- and post-heating associated with the initial incubation steps (e.g., denaturation, followed by sulphonation and deamination). Figure adapted from Turiello et al. 2023.[49]

and their ability to complete unit operations during discrete reactions, fluidic dye studies were completed. **Figure 2-14** shows the progress of one representative dye study as it progresses through each of the BSC steps, including sulphonation and deamination, bead binding, wash steps, desulphonation, and the final DNA elution. Alternating blue and yellow dye solutions were moved throughout each domain of a 4-plex disc through the requisite channels and chambers successfully, indicating fluidic control and reproducibility. A schematic detailing the placement and radial position of valves on each domain of the microdevice is depicted in **Figure 2-15**. Complete adaptation to the microdevice requires that all incubations be completed on disc. Following the shortening of reaction intervals described above, it stands that the longest on-disc heating interval occurs during the sulphonation and deamination step (54°C for 45 min), preceded by a brief denaturation in the same chamber (95°C for 1 min). Upon visual inspection, it appeared some fluid loss was reproducibly occurring during this step (**Fig. 2-16**). A dye study was completed to quantify this loss per a previously described protocol, known as 'The Crop-Threshold-and-Go' method of image segmentation and analysis.[33] Here, a calibration curve correlating average pixel area and fluid volume was constructed from digital scans of bisulfite conversion chambers loaded with Allura Red dye at regular intervals,

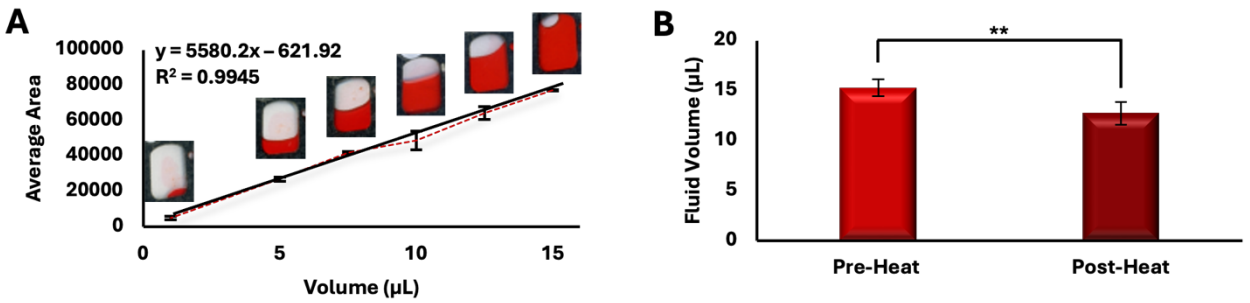

Figure 2-17. Quantification of fluid loss from initial reactions. (A) Calibration curve corresponding to the average pixel areas of digital scans of bisulfite conversion chambers loaded with Allura red dye. (B) Quantification of fluid loss pre- and post-heating protocol. Figure adapted from Turiello et al. 2023.[49]

including 1, 5, 7.5, 10, 12.5, and 15 µL (R^2 = 0.9945, y = 55.80.2x – 621.92) (**Fig. 2-17a**). Subsequent scans were taken of the conversion chambers pre- and post-heating, and the corresponding volumes were extrapolated from image analysis and according to their placement along the standard curve. Results indicated that ~83% of the fluid was retained following this heated incubation step, with pre- and post-heat volumes approximated to be 15.28 $\pm$ 0.95 and 12.73 $\pm$ 1.28, respectively (**Fig. 2-17b**). It can be speculated that fluid is being lost to the intermediate layers surrounding the chamber, given all outlets are closed to the external environment. In particular, the chamber vent incorporates a hydrophobic PTFE membrane to prevent fluid loss and the loading port channel is thermally occluded (e.g., 'closed') prior to heating (**Fig. 2-16, 'Post-Heat' inset**). Thus, it cannot be confirmed whether the loss of fluid leads to DNA loss from the chamber or simply concentration of the DNA into a reduced aliquot of fluid.

2.3.6. Microdevice Testing with Methylation Standards. To compare the performance of the conventional 'gold-standard' method and the optimized on-disc method, non-methylated controls were converted at equivalent concentrations and subsequently assessed for relative DNA recovery and conversion efficiency. Post-BSC, the total amount of DNA in each corresponding

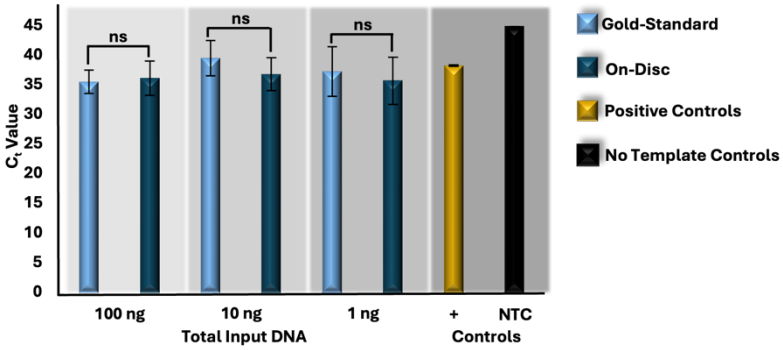

Figure 2-18. On disc recovery relative to the gold-standard method. RT-PCR results originating from non-methylated DNA standards, bisulfite converted gold-standard approach and microfluidic 'on-disc' approaches. Figure adapted from Turiello et al. 2023.[49]

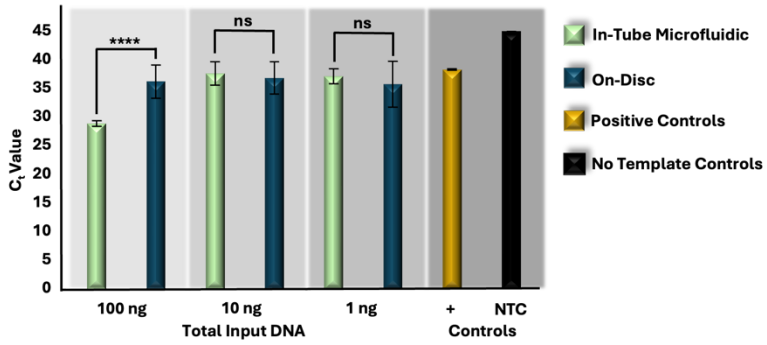

Figure 2-19. On disc recovery relative to the 'in-tube microfluidic' approach. RT-PCR results originating from non-methylated DNA standards, bisulfite converted microfluidic 'in-tube' and 'on-disc' and 'approaches. Figure adapted from Turiello et al. 2023.[49]

amplification reaction totaled 100, 10, and 1 ng (e.g., 4 ng/µL, 400 pg/µL, and 40 pg/µL, respectively); unpaired t-tests of resultant C_t values were not statistically different at each concentration (α = 0.05, p-values = 0.6083, 0.0804, 0.4596, respectively), indicating similar recovery between the gold-standard and on-disc methods (**Fig. 2-18**). Equivalent concentrations of non-methylated standards were also prepared in-tube using the microfluidic volumes and incubation parameters. Relative recovery results indicate similar recovery across conditions for samples prepared with DNA input amounts of 10 and 1 ng total (unpaired t-tests, α = 0.05, p-values = 0.5368 and 0.3693, respectively); however, the in-tube microfluidic method demonstrated markedly increased recovery compared to the on-disc method at 100 ng total (unpaired t-test, α = 0.05, p-value = <0.0001), with average C_t values of 28.89 $\pm$ 0.51 and 36.23 $\pm$ 2.89, respectively (**Fig. 2-19**). This may indicate the potential of the microfluidic method at

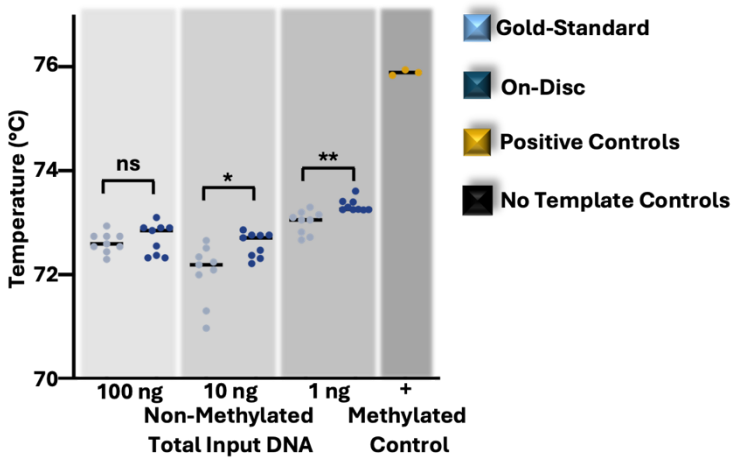

Figure 2-20. On disc conversion efficiency relative to the gold-standard method. HRM results originating from non-methylated DNA standards, bisulfite converted gold-standard approach and microfluidic 'on-disc' approaches. Figure adapted from Turiello et al. 2023.[49]

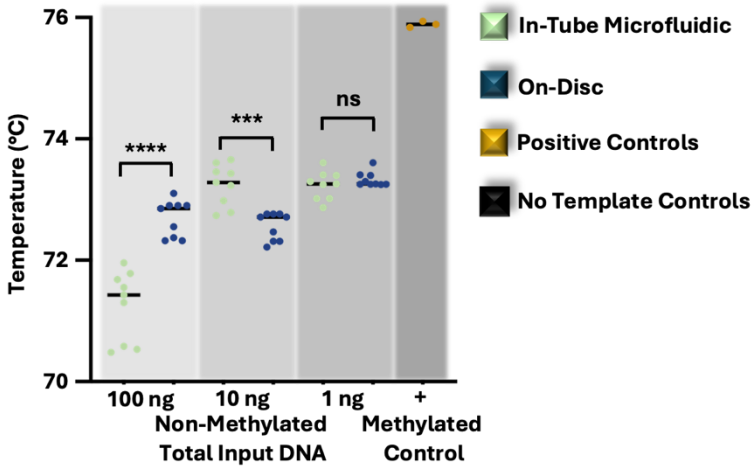

Figure 2-21. On disc conversion efficiency relative to the 'in-tube microfluidic' approach. HRM results originating from non-methylated DNA standards, bisulfite converted microfluidic 'in-tube' and 'on-disc' and 'approaches. Figure adapted from Turiello et al. 2023.[49]

concentrations higher than 4 ng/µL with optimal microdevice performance. At this point, the microdevice provides a faster, automated BSC alternative that performs comparably in terms of DNA recovery, and with only ~1/10th of the reagent volumes, theoretically decreasing cost at scale.

As before, relative conversion efficiency was assessed with HRM following the RT-PCR reaction. While no statistical difference was determined at the higher concentration (unpaired t-test, α = 0.05, p-value = 0.5477), differences were observed with the lower DNA input amounts, including 10 ng (unpaired t-test, α = 0.05, p-value = 0.0152), and 1 ng (unpaired t-test, α = 0.05, p-value = 0.0014). However, the differences between T_m values were negligible overall; on average, differences between 10 ng eluates ranged 0.55°C $\pm$ 0.20°C and 1 ng eluates were only

different by 0.32°C ± 0.08°C (**Fig. 2-20**). Comparing these results to the same concentrations of standards prepared using the in-tube microfluidic method, trends reverse with no statistical difference at the lowest concentration (unpaired t-test, α = 0.05, p-value = 0.0001) and noticeable differences at the higher DNA input amounts of 100 and 10 ng total (unpaired t-tests, α = 0.05, p-values = <0.0001 and 0.0001, respectively) (**Fig. 2-21**). At 100 ng total, the in-tube microfluidic method exhibits lower T_m values of 0.68°C ± 0.14°C compared to its on-disc counterpart, once again indicating the potential of the microfluidic scheme, if fully optimized to reduce fluid loss. Overall, the standard deviations, or *spread*, of T_m values was the lowest with the automated, on-disc method when comparing all conditions and concentrations, speaking to the reproducibility of this mode. Interestingly, a comparison of each method across concentrations, reveals a statistical difference between them (two-way ANOVA, α = 0.05, p-value = < 0.0001). While this may seem peculiar, studies here are completed in a stochastic regime so as to be forensically-relevant (e.g., 4, 0.4, and 0.04 ng/μL), where starting DNA template is known to impact the

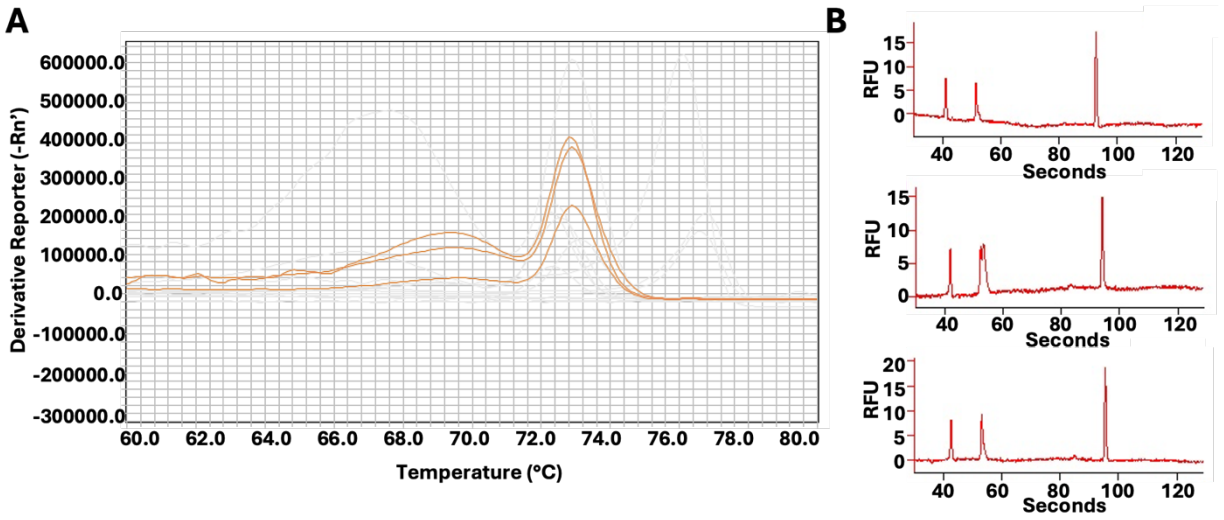

Figure 2-22. Artifact characterization. (A) Melt curve results depicting the profiles from samples prepared on-disc with a total DNA input of 100 ng. (B) Electropherograms from the samples prepared on-disc at 100 ng total, post RT-PCR and HRM. An electrophoretic artifact, or 'split-peak' is observed in the second (middle) replicate. Figure adapted from Turiello et al. 2023.[49]

resulting T_m.[36] This same trend is demonstrated later in this work, with conversion by an alternative commercial method in this same concentration range. Diving deeper into the variation across BSC preparation conditions and the estimation of conversion efficiency, at the highest DNA input amount (e.g., 100 ng total in the PCR reaction), an additional peak was reproducibly observed with HRM (**Fig. 2-22A**). Generally, multiple melt curves suggest nonspecific amplification; however, the NTCs did not indicate contamination and the additional 'peak' exhibited low amplitude and appeared broad and unresolved (**Fig. 2-22A**). This brings up a shortcoming of HRM, whereby an assumption is made that DNA melting is a 2-stage process resulting in only the detection of amplicons in their double- and single-stranded states. In reality, there may often be an intermediate state wherein the G/C rich portions of the amplicon maintain a double-stranded configuration and A/T rich regions disassociate first.[37] To confirm this phenomenon with the FHL2 amplicons at the highest concentrations and with on-disc BSC eluates, resultant amplicons were separated via microchip electrophoresis. Results indicate the presence of only one amplicon at 133 base pairs (bp), as anticipated[25], and suggest a multi-stage melt may occur at higher concentrations with this particular target (**Fig. 2-22B**).This may also account for the variation observed here between T_m values across all sample preparation conditions at 100 ng total.

To evaluate the potential for DNA degradation resulting from conversion-related fragmentation, the Quantifiler Trio DNA Quantification Kit was used. This kit is typically used in forensic DNA analysis workflows to quantify DNA, test for the contribution of male genetic material, and assess the quality of forensic samples that are often subject to environmental influences that lead to nucleic acid degradation.[38, 39] Degradation indices are automatically

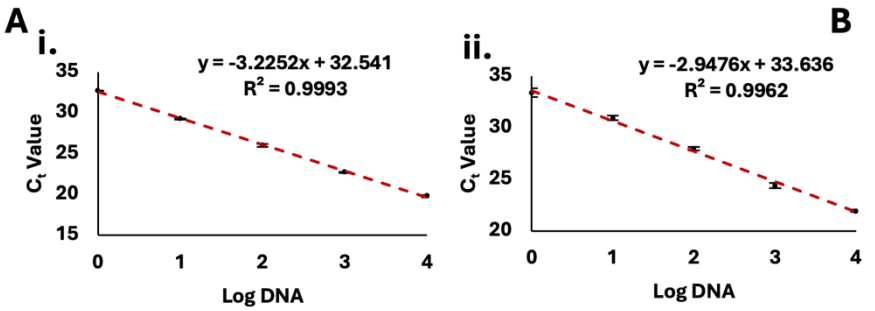

B

Samples	Degradation Index	
	Average	SD
1	0.318	0.029
2	0.319	0.021
3	0.321	0.019

Figure 2-23. Degradation Study. (A) Standard curves constructed for large (i.) and small (ii.) autosomal targets. (B) degradation indices calculated for three replicates prepared via the on-disc method. Figure adapted from Turiello et al. 2023.[49]

calculated by the associated software and based upon C_t values of diluted standards for large and small autosomal targets. Here, R^2 values were high (>0.99) (**Fig. 2-23A**) and the associated Internal PCR Control (IPC) amplified as expected, indicating the amplification reaction was not affected by any inhibitors and efficiency was as expected.[40] Calculated degradation indices from non-methylated DNA standards converted on-disc via the µCD method are <1, indicating that the DNA is not degraded or inhibited.[40] Additionally, indices are fairly consistent between conversion replicates and indicate consistency with regard to degradation (**Fig. 2-23B**). These results are both relevant to forensic use of the workflow and confirm that degradation via the µCD method should not interfere with interpretation at this concentration (~1.25 ng/µL).

2.3.7. Comparison to an Enzymatic Method for Cytosine Deamination. In response to the aforementioned issues associated with gold-standard bisulfite conversion, namely DNA fragmentation and loss, alternative methods for the conversion of cytosines for epigenetic analysis have been developed commercially.[41, 42, 43, 44] One such commercialized method forgoes chemical conversion and relies upon an apolipoprotein B mRNA-editing enzyme, catalytic peptide (APOBEC) for the deamination of cytosine to uracil, leaving modified cytosines (e.g., 5-

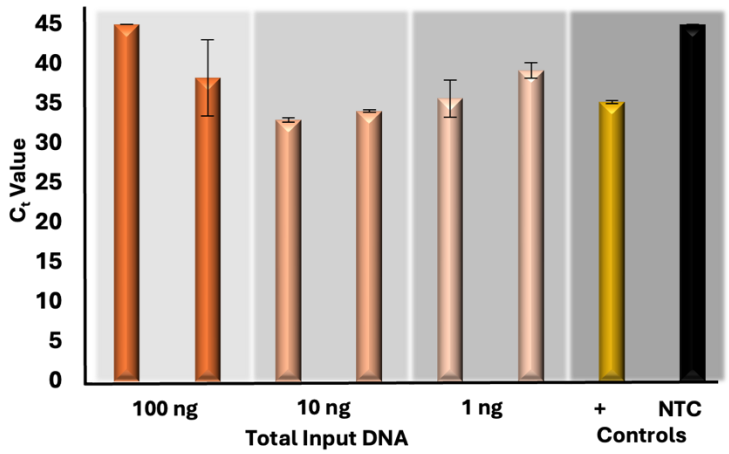

Figure 2-24. Preliminary recovery data from an enzymatic approach to cytosine conversion. RT-PCR results originating from enzymatically converted non-methylated DNA standards. Figure adapted from Turiello et al. 2023.[49]

methylcytosines and 5-hydroxymethylcytosines) intact via enzymatic modification by a ten-eleven translocation 2 (TET2) enzyme and Oxidation Enhancer.[45, 46] To compare the results from µCD dSP-BSC with this alternative method for conversion, non-methylated control DNA was enzymatically converted at equivalent amounts of input DNA, as before. **Figures 2-24** and **2-25** show the results from duplicate enzymatic conversion reactions in terms of relative DNA recovery and conversion efficiency, respectively. Generally, relative recovery results were inconsistent in comparison with the µCD method, indicating that the microdevice method showed greater DNA recovery at total DNA input amounts of 100 ng (µCD mean C_t values 5.42 $\pm$ 2.13 lower) and lower recovery at 10 ng total (µCD mean C_t values 3.37 $\pm$ 1.26 higher) (**Fig. 2-24**). While recovery at 1 ng total, perhaps the most forensically-relevant range, was found to show no statistical differences between average C_t values (unpaired t-test, α = 0.05, p-value = 0.4174). However, this is likely the result of stochastic differences across all samples processed within this concentration range; a direct comparison of units reveals a lower mean C_t difference of 1.28 $\pm$ 0.06 for samples prepared via the microdevice, indicating overall higher recovery (**Fig. 2-24**). When comparing T_m values associated with the enzymatic approach, temperatures are statistically different across

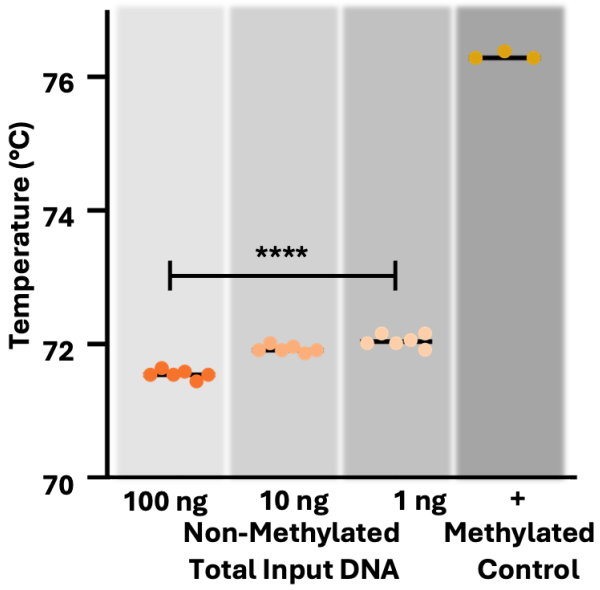

Figure 2-25. Preliminary recovery data from an enzymatic approach to cytosine conversion. RT-PCR results originating from enzymatically converted non-methylated DNA standards. Figure adapted from Turiello et al. 2023.[49]

concentrations (one-way ANOVA, α = 0.05, p-value = <0.0001), potentially indicating that DNA input amount influences conversion efficiency (**Fig. 2-25**). However, in estimations of conversion efficiency via HRM, the enzymatic method outperformed the microfluidic approach by a mean temperature difference of 1.02 $\pm$ 0.11°C; these differences were also found to be statistically significant (unpaired t-test, α = 0.05, p-value = <0.0001). In total, preliminary results comparing the µCD and enzymatic approaches indicate that performance is likely dependent upon DNA input amount with regard to recovery and slightly improved in terms of conversion efficiency with the enzymatic method. Of course, the data set and analytical range tested here is relatively small and further testing is required for a true comparison. With regard to manual intervention and time at the bench, the enzymatic approach required DNA pre-processing (e.g., shearing), 11 more reagents and associated manual handling steps/tube transfers, and 6 additional hours of processing time compared to the µCD method.

2.4. Conclusions

The chemical modification of cytosine residues to uracil via bisulfite conversion has remained largely steadfast since its conception several decades ago[47] and is widely accepted to be associated with DNA degradation and loss[48]. For the preponderance of epigenetic applications, this loss may be compensated for by using samples known to contain higher concentrations of nucleic acids and/or by incorporating upstream enrichment techniques to increase DNA concentration from a large volume of sample. Unfortunately, forensic casework samples are known to have limited DNA contributions that are often fragmented for a number of reasons, including limited sample deposits, environmental exposure, or sample partitioning for individualizing identification efforts, to name a few. Thus, applications in forensic epigenetics, wherein DNA is subject to an additional, deleterious sample preparation process post-extraction, may result in complete loss of the sample and are, therefore, not ideal for integration with the forensic workflow in their current form. Additionally, the adage of another 'open-tube' process with several labor-intensive pipetting steps increases time at the bench, the risk for contamination, and opportunities for errors by the analyst.

The above work describes a microfluidic solution for forensic epigenetic sample preparation that decreases contamination risks and the potential for interoperability issues that are often associated with manual handling.[49] By leveraging decreased, microfluidic volumes, the described method enables reduced incubation times by ~40% compared to the gold-standard and modified in-tube approaches, and preliminary results indicate increased recovery compared to a gold-standard method. The µCD itself incorporates centrifugal force and sacrificial, laser-based valving for fluidic control and the performance of discrete unit operations, permitting automation, reproducibility, and an overall small footprint for preparation of up to four samples

in parallel. The fully-integrated device does exhibit some fluid loss through uptake to the surrounding material during the longest incubation step (e.g., sulphonation and deamination) that may be associated with loss of sensitivity compared to an in-tube microfluidic approach; yet, when comparing controls converted with both gold-standard and on-disc approaches at multiple concentrations, there are no statistical differences in recovery and only negligible differences in conversion efficiency. Likewise, samples prepared via the µCD show no evidence of DNA degradation or inhibition from residual reagents (e.g., ethanol) in the converted eluate, as indicated by a commercial kit intended for forensic characterization of these particular factors. Finally, in a limited comparison of the µCD method and an alternative, enzymatic approach for cytosine conversion, the results were largely stochastic, but indicate that DNA input concentration may be a key factor of performance. Additionally, the enzymatic method necessitated shearing the DNA up front for successful conversion and required a 300x increase in time at the bench, several manual handling steps, and 11 more reagents when compared with the µCD approach. In summary, this work demonstrates progress toward a microfluidic bisulfite conversion method that is more amenable to integration with the forensic DNA workflow but will benefit from further quantitative validation and characterization in the future. Looking to the future, there are a variety of methylation-based applications that would benefit from an automated and miniaturized sample preparation workflow across multiple sectors, as predictive biomarkers have been identified for cancer,[50] neurodegenerative[51] and psychiatric[52] disorders, and therapeutic outcomes,[53] to name a few.

2.5. Acknowledgements

Special thanks to the National Institute of Justice (NIJ), U.S. Department of Justice (DOJ) for the Graduate Research Fellowship support (2020-R2-CX-0030), the Forensic Sciences Foundation, Inc. for the Jan S. Bashinski Criminalistics Graduate Thesis Grant, the University of Virginia (UVA) Graduate School of Arts and Sciences Council for the Research Grant, and the Achievement Rewards for College Scientists (ARCS) Foundation for Fellowship support. I would also like to recognize the International Society for Forensic Genetics (ISFG), the International Society for Applied Biological Sciences (ISABS) and the University of Virginia for their acknowledgement and support of this work.

2.6. References

(1) Butler, J. M. *Advanced Topics in Forensic DNA Typing: Methodology*; Elsevier/Academic Press: Walthan, MA, 2012.

(2) Bass, W. M. *Human Osteology: A Laboratory and Field Manual*, Fifth edition.; Special publication no. 2 of the Missouri Archaeological Society; Missouri Archaeological Society: Columbia, Mo, 2005.

(3) Wiersema, J. M. Evolution of Forensic Anthropological Methods of Identification. *Academic Forensic Pathology* **2016**, *6* (3), 361–369. https://doi.org/10.23907/2016.038.

(4) Naito, E.; Dewa, K.; Yamanouchi, H.; Takagi, S.; Kominami, R. Sex Determination Using the Hypomethylation of a Human Macro-Satellite DXZ4 in Female Cells. *Nucl Acids Res* **1993**, *21* (10), 2533–2534. https://doi.org/10.1093/nar/21.10.2533.

(5) Li, C.; Zhang, S.; Que, T.; Li, L.; Zhao, S. Identical but Not the Same: The Value of DNA Methylation Profiling in Forensic Discrimination within Monozygotic Twins. *Forensic*

Science International: Genetics Supplement Series **2011**, *3* (1), e337–e338. https://doi.org/10.1016/j.fsigss.2011.09.031.

(6) Frumkin, D.; Wasserstrom, A.; Budowle, B.; Davidson, A. DNA Methylation-Based Forensic Tissue Identification. *Forensic Science International: Genetics* **2011**, *5* (5), 517–524. https://doi.org/10.1016/j.fsigen.2010.12.001.

(7) Vidaki, A.; Kayser, M. From Forensic Epigenetics to Forensic Epigenomics: Broadening DNA Investigative Intelligence. *Genome Biol* **2017**, *18* (1), 238. https://doi.org/10.1186/s13059-017-1373-1.

(8) Bocklandt, S.; Lin, W.; Sehl, M. E.; Sánchez, F. J.; Sinsheimer, J. S.; Horvath, S.; Vilain, E. Epigenetic Predictor of Age. *PLoS ONE* **2011**, *6* (6), e14821. https://doi.org/10.1371/journal.pone.0014821.

(9) Maulani, C.; Auerkari, E. I. Age Estimation Using DNA Methylation Technique in Forensics: A Systematic Review. *Egypt J Forensic Sci* **2020**, *10* (1), 38. https://doi.org/10.1186/s41935-020-00214-2.

(10) Freire-Aradas, A.; Phillips, C.; Lareu, M. V. Forensic Individual Age Estimation with DNA: From Initial Approaches to Methylation Tests. *Forensic Sci Rev* **2017**, *29* (2), 121–144.

(11) Zbieć-Piekarska, R.; Spólnicka, M.; Kupiec, T.; Makowska, Ż.; Spas, A.; Parys-Proszek, A.; Kucharczyk, K.; Płoski, R.; Branicki, W. Examination of DNA Methylation Status of the ELOVL2 Marker May Be Useful for Human Age Prediction in Forensic Science. *Forensic Science International: Genetics* **2015**, *14*, 161–167. https://doi.org/10.1016/j.fsigen.2014.10.002.

(12) Zbieć-Piekarska, R.; Spólnicka, M.; Kupiec, T.; Parys-Proszek, A.; Makowska, Ż.; Pałeczka, A.; Kucharczyk, K.; Płoski, R.; Branicki, W. Development of a Forensically Useful Age Prediction Method Based on DNA Methylation Analysis. *Forensic Science International: Genetics* **2015**, *17*, 173–179. https://doi.org/10.1016/j.fsigen.2015.05.001.

(13) Freire-Aradas, A.; Phillips, C.; Mosquera-Miguel, A.; Girón-Santamaría, L.; Gómez-Tato, A.; Casares de Cal, M.; Álvarez-Dios, J.; Ansede-Bermejo, J.; Torres-Español, M.; Schneider, P. M.; Pośpiech, E.; Branicki, W.; Carracedo, Á.; Lareu, M. V. Development of a Methylation Marker Set for Forensic Age Estimation Using Analysis of Public Methylation Data and the Agena Bioscience EpiTYPER System. *Forensic Science International: Genetics* **2016**, *24*, 65–74. https://doi.org/10.1016/j.fsigen.2016.06.005.

(14) Park, J.-L.; Kim, J. H.; Seo, E.; Bae, D. H.; Kim, S.-Y.; Lee, H.-C.; Woo, K.-M.; Kim, Y. S. Identification and Evaluation of Age-Correlated DNA Methylation Markers for Forensic Use. *Forensic Science International: Genetics* **2016**, *23*, 64–70. https://doi.org/10.1016/j.fsigen.2016.03.005.

(15) Naue, J.; Hoefsloot, H. C. J.; Mook, O. R. F.; Rijlaarsdam-Hoekstra, L.; van der Zwalm, M. C. H.; Henneman, P.; Kloosterman, A. D.; Verschure, P. J. Chronological Age Prediction Based on DNA Methylation: Massive Parallel Sequencing and Random Forest Regression. *Forensic Science International: Genetics* **2017**, *31*, 19–28. https://doi.org/10.1016/j.fsigen.2017.07.015.

(16) Feng, L.; Peng, F.; Li, S.; Jiang, L.; Sun, H.; Ji, A.; Zeng, C.; Li, C.; Liu, F. Systematic Feature Selection Improves Accuracy of Methylation-Based Forensic Age Estimation in Han Chinese

Males. *Forensic Science International: Genetics* **2018**, *35*, 38–45. https://doi.org/10.1016/j.fsigen.2018.03.009.

(17) Hong, S. R.; Jung, S.-E.; Lee, E. H.; Shin, K.-J.; Yang, W. I.; Lee, H. Y. DNA Methylation-Based Age Prediction from Saliva: High Age Predictability by Combination of 7 CpG Markers. *Forensic Science International: Genetics* **2017**, *29*, 118–125. https://doi.org/10.1016/j.fsigen.2017.04.006.

(18) Hong, S. R.; Shin, K.-J.; Jung, S.-E.; Lee, E. H.; Lee, H. Y. Platform-Independent Models for Age Prediction Using DNA Methylation Data. *Forensic Science International: Genetics* **2019**, *38*, 39–47. https://doi.org/10.1016/j.fsigen.2018.10.005.

(19) Jung, S.-E.; Lim, S. M.; Hong, S. R.; Lee, E. H.; Shin, K.-J.; Lee, H. Y. DNA Methylation of the ELOVL2, FHL2, KLF14, C1orf132/MIR29B2C, and TRIM59 Genes for Age Prediction from Blood, Saliva, and Buccal Swab Samples. *Forensic Science International: Genetics* **2019**, *38*, 1–8. https://doi.org/10.1016/j.fsigen.2018.09.010.

(20) Lee, H. Y.; Jung, S.-E.; Oh, Y. N.; Choi, A.; Yang, W. I.; Shin, K.-J. Epigenetic Age Signatures in the Forensically Relevant Body Fluid of Semen: A Preliminary Study. *Forensic Science International: Genetics* **2015**, *19*, 28–34. https://doi.org/10.1016/j.fsigen.2015.05.014.

(21) Li, L.; Song, F.; Huang, Y.; Zhu, H.; Hou, Y. Age-Associated DNA Methylation Determination of Semen by Pyrosequencing in Chinese Han Population. *Forensic Science International: Genetics Supplement Series* **2017**, *6*, e99–e100. https://doi.org/10.1016/j.fsigss.2017.09.042.

(22) Giuliani, C.; Cilli, E.; Bacalini, M. G.; Pirazzini, C.; Sazzini, M.; Gruppioni, G.; Franceschi, C.; Garagnani, P.; Luiselli, D. Inferring Chronological Age from DNA Methylation Patterns of

Human Teeth: INFERRING AGE FROM DNA METHYLATION OF HUMAN TEETH. *Am. J. Phys. Anthropol.* **2016**, *159* (4), 585–595. https://doi.org/10.1002/ajpa.22921.

(23) Nguyen, N.-T.; Wereley, S. T.; Shaegh, S. A. M. *Fundamentals and Applications of Microfluidics*, Third edition.; Artech House integrated microsystems series; Artech House: Norwood, Massachusetts, 2019.

(24) Reyes, D. R.; Iossifidis, D.; Auroux, P.-A.; Manz, A. Micro Total Analysis Systems. 1. Introduction, Theory, and Technology. *Anal. Chem.* **2002**, *74* (12), 2623–2636. https://doi.org/10.1021/ac0202435.

(25) Hamano, Y.; Manabe, S.; Morimoto, C.; Fujimoto, S.; Ozeki, M.; Tamaki, K. Forensic Age Prediction for Dead or Living Samples by Use of Methylation-Sensitive High Resolution Melting. *Legal Medicine* **2016**, *21*, 5–10. https://doi.org/10.1016/j.legalmed.2016.05.001.

(26) Nouwairi, R. L.; Cunha, L. L.; Turiello, R.; Scott, O.; Hickey, J.; Thomson, S.; Knowles, S.; Chapman, J. D.; Landers, J. P. Ultra-Rapid Real-Time Microfluidic RT-PCR Instrument for Nucleic Acid Analysis. *Lab Chip* **2022**, 10.1039.D2LC00495J. https://doi.org/10.1039/D2LC00495J.

(27) Dignan, L. M.; Woolf, M. S.; Tomley, C. J.; Nauman, A. Q.; Landers, J. P. Multiplexed Centrifugal Microfluidic System for Dynamic Solid-Phase Purification of Polynucleic Acids Direct from Buccal Swabs. *Anal. Chem.* **2021**, acs.analchem.1c00842. https://doi.org/10.1021/acs.analchem.1c00842.

(28) Turiello, R.; Dignan, L. M.; Thompson, B.; Poulter, M.; Hickey, J.; Chapman, J.; Landers, J. P. Centrifugal Microfluidic Method for Enrichment and Enzymatic Extraction of Severe Acute

Respiratory Syndrome Coronavirus 2 RNA. *Anal. Chem.* **2022**, *94* (7), 3287–3295. https://doi.org/10.1021/acs.analchem.1c05215.

(29) Woolf, M. S.; Dignan, L. M.; Lewis, H. M.; Tomley, C. J.; Nauman, A. Q.; Landers, J. P. Optically-Controlled Closable Microvalves for Polymeric Centrifugal Microfluidic Devices. *Lab Chip* **2020**, *20* (8), 1426–1440. https://doi.org/10.1039/C9LC01187K.

(30) Garcia-Cordero, J. L.; Kurzbuch, D.; Benito-Lopez, F.; Diamond, D.; Lee, L. P.; Ricco, A. J. Optically Addressable Single-Use Microfluidic Valves by Laser Printer Lithography. *Lab Chip* **2010**, *10* (20), 2680. https://doi.org/10.1039/c004980h.

(31) DuVall, J. A.; Le Roux, D.; Tsuei, A.-C.; Thompson, B. L.; Birch, C.; Li, J.; Nelson, D. A.; Mills, D. L.; Ewing, M. M.; McLaren, R. S.; Storts, D. R.; Root, B. E.; Landers, J. P. A Rotationally-Driven Polyethylene Terephthalate Microdevice with Integrated Reagent Mixing for Multiplexed PCR Amplification of DNA. *Anal. Methods* **2016**, *8* (40), 7331–7340. https://doi.org/10.1039/C6AY01984F.

(32) Thompson, B. L.; Ouyang, Y.; Duarte, G. R. M.; Carrilho, E.; Krauss, S. T.; Landers, J. P. Inexpensive, Rapid Prototyping of Microfluidic Devices Using Overhead Transparencies and a Laser Print, Cut and Laminate Fabrication Method. *Nat Protoc* **2015**, *10* (6), 875–886. https://doi.org/10.1038/nprot.2015.051.

(33) Woolf, M. S.; Dignan, L. M.; Scott, A. T.; Landers, J. P. Digital Postprocessing and Image Segmentation for Objective Analysis of Colorimetric Reactions. *Nat Protoc* **2021**, *16* (1), 218–238. https://doi.org/10.1038/s41596-020-00413-0.

(34) Cho, S.; Jung, S.-E.; Hong, S. R.; Lee, E. H.; Lee, J. H.; Lee, S. D.; Lee, H. Y. Independent Validation of DNA-Based Approaches for Age Prediction in Blood. *Forensic Science International: Genetics* **2017**, *29*, 250–256. https://doi.org/10.1016/j.fsigen.2017.04.020.

(35) Hernández, H. G.; Tse, M. Y.; Pang, S. C.; Arboleda, H.; Forero, D. A. Optimizing Methodologies for PCR-Based DNA Methylation Analysis. *BioTechniques* **2013**, *55* (4), 181–197. https://doi.org/10.2144/000114087.

(36) Applied Biosystems. A Guide to High Resolution Melting (HRM) Analysis, 2010. https://assets.thermofisher.com/TFS-Assets/LSG/manuals/cms_070283.pdf.

(37) Downey, N.; Dwight, Z.; Wittwer, C. *Explaining Multiple Peaks in qPCR Melt Curve Analysis*. https://www.idtdna.com/pages/education/decoded/article/interpreting-melt-curves-an-indicator-not-a-diagnosis.

(38) Gouveia, N.; Brito, P.; Serra, A.; Balsa, F.; Andrade, L.; São Bento, M.; Cunha, P.; Bogas, V.; Lopes, V.; Porto, M. J. Validation of Quantifiler ® Trio DNA Quantification Kit in Forensic Samples. *Forensic Science International: Genetics Supplement Series* **2015**, *5*, e24–e25. https://doi.org/10.1016/j.fsigss.2015.09.010.

(39) Vernarecci, S.; Ottaviani, E.; Agostino, A.; Mei, E.; Calandro, L.; Montagna, P. Quantifiler ® Trio Kit and Forensic Samples Management: A Matter of Degradation. *Forensic Science International: Genetics* **2015**, *16*, 77–85. https://doi.org/10.1016/j.fsigen.2014.12.005.

(40) Lackey, A. *How To Evaluate Forensic DNA Quality With Quantifiler Trio DNA Quantification Kit*. ThermoFisher Scientific. https://www.thermofisher.com/blog/behindthebench/how-to-evaluate-forensic-dna-quality-with-quantifiler-trio-dna-quantification-kit/.

(41) Yu, M.; Hon, G. C.; Szulwach, K. E.; Song, C.-X.; Zhang, L.; Kim, A.; Li, X.; Dai, Q.; Shen, Y.; Park, B.; Min, J.-H.; Jin, P.; Ren, B.; He, C. Base-Resolution Analysis of 5-Hydroxymethylcytosine in the Mammalian Genome. *Cell* **2012**, *149* (6), 1368–1380. https://doi.org/10.1016/j.cell.2012.04.027.

(42) Booth, M. J.; Branco, M. R.; Ficz, G.; Oxley, D.; Krueger, F.; Reik, W.; Balasubramanian, S. Quantitative Sequencing of 5-Methylcytosine and 5-Hydroxymethylcytosine at Single-Base Resolution. *Science* **2012**, *336* (6083), 934–937. https://doi.org/10.1126/science.1220671.

(43) Zhang, L.; Szulwach, K. E.; Hon, G. C.; Song, C.-X.; Park, B.; Yu, M.; Lu, X.; Dai, Q.; Wang, X.; Street, C. R.; Tan, H.; Min, J.-H.; Ren, B.; Jin, P.; He, C. Tet-Mediated Covalent Labelling of 5-Methylcytosine for Its Genome-Wide Detection and Sequencing. *Nat Commun* **2013**, *4* (1), 1517. https://doi.org/10.1038/ncomms2527.

(44) Schutsky, E. K.; DeNizio, J. E.; Hu, P.; Liu, M. Y.; Nabel, C. S.; Fabyanic, E. B.; Hwang, Y.; Bushman, F. D.; Wu, H.; Kohli, R. M. Nondestructive, Base-Resolution Sequencing of 5-Hydroxymethylcytosine Using a DNA Deaminase. *Nat Biotechnol* **2018**, *36* (11), 1083–1090. https://doi.org/10.1038/nbt.4204.

(45) Vaisvila, R.; Ponnaluri, V. K. C.; Sun, Z.; Langhorst, B. W.; Saleh, L.; Guan, S.; Dai, N.; Campbell, M. A.; Sexton, B. S.; Marks, K.; Samaranayake, M.; Samuelson, J. C.; Church, H. E.; Tamanaha, E.; Corrêa, I. R.; Pradhan, S.; Dimalanta, E. T.; Evans, T. C.; Williams, L.; Davis, T. B. Enzymatic Methyl Sequencing Detects DNA Methylation at Single-Base Resolution from Picograms of DNA. *Genome Res.* **2021**, *31* (7), 1280–1289. https://doi.org/10.1101/gr.266551.120.

(46) Williams, L.; Bei, Y.; Church, H. E.; Dai, N.; Dimalanta, E. T.; Ettwiller, L. M.; Evans, T. C., Jr.; Langhorst, B. W.; Borgaro, J. G.; Guan, S.; Marks, K.; Menin, J., F.; Nichols, N., M.; Ponnaluri, V. K. C.; Saleh, L.; Samaranayake, M.; Sexton, B. S.; Sun, Z.; Tamanaha, E.; Vaisvilla, R.; Yigit, E.; Davis, T. B. Enzymatic Methyl-Seq: The Next Generation of Methylome Analysis. *New England Biolabs*. https://www.neb.com/tools-and-resources/feature-articles/enzymatic-methyl-seq-the-next-generation-of-methylome-analysis.

(47) Shapiro, R.; Servis, R.; Welcher, M. Reactions of Uracil and Cytosine Derivatives with Sodium Bisulfite. A Specific Deamination Method. *Journal of American Chemical Society 92* (2).

(48) Leontiou, C. A.; Hadjidaniel, M. D.; Mina, P.; Antoniou, P.; Ioannides, M.; Patsalis, P. C. Bisulfite Conversion of DNA: Performance Comparison of Different Kits and Methylation Quantitation of Epigenetic Biomarkers That Have the Potential to Be Used in Non-Invasive Prenatal Testing. *PLoS ONE* **2015**, *10* (8), e0135058. https://doi.org/10.1371/journal.pone.0135058.

(49) Turiello, R.; Nouwairi, R. L.; Keller, J.; Cunha, L. L.; Dignan, L. M.; Landers, J. P. A Rotationally-Driven Dynamic Solid Phase Sodium Bisulfite Conversion Disc for Forensic Epigenetic Sample Preparation. *Lab Chip* **2024**, *24* (1), 97–112. https://doi.org/10.1039/D3LC00867C.

(50) Locke, W. J.; Guanzon, D.; Ma, C.; Liew, Y. J.; Duesing, K. R.; Fung, K. Y. C.; Ross, J. P. DNA Methylation Cancer Biomarkers: Translation to the Clinic. *Front. Genet.* **2019**, *10*, 1150. https://doi.org/10.3389/fgene.2019.01150.

(51) the Australian Imaging Biomarkers and Lifestyle study; the Alzheimer's Disease Neuroimaging Initiative; Nabais, M. F.; Laws, S. M.; Lin, T.; Vallerga, C. L.; Armstrong, N. J.; Blair, I. P.; Kwok, J. B.; Mather, K. A.; Mellick, G. D.; Sachdev, P. S.; Wallace, L.; Henders, A.

K.; Zwamborn, R. A. J.; Hop, P. J.; Lunnon, K.; Pishva, E.; Roubroeks, J. A. Y.; Soininen, H.; Tsolaki, M.; Mecocci, P.; Lovestone, S.; Kłoszewska, I.; Vellas, B.; Furlong, S.; Garton, F. C.; Henderson, R. D.; Mathers, S.; McCombe, P. A.; Needham, M.; Ngo, S. T.; Nicholson, G.; Pamphlett, R.; Rowe, D. B.; Steyn, F. J.; Williams, K. L.; Anderson, T. J.; Bentley, S. R.; Dalrymple-Alford, J.; Fowder, J.; Gratten, J.; Halliday, G.; Hickie, I. B.; Kennedy, M.; Lewis, S. J. G.; Montgomery, G. W.; Pearson, J.; Pitcher, T. L.; Silburn, P.; Zhang, F.; Visscher, P. M.; Yang, J.; Stevenson, A. J.; Hillary, R. F.; Marioni, R. E.; Harris, S. E.; Deary, I. J.; Jones, A. R.; Shatunov, A.; Iacoangeli, A.; Van Rheenen, W.; Van Den Berg, L. H.; Shaw, P. J.; Shaw, C. E.; Morrison, K. E.; Al-Chalabi, A.; Veldink, J. H.; Hannon, E.; Mill, J.; Wray, N. R.; McRae, A. F. Meta-Analysis of Genome-Wide DNA Methylation Identifies Shared Associations across Neurodegenerative Disorders. *Genome Biol* **2021**, *22* (1), 90. https://doi.org/10.1186/s13059-021-02275-5.

(52) Shirvani-Farsani, Z.; Maloum, Z.; Bagheri-Hosseinabadi, Z.; Vilor-Tejedor, N.; Sadeghi, I. DNA Methylation Signature as a Biomarker of Major Neuropsychiatric Disorders. *Journal of Psychiatric Research* **2021**, *141*, 34–49. https://doi.org/10.1016/j.jpsychires.2021.06.013.

(53) Romero-Garcia, S.; Prado-Garcia, H.; Carlos-Reyes, A. Role of DNA Methylation in the Resistance to Therapy in Solid Tumors. *Front. Oncol.* **2020**, *10*, 1152. https://doi.org/10.3389/fonc.2020.01152.

Chapter 3. Toward an Integrated Microfluidic Method for Forensic Epigenetic Sample Preparation

Publication(s) included in Chapter 3:

- **Turiello, R.**; Chambers, T. G.; Enwere, M.; Straub, M. N.; Williamson, N.; Nouwairi, R. L.; Landers, J. P. Toward an Integrated Microfluidic Method for Forensic Epigenetic Sample Preparation. *Lab on a Chip*, In Preparation.

3.1. Introduction

Forensic human identification is based upon genetic variation, with the preponderance of testing relying on a unique set of repeating sequences known as short tandem repeats (STRs) that are capable of differentiating one person from another with high discriminatory power.[1] As an alternative, single nucleotide polymorphisms (SNPs) may be exploited to shed investigative light on an individual's bio-geographical ancestry, lineage, or phenotypic traits, such as hair, skin, or eye color.[2,3,4] Likewise, probing *epigenetic* variation can provide information related to both identification and contextual information, such as human age and tissue source attribution (i.e., body fluid identification), respectively.[5,6] In particular, the phenotypic information that may be inferred from methylation-based epigenetic signatures have proven to be as confounding as they are informative in some cases[7]; and yet, several interrogation panels have been developed that are robust enough to differentiate between monozygotic twins,[8] predict smoking habits,[9] and determine chronological age within less than a year of accuracy[10]. Unlike STR and SNP analysis, methylation interrogation requires a labor-intensive sample preparation process that includes

both DNA extraction and bisulfite conversion (BSC), processes that independently result in a magnitude of DNA loss.

Gold-standard methods for forensic DNA extraction involve cellular lysis, followed by the silica-assisted purification of the nucleic acid (NA) in a packed column or dynamic solid phase (i.e. silica beads).[1] For purification, the DNA is bound to the silica surface in the presence of a chaotrope via hydrogen bonding and hydrophobic interactions so that NAs may be separated from bulk cell lysate and contaminants.[11] This DNA-silica adsorption is variable and highly dependent on pH, buffer constituents, and the concentration of DNA in solution; in fact, some percentage of the DNA will be unrecoverable as a result of either becoming irreversibly bound to silica or not bound at all.[12] For epigenetic analysis, purified DNA eluates will then be subjected to BSC, a method that preferentially deaminates all cytosines not containing a methyl tag to uracil; in the amplification reaction that follows, converted uracil bases are copied as thymine.[13] The conversion reaction results in DNA loss through chemical decomposition, whereby the *N*-glycosyl bond of pyrimidine bases (i.e., cytosine, uracil, and thymine) is cleaved to produce abasic sites following prolonged incubation with ammonium bisulfite.[14] In essence, the reaction causes DNA fragmentation by abasic site-related strand scission, making downstream detection by amplification more challenging.[14] Mitigating this phenomenon is difficult, as bisulfite-related DNA loss increases linearly with incubation time, but shorter incubation times using standard reaction volumes result in low conversion efficiency and poor prediction results (i.e., false positives/negatives).[15]

The loss of genetic material resulting from both extraction and conversion are less problematic for clinical applications in which a large volume of sample is taken; this of course

does not include those applications focused on extremely limited NA concentrations such as cell free or circulating tumor DNA testing (i.e., liquid biopsy).[16] However, the DNA encountered in the forensic context is limited and often highly degraded for a variety of reasons, largely having to do with its deposition in environments that subject it to unfavorable temperature, humidity, and ultraviolet (UV) radiation conditions.[17] Therefore, additional DNA loss as a result of the coupled sample preparation processes is suboptimal, especially when the conservation of that DNA is of the upmost importance. In addition, adding another step (i.e., epigenetic conversion) to the time-consuming and labor-intensive workflow of forensic DNA typing is a barrier-to-entry in already overburdened laboratories with strict standards for quality and assay performance.[18] In response, we previously developed an automated method for forensic epigenetic conversion that utilizes rotational force and a microfluidic format to automate the BSC process with the goal of enhancing DNA recovery compared to a gold-standard method.[19] Characterization of the microCD (μCD) method was completed with differentially-methylated DNA standards and multiple downstream analytical modes to assess relative DNA recovery, conversion efficiency, and resultant degradation.[19] Despite the system's general success in terms of DNA recovery and analytical time saved with conversion, the reality is that the method described[19] requires the introduction of previously extracted genetic material from human cells.

In an effort to streamline the entire sample preparation workflow for forensic epigenetic use and further enhance DNA recovery, the following chapter examines the incorporation of an enzymatic method for DNA release to be incorporated upstream of the microfluidic conversion process. In contrast to the conventional solid-phase approaches considered the "gold-standard" for DNA extraction, the enzymatic method requires no purification and thus, allows the analyst

to avoid loss due to sequential silica washes. As a proof-of-concept, this chapter evaluates whether or not enzymatic extraction is compatible with downstream conversion by ammonium bisulfite using standards, cloned K-562 cells, and venous blood samples. Compatibility is evaluated in terms of real-time polymerase chain reaction (RT-PCR), high resolution melting (HRM), electrophoresis, and pyrosequencing, using targets known for their utility in human age prediction.[19,20,21,22] Toward a fully integrated approach to epigenetic sample preparation, a rotationally-driven device design in proposed and assessed using colorimetric dye studies and preliminary testing with venous blood samples.

3.2. Materials and Methods

3.2.1. Sample Materials. Amplification and detection chemistry was tested with the Human Methylated and Non-Methylated DNA Set (Zymo Research, Irvine, CA, USA) at a stating concentration of 250 ng/μL. K-562 cells were purchased and prepared at a concentration of 125k according to manufacturer recommendations (ATTCC, Manassas, VA, USA) and resuspended in phosphate buffered saline (PBS) (Thermo Fisher Scientific. Waltham, MA, USA). Blood samples were collected, de-identified, and prepared by University of Virginia Hospital. As a positive control, 1 μL of the Universal Methylation Human DNA Standard (Zymo Research, Irvine, CA, USA) at an initial concentration of 20 ng/μL was used for each reaction. Negative controls substituted nuclease-free water for sample for both extraction and bisulfite conversion to ensure no contamination due to handling. No template controls consisting of nuclease-free water were also used in place of converted extract for all amplification reactions. USA).

3.2.2. DNA Extraction. Extraction by the "gold-standard" method used the DNeasy Blood & Tissue Kit (QIAGEN, Hilden, Germany) according to manufacturer's instructions, but with a 50 μL elution volume. To ensure maximum recovery from silica columns, the total volume of elution buffer was run through the column a total of 3x by pipette. EA1 extractions were completed in parallel with a reaction volume of 50 μL for ease of comparison. Each reaction consisted of 5 μL of BLUE Buffer (MicroGEM International, PLC, Charlottesville, VA, USA), 1 μL EA1 Enzyme (MicroGEM International, PLC), and a variable amount of DNA-free water, based upon the input volume of aqueous sample. For K-562 cells, 44 μL of water was added; thus, the reaction chemistry was used to rehydrate flash frozen cell pellets. To test the chemistry with aqueous blood samples, 10 μL of whole blood was mixed with 34 μL of DNA-free water. The same reagent volumes were used for samples prepared via FLOQSwabs® (Copan Diagnostics, Murrieta, CA, USA).

3.2.3. Assessment of DNA Recovery and Template Conversion. Amplification by and detection by RT-PCR of eluates resulting from extraction and conversion leveraged the ZymoTaq™ PreMix (Zymo Research, Irvine, CA, USA) chemistry. According to manufacturer recommendations, 50 μL reactions were comprised of 25 μL of ZymoTaq™ PreMix, 1.25 μL of 10 μM forward and reverse primers (0.25 μM) (Integrated DNA Technologies, Coralville, Iowa, USA), 20.5 μL of nuclease-free water, and 2 μL of input DNA. Half reactions consisted of exactly half the volume of reagents used in 50 μL reactions and those half reactions containing 2x DNA and 2x primers used 2 μL of input DNA and 1.25 μL of 10 μM forward and reverse primers (0.5 μM) in a 25 μL reaction. Samples were amplified and melted in triplicate on the QuantStudio 5 Real-Time PCR System with detection in the FAM channel (Thermo Fisher Scientific, Waltham, MA, USA). Thermal conditions

included initial denaturation (95°C, 600 s), 45 cycles of denaturation (95°C, 30 s), annealing (49.5°C, 45 s), and extension (72°C, 60 s), and a final extension step (72°C, 420 s). For the annealing temperature study, the Flex function was used to test multiple annealing temperatures simultaneously, including 49, 49.5, 50, 50.5, 51, and 51.5°C. Samples were considered positive if they crossed the instrument threshold, generating a C_t value. HRM was also completed using the QuantStudio 5 system; immediately following RT-PCR, the reaction was heated to 95°C for 1 s for denaturation, subsequently cooled to 50°C and held for 20 s, before being incrementally heated to 95°C at a rate of 0.1°C/s. Data acquisition occurred at each temperature interval and the instrument's software produced T_m values for each samples based upon its own algorithm.

3.2.4. Microfluidic Device Design and Fabrication. Microdevices were designed using AutoCAD software (Autodesk, Inc., Mill Valley, CA, USA) with channels enabling fluid flow via valve actuation and rotational force; channels were designed to be approximately 100 µm deep and have widths between 400 and 500 µm. Engineered renderings were translated to polymeric materials via a CO_2 laser (VLS 3.50, Universal Laser Systems, Scottsdale, AZ, USA). The core device is primarily constructed from five poly(ethylene terephthalate) (PeT) layers (Film Source, Inc., Maryland Heights, MO, USA). Layers 2 and 4 are encapsulated in a heat-sensitive adhesive (HSA) (EL-7970-29, Adhesives Research, Inc., Glen Rock, PA, USA) to enable thermal bonding via the "print, cut, laminate" (PCL) method[23] by a commercial-off-the-shelf laminator (Ultralam 250B, Akiles Products, Inc., Mira Loma, CA, USA). Layer 3 consisted of a black PeT (bPeT) (Lumirror X30, Toray Industries, Inc., Chuo-ku, Tokyo, Japan) layer to enable laser-based valving, as previously described.[24,25] Chamber thicknesses were enhanced compared to previous iterations,[19] whereby

accessory pieces consisting of poly-(methyl methacrylate) (PMMA) (1.5 mm thickness, McMaster Carr, Elmhurst, IL, USA) capped with PeT and bonded by pressure-sensitive adhesive (PSA) transfer tape (MSX-7388, 3M, Saint Paul, MN, USA) were added to the top and bottom of the device. To ensure fluid retention during heated incubations, polytetrafluoroethylene (PTFE) hydrophobic membranes (0.2 µm, Sterlitech, Auburn, WA, USA) were added to select vents.

3.2.5. Mechatronic Systems for Microfluidic Operation. Mechatronic systems that permit centrifugal force, enable laser-based valving, allow for magnetic mixing of silica particles, and heating on the device were all designed in-house, as previously described. [25,26,27] Each system is controlled by 8-core microcontrollers (Propeller P8X32A-M44; Propeller, Inc., Rockland, CA, USA) that are coded for functionality by a custom software program, *Spin*, from a corresponding external laptop. The Power, Time, and Z-Height Actuated (PrTZAL) System enables laser-based valving and imparts centrifugal force onto the device.[25] Valves consisting of bPeT are opened and channels are closed when the 638 nm laser diode is adjusted in terms of laser power, time, and distance from the surface of the disc, as before.[19] Laser valves were 'opened' by setting the power, time, and z-height parameters to 500 mW, 500 ms, and 15 mm above the surface of the disc, respectively. As before, laser valves were 'closed' with corresponding settings of 700 mW, 2500 ms, and a z-height distance of 26 mm. On-disc heating was completed with the help of a dual-clamped Pelter system.[28] Similarly, a dynamic solid phase extraction (dSPE) system enabled "sweeping" of magnetic beads during the integrated dye study.[26] Each mechatronic system may be programmed to complete a set of commands using the *Spin* code graphical user interface (GUI).

3.2.6. Dye Studies and Image Analysis. Aqueous dye solutions were used to visually represent reagents slated for microfluidic extraction. For colorimetric image analysis, yellow and blue dyes were representative of extracted lysate and ammonium bisulfite, respectively. Disc images were captured with an Epson Perfection V100 Photo desktop scanner (Seiko Epson Corporation, Suwa, Nagano Prefecture, Japan) and converted to HSB stacks using the Fiji ImageJ freeware. Transformed data was analyzed via the "crop-and-go" technique, whereby the hue of a designated region of interest within each chamber and parallel measurements of control dye solutions were compared to extrapolate the volume of metered lysate. For the second generation integrated design dye study, FLOQSwabs (Copan Diagnostics, Murrieta, CA, USA) were saturated with 0.1 M Allura red dye solution (Sigma-Aldrich, St. Louis, MO, USA) diluted in 1x Tris-EDTA Buffer, pH 7.5 (Sigma-Aldrich, St. Louis, MO, USA).

3.2.7. Microfluidic Enzymatic Extraction. The microfluidic extraction process can be followed in a representative schematic, shown below. A full FLOQSwab (Copan Diagnostics) was introduced to the corresponding swab chamber and capped with a laser-ablated PeT coverlet by PSA. A 50 μL volume of extraction cocktail, comprised of 5 μL BLUE Buffer (MicroGEM International), 1 μL of EA1 Enzyme (MicroGEM International), and 44 μL of DNA-free water, is added to the extraction chamber through the associated loading arm. The channel leading to the loading arm (valve 1) is then laser ablated (or 'closed') via the PrTZAL system.[25] Lysate metering occurred following the laser actuation of valve 2 to introduce fluid from the enzymatic lysis swab chamber to the lysate

metering and overflow chambers. For the purposes of this stage of optimization, fluid was recovered at this stage of the process of conventional conversion processing.

3.2.8. Electrophoresis. Size-based separation of DNA was completed with the 2100 Bioanalyzer Instrument (Agilent Technologies, Santa Clara, CA, USA). The Agilent DNA Kit (Agilent) was used according to manufacturer recommendations with 9 μL of Gel-Dye Matrix, 5 μL of DNA 1000 Marker, 1 μL of DNA 1000 Ladder, and 1 μL of converted DNA eluate added to the corresponding wells in the microfluidic chip. The 2100 Expert Software (Agilent) was used for analysis.

3.2.9. Pyrosequencing. Bisulfite-converted material was amplified in the ELOVL2 target region, according to specifications from Kampmann et al. 2024.[22] Each eluate was amplified in a total reaction volume of 25 μL consisting of 12.5 μL 2x PyroMark PCR Master Mix (Qiagen), 2.5 μL CoralLoad Concentrate (Qiagen), 1.5 μL of combined forward and reverse primers (0.6 μM final concentration) (Qiagen), 3 μL of DNA-free water, and 5 μL of sample. Per author's recommendation, the PCR cycling parameters consisted of PCR activation (95°C, 15 min), 50 cycles of denaturation (95°C, 30 s), annealing (48°C - 52°C, 20 s), and extension (72°C, 30 s), and a final extension (72°C, 10 min). The annealing temperature ramped from 48°C - 52°C during the first 10 cycles of the reaction, using the Veriti Thermal Cycler (Thermo Fisher Scientific).

Pyrosequencing was completed on the PyroMark Q48 Autoprep (Qiagen) according to manufacturer's instructions and with sequencing primer at a concentration of 6 μM. Each well on the PyroMark Q48 discs were loaded with 10 μL of sample and 3 μL of beads. Eluates were amplified in duplicate and volumes were combined to allow for pyrosequencing of each extracted

and converted replicate in triplicate. The PyroMark Q48 software was used to estimate methylation percentages at each locus and indicate whether sequencing runs passed, required checking, or failed via a color coding system of blue, yellow, and red, respectively.

3.2.10. Statistics and Reproducibility. C_t and T_m values were described as the mean $\pm$ standard deviations for all technical BSC replicates and/or amplification replicates. Significance testing by t-test and ANOVA were completed with GraphPad Prism Software (San Jose, CA, USA). All described t-tests are two-tailed, using unpaired comparison parameters, and with a significance (α) of 0.05 (e.g., 95% confidence interval). Any analysis of variance (ANOVA) used a one-way framework and with a the same 95% confidence interval parameters.

3.3. Experimental

3.3.1. DNA Extraction Method Selection. The conventional method for forensic DNA extraction (**Fig. 3-1**) utilizes sodium dodecyl sulfate (SDS) and a serine protease (i.e., proteinase K, pro K) to effectively lyse cells and digest structural proteins and enzymes that would otherwise lead to the

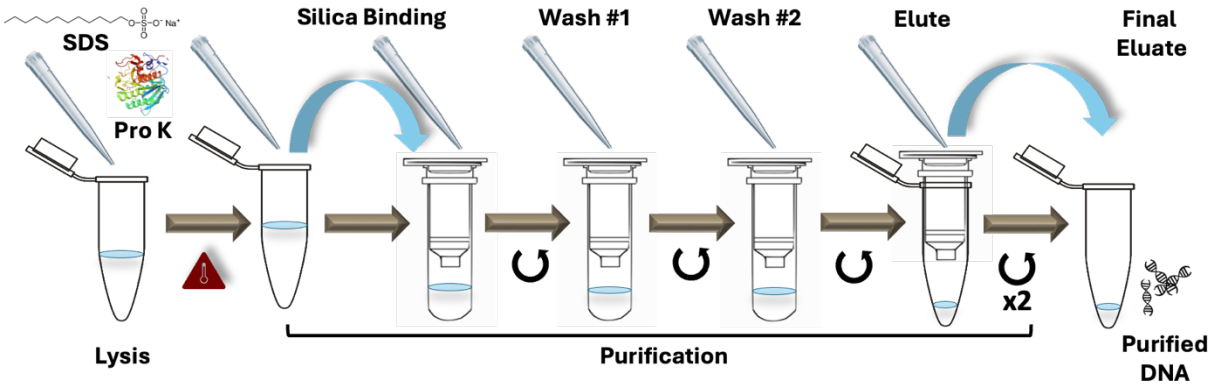

Figure 3-1. Typical solid-phase extraction process. Cellular lysis by proteinase K and SDS is followed by silica-based purification by column.

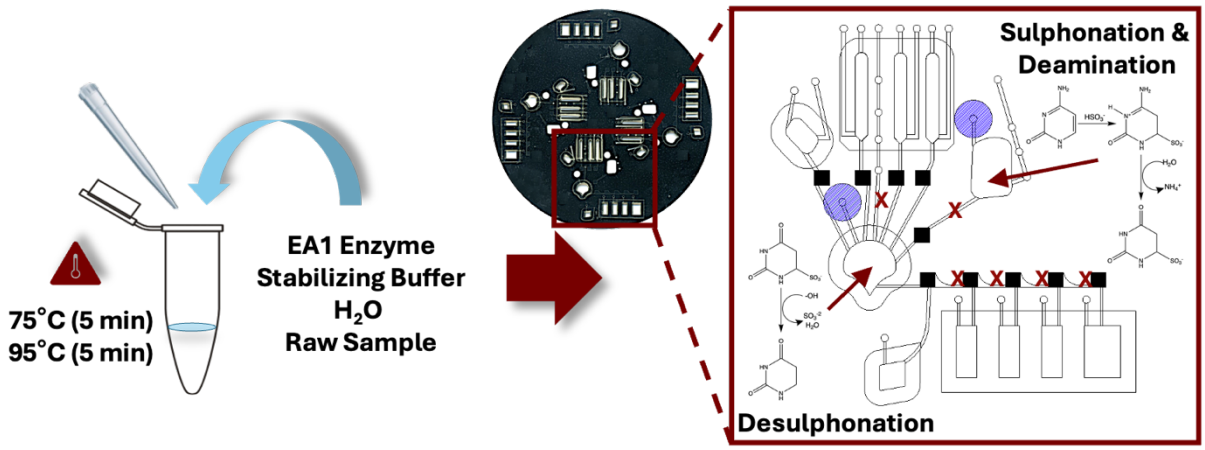

Figure 3-2. Enzymatic NA extraction. Cellular lysis accomplished with neutral protease EA1 at 75°C and subsequently rendered inactive at 95°C. This step would be integrated upstream from epigenetic conversion using the previously disclosed microfluidic system.

degradation of genetic material or inhibition of downstream target amplification.[29] These inhibitory reagents and denatured proteins, such as DNases, are removed during purification, whereby they are filtered out in a silica solid phase, ultimately producing a purified DNA eluate. This purification process leads to variable loss of unrecoverable DNA in response to several factors having to do with the pH, buffer constituents, and DNA concentration compared to the silica substrate.[12] To mitigate the loss of genetic material as a result of silica-based purification, this work incorporates an alternative method for DNA extraction based upon the introduction of a highly thermostable neutral protease from *Bacillus* sp. strain EA1.[30] Extraction by the EA1 enzyme permits nucleic acid preparation in a single tube, whereby the enzyme's action is dependent upon temperature alone (**Fig. 3-2**). Furthermore, the enzyme is functional in a buffer compatible with downstream amplification, removing the need for pro K, SDS, harsh chemicals, and silica purification altogether. The EA1 method has been explored for its utility with forensic DNA extraction from both biological samples and degraded stains,[31,32] and was recently developmentally validated for this purpose.[33] Here, I propose the coupling of DNA extraction, by

the EA1 method, with epigenetic conversion by bisulfite (**Fig. 3-2**). This work demonstrates that non-purified eluates resulting from EA1 lysis are compatible with epigenetic conversion and downstream testing. To the author's knowledge, this is the first time enzymatic lysis by EA1 has been coupled with bisulfite conversion for epigenetic analysis.

3.3.2. Assessment of DNA Recovery and Template Conversion. To evaluate the relative DNA recovery and template conversion originating from different sample preparation modes and parameters, cycle threshold (C_t) and melting temperature (T_m) values were compared following amplification by RT-PCR and HRM of the FHL2 target. This target has been associated with human age prediction by HRM post-amplification,[20] and was previously used for conversion optimization using RT-PCR and HRM on a microfluidic system.[19] Thus, these particular FHL2 primer sequences have been tested for relevance, function, and performance with the associated conversion

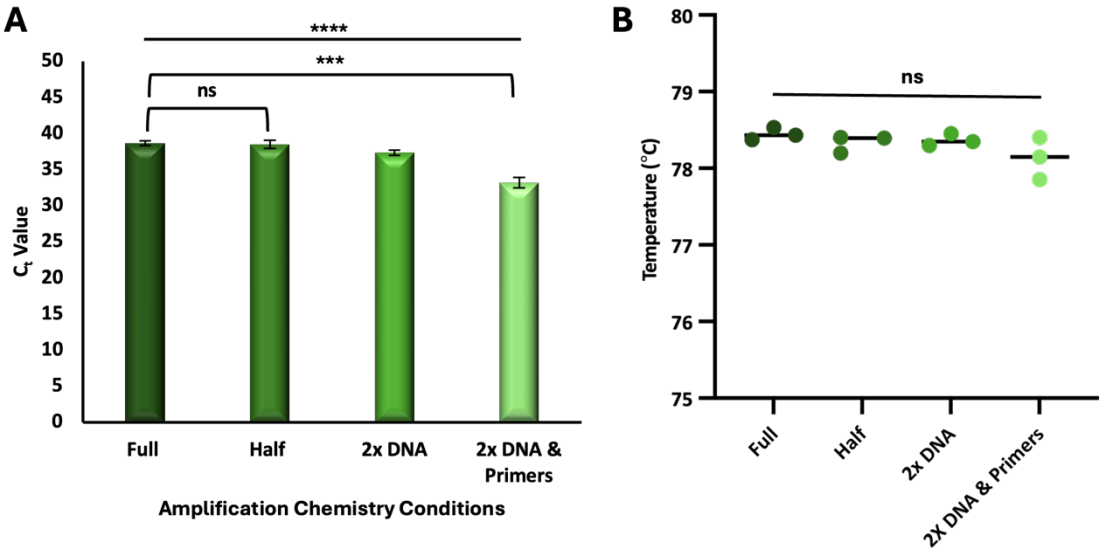

Figure 3-3. Optimization of chemistry for recovery and conversion efficiency estimation. (A) RT-PCR and (B) HRM results, comparing methylation standards amplified with a manufacturer recommended protocol versus those containing altered half-volume reactions.

chemistry. However, this work utilizes a different amplification chemistry, necessitating additional optimization. Herein, amplification and detection leveraged the ZymoTaq™ PreMix, in which the interchelating dye is premixed into a solution designed to limit non-specific amplification products in low-complexity, bisulfite-treated templates. This chemistry was tested with bisulfite converted, methylated DNA standards according to manufacturer recommendations and at half-reaction volumes under three conditions: 1) using manufacturer recommended concentrations, 2) with 2x the amount of DNA, and 3) with 2x the recommended concentration of DNA and primers. **Figure 3-3A** depicts resultant C_t values originating from each condition. No statistical differences between full and half-volume reactions are observed (unpaired *t*-test, α = 0.05, *p*-value = 0.686) and samples prepared with 2x the concentration of primers and DNA showed enhanced detection sensitivity by ~5.517 ($\pm$ 0.389) C_t units. No template controls were run according to each parameter described; results (data not shown) showed no signal beyond baseline noise, indicating no non-specific amplification (NSA). HRM profiles for methylated standards showed only one peak (78.319 $\pm$ 0.182) and demonstrated no statistical differences between parameters (One-way ANOVA, α = 0.05, *p*-value = <0.0001), confirming amplification results that indicated no NSA (**Fig. 3-3B**). Moving forward, amplification conditions leveraging twice the concentration of primers and volume of input DNA were selected for further testing.

Given the disparity of guanine and cytosine (GC) content that is innate to methylated and non-methylated standards post-conversion, it is understandable that there will be a disparity in amplification efficiency (i.e., PCR bias) and T_m. **Figure 3-4** shows the differences between replicates of converted methylated and non-methylated standards, amplified with multiple annealing temperatures ranging from 49°C to 51.5°C. Generally, methylated standards produce

A

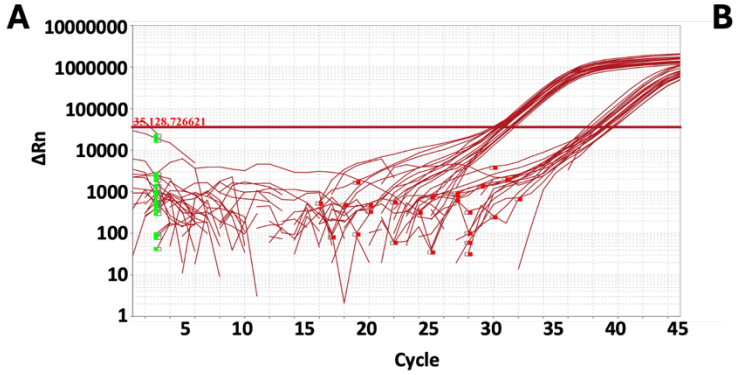

B

Annealing Temperature	Methylation Status	Average	Standard Deviation	Cycle Threshold Difference
49°C	U	30.784	0.477	7.939
	M	38.723	0.619	
49.5°C	U	30.555	0.142	7.191
	M	37.746	0.206	
50°C	U	30.931	0.609	7.734
	M	38.665	0.338	
50.5°C	U	30.796	0.574	8.205
	M	39.001	0.165	
51°C	U	30.810	0.331	7.915
	M	38.726	0.184	
51.5°C	U	30.540	0.664	8.635
	M	39.174	0.588	

Figure 3-4. Annealing temperature testing of differentially-methylated amplicons by RT-PCR. (A) Amplification plot and (B) C_t values originating from annealing temperature testing with methylated and non-methylated amplicons.

much later C_t values, as their GC content is preserved and repeated denaturation and extension is slower thanks to a higher hydrogen bond content in comparison to their unmethylated counterparts. In an effort to mitigate the favoring of one transcript over another, an annealing temperature of 49.5°C was selected, as it exhibited the lowest differences between C_t values (**Figure 3-4B**). Average T_m values for the non-methylated and methylated amplicons using this chemistry can be visualized in **Figure 3-5**. In the following section, these melt temperatures will be used to assess comparative conversion efficiency following extraction by EA1 and a commercialized, gold-standard method.

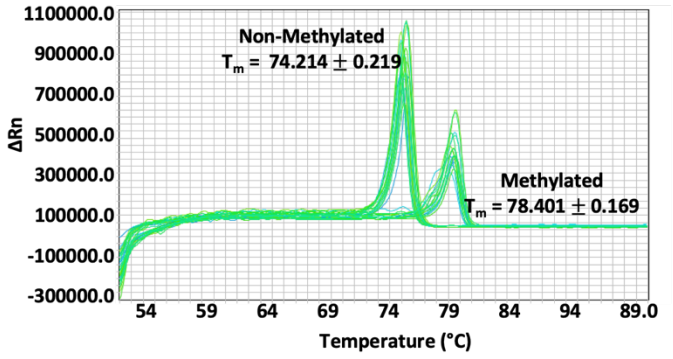

Figure 3-5. Annealing temperature testing of differentially-methylated amplicons by HRM. Melt curve profiles originating from annealing temperature testing with methylated and non-methylated amplicons.

3.3.3. Assessment of Relative DNA Recovery from EA1 and a Gold-Standard Method for DNA Extraction.

The enzymatic method for NA extraction does

not require purification by silica beads or a packed column, as the gold-standard methods do. As discussed, a significant amount of genetic material is lost to the purification process as some NAs may fail to bond, while others are bound irreversibly.[12] The assumption follows that extraction by the EA1 method will result in a significant increase in DNA recovery, compared to gold-standard silica methods; for precedent, preliminary data suggests this is true for RNA lysed from SARS-CoV-2 virions.[27] To compare relative recovery as a result of the purification process alone and coupled with conversion, pre-purified non-methylated and methylated standards were "extracted" in parallel by the EA1 method and a Qiagen solid-phase approaches. For comparison, these same standards were used to generate standard curves for each condition within a relevant concentration range (**Fig. 3-6**). A standard curve was constructed using both non-methylated and

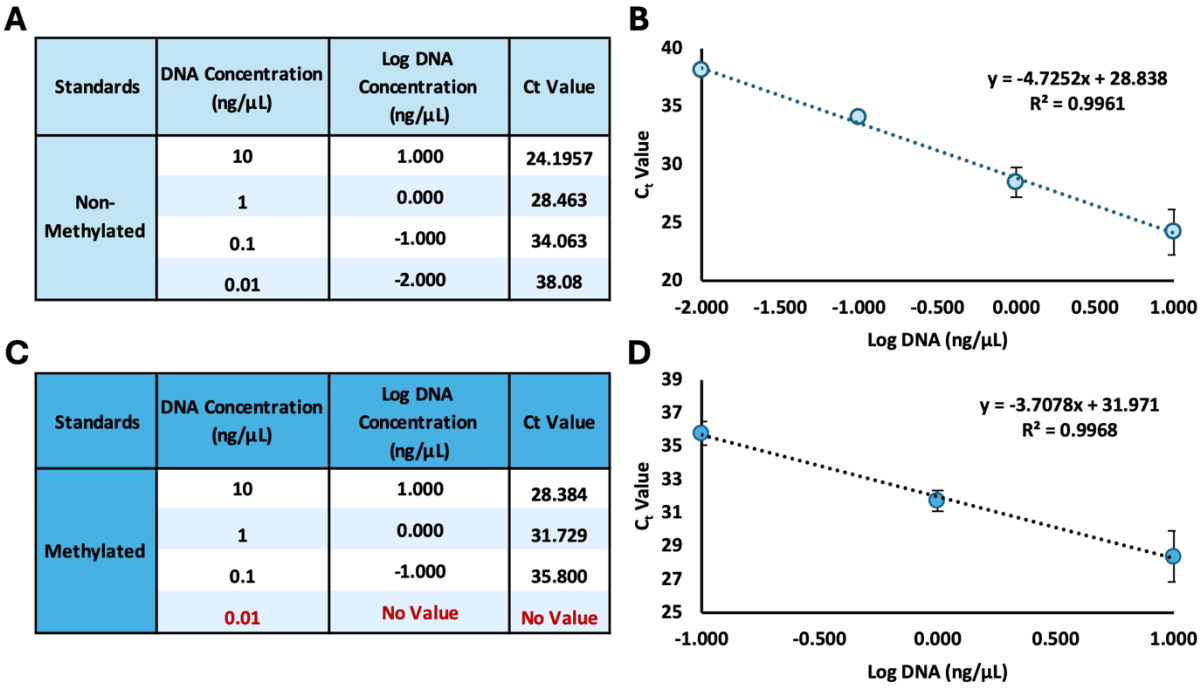

Standards	DNA Concentration (ng/µL)	Log DNA Concentration (ng/µL)	Ct Value
Non-Methylated	10	1.000	24.1957
	1	0.000	28.463
	0.1	-1.000	34.063
	0.01	-2.000	38.08

Standards	DNA Concentration (ng/µL)	Log DNA Concentration (ng/µL)	Ct Value
Methylated	10	1.000	28.384
	1	0.000	31.729
	0.1	-1.000	35.800
	0.01	No Value	No Value

Figure 3-6. Standard curves for relative quantification. C_t values generated for concentrations ranging from 10 – 0.01 ng/µL from (A – B) non-methylated standards and (C – D) methylated standards post-conversion. Note that there was no C_t value generated from methylated standards amplified at 0.01 ng/µL (C) and this point was therefore not included on the requisite standard curve (D).

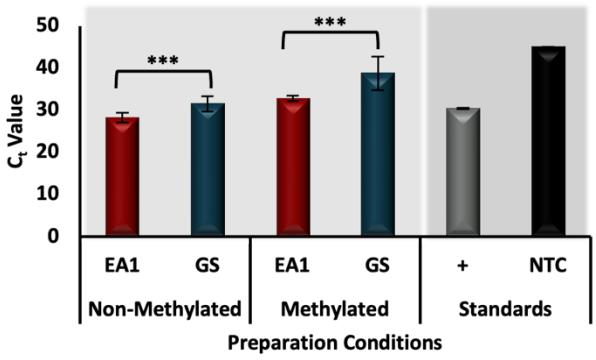

Figure 3-7. Comparative standard DNA recovered post extraction and epigenetic conversion. Statistically different C_t values originating from extraction of non-methylated and methylated DNA standards by the enzymatic (EA1) and gold-standard (solid-phase chemistry) methods.

methylated standards for direct comparison, as PCR bias can influence any relative recovery estimations.[19] Each curve demonstrated excellent linearity (non-methylated R^2 = 0.996, methylated R^2 = 0.997) and was thus used to extrapolate relative DNA concentrations in ng/μL, substituting the C_t value of any "unknown" samples for the "y-intercept" value.

Figure 3-7 compares the C_t values generated following DNA extraction by either EA1 or gold-standard methods for both non-methylated and methylated standards. For each, significant statistical differences were observed between conditions (unpaired *t*-tests, α = 0.05, non-methylated *p*-value = 0.0004, methylated *p*-value = 0.001), suggesting some amount of genetic material is lost to the purification process by the gold-standard method when compared to EA1. Examining the data further, the relative average concentrations were calculated and depicted in **Table 3-1**, where the percentage of DNA recovered was determined to be ~29% and ~50% with EA1 and ~2% and ~24% with gold-standard extraction. While these results cannot be used to surmise the total DNA loss as a result of extraction alone, as a significant portion of NA material is lost to epigenetic conversion by bisulfite,[14] they can be used

Preparation Conditions		Average Concentration (ng/μL)	DNA Recovered (%)
Non-Methylated	EA1	0.359 ± 0.213	28.680 ± 17.066
	GS	0.025 ± 0.026	2.034 ± 2.119
Methylated	EA1	0.359 ± 0.078	49.947 ± 6.213
	GS	0.025 ± 0.070	23.775 ± 5.583

Table 3-1. Estimated recoveries by method. The average concentrations and relative DNA recovered from each method.

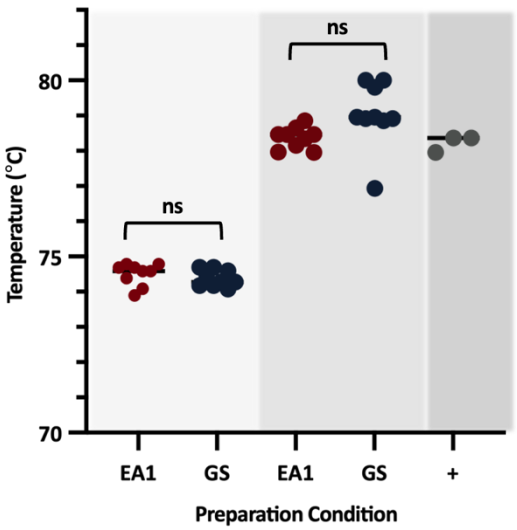

Figure 3-8. Comparison of conversion efficiency post extraction and epigenetic conversion. Statistically similar T_m values originating from extraction of non-methylated and methylated DNA standards by the enzymatic (EA1) and gold-standard (solid-phase chemistry) methods.

to calculate relative total loss due to extraction. It was extrapolated that approximately 26% of DNA is lost to the gold-standard method, in comparison to EA1, likely during the purification phase of the workflow. This estimate was consistent across methylated and unmethylated standards, providing replicate results as to the approximated percentage of total DNA lost.

Whether or not DNA extraction method had any effect on downstream conversion could be gauged with HRM, at least as it relates to our target of interest. Of course, the most relevant results would originate from non-methylated standard DNA, as any cytosines sans methylation would be subject to uracil conversion and demonstrate differences in conversion efficiency that might arise from altered reaction conditions. **Figure 3-8** shows the relative melt temperatures, which demonstrate no statistical differences when preparation conditions are compared using unpaired t-tests for both non-methylated and methylated standards ($\alpha = 0.05$, *p*-values = <0.411 and 0.055, respectively). These data indicate there are no repercussions as a result of either extraction method as far as cytosine conversion is concerned. In summary, the EA1 method demonstrates increased DNA recovery compared to a gold-standard method requiring silica-based purification and the EA1 method confers no effects to conversion.

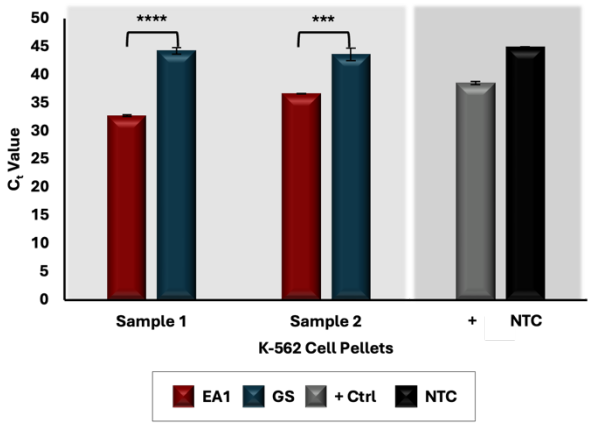

Figure 3-9. Relative DNA recovery with K-562 cells. A comparison of C_t values post extraction and bisulfite conversion by the enzymatic and gold-standard methods indicates increased recovery by the enzymatic method.

3.3.4. Compatibility of EA1 with Epigenetic Conversion by Bisulfite using K-562 Cells. To this point, the EA1 extraction method has not been coupled with downstream epigenetic conversion from DNA originating from human cells. As such, there is no data indicating whether or not the non-purified eluate that results from an enzymatic extraction is amenable to downstream conversion. Simply put, the extract resulting from an enzymatic lysis protocol will contain extracellular and cellular debris that may confer effects detrimental to the conversion process, which is known to require "purified" NA.

To assess compatibility in terms of DNA recovery and conversion efficiency, preliminary testing was completed with cultured cells from the a human erythroleukemic K562 cell line.[34] Samples were bisulfite converted and amplified following extraction by the EA1 method, as well as a Qiagen approach to serve as the *gold-standard* for comparison. **Figure 3-9** displays the resultant C_t values from the preparation of two cloned samples; a visible statistical difference is demonstrated as a result of the different preparation procedures (unpaired *t*-tests, $\alpha = 0.05$, *p*-values = <0.0001 and 0.0009, respectively). The EA1 method generated amplicons with averaged and combined C_t values approximately 9 units lower than the GS method. Melt temperatures (i.e. T_m values) were also compared to indicate heterogeneity of the amplicon product following conversion, and the relative conversion efficiency between methods. **Figure 3-10** shows that

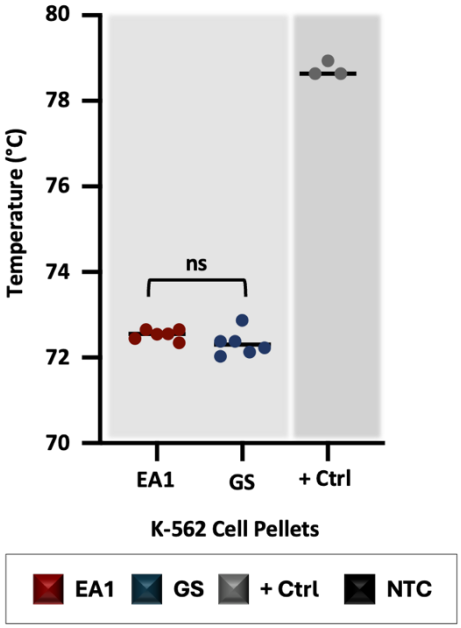

Figure 3-10. Compared conversion efficiency with K-562 cells. A comparison of T_m values post extraction and bisulfite conversion by the enzymatic and gold-standard methods indicates no statistical differences.

average T_m values from gold-standard and EA1 extraction methods have no statistical differences between replicates (unpaired *t*-test, $\alpha = 0.05$, *p*-value = 0.1544). In addition to signifying comparable relative conversion efficiency between methods, the presence of a singular 'peak' demonstrates the presence of only one PCR product and indicates complete conversion of the FHL2 target. A comparison of the combined data with K-562 cells indicates that extraction by EA1 is not only compatible with downstream conversion and targeted RT-PCR, but that it may results in increased sensitivity of the total assay with no hindrance to conversion efficiency.

3.3.5. Compatibility of EA1 with Epigenetic Conversion by Bisulfite using Blood Samples. The compatibility demonstrated with K-562 cells is promising, but certainly preliminary and not indicative of the chemistry's practical utility for a forensic epigenetic application. The preponderance of cellular mixtures used for forensic epigenetic analyses originate from blood samples containing a variety of contributions including red and white blood cells, platelets, and plasma. For forensic identification, DNA purification by a gold-standard silica process is purported to isolate the NA material away from potential inhibitors, such as hemoglobin and immunoglobulin G that would adversely affect amplification via diminished polymerase activity, and fluorescent molecule/single-stranded DNA binding.[35]

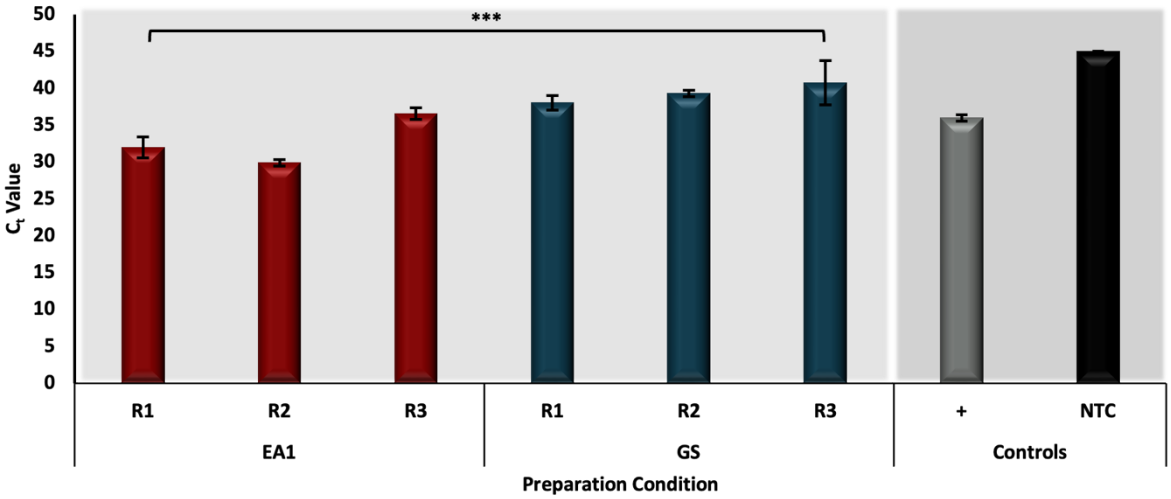

Figure 3-11. Relative DNA recovery with aqueous blood samples. A comparison of C_t values post extraction and bisulfite conversion by the enzymatic and gold-standard methods indicates increased recovery and variability between technical replicates by the enzymatic method.

The results from an initial study using aqueous blood samples to compare the EA1 method with a solid-phase approach, both coupled with epigenetic conversion, is shown in **Figure 3-11.** Triplicate analysis demonstrated statistical differences between preparation conditions (unpaired *t*-test, $\alpha = 0.05$, *p*-value = 0.0001). Similar to previous testing with non-methylated standards and K-562 cells, results demonstrated increased DNA recovery at this locus compared to the gold-standard method; average C_t values derived from EA1 and GS prepared samples were ~32.82 and ~39.36, respectively. However, there was a slight increase in variation between extraction replicates prepared by the enzymatic method, as the average standard deviation increased ~0.796 units for EA1 preparations. Regarding conversion efficiency, no statistical differences emerged from an unpaired *t*-test comparing all T_m values ($\alpha = 0.05$, *p*-value = 0.323), data not shown. In essence, a first pass at testing blood samples indicated increased DNA recovery with EA1, but perhaps resulting in increased stochasticity between sample replicates as well.

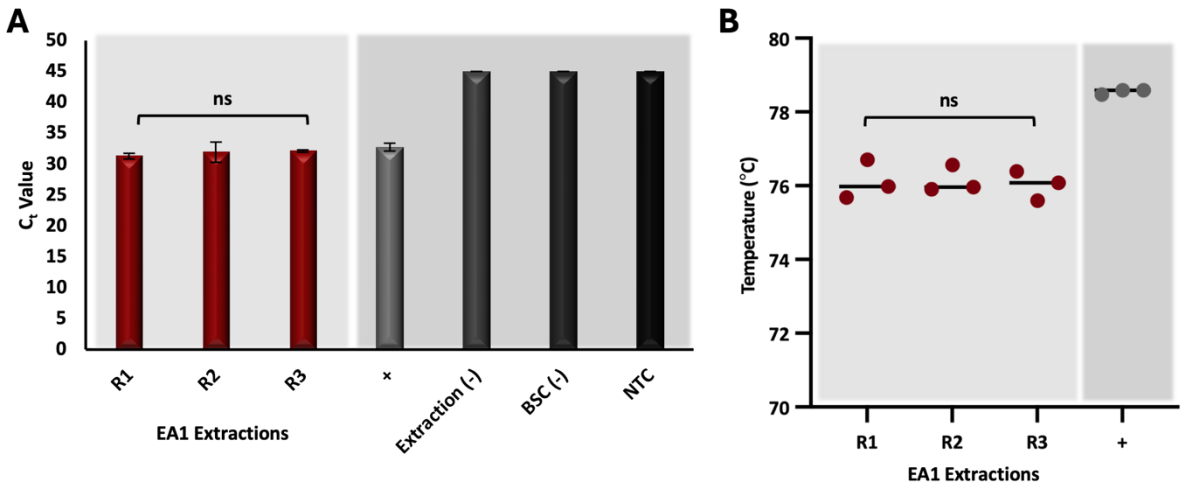

Figure 3-12. Coupling enzymatic extraction with epigenetic conversion using blood samples. (A) A comparison of C_t values post extraction and bisulfite conversion by the enzymatic method indicates consistent performance between replicates. (B) T_m values also demonstrate no differences in conversion efficiency between technical replicates.

The potential for variable performance with enzymatic lysis was addressed with additional replicate testing. For context, it was determined after testing the blood samples portrayed in **Figure 3-11** that the large-volume blood aliquots were subject to several freeze-thaw cycles, likely contributing to irregular cellular lysis and DNA degradation.[36] Thus, freshly prepared blood samples were extracted in triplicate by EA1 in a follow-up experiment. **Figure 3-12** shows the resultant C_t and T_m values, both of which demonstrate no statistical differences between technical replicates (One-way ANOVAs, α = 0.05, *p*-values = 0.707 and 0.070, respectively). Taken into context with previous results, extraction of blood samples with EA1 confirmed compatibility of the method with forensically-relevant cell types and matrices slated for epigenetic analyses, at least as it relates to RT-PCR and HRM analyses. Furthermore, the results showed selection of this method would result in increased DNA recovery and comparable conversion efficiency compared to a gold-standard approach, a feature that would improve epigenetic prediction accuracy.

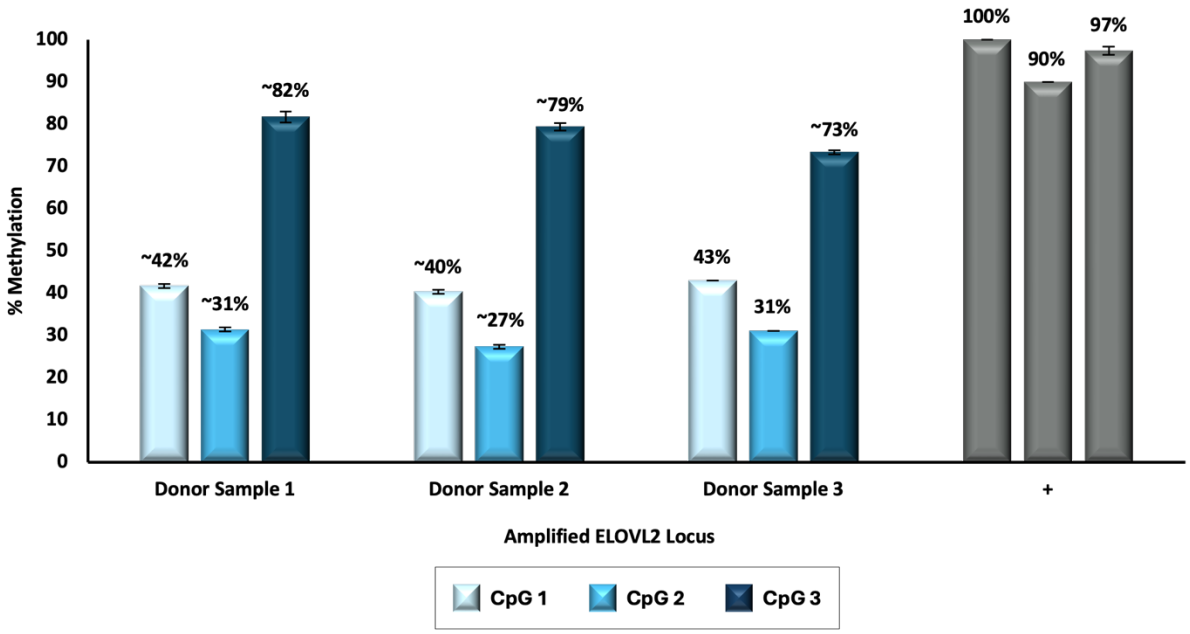

Figure 3-13. Compatibility with pyrosequencing. Average methylation levels across three age-related CpG sites from peripheral blood across three donors, along with a methylated and bisulfite-converted positive control standard.

Interestingly, the presumably "damaged" samples showed increased variability in terms of DNA recovery (**Fig. 3-11**), which indicated to us that the enzymatic method may not perform to its full potential in differentially degraded samples, such as those that would be encountered in a forensic setting. However, in considering all of the data, the demonstrated variation was increased compared to samples prepared by the silica method, but by less than 1 C_t unit overall.

To assess compatibility with downstream pyrosequencing, the most ubiquitously used method for forensic age approximation, replicates extracted by the EA1 method and converted downstream were examined via the ELOVL2 locus. The ELOVL2 region is the most rigorously evaluated epigenetic marker as it relates to human age prediction, and has demonstrated prediction with degraded bloodstains and a variety of other tissues.[21] Herein, three CpG sites along the locus are examined according to an assay designed by Piekarska et al.[21] and validated by Kampmann and others.[22] **Figure 3-13** shows the estimated methylation levels (percentages)

Sample Conditions		CpG 1 (%)	CpG 2 (%)	CpG 3 (%)	Sample Conditions		CpG 1 (%)	CpG 2 (%)	CpG 3 (%)
Donor Sample 1	Extract 1	42	31	80	Donor Sample 3	Extract 1	43	31	73
	Extract 2	41	32	83		Extract 2	43	31	73
	Extract 3	42	31	82		Extract 3	43	31	74
Averages		41.66667	31.33333	81.666667	Averages		43	31	73.333333
Std. Dev.		0.471405	0.471405	1.2472191	Std. Dev.		0	0	0.4714045
Donor Sample 2	Extract 1	40	27	80	100% Methylated Controls	+	100	90	96
	Extract 2	40	28	78		+	100	90	98
	Extract 3	41	27	80		+	100	90	98
Averages		40.33333	27.33333	79.333333	Averages		100	90	97.333333
Std. Dev.		0.471405	0.471405	0.942809	Std. Dev.		0	0	0.942809

Table 3-2. Percent methylation of each technical replicate. Individual methylation level estimations from the PyroMark Q48 Software.

for each variable position from venous blood originating from a total of three donors, as well as for a methylated and bisulfite converted positive control. While a comparison of donor age to methylation status could not be made for privacy reasons, the data does suggest high DNA recovery, as all replicates "passed" analysis using the instrument software. Furthermore, very low standard deviations are calculated between replicates of each extract, suggesting uniformity of workflow performance and indicating compatibility with pyrosequencing for age approximation. Exact figures associated with each replicate are detailed in **Table 3-2**.

3.3.6. Reducing EA1 Reaction Intervals for Microfluidic Integration. Toward ultimate microfluidic integration upstream of epigenetic conversion, further shortening of the already significantly abbreviated incubations with the EA1 method was investigated. Reducing heated incubation times prior to microfluidic incorporation is advantageous, as prolonged heating on-disc increases the likelihood of device failure by multiple modes, including delamination, PSA failure, PTFE membrane stress, and fluid loss through previously closed channels overcome with pressure from

thermal pumping. This is especially the case for large volume reaction chambers that may put more stress on the device as a whole. As an adage, further shortening incubation intervals decreases total sample preparation time; as time is of the essence in forensic use cases, further reducing total analytical time is always in favor.

Enzymatic conversion consists of two heated incubations, based upon the optimal activation and thermal denaturation temperatures associated with the EA1 proteinase.[37] Coolbear et al. describe the enzyme activity of EA1 based upon temperature, reporting the activation energy for EA1 to be approximately 70 KJ/mol at 75°C.[37] Likewise, Saul et al. demonstrate rapid activity loss for EA1 subjected to incubation at 95°C, indicating the enzyme may be denatured so as not to hinder amplification downstream.[30] While publication- and standard operating procedure-based protocols vary regarding incubation times, the most rapid approach suggests incubations at 75°C and 95°C for 5 minutes each.[33] Furthermore, in Chapter 4, we demonstrate that these incubation times can be further reduced for the lysis of SARS-CoV-2 virions and that it is possible to remove the 75°C without significant repercussion to NA recovery.[38,27]

Extraction Condition	Enzymatic Lysis		Enzyme Denaturation	
	Temperature	Time	Temperature	Time
Condition 1	75 °C	300 s	95 °C	300 s
Condition 2	75 °C	60 s	95 °C	60 s
Condition 3	75 °C	60 s	95 °C	30 s
Condition 4	75 °C	0 s	95 °C	30 s
Condition 5	75 °C	0 s	95 °C	15 s

Table 3-3. EA1 extraction conditions. A total of five conditions are tested, with condition 1 being the most rapid recommendation protocol, and condition 5 being the least conservative in terms of enzyme efficiency and denaturation.

Herein, comparative results for blood samples extracted by EA1 under various incubation conditions are demonstrated in terms of relative DNA recovery and conversion efficiency. Different incubation conditions are outlined in **Table 3-3** and range drastically from a

total time of 10 min (600 s) with *Condition 1* and only 15 s at 95°C with *Condition 5*. The amplification results from liquid blood samples extracted by each condition are demonstrated in **Figure 3-14**; C_t value differences were demonstrated across conditions (One-way ANOVA, α = 0.05, *p*-value = 0.0006) and ranged from 29.65 to 34.15. Overall, this indicates encouraging results that enzymatic extraction from blood is possible in only 15 s without a meaningful difference in DNA recovery. For *optimal* performance, the lowest units were observed with conditions 1 and 2 which showed no significant differences overall (unpaired *t*-test, α = 0.05, *p*-value = 0.842), however, a much more drastic variation between replicates was observed with condition 1 parameters. These data are more clearly illustrated in **Figure 3-14A** when compared with other recovery plots, as the individual data points have been included. Perhaps the more interesting data as it relates to the enzymatic chemistry and the reduction of incubation intervals is depicted

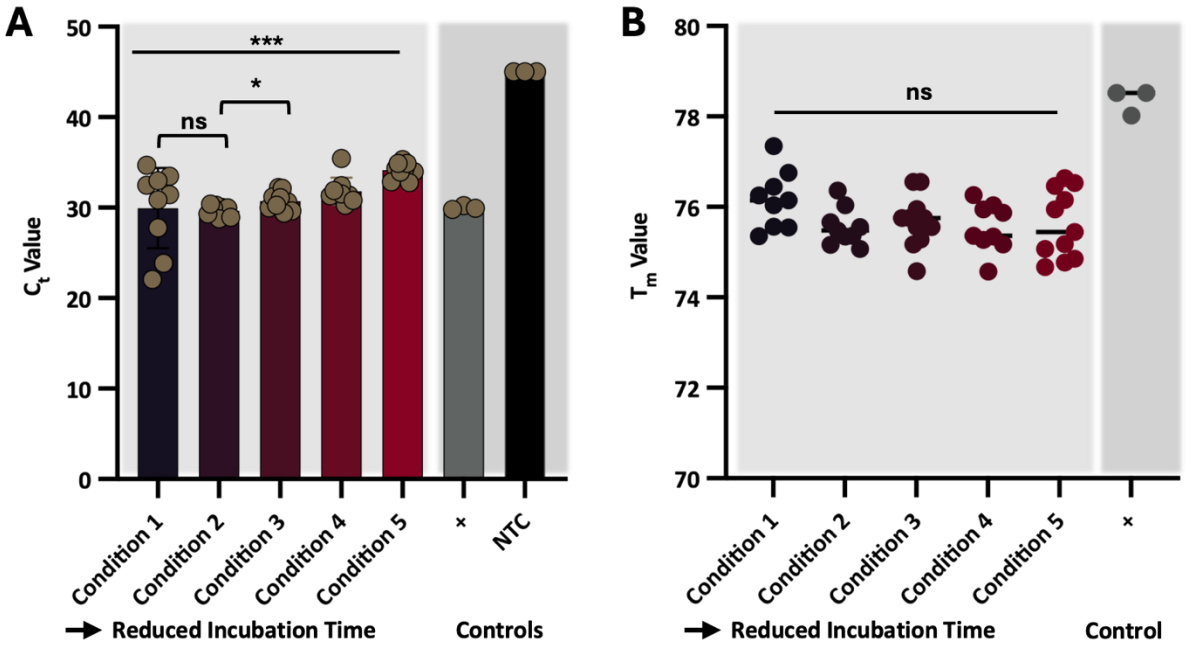

Figure 3-14. Relative recovery and conversion efficiency following altered extraction conditions with liquid blood samples. (A) C_t and (B) T_m values originating from enzymatic extraction protocols ranging from 10 min with condition 1 to only 15 s with condition 5.

in **Figure 3-14B**. The melt temperatures of amplicons indicate that even with 15 s extractions by the enzymatic method, bisulfite conversion efficiency is not altered in a statistically impactful way (One-way ANOVA, $\alpha = 0.05$, *p*-value = 0.174). This may indicate that "pure" DNA is not necessarily required for efficient conversion by bisulfite, at least so far as the sulphonation and deamination step is concerned.

The results demonstrated with liquid blood samples are promising, but perhaps not representative of the functionality of the method for its intended application, as liquid blood is rarely tested in forensic laboratories. Thus, **Figure 3-15** illustrates replicated experimental conditions, but with blood deposited onto nylon-flocked swabs. Nylon-flocked swabs were selected over cotton or rayon alternatives as they exhibit better sample release and less entrapment, and because they are available in sizes more amenable to microfluidic

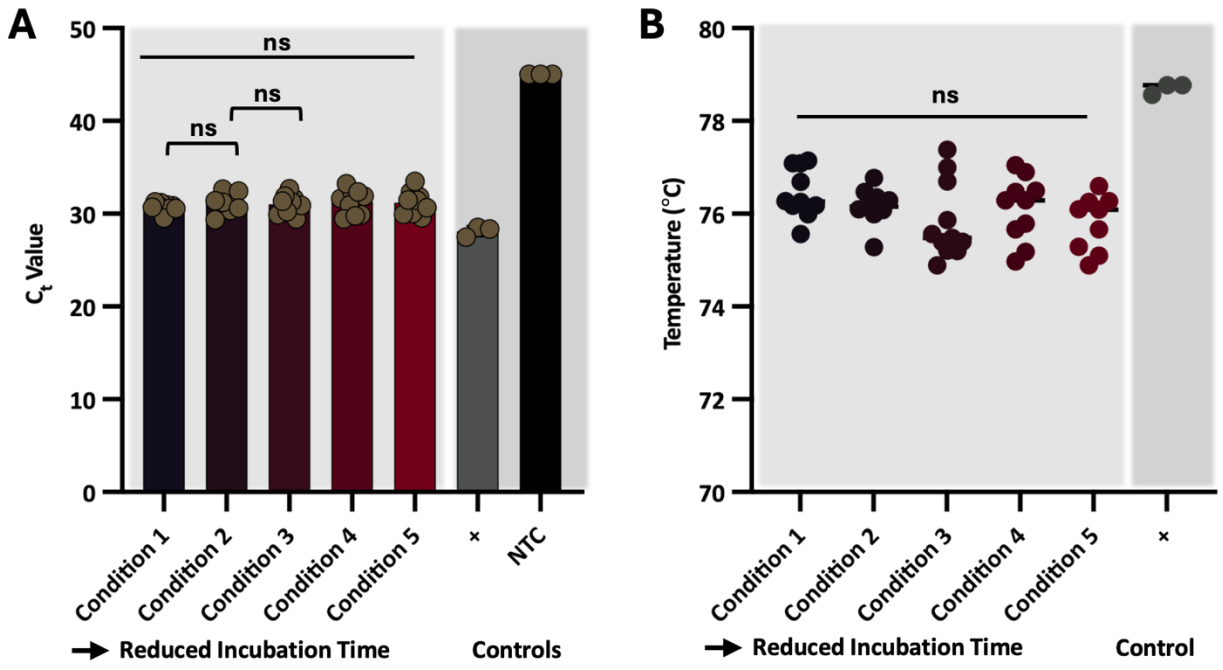

Figure 3-15. Relative recovery and conversion efficiency following altered extraction conditions with blood swabs. (A) C_t and (B) T_m values from extracted blood swabs with reduced incubation times.

incorporation.[39] Enzymatic extraction with swabs performed consistently across all sample replicates and conditions (**Fig. 3-15A**) (One-way ANOVA, α = 0.05, *p*-value = 0.831), providing additional evidence that incubation times may be shortened significantly. Likewise, conversion of the FHL2 target remained consistent in terms of T_m value across each extraction condition (**Fig. 3-15B**) (One-way ANOVA, α = 0.05, *p*-value = 0.159), supporting the hypothesis that epigenetic conversion is successful without silica-facilitated purification.

3.3.7. A Microfluidic Approach to Integrated Epigenetic Sample Preparation. With sufficient data suggesting the compatibility of an enzyme-based DNA extraction method and downstream bisulfite conversion, a microfluidic disc was designed to couple these processes in an automated fashion. Herein, testing of the architecture as it relates to the extraction and lysate metering

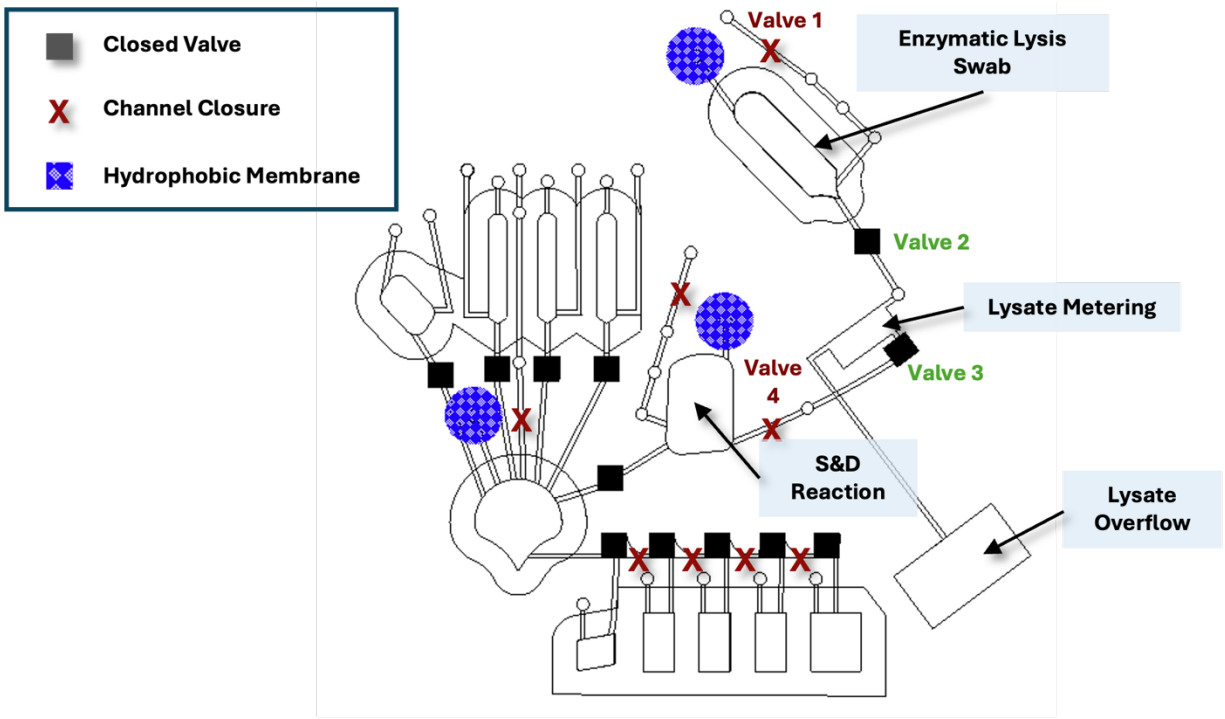

Figure 3-16. Proposed microfluidic architecture for epigenetic sample preparation. AutoCAD rendering of one sample domain that includes architectural features for integrated enzymatic extraction and dynamic solid phase bisulfite conversion

portions of the workflow is completed, with an emphasis on colorimetric dye studies and analytical performance, as before.

3.3.7.1. On-Disc Colorimetric Dye Studies. An integrated microfluidic workflow coupling enzymatic NA extraction and epigenetic conversion by bisulfite is proposed in **Figure 3-16**. The core architecture enabling conversion was adapted from previous work,[19] with additional features to permit direct-from-swab enzymatic lysis. To prevent issues associated with stochastic sampling on-disc, extraction architecture was designed to house both the swab and a total volume of at 50 µL with the help of PMMA constructed chambers. Beyond the swab chamber, features that enabled precise lysate metering and overflow chambers for off-disc comparative analysis were incorporated.

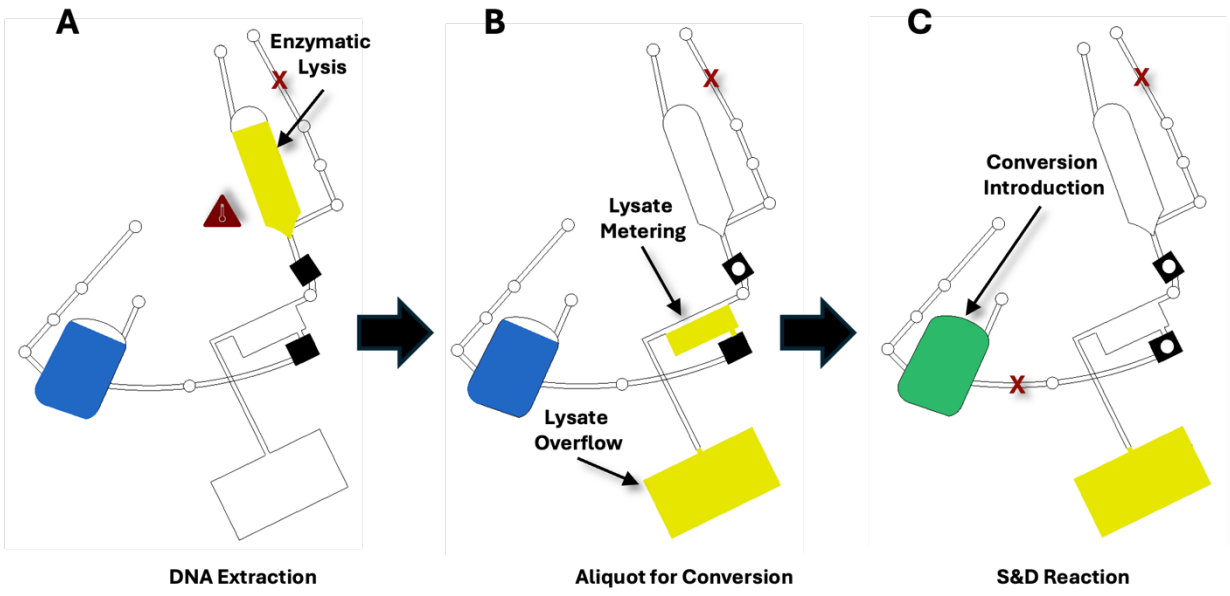

Figure 3-17. Proposed architecture for enzymatic extraction and lysate metering into conversion. Schematic depicting the fluidic workflow from enzymatic lysis to conversion introduction.

The ‘on-disc’ chemical workflow is depicted in **Figure 3-17**, whereby the extraction cocktail, also referred to as “lysate” post-heating, is represented by yellow dye and ammonium bisulfite is represented by blue dye. Following heating of the extraction cocktail and valve actuation to introduce the lysate into the metering chamber, 2 µL of lysate is introduced into the conversion chamber for sulphonation and deamination, represented in green. The reliability of the metering architecture to deliver precisely 2 µL of lysate is essential to ensure reproducible DNA recovery and device performance. To quantitatively estimate that performance, dye studies were completed along with corresponding image analysis to estimate the hue shifts as yellow dye, or lysate, was introduced into blue dye, (i.e., ammonium bisulfite). To estimate the volume of yellow dye metered into blue dye, a standard curve (**Fig 3-18A**) was constructed from hue measurements taken from serially diluted dye standards ranging from 0% to 10% yellow dye. The standard curve showed a strong linear correlation (R^2 = ~0.979 in the relevant analytical range.

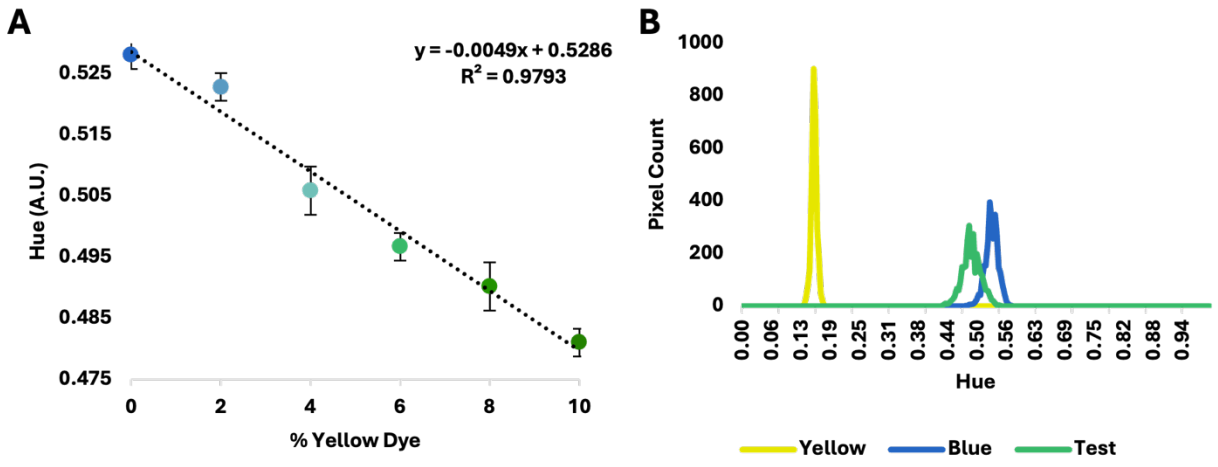

Figure 3-18. Colorimetric dye study to estimate lysate metering volume. (A) Calibration curve of hue against percentage of yellow dye solution mixed with blue dye solution and used to determine the volume of lysate metered into the conversion chamber. (B) Line graph depicting the hue of yellow and blue control dye solutions and the mixed solutions resulting from microfluidic introduction of the lysate (yellow) into the ammonium bisulfite solution (blue).

The normalized hue of the dye mixture post-metering was approximately 0.490 ± 0.004, compared to the normalized hue for blue alone, it was extrapolated that approximately 7.838% of the mixture consisted of yellow dye, deviating only 0.142% from the expected percentage (**Fig 3-18B**). These data were further used to calculate the volume of yellow dye metered into the corresponding chamber for conversion to be ~2.039 μL. Colorimetric results confirmed the metering architecture was dispensing the desired volume of lysate for conversion.

3.3.7.2. On-Disc Analytical Performance. To evaluate microdevice performance in terms of enzymatic DNA lysis, swabs containing donor blood were enclosed into requisite swab chambers and heated with an external mechatronic system. In the trade-off between DNA recovery and rapid extraction, *condition 3* parameters were selected (recall **Table 3-3**), to provide sufficient ramp time for the system and reaction fluid to reach target temperatures while protecting the integrity of the disc, as delamination around chambers has been known to occur

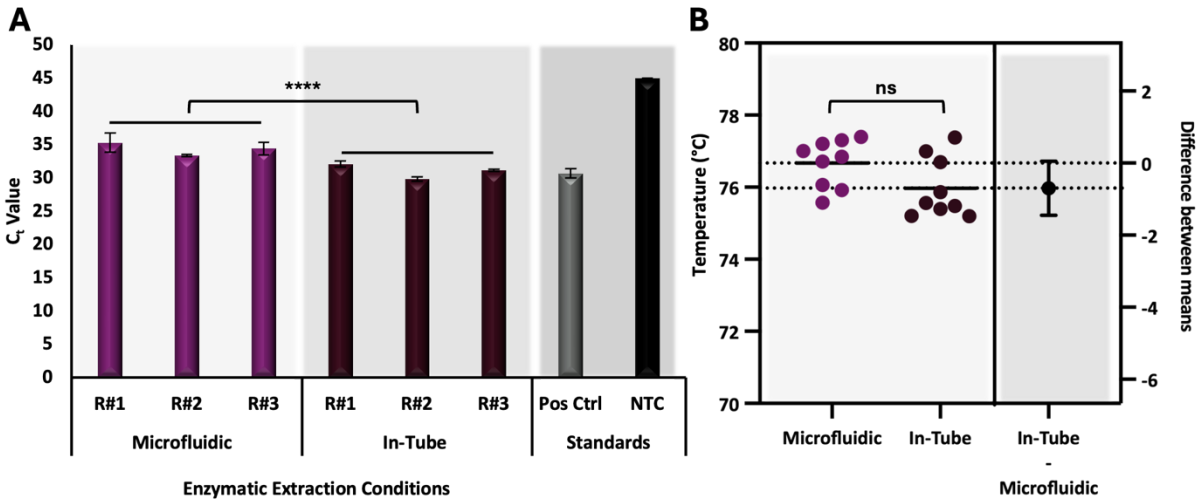

Figure 3-19. Microfluidic performance compared to in-tube extraction by EA1. (A) C_t and (B) T_m values from extracted blood swabs with the microfluidic system and in-tube, using incubations of 75°C for 1 min and 95°C for 30 s.

with PCL discs when held at high temperatures (i.e., 95°C)[40]. **Figure 3-19A** depicts relative C_t values and a significant statistical difference (unpaired *t*-test, α = 0.05, *p*-value = <0.0001) between samples extracted using the microfluidic method compared to the in-tube enzymatic approach. In total, C_t values increased an average of 3.340 ± 0.568 units for eluates resulting from the microfluidic mode, indicating that DNA recovery decreased slightly. The reduction in recovery was attributed to a microfluidic failure mode whereby the pressure from thermal pumping when heating to 95°C resulted in fluid loss through a downstream valve and into the lysate overflow chamber. Still, this loss in recovery had no effect on the conversion efficiency of downstream conversion, as evidenced by the T_m values detailed in **Figure 3-19B**, which show no statistical differences between approaches (unpaired *t*-test, α = 0.05, *p*-value = <0.066). Additional confirmation of only one FHL2 amplicon of similar length was confirmed with downstream electrophoresis. **Figure 3-20** shows the electrophoretic peaks associated with three products resulting from the microfluidic workflow (**Fig. 3-20A**) and one positive control (**Fig. 3-20B**). Upper and lower markers indicate successful separation and sizing, and the presence of only one high

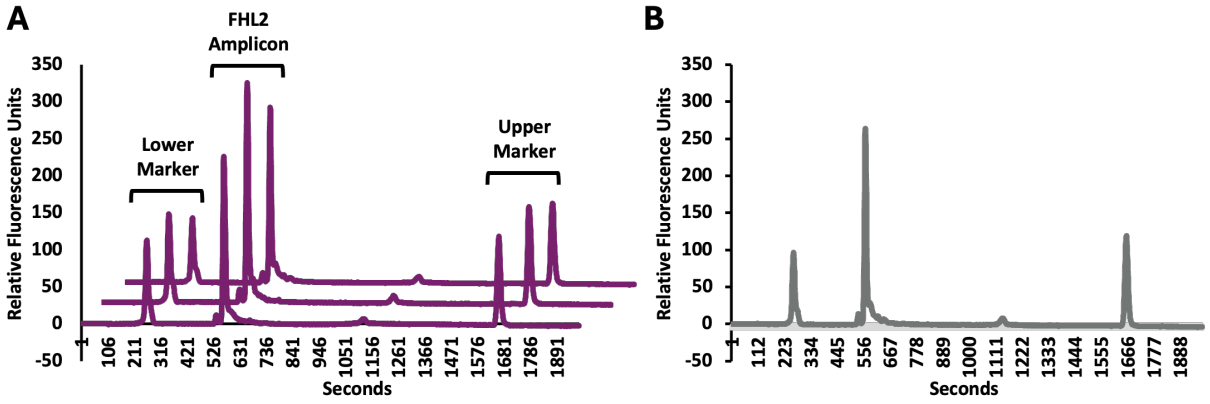

Figure 3-20. Electrophoretic separation of amplicons resulting from microfluidic extraction. FHL2 amplicons ranging from 128 to 131 base pairs for (A) samples prepared on-disc and a positive control. Only one representative replicate of three is shown for donor sample and methylation control.

amplicon peak above the analytical threshold. Average peak heights of extracted samples were 129 ± 0.943, close enough to the 133 bp amplicon length expected for FHL2, since instrument sizing resolution for amplicons from 50 – 600 bp are expected to have a variance of ± 10%.[41]

Results from pyrosequencing of three relevant CpGs in the ELOVL2 region following on-disc extraction of blood demonstrate compatibility of the EA1 extraction method with this technique (**Fig. 3-21**). However, results are variable between replicates with lower methylation percentages reported for extract 1 compared to extracts 2 and 3. Overall, the Q48 software flagged extracts originating from replicates 1 and 2 yellow, while peaks from replicate 3 were flagged red and reported warnings including *low peak height* and *uncertainty due to baseline drift*. Furthermore, there was some variation between the predicted methylation percentages at each CpG across extracts, with extract 3 showing a significant standard deviation in CpG 2. Recall that extract 3 was flagged red, making % methylation calls by the software "uncertain." For comparative purposes, it is important to look to the variation between replicates for standards

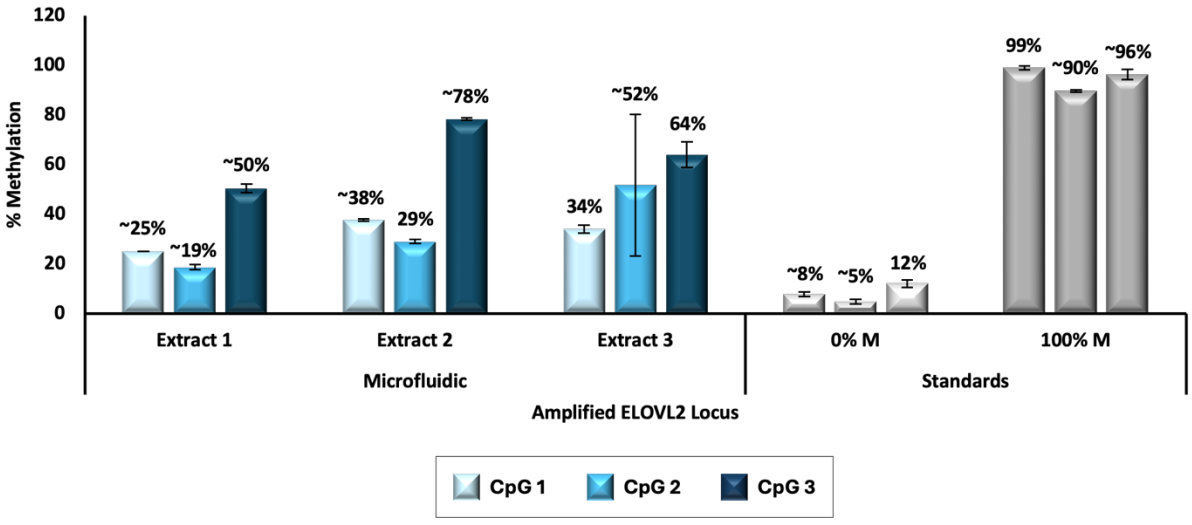

Figure 3-21. Microfluidic compatibility with pyrosequencing. Average methylation levels across three age-related CpG sites from peripheral blood from one donor (n = 3), along with a methylation controls of fully non-methylated or methylated genomic DNA.

prepared with 0% and 100% methylation statuses whereby system predications swing from a difference of 1% to 12% depending upon the CpG site. Therefore, it may be appropriate to develop some kind of correction factor. Nevertheless, the differences between extracts is apparent and may be attributed to inhibition caused by leaching disc materials. The potential for this phenomenon is discussed further in Chapter 5.

3.3.7.3. Toward A Fully-Integrated and Multiplexed Method. Ongoing work is focused on validated the integrated workflow on-disc; that is, performing complete sample preparation from swab-to-converted-eluate. To this end, a new disc design has been proposed, aimed at increasing the ease with which the disc is fabricated, increasing the multiplex capacity, and enhancing the

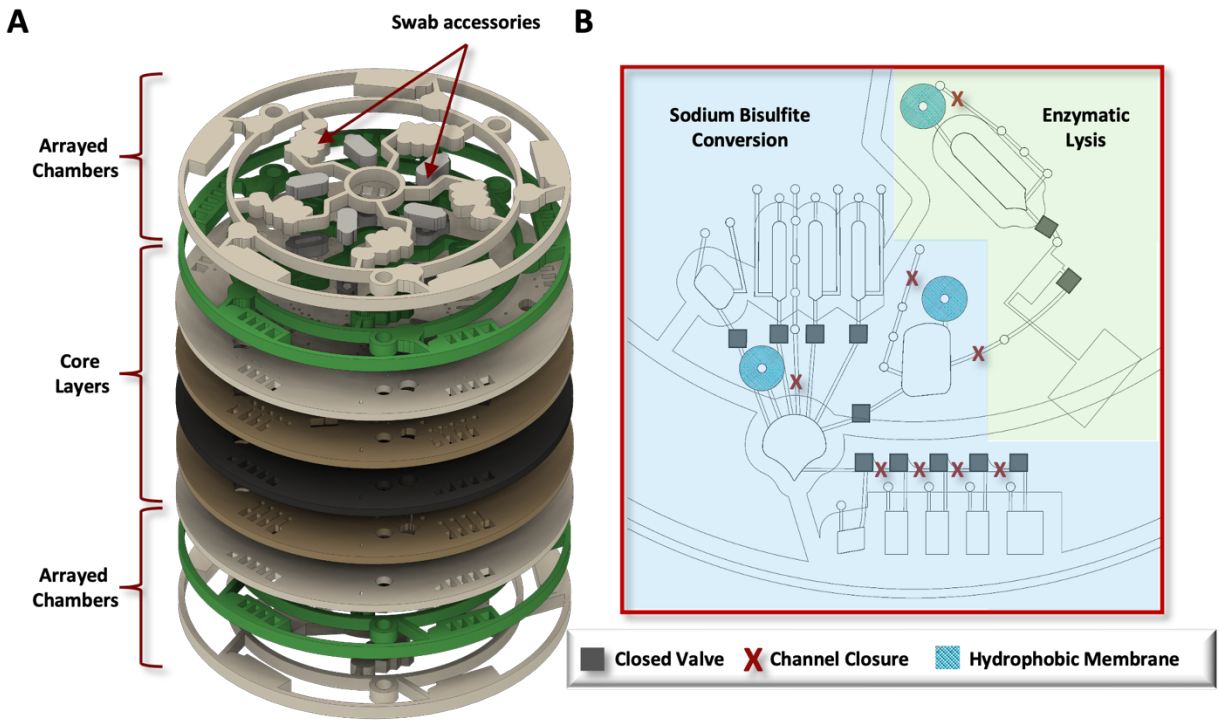

Figure 3-22. Multiplexed microfluidic architecture for epigenetic sample preparation. (A) AutoCAD rendering of exploded disc layers, including the arrayed PMMA accessory chambers. (B) Schematic delineating the enzymatic lysis and bisulfite conversion architectural details.

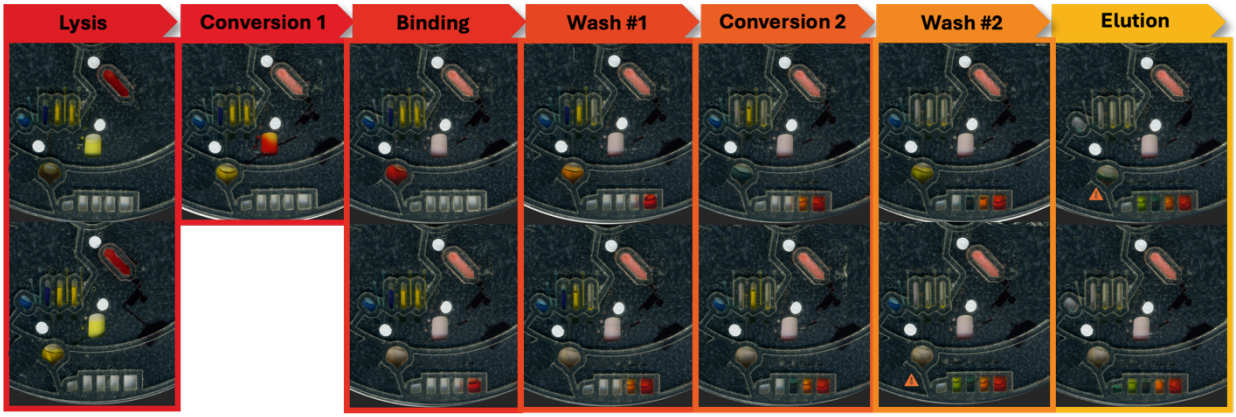

Figure 3-23. Fluidic dye study for integrated disc. Digital scans following the progression of one representative dye study, beginning with direct-from-swab enzymatic lysis and ending with DNA elution of the converted extract.

stability of the disc for optimal performance. **Figure 3-22** displays the multi-layered disc, featuring PMMA chambers and scaffolding to be installed on both the top and bottom of the device. The addition of PMMA to both sides of the device increases the z-height of each chamber significantly to enable the narrowing of each fluidic 'domain' to allow for the incorporation of an addition reaction unit. With this change, a total of five domains are incorporated to allow for three sample replicates and a positive and negative control per reaction disc. The PMMA chambers have been added to a series of concentric rings to act as scaffolding, permitting disc stability with heated incubations and ease of fabrication; rather than placing individual chambers to the disc all architecture may be aligned in one step (**Fig. 3-22A**). The scaffolding details are designed strategically to avoid overlap with loading vents and valves, hydrophobic membrane patches, and valves, as shown in **Figure 3-22B**. To ensure functionality in terms of fluid flow, valve performance, magnetic mixing, etc., a dye study was completed. The full fluidic workflow can be traced in **Figure 3-23**. Notably, the disc demonstrated consistent performance across domains with visual

confirmation of fluid flow, metering from the enzymatic lysis swab chamber, magnetic bead actuation and retention, and waste disposal.

3.4. Conclusions

Conventional epigenetic sample preparation consists of two laborious analytical workflows, DNA extraction and epigenetic conversion by bisulfite, known to result in significant DNA loss. For an application in forensic genetics, whereby starting material is known to be fragmented and in low abundance generally, the additional loss can be extremely detrimental to the predictive outcome. Previously, I demonstrated the success of a rotationally-driven microfluidic disc aimed to reduce the burden associated with bisulfite conversion and work toward increasing DNA recovery via microfluidic intervention.[19] In this chapter, the focus was placed on DNA extraction; more specifically, the conventional "gold-standard" method for DNA extraction and subsequent purification was supplanted by an enzymatic approach with the neutral protease EA1. To the author's knowledge, this was the first account of the coupling of enzymatic extraction by EA1 and conversion by bisulfite. Experiments demonstrated that, in comparison to the EA1 approach, approximately 26% of DNA was lost to extraction by the conventional method, whether the standards in question are heavily methylated or not. Testing also confirmed that extraction by EA1 is compatible with downstream conversion and detection by RT-PCR, HRM, and pyrosequencing of forensically-relevant targets across standards, cloned cells, and peripheral blood samples. Likewise, that the 'non-purified' elates did not result in any changes to conversion efficiency when compared to those prepared by the gold-standard method. Success by RT-PCR and HRM was also demonstrated with reduced incubation times, indicating extraction and

successful conversion is still possible following only 15 s of incubation with EA1. Finally, a microfluidic architecture is described to couple direct-from-swab lysis with downstream conversion. The extraction process is tested via colorimetric dye studies indicating proper fluid flow and precise metering across replicates. Likewise, samples are extracted from swabs in only 90 s with minimal differences in recovery and electrophoretic evidence of target specificity. Pyrosequencing results were variable across replicates and require further optimization. Toward validation of the fully-integrated disc, a 5-plex disc was designed for ease of fabrication and increase fluid capacity that has already demonstrated success in terms of fluid flow.

3.5. Acknowledgements

I would like to acknowledge the National Institute of Justice (NIJ), U.S. Department of Justice (DOJ) for the Graduate Research Fellowship support (2020-R2-CX-0030), the Forensic Sciences Foundation, Inc. for the Jan S. Bashinski Criminalistics Graduate Thesis Grant, the University of Virginia (UVA) Graduate School of Arts and Sciences Council for the Research Grant, and the Achievement Rewards for College Scientists (ARCS) Foundation for Fellowship support. I would also like to recognize the International Society for Forensic Genetics (ISFG), the International Society for Applied Biological Sciences (ISABS) and the University of Virginia for their acknowledgement and support of this work.

3.6. References

(1) Butler, J. M. *Advanced Topics in Forensic DNA Typing: Methodology*; Elsevier/Academic Press: Walthan, MA, 2012.

(2) Kayser, M. Forensic DNA Phenotyping: Predicting Human Appearance from Crime Scene Material for Investigative Purposes. *Forensic Science International: Genetics* **2015**, *18*, 33–48. https://doi.org/10.1016/j.fsigen.2015.02.003.

(3) Schneider, P. M.; Prainsack, B.; Kayser, M. The Use of Forensic DNA Phenotyping in Predicting Appearance and Biogeographic Ancestry. *Deutsches Aerzteblatt Online* **2019**. https://doi.org/10.3238/arztebl.2019.0873.

(4) Kayser, M.; Branicki, W.; Parson, W.; Phillips, C. Recent Advances in Forensic DNA Phenotyping of Appearance, Ancestry and Age. *Forensic Science International: Genetics* **2023**, *65*, 102870. https://doi.org/10.1016/j.fsigen.2023.102870.

(5) Vidaki, A.; Kayser, M. Recent Progress, Methods and Perspectives in Forensic Epigenetics. *Forensic Science International: Genetics* **2018**, *37*, 180–195. https://doi.org/10.1016/j.fsigen.2018.08.008.

(6) Williams, G.; Horn, B. Forensic Epigenetics Methods and Applications. In *Epigenetics Methods*; Elsevier, 2020; pp 647–669. https://doi.org/10.1016/B978-0-12-819414-0.00031-8.

(7) Vidaki, A.; Kayser, M. From Forensic Epigenetics to Forensic Epigenomics: Broadening DNA Investigative Intelligence. *Genome Biol* **2017**, *18* (1), 238. https://doi.org/10.1186/s13059-017-1373-1.

(8) Li, C.; Zhang, S.; Que, T.; Li, L.; Zhao, S. Identical but Not the Same: The Value of DNA Methylation Profiling in Forensic Discrimination within Monozygotic Twins. *Forensic Science International: Genetics Supplement Series* **2011**, *3* (1), e337–e338. https://doi.org/10.1016/j.fsigss.2011.09.031.

(9) Kaur, G.; Begum, R.; Thota, S.; Batra, S. A Systematic Review of Smoking-Related Epigenetic Alterations. *Arch Toxicol* **2019**, *93* (10), 2715–2740. https://doi.org/10.1007/s00204-019-02562-y.

(10) Freire-Aradas, A.; Phillips, C.; Lareu, M. V. Forensic Individual Age Estimation with DNA: From Initial Approaches to Methylation Tests. *Forensic Sci Rev* **2017**, *29* (2), 121–144.

(11) Vogelstein, B.; Gillespie, D. Preparation and Analytical Purification of DNA from Agarose. *PNAS* **1979**, *76* (2), 615–619. https://doi.org/10.1073/pnas.76.2.615.

(12) Katevatis, C.; Fan, A.; Klapperich, C. M. Low Concentration DNA Extraction and Recovery Using a Silica Solid Phase. *PLoS ONE* **2017**, *12* (5), e0176848. https://doi.org/10.1371/journal.pone.0176848.

(13) Shapiro, R.; Servis, R.; Welcher, M. Reactions of Uracil and Cytosine Derivatives with Sodium Bisulfite. A Specific Deamination Method. *Journal of American Chemical Society 92* (2).

(14) Tanaka, K.; Okamoto, A. Degradation of DNA by Bisulfite Treatment. *Bioorganic & Medicinal Chemistry Letters* **2007**, *17* (7), 1912–1915. https://doi.org/10.1016/j.bmcl.2007.01.040.

(15) Darst, R. P.; Pardo, C. E.; Ai, L.; Brown, K. D.; Kladde, M. P. Bisulfite Sequencing of DNA. *CP Molecular Biology* **2010**, *91* (1). https://doi.org/10.1002/0471142727.mb0709s91.

(16) Gai, W.; Sun, K. Epigenetic Biomarkers in Cell-Free DNA and Applications in Liquid Biopsy. *Genes* **2019**, *10* (1), 32. https://doi.org/10.3390/genes10010032.

(17) Bhoyar, L.; Mehar, P.; Chavali, K. An Overview of DNA Degradation and Its Implications in Forensic Caseworks. *Egypt J Forensic Sci* **2024**, *14* (1), 15. https://doi.org/10.1186/s41935-024-00389-y.

(18) Turiello, R.; Nouwairi, R. L.; Landers, J. P. Taking the Microfluidic Approach to Nucleic Acid Analysis in Forensics: Review and Perspectives. *Forensic Science International: Genetics* **2023**, *63*, 102824. https://doi.org/10.1016/j.fsigen.2022.102824.

(19) Turiello, R.; Nouwairi, R. L.; Keller, J.; Cunha, L. L.; Dignan, L. M.; Landers, J. P. A Rotationally-Driven Dynamic Solid Phase Sodium Bisulfite Conversion Disc for Forensic Epigenetic Sample Preparation. *Lab Chip* **2024**, *24* (1), 97–112. https://doi.org/10.1039/D3LC00867C.

(20) Hamano, Y.; Manabe, S.; Morimoto, C.; Fujimoto, S.; Ozeki, M.; Tamaki, K. Forensic Age Prediction for Dead or Living Samples by Use of Methylation-Sensitive High Resolution Melting. *Legal Medicine* **2016**, *21*, 5–10. https://doi.org/10.1016/j.legalmed.2016.05.001.

(21) Zbieć-Piekarska, R.; Spólnicka, M.; Kupiec, T.; Parys-Proszek, A.; Makowska, Ż.; Pałeczka, A.; Kucharczyk, K.; Płoski, R.; Branicki, W. Development of a Forensically Useful Age Prediction Method Based on DNA Methylation Analysis. *Forensic Science International: Genetics* **2015**, *17*, 173–179. https://doi.org/10.1016/j.fsigen.2015.05.001.

(22) Kampmann, M.-L.; Fleckhaus, J.; Børsting, C.; Jurtikova, H.; Piters, A.; Papin, J.; Gauthier, Q.; Ghemrawi, M.; Doutremepuich, C.; McCord, B.; Schneider, P. M.; Drabek, J.; Morling, N. Collaborative Exercise: Analysis of Age Estimation Using a QIAGEN Protocol and the PyroMark Q48 Platform. *Forensic Sciences Research* **2024**, *9* (1), owad055. https://doi.org/10.1093/fsr/owad055.

(23) Thompson, B. L.; Ouyang, Y.; Duarte, G. R. M.; Carrilho, E.; Krauss, S. T.; Landers, J. P. Inexpensive, Rapid Prototyping of Microfluidic Devices Using Overhead Transparencies and a Laser Print, Cut and Laminate Fabrication Method. *Nat Protoc* **2015**, *10* (6), 875–886. https://doi.org/10.1038/nprot.2015.051.

(24) Garcia-Cordero, J. L.; Kurzbuch, D.; Benito-Lopez, F.; Diamond, D.; Lee, L. P.; Ricco, A. J. Optically Addressable Single-Use Microfluidic Valves by Laser Printer Lithography. *Lab Chip* **2010**, *10* (20), 2680. https://doi.org/10.1039/c004980h.

(25) Woolf, M. S.; Dignan, L. M.; Lewis, H. M.; Tomley, C. J.; Nauman, A. Q.; Landers, J. P. Optically-Controlled Closable Microvalves for Polymeric Centrifugal Microfluidic Devices. *Lab Chip* **2020**, *20* (8), 1426–1440. https://doi.org/10.1039/C9LC01187K.

(26) Dignan, L. M.; Woolf, M. S.; Tomley, C. J.; Nauman, A. Q.; Landers, J. P. Multiplexed Centrifugal Microfluidic System for Dynamic Solid-Phase Purification of Polynucleic Acids Direct from Buccal Swabs. *Anal. Chem.* **2021**, acs.analchem.1c00842. https://doi.org/10.1021/acs.analchem.1c00842.

(27) Turiello, R.; Dignan, L. M.; Thompson, B.; Poulter, M.; Hickey, J.; Chapman, J.; Landers, J. P. Centrifugal Microfluidic Method for Enrichment and Enzymatic Extraction of Severe Acute Respiratory Syndrome Coronavirus 2 RNA. *Anal. Chem.* **2022**, *94* (7), 3287–3295. https://doi.org/10.1021/acs.analchem.1c05215.

(28) DuVall, J. A.; Le Roux, D.; Tsuei, A.-C.; Thompson, B. L.; Birch, C.; Li, J.; Nelson, D. A.; Mills, D. L.; Ewing, M. M.; McLaren, R. S.; Storts, D. R.; Root, B. E.; Landers, J. P. A Rotationally-Driven Polyethylene Terephthalate Microdevice with Integrated Reagent Mixing for Multiplexed PCR Amplification of DNA. *Anal. Methods* **2016**, *8* (40), 7331–7340. https://doi.org/10.1039/C6AY01984F.

(29) Qamar, W.; Khan, M. R.; Arafah, A. Optimization of Conditions to Extract High Quality DNA for PCR Analysis from Whole Blood Using SDS-Proteinase K Method. *Saudi Journal of Biological Sciences* **2017**, *24* (7), 1465–1469. https://doi.org/10.1016/j.sjbs.2016.09.016.

(30) Saul, D. J.; Williams, L. C.; Toogood, H. S.; Daniel, R. M.; Bergquist, P. L. Sequence of the Gene Encoding a Highly Thermostable Neutral Proteinase from Bacillus Sp. Strain EA1: Expression in Escherichia Coli and Characterisation. *Biochimica et Biophysica Acta (BBA) - Gene Structure and Expression* **1996**, *1308* (1), 74–80. https://doi.org/10.1016/0167-4781(96)00074-7.

(31) Moss, D.; Harbison, S.-A.; Saul, D. J. An Easily Automated, Closed-Tube Forensic DNA Extraction Procedure Using a Thermostable Proteinase. *International Journal of Legal Medicine* **2003**, *117* (6), 340–349. https://doi.org/10.1007/s00414-003-0400-9.

(32) Lounsbury, J. A.; Coult, N.; Miranian, D. C.; Cronk, S. M.; Haverstick, D. M.; Kinnon, P.; Saul, D. J.; Landers, J. P. An Enzyme-Based DNA Preparation Method for Application to Forensic Biological Samples and Degraded Stains. *Forensic Science International: Genetics* **2012**, *6* (5), 607–615. https://doi.org/10.1016/j.fsigen.2012.01.011.

(33) Conte, J.; Kishbaugh, J. M.; Baxter, D. J.; Thompson, R.; Pankaj, S.; Chilukuri, R. V. E.; Marshall, P. Developmental Validation of the Forensic GEM Universal Kit for the Extraction of Genomic DNA. *Forensic Genomics* **2022**, *2* (3), 71–80. https://doi.org/10.1089/forensic.2022.0008.

(34) Andersson, L. C.; Nilsson, K.; Gahmberg, C. G. K562—A Human Erythroleukemic Cell Line. *Intl Journal of Cancer* **1979**, *23* (2), 143–147. https://doi.org/10.1002/ijc.2910230202.

(35) Sidstedt, M.; Hedman, J.; Romsos, E. L.; Waitara, L.; Wadsö, L.; Steffen, C. R.; Vallone, P. M.; Rådström, P. Inhibition Mechanisms of Hemoglobin, Immunoglobulin G, and Whole Blood in Digital and Real-Time PCR. *Anal Bioanal Chem* **2018**, *410* (10), 2569–2583. https://doi.org/10.1007/s00216-018-0931-z.

(36) Shao, W.; Khin, S.; Kopp, W. C. Characterization of Effect of Repeated Freeze and Thaw Cycles on Stability of Genomic DNA Using Pulsed Field Gel Electrophoresis. *Biopreservation and Biobanking* **2012**, *10* (1), 4–11. https://doi.org/10.1089/bio.2011.0016.

(37) Coolbear, T.; Eames, C. W.; Casey, Y.; Daniel, R. M.; Morgan, H. W. Screening of Strains Identified as Extremely Thermophilic Bacilli for Extracellular Proteolytic Activity and General Properties of the Proteinases from Two of the Strains. *Journal of Applied Bacteriology* **1991**, *71* (3), 252–264. https://doi.org/10.1111/j.1365-2672.1991.tb04456.x.

(38) Dignan, L. M.; Turiello, R.; Layne, T. R.; O'Connell, K. C.; Hickey, J.; Chapman, J.; Poulter, M. D.; Landers, J. P. An Ultrafast SARS-CoV-2 Virus Enrichment and Extraction Method Compatible with Multiple Modalities for RNA Detection. *Analytica Chimica Acta* **2021**, *1180*, 338846. https://doi.org/10.1016/j.aca.2021.338846.

(39) Bruijns, B. What Are the Limitations and Challenges of Swab-Based DNA Sampling? *Forensic Sciences* **2024**, *4* (1), 76–95. https://doi.org/10.3390/forensicsci4010006.

(40) Dignan, L. M. Microfluidic Integration of Multi-Step Bioanalytical Assays. PhD Dissertation, University of Virginia, Charlottesville, VA 22904, 2022. https://libraetd.lib.virginia.edu/public_view/3b5919687.

(41) Agilent Technologies. *Performance Characteristics of the High Sensitivity DNA Kit for the Agilent 2100 Bioanalyzer System*; Technical Note Publication Number 5990-4417EN; 2016. https://www.agilent.com/cs/library/technicaloverviews/public/5990-4417EN.pdf.

Chapter 4. A Microfluidic Approach to Viral Sample Preparation by Nanoparticle Enrichment and Enzymatic Nucleic Acid Extraction

Publication(s) included in Chapter 4:

- **Turiello, R.**; Dignan, L. M.; Thompson, B.; Poulter, M.; Hickey, J.; Chapman, J.; Landers, J. P. A Centrifugal Microfluidic Method for Enrichment and Enzymatic Extraction of SARS-CoV-2 RNA. *Analytical Chemistry*, 2022, 94 (7), 3287 - 3295. doi: 10.1021/acs.analchem.1c05215.
- *Dignan, L. M. & ***Turiello, R.**; Layne, T. R.; O'Connell, K. C.; Hickey, J.; Chapman, J.; Poulter, M. D.; Landers, J. P. An Ultrafast Sars-Cov-2 Virus Enrichment and Extraction Method Compatible with Multiple Modalities for RNA Detection. *Analytica Chimica Acta*, 2021, 1180. doi: 10.1016/j.aca.2021.338846
- Marshall, J. S.; **Turiello, R.**; Cunha, L. L.; Frazier, E. V.; Hickey, J.; Chapman, J.; Poulter, M. D.; Fehling, H. L.; Landers, J. P. Rapid SARS-CoV-2 Virus Enrichment and RNA Extraction for Efficient Diagnostic Screening of Pooled Nasopharyngeal or Saliva Samples for Dilutions up to 1:100. *Diagnostics*, 2022, 12 (6). doi: 10.3390/diagnostics12061398

*Both contributed equally to this manuscript as co-first authors

4.1. Introduction

Severe acute respiratory syndrome coronavirus 2 (SARS-CoV- 2) was determined to be the causative agent of the COVID-19 pandemic in December of 2019.[1] Since then, the most ubiquitous laboratory method for diagnostic testing and surveillance monitoring has been real-time reverse transcriptase polymerase chain reaction (real-time RT-PCR) amplification of viral

RNA.[2] RT-PCR is recognized as a robust technique with high analytical sensitivity and target specificity; however, detection depends directly on successful upstream RNA isolation from crude samples. In the case of viral pathogens, this involves lysis of virion envelopes followed by purification of the liberated RNA. “Gold-standard” RNA isolation methods require sample incubation with lytic enzymes, followed by RNA purification via flow through a packed column or silica beads suspended in the lysate.[3] While these methods are ostensibly successful, practical challenges remain, including high cost and supply chain limits. Specifically, reliance on a narrow panel of viral nucleic acid (NA) preparation techniques during an epidemiological outbreak is problematic, as the availability of conventional kits may become limited.[4] Furthermore, their time-consuming, labor-intensive workflows require multiple open-tube washing and transfer steps, making many kits susceptible to sample contamination, analyst exposure, and nucleic acid (NA) loss.[5] Thus, complete reliance on gold standard RNA extraction methods may ultimately be detrimental to the effectiveness of surveillance and transmission control due to stalled containment and/or treatment efforts.[6]

Beyond the aforementioned limitations, conventional methods for RNA isolation do not involve a mechanism for upstream virion enrichment, leveraging either centrifugation, nuclease treatment, or affinity capture particles to improve detection sensitivity.[7,8] Enrichment is particularly advantageous for low titer samples in which preconcentration of the target analyte could mean the difference between detection and a negative result.[9] Furthermore, many enrichment methods facilitate the removal of sample matrices, often containing products that may influence sample extraction and hinder detection.[10,11] In essence, inclusion of a method for virion enrichment and matrix removal may increase the effectiveness of RNA extraction and

improve the assay sensitivity. Recently, successful virion enrichment from multiple matrices has been demonstrated using affinity-capture hydrogel Nanotrap particles.[9] Composed of cross-linked polymer networks, these nanoparticles (NPs) are decorated with chemical affinity baits that promote virion capture via interactions with viral surface spike proteins.[12] Nanotrap enrichment, in conjunction with one-step enzymatic extraction, has proved successful in detecting SARS-CoV-2 from clinical nasopharyngeal swabs, surveillance sample mimics, and contrived saliva samples.[13]

To address the shortcomings of conventional RNA isolation, a multiplexed microfluidic centrifugal device (μCD) for expedited, automated virion enrichment and enzymatic extraction of SARS-CoV-2 RNA from clinical samples is proposed.[14] Specifically, on-disc NP-based enrichment is coupled with a rapid, single-step method for virion lysis of PCR-ready RNA.[15,16] Each μCD contains six domains for parallel processing in an enclosed format that mitigates the risk of contamination and analyst exposure to SARS-CoV-2. Reliance on rotationally driven flow eliminates the need for bulky external hardware (e.g., syringe pumps), enabling the creation of smaller, field-forward instrumentation.[17,18] Notably, the NPs are functionalized with iron oxide, allowing for efficient mixing in the system via application of an external, bidirectional rotating magnetic field (bRMF) that facilitates NP "sweeping".[19] Furthermore, active, laser-actuated valving permits both valve opening and channel closures to enable reliable implementation of numerous sequential unit operations.[20] This work demonstrates the compatibility of an optimized method for rapid SARS-CoV-2 sample preparation with full process controls and clinical samples in multiple, clinically relevant matrices.

Additional preliminary research was completed to further position this work for sample-to-answer integration at the point-of-need in one, integrated microfluidic system. While the development of a microfluidic scheme for RT-PCR that integrates with the sample preparation method detailed here is outside of the scope of this dissertation, studies were completed to enable a sample-to-answer workflow that does not require cold-chain storage. That is, amplification reagents were modified and tested so that they might be stored at room temperature, similar to the reagents necessary for enrichment and NA extraction. Likewise, an alternative method for rapid, integrated Nanotrap particle enrichment and enzymatic lysis was tested for its potential for population surveillance by sample pooling. Pooling of samples up to 1:20 were completed here, with collaborative efforts using the same method to show sensitivity with pools of up to 1:100.[21]

4.2. Materials and Methods

4.2.1. Clinical Sample Preparation and Analysis. Nasopharyngeal clinical specimens were collected, prepared, and tested by real-time RT-PCR at the University of Virginia Health System for subject diagnosis and stored at −20 °C in a viral transport medium (VTM). Prior to receipt, samples were deidentified according to the IRB-approved protocol. Standard of care testing was performed with methods granted emergency use authorization (EUA) from the FDA according to manufacturer's instructions, these included the Abbott-Alinity-m SARS-CoV-2 assay, the Abbott M2000 Real-Time SARS-CoV-2 assay, and the Xpert Xpress SARS-CoV-2 assay. Prior to analysis, each sample was vortexed for 10 s, and 600 µL of liquid was transferred to a 2 mL screw-cap

microcentrifuge tube. VTM samples were inactivated by heating for 30 min at 65 °C, transferred to a sealed bag, and stored at −80 °C until further analysis.

4.2.2. Sample Materials. Any sample assigned a cycle threshold (C_t) value by the clinical laboratory was considered positive for SARS-CoV-2; C_t values were used to determine relative viral titers. A SARS-CoV-2 reference material (100 000 copies/mL, AccuPlex SARS-CoV-2 Reference Material, SeraCare, Milford, MA) was diluted from 100 copies/µL to 50 and 25 copies/µL in either PCR-grade water (Molecular Biologicals International, Inc.), clinically negative SARS-CoV-2 samples in VTM, or human saliva to serve as on-disc full-process analytical controls.

4.2.3. In-Tube Nanotrap Enrichment and RNA Extraction. In-tube studies were completed with 100 µL of inactivated clinical samples at high, moderate, and low viral titers. Nanotrap Magnetic Virus Particles (CERES Nanosciences, Inc., Manassas, VA) were spiked into full-process controls and SARS-CoV-2 clinical samples at 5, 10, 20, 30, or 50% of the total sample volume and incubated at room temperature for 0.5, 1, 5, 10, or 20 min. NPs were magnetically pelleted, the supernatant was removed, and NPs were resuspended in an enzymatic RNA extraction cocktail (rnaGEM, MicroGEM International, PCL, Charlottesville, VA) consisting of 88 µL of water, 10 µL of BLUE buffer, and 2 µL of rnaGEM enzyme solution prior to incubation for 5 min at 95 °C. Samples were also prepared with the RNeasy Mini Kit (Qiagen, Valencia, CA) according to the manufacturer's instructions. In-tube matrix effects were tested with clinical samples neat and diluted with fresh saliva to 1:1, 1:4, and 1:8. For comparison of eluates from the in-tube and on-disc methods,

elution volumes were decreased from 100 to 50 µL (44 µL of water, 5 µL of BLUE buffer, and 1 µL of rnaGEM enzyme solution); the NP input volume was adjusted to maintain a 20% concentration.

4.2.4. Comparison of Commercial, Enriched, and rnaGEM Approaches. Patient samples were previously analyzed by real-time RT-PCR in the clinical laboratory at the University of Virginia Health System for diagnostic purposes. Here, any sample received with a clinically assigned C_t value was considered clinically-positive. Clinical C_t values were also used to infer comparative viral titers. In 'commercial' extractions, RNA was isolated from 250 mL of inactivated patient sample using the RNeasy Mini Kit (Qiagen, Valencia, CA, USA) with a DNase I treatment (New England Biolabs, Ipswich, MA, USA) according to manufacturer's instructions. Enriched rnaGEM extractions include a pre-concentration step in which 25 mL Nanotrap Magnetic Virus Particles (CERES Nanosciences, Inc. Manassas, VA, USA) were mixed with 250 mL of heat-inactivated patient sample. Following a brief incubation, the particles were magnetically separated and the supernatant was removed. Nanotrap particles were resuspended in a rnaGEM cocktail comprised of 44 µL water, 5 µL BLUE buffer, and 1 µL rnaGEM enzyme solution. Following incubation for 10 min at 75 °C and 5 min at 95 °C in a thermal cycler, the particles were again separated magnetically and the supernatant RNA solution was collected and ~~retained RNA extracts were~~ stored at -80 °C until analysis.

4.2.5. Device Design and Fabrication. Microdevice architecture was designed using AutoCAD software (Autodesk, Inc., Mill Valley, CA) and laser-ablated into thermoplastic substrates using a CO_2 laser (VLS 3.50, Universal Laser Systems, Scottsdale, AZ). The primary device consists of five

poly(ethylene terephthalate) (PeT) layers (Film Source, Inc., Maryland Heights, MO). Capping layers 1 and 5 are composed of PeT, whereas primary fluidic layers 2 and 4 are composed of heat sensitive adhesive (EL-7970-39, Adhesives Research, Inc., Glen Rock, PA)-coated PeT. Layer 3, composed of black PeT (bPeT) (Lumirror X30, Toray Industries, Inc., Chuo-ku, Tokyo, Japan), acts as an intervening layer between the two primary fluidic layers to permit laser valving.[20] Layers were aligned and heat-bonded using a laminator (UltraLam 250B, Akiles Products, Inc., Mira Loma, CA) according to the "print, cut, laminate" method, described elsewhere.[22] The poly-(methyl methacrylate) (PMMA) accessory layer (1.5 mm thickness, McMaster Carr, Elmurst, IL) was affixed to layer 1 by a pressure-sensitive adhesive (PSA) transfer tape (MSX- 7388, 3M, Saint Paul, MN), capped with PeT, and used to increase the chamber depth and fluid capacity.[19] Fluidic channels connecting microdevice chambers had a depth of approximately 100 μm and approximate widths between 400 and 500 μm.

4.2.6. Spin System Construction and Operation. Valve opening,[23] channel closures,[20] rotationally driving flow, and magnetic mixing[19] were enabled by in-house mechatronic systems regulated by 8-core microcontrollers (Propeller P8X32A-M44; Propeller, Inc., Rockland, CA) and custom programs written in Spin, Propeller's coding language, run from a laptop computer. On-disc heating was facilitated by a clamped, dual-Peltier system.

***4.2.6.1. Power, Time, and Z-Height Adjustable Laser (PrTZAL) System*.** Laser valving events and rotationally driven flow were accomplished with the PrTZAL system, described elsewhere.[20] Active valving via a 638 nm laser diode occurred when the disc was stationary and

situated under the laser at the corresponding radial distance from the center of rotation (r), measured in mm. To open the valves, the laser was positioned 15 mm above the disc, and irradiation occurred at 500 mW for 500 ms.[20] Channels were occluded by situating the disc 27 mm below the laser and with a power output of 700 mW for 2500 ms. A DC brushless motor was used to drive device rotation, enabling fluidic control.

4.2.6.2. Dynamic Solid-Phase Extraction (dSPE) Platform. The dSPE platform[19] was used to impart external magnetic control of the paramagnetic affinity-capture hydrogel NPs for efficient mixing with both the SARS-CoV-2 samples and the enzymatic extraction reagents. The platform houses a PMMA disc (diameter = 150 mm, thickness = 1.50 mm) placed 7.50 mm above the sample disc platform and featuring two Neodymium magnets to generate the bRMF[19] that facilitates back-and-forth NP sweeping within a chamber with reversal of rotational direction.

4.2.7. On-Disc Enrichment and Enzymatic Extraction Protocol. Liquid sample (50 µL), enzymatic extraction cocktail (50 µL), and NPs (10 µL) were introduced to corresponding chambers via pipette loading. After actuation of valve 1, disc rotation drove the fluid from the sample input chamber to the central magnetic manipulation chamber (1500 g, 30 s). Here, SARS-CoV-2 virions were adsorbed to NPs during bRMF application for a total of 300 s, switching direction every 20 s. NPs were centrifugally pelleted (2000 g, 60 s) before valve 2 (r = 45.4 mm) was opened and supernatant was pumped (1500 g, 30 s) into the waste chamber. The channel upstream of the waste chamber was laser-sealed to prevent further fluid flow. Valve 3 was then opened to permit the lysis cocktail to flow (1500 g, 30 s) into the magnetic manipulation chamber for another

mixing step. The central chamber was then heated to 95 °C for 1 min prior to NP pelleting (2000 g, 60 s). Sample elution to the viral RNA elution chamber occurred after the opening of valve 4 and disc rotation (1500 g, 30 s). The RNA eluate was then retrieved by pipette after puncturing the capping layer PeT.

4.2.8. Performance and Analysis of Dye Visualization Studies. Blue and yellow aqueous dye solutions were used to visually represent the sample and extraction cocktail, respectively. Device images were captured using an Epson Perfection V100 Photo desktop scanner (Seiko Epson Corporation, Suwa, Nagano Prefecture, Japan). Raw images were converted to HSB stacks using the Fiji ImageJ freeware and analyzed using the "crop-and-go" technique.[24] Briefly, the hue of a rectangular region of interest (ROI) within each chamber (n = 6) and parallel measurements were compared to control dye solutions of known constituency on-disc. Control solutions were comprised of serially diluted blue dye in yellow dye from 100% to 0% (each n = 3).

4.2.9. Real-Time Polymerase Chain Reaction. Detection of SARS-CoV-2 was accomplished using the Centers for Disease Control and Prevention (CDC) assay.[25] Per manufacturer's instructions, each 20 µL reaction was composed of 5 µL of TaqPath 1-Step RT-qPCR Master Mix, CG (Thermo Fisher Scientific, Waltham, MA), 1.5 µL of SARS-CoV-2 (2019- nCoV) CDC RUO N1 primer-probe mix (Integrated DNA Technologies, Coralville, IA), 8.5 µL of PCR-grade water (Molecular Biologicals International, Inc.), and 5 µL of eluate. For positive controls, the 2019-nCoV_N_ Positive Control plasmid (100 000 copies/µL, Integrated DNA Technologies) was diluted to 1000 copies/µL in PCR-grade water (Molecular Biologicals International, Inc.). All samples were run in

triplicate on a QuantStudio 5 Real-Time PCR System with detection in the FAM channel (Thermo Fisher Scientific). Thermal conditions included reverse transcription (50 °C, 900 s), denaturation (95 °C, 180 s), 40 cycles of denaturation (95°C, 3 s), and annealing (60 °C, 30 s), with a final hold step at 25 °C. The 60 °C annealing temperature was determined optimal over the manufacturer's recommended temperature of 55 °C previously.[13] Amplification was considered successful if the signal amplitude crossed the instrument-defined threshold, providing a C_t value, before the 40 cycle cutoff.

4.2.10. On-Disc Reagent Storage via Vacufuge. A 5305 Vacufuge Plus Concentrator (Eppendorf, Hamburg, Germany) was used to dry down 15 µL aliquots of reaction mixes for a total of 60 min in all circumstances described. The reagent 'pellet' was then rehydrated with 20 µL of extracted eluate or diluted CDC plasmid (100 000 copies/µL, Integrated DNA Technologies). Prior to being introduced into the amplification reaction, SeraCare samples were extracted by the enzymatic method, described previously (rnaGEM, MicroGEM International, PCL, Charlottesville, VA). Extraction proceeded according to manufacturer recommendations, with reactions consisting of 88 µL of water, 10 µL of BLUE buffer, and 2 µL of rnaGEM enzyme solution prior to incubation for 10 min at 75 °C and 5 min at 95 °C. For amplification, two chemistries from Meridian Bioscience (London, UK) were used for detection of SARS-CoV-2 RNA with a view toward long-term reagent storage. The SensiFAST™ Probe Lo-ROX One-Step Kit (Meridian Bioscience) was used to construct 15 µL reactions composed of 10 µL SensiFast™ Probe Lo-ROX One-Step Mix (2x) (Meridian Bioscience), 1.6 µL Forward Primer (10 µM) and 1.6 µL Reverse Primer (10 µM) (Integrated DNA Technologies, Coralville, IA), 0.2 µL Probe (10 µM) (Integrated DNA Technologies), 0.2 µL Reverse

Transcriptase (Meridian Bioscience), 0.4 µL of RiboSafe RNase Inhibitor (Meridian Bioscience), and 1 µL of PCR-grade water (Molecular Biologicals International, Inc.). Likewise, the Lyo-Ready™ 1-Step RT-qPCR Mix (Meridian Bioscience) was used to construct 20 µL reactions composed of 10 µL Lyo-Ready™ 1-Step RT-qPCR Mix (2x) (Meridian Bioscience), 1.6 µL Forward Primer (10 µM) and 1.6 µL Reverse Primer (10 µM) (Integrated DNA Technologies, Coralville, IA), 0.2 µL Probe (10 µM) (Integrated DNA Technologies), 0.2 µL Lyo-Compatible MMLV-RT (Meridian Bioscience), and 1.4 µL of PCR-grade water (Molecular Biologicals International, Inc.). In each case, the N gene was targeted and a corresponding probe was designed (sequences not disclosed). All samples were run in triplicate on a 7500 Fast Real-Time PCR System (Thermo Fisher with detection in the FAM channel (Thermo Fisher Scientific). Thermal conditions included reverse transcription (45 °C, 300 s), denaturation (95 °C, 60 s), 40 cycles of denaturation (95°C, 3 s), and annealing (65 °C, 30 s), with a final hold step at 25 °C. Amplification was considered successful if the signal amplitude crossed the instrument-defined threshold, providing a C_t value, before the 40 cycle cutoff. For dehydration studies involving cyclic olefin copolymer (COC), 2 mm punches are retrieved from two separate COC substrates (manufacturers not disclosed) and placed into 0.2 mL tubes along with amplification reagents, vacufuged for 60 min, and subsequently rehydrated with CDC plasmid diluted to 100 copies/µL, as before.

4.2.11. Pooling Study. Nasopharyngeal clinical specimens suspended in VTM were pooled so positive and negative samples were mixed in ratios neat and in dilutions of 1:5, 1:10, or 1:20 (positive: negative). Three positive clinical samples of comparatively, high, moderate, and low concentrations were used. Pooled samples were enriched and extracted using a method

previously described,[13] wherein a PDQeX instrument (MicroGEM International, PCL, Charlottesville, VA) is used to sequester the virus and retain the 50 µL of Nanotrap Magnetic Virus Particles (CERES Nanosciences, Inc., Manassas, VA) used for enrichment. For amplification, the SensiFAST™ Probe Lo-ROX One-Step Kit (Meridian Bioscience) was used to construct 20 µL reactions composed of 10 µL SensiFast™ Probe Lo-ROX One-Step Mix (2x) (Meridian Bioscience), 1.6 µL Forward Primer (10 µM) and 1.6 µL Reverse Primer (10 µM) (Integrated DNA Technologies, Coralville, IA), 0.2 µL Probe (10 µM) (Integrated DNA Technologies), 0.2 µL Reverse Transcriptase (Meridian Bioscience), 0.4 µL of RiboSafe RNase Inhibitor (Meridian Bioscience), 1 µL of PCR-grade water (Molecular Biologicals International, Inc.), and 5 µL of extract. All samples were run in triplicate on a 7500 Fast Real-Time PCR System (Thermo Fisher with detection in the FAM channel (Thermo Fisher Scientific). Thermal conditions included reverse transcription (45 °C, 300 s), denaturation (95 °C, 60 s), 40 cycles of denaturation (95°C, 3 s), and annealing (65 °C, 30 s), with a final hold step at 25 °C. Amplification was considered successful if the signal amplitude crossed the instrument-defined threshold, providing a C_t value, before the 40 cycle cutoff.

4.3. Experimental

The development of a method for virion enrichment and enzymatic RNA extraction from SARS-CoV-2 samples is described. Here, sample preparation required in-tube chemistry optimization to maximize the enrichment efficacy, assessed through a comparison with a commercial method. Furthermore, the effects of different sample matrices on preparation were evaluated. Successful µCD integration necessitated precise fluidic control to permit implementation of discrete unit operations. To demonstrate analytical performance, C_t values

obtained via real-time RT-PCR amplification of extracted viral RNA were compared; because C_t values are indicative of relative starting concentrations, optimal conditions for sample preparation would produce more rapid amplification (i.e., lower C_t values). I show that virions can be effectively enriched from multiple matrices and lysed to release amplification-ready viral RNA by this method. Additional research aimed toward the integration of this technology with PON testing is also described, including studies involving the drying down of RT-PCR reagents by vacufugation and pooling studies for up to 20 patients.

4.3.1. A Sample Preparation Workflow for Viral Enrichment and Enzymatic Nucleic Acid Extraction from SARS-CoV-2 Virions. The sample preparation workflow (**Figure 4-1**) was optimized from a protocol described in Dignan and Turiello et al.[13] which combined a nanoparticle-based enrichment, coupled with a rapid, one-step enzymatic extraction method to provide SARS-CoV-2 RNA from clinically-relevant matrices in under 10 minutes. In the workflow described here, magnetically actuated NPs were used for virion capture and isolation from clinical matrices.[26] Lysis of the viral envelope and liberation of RNA was accomplished with *rna*GEM chemistry; a proprietary chemistry that includes a buffer system and neutral

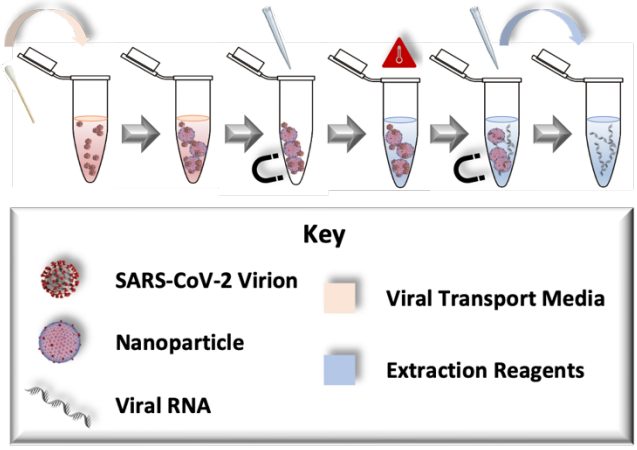

Figure 4-1. In-tube proposed sample preparation workflow. Enrichment from the sample leverages affinity NPs for virion adsorption. Following magnetic actuation and removal of the supernatant, RNA extraction is achieved in a PCR compatible buffer. The reaction mixture is heated to 95 °C before a second magnetic step and the pipette removal of the viral RNA eluate. Adapted from Turiello et al. 2022, *Lab Chip.*[13]

protease that targets cell surface proteins.[16] This single-step, enzyme-based extraction method does not require time- and labor-intensive column-purification and circumvents centrifugation by leveraging temperature control. Optimal release of nucleic acids from intact cells and/or virions is achieved at a temperature of 75 °C,[16] with termination of the reaction at 95 °C to diminish activity and prevent detection inhibition downstream.[27] The process time can be reduced by controlling the rate of heating, so long as target temperatures are achieved. Furthermore, data suggests that a protocol in which the 75 °C step is eliminated entirely is plausible, so long as the sample ramps past its optimal temperature for efficiency on the way to the 95 °C heat-kill step.[13]

Preliminary characterization of this workflow was completed with clinical samples of a known positive status using three different sample preparation parameters, including the gold-standard 'commercial' extraction method, the enzymatic 'Enriched rnaGEM' approach, and an

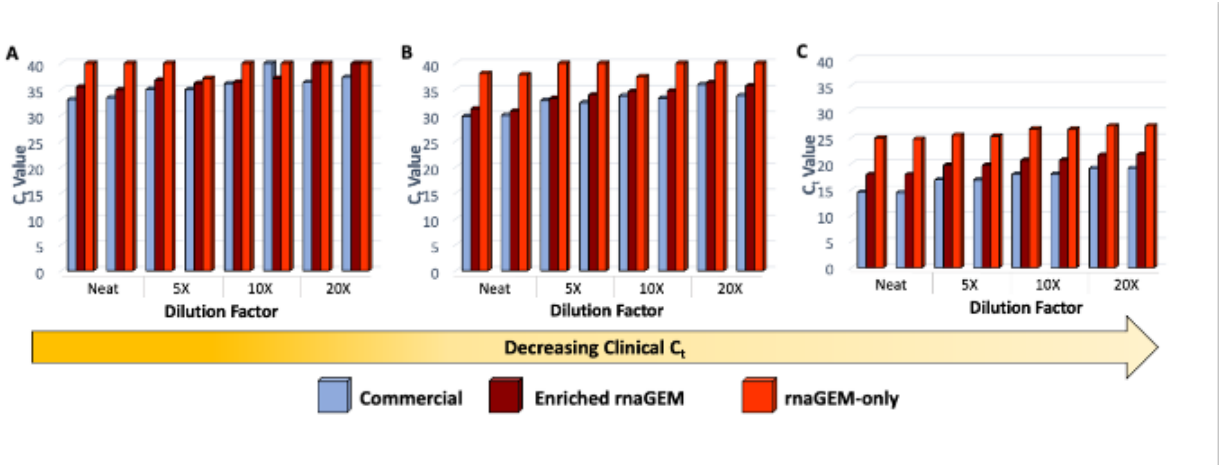

Figure 4-2. Comparison of enzymatic extraction methods with a commercial kit. SARS-CoV-2 RNA was extracted from known positive clinical samples in parallel using two methods – a commercial solid phase spin-basket kit, and enzymatic extractions with viral preconcentration. Three samples with comparatively (A) high, (B) moderate, and (C) low Ct values were selected for comparison. Extracts were analyzed neat and serially diluted at factors of 5X, 10X, and 20X, each in duplicate. Ct values obtained from the enriched enzymatic extracts were only slightly higher than extracts obtained using the commercial kit.

approach using 'rnaGEM only'.[13] **Figure 4-2** shows the C_t values associated with three of these clinical samples, of high, moderate, and low relative concentrations. Broadly, SARS-CoV-2 RNA was detected in all extracts with exceptional concordance of C_t values. Given that clinical laboratories only report a binary response to practitioners to provide patient diagnoses, the minor (1-2 cycle) differences between the methods overall has negligible practical import. To provide a more complete picture of comparative performance, neat samples were diluted by factors of 5X, 10X, and 20X before being prepared by each sample preparation method (**Figure 2**). Again, the C_t values from parallel extracts were largely concordant between methods. At each dilution of the moderate titer extract, the C_t values were within approximately one unit of each other across methods and viral RNA was detected in all dilutions, down to 20X (**Fig. 4-2B**). Similar trends were observed in analysis of the low viral titer sample with a single discrepancy, wherein the 20X dilution of the enriched rnaGEM extract exhibited no amplification but the parallel extract prepared by the commercial method did (**Fig. 4-2A**). Still, it was hypothesized that the concentrations in this regime were largely stochastic and the distribution of RNA in these dilutions were inhomogeneous and failed to adhere to a normal distribution.

Interestingly, the most pronounced differences across methods is observed in the sample representing the highest relative titer (**Fig. 4-2C**). Although RNA obtained via enriched rnaGEM extraction was readily detected with C_t values of 20 ± 2 units in all dilutions, the values of commercial extracts were ~3 cycles lower. A similar phenomenon was observed by Barclay et al., who suspected viral saturation of the nanoparticles at very high titers[9]; virions were likely sterically prevented from binding with the particles and were lost in the discarded supernatant prior to extraction. Still, Barclay et al. suggests that nanoparticle saturation does not affect the

utility of enrichment-aided extractions since it does not prevent qualitative SARS-CoV-2 identification.[9] I believe this to be especially true as it pertains to high titer samples such as the one in question, since regardless of extraction method, amplification occurred well below the cut-off cycle and SARS-CoV-2 was readily detected. It can be added that the use of nanoparticle enrichment removes free RNA not contained in a viral envelope, known to persist in sample matrices well beyond patient infectivity.[28] Column based methods are unable to differentiate RNA from infectious virus and naked RNA, thus confounding PCR-based diagnostics and efforts by public health officials to determine key metrics, such as required quarantine duration.[28] Since our method uses nanoparticle-based viral enrichment upstream of virion lysis, free, non-infectious RNA is not retained, potentially providing more accurate, useful information regarding patient infectivity.

4.3.2. Nanotrap Particle Enrichment Optimization. For virion enrichment, parameters including NP input volume and incubation time were optimized with consideration given to resultant C_t values, reagent conservation, and total analysis time. **Figure 4-3** shows the C_t values derived from parallel aliquots of three positive clinical samples at high, moderate, and low concentrations, analyzed with NP percentages between 5 and 50%. Optimal NP input volume was determined to be 20% of the total sample volume, as 5% and 10% enrichment parameters were found to produce higher relative C_t values, indicating lower post extraction RNA concentrations, whereas input volumes higher than 20% did not exhibit appreciably different C_t values across sample concentrations.

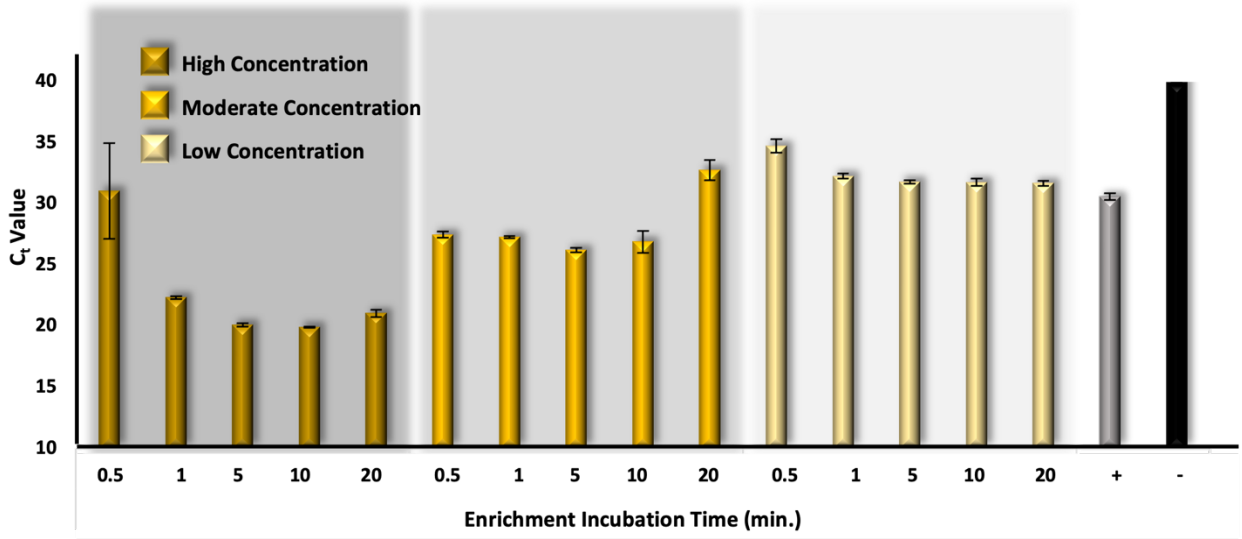

Figure 4-3. Determination of the optimal nanoparticle incubation time for enrichment in-tube. Three positive patient samples in VTM at different sample concentrations were incubated with nanoparticles for 0.5, 1, 5, 10, and 20 minutes before the nanoparticles were actuated on a magnetic stand and the supernatant was removed. Eluates were amplified in triplicate and C_t values indicated that 5-minute incubation periods are optimal for capture of SARS-CoV-2. Adapted from Turiello et al. 2022, *Lab Chip.*[13]

Moving forward, the 20% NP concentration was used to determine the optimal NP incubation time from 30 s to 20 min using clinical samples with variable relative titers, as before. Provided the relative distribution of C_t values, shown in **Figure 4-4**, the ideal incubation time was determined to be 5 min, with all other incubation intervals producing either significantly higher or comparable C_t values; for instance, low-concentration samples incubated for 10 and 20 min show the same mean C_t units. Enrichment conditions both in-tube and with the µCD were dictated by these results in the proceeding studies.

The recovery of the enriched in-tube method was determined using two positive controls for relative comparison, including the nCoV-N1 complementary DNA (cDNA) Plasmid and armored SARS-CoV-2 RNA from SeraCare. The principle being that a cDNA plasmid represents maximum recovery at a given concentration, as it comes pre-purified, reverse transcribed into cDNA, and ready for RT-PCR. Here, the plasmid control is used as a baseline for the *best case*

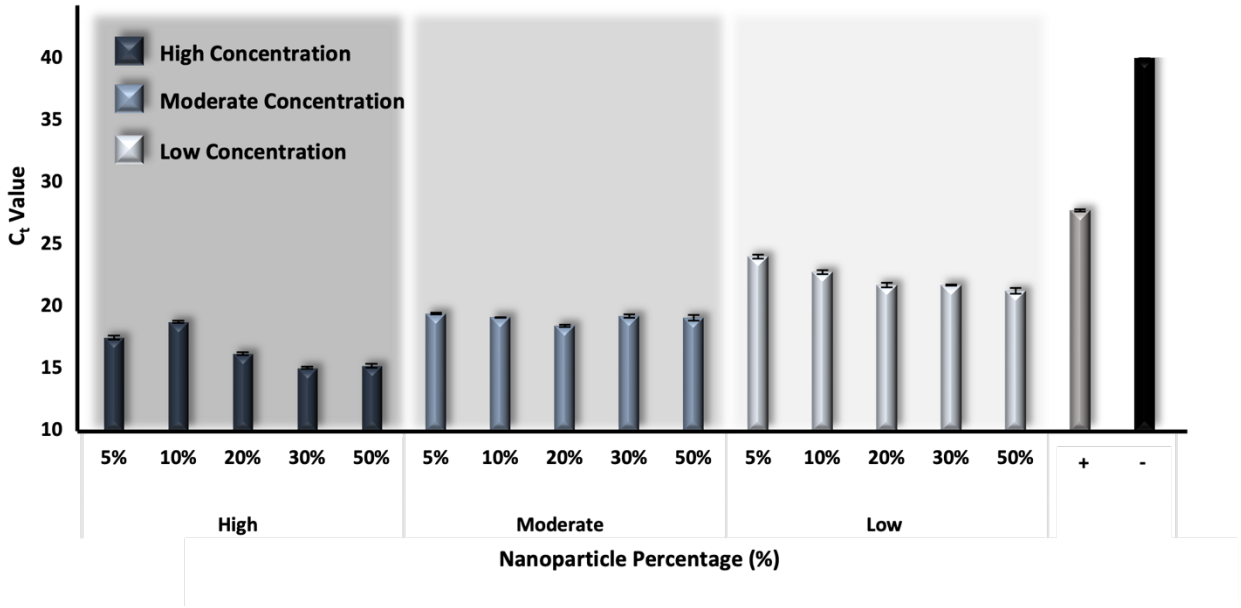

Figure 4-4. Determination of the optimal nanoparticle concentration for enrichment in-tube. Three positive patient samples in VTM at different sample concentrations were selected for this study and incubated with nanoparticles at 5, 10, 20, 30 and 50% the total volume of sample, 100 µL. Eluates were amplified in triplicate. Results suggest that across sample concentrations, an input volume of 20% nanoparticles is sufficient for SARS-CoV-2 capture. Adapted from Turiello et al. 2022, *Lab Chip.*[13]

scenario in terms of DNA recovery. As a comparison, the armored SeraCare control is designed to mimic the SARS-CoV-2 virion and is adorned with exterior Spike (S) proteins that enrichment NPs have an electrostatic affinity for; this way, the SeraCare samples may act as full process positive controls. Given that both controls are assigned a concentration provided by the manufacturer, the resultant C_t values may be compared to estimate the recovery of the proposed sample preparation workflow. Experimentally, the nCoV-N1 Control Plasmid cDNA was serially diluted from 100 copies/µL – 1 copy/µL and amplified using the aforementioned CDC chemistry and the N1 target for COVID-19. **Figure 4-5A** shows a standard curve constructed from the associated C_t values with excellent linearity, as evidenced by a correlation coefficient (R^2 value) of 0.9798. In parallel, SeraCare Positive Reference Material was serially diluted in water to 80, 60, 40, 20, 10, and 5 copies/µL and extracted via the in-tube method with and without the enrichment step. The

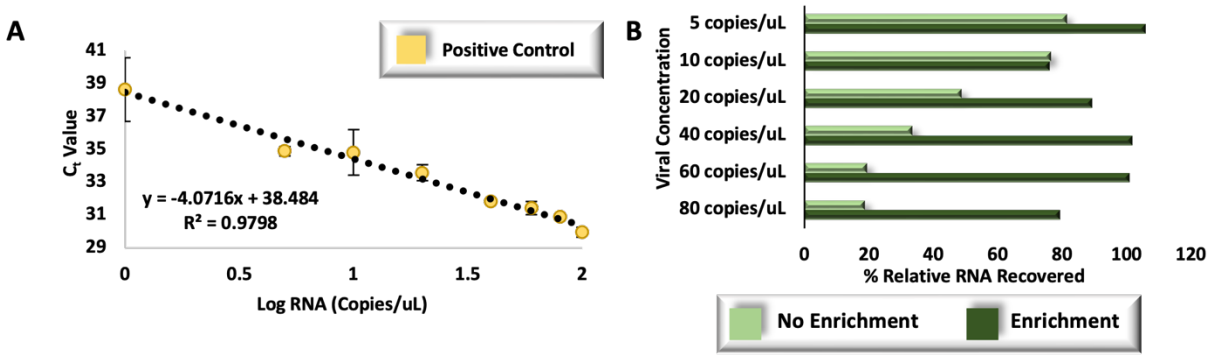

Figure 4-5. Extraction efficiency with and without NP enrichment using the in-tube method. (A) A standard curve was constructed with CDC plasmid SAS-CoV-2 cDNA standards, demonstrating suitable linearity (R^2 of 0.9798). (B) Relative RNA recovery estimated based upon cDNA standards and isolated SARS-CoV-2 positive reference material using the in-tube method with and without the enrichment step with NPs. Results indicate enhanced DNA recovery with enrichment overall.

linear regression trendline (**Fig. 4-5A**) was used to mathematically derive the relative concentrations of samples produced under each condition, that is, with or without enrichment by the NPs. The final RNA concentration recovered by each method was calculated by dividing the derived RNA concentration in each extract by the amount of input RNA and multiplying by 100. **Figure 5B** demonstrates the variability associated with the experimental results across viral concentrations. Broadly, enriched extracts exhibited recovery rates between 76 – 100% with a mean rate of ~92%, whereas parallel samples prepared without enrichment exhibited much lower recovery rates, between 18 – 81% with a mean recovery rate of ~46%. It can be concluded from these results that NP enrichment does enhance recovery overall, but not uniformly across concentrations. This may also be further complicated by the synthesis of full process controls, which may result in mock virions which are 'empty' or free of RNA template; this phenomenon was confirmed as one that may occur during the construction of SeraCare reference material, leading to incongruence between the reported concentrations and those estimated via RT-PCR.

Nevertheless, the results demonstrate enhanced detection performance with the inclusion of enrichment by NPs.

4.3.3. Performance of Optimized Enrichment Method Coupled with Rapid Enzymatic Extraction.

To compare enriched rnaGEM eluates with a commercial technique, samples were prepared in-tube using the proposed method and a Qiagen solid-phase method for RNA extraction. RNA isolated from samples with relatively low, moderate, and high viral titers using both methods in parallel was amplified (**Fig. 4-6A**), and resultant C_t values were compared (**Fig. 4-6B**). A two-way analysis of variance (ANOVA) with replication indicates the null hypothesis (equivalence of means) could not be rejected ($\alpha = 0.05$, p-value = 0.116); stated another way, the C_t values produced by amplification of RNA prepared using both methods were statistically similar at each viral titer. That is, after preparation by a column-based, labor-intensive approach and the simplified method described, eluates produce the same amplification results.

To demonstrate applicability of this method to various types of clinical samples, the presence of a biological matrix, namely, saliva, was tested. Using the in-tube method, parallel

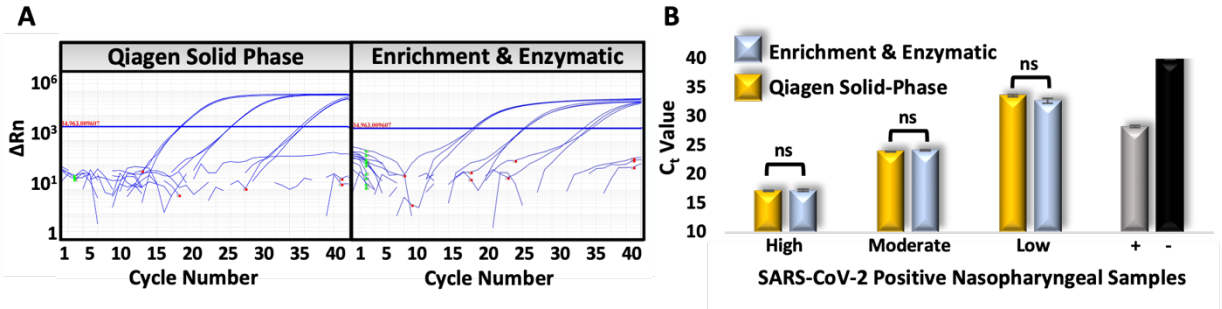

Figure 4-6. Comparison of gold-standard and optimized enrichment and enzyme-based extraction methods. (A, B) Clinical samples were extracted by the solid-phase or proposed method in-tube. No statistical differences were observed between Ct values resulting from amplification of eluates produced by either method. Adapted from Turiello et al. 2022, *Lab Chip.*[13]

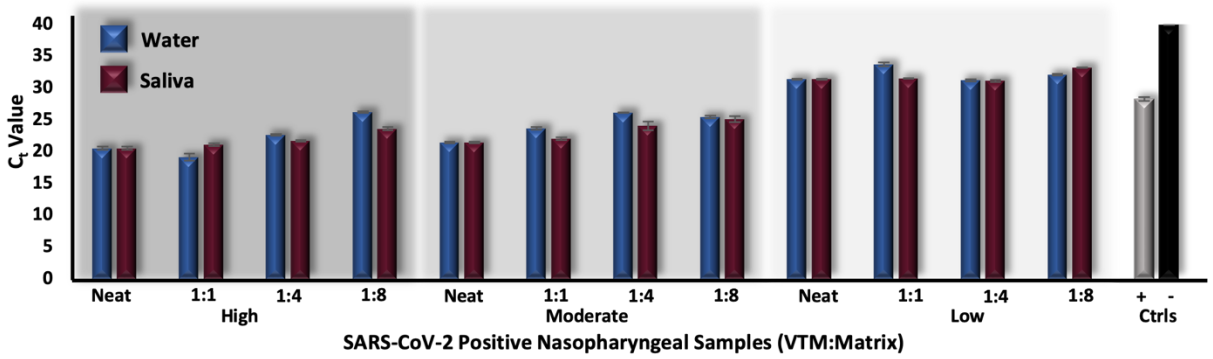

Figure 4-7. Sample preparation method matrix performance. Clinical samples were prepared neat and serially diluted in water (blue) and saliva (burgundy) in parallel. Resultant C_t values demonstrate average differences below two C_t units. Adapted from Turiello et al. 2022, *Lab Chip.*[13]

aliquots from clinical samples were tested neat and diluted in either water or saliva, at various titers (**Fig. 4-7**). It was hypothesized that because NP enrichment permits matrix removal prior to RNA extraction, any adverse effects of the matrix on downstream amplification, and ultimately detection sensitivity, would be mitigated. Although resultant C_t values appeared comparable at each dilution factor, separate two-way ANOVA tests for high-, moderate-, and low-concentration samples demonstrated statistical differences in values across matrices ($\alpha = 0.05$, p-values = 0.007, 1.061×10^{-5}, and 0.017, respectively). However, mean differences between values from each donor sample diverge by less than 2 units (1.150−1.854). Furthermore, differences between values across sample concentrations, matrices, and dilutions appear to be stochastic, with no clear trend suggesting one matrix as preferable over the other. Moreover, results indicate no appreciable difference between detection results from samples diluted in either water or saliva matrices.

Following the optimization of the enrichment step for microfluidic integration, the incubation interval associated with enzymatic lysis was also tested to determine whether a 5 min duration was necessary for downstream detection of the viral RNA. As discussed previously, the

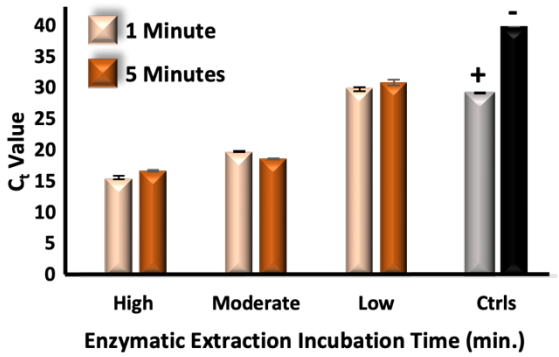

Figure 4-8. The effect of shortening heated incubation time during enzymatic extraction. Three positive patient samples in VTM at different relative sample concentrations were enriched and heated with enzymatic extraction reagents in-tube for either 5 minutes or 1 minute. Extracted samples were amplified in triplicate and resultant Ct values indicated the data sets are equal and there is no statistical difference between them. Adapted from Turiello et al. 2022, *Lab Chip.*[13]

75 °C incubation step was previously eliminated, meaning that the lysis was truly a one-step extraction based only on a 95 °C incubation. Still, contact heating at such an elevated temperature on a polymer-based device can lead to both deformation and delamination, enhancing the potential for failure modes. Thus, minimizing the incubation period is ideal for this particular mode of automated extraction. As before, three clinical samples denoted as having relatively high, moderate, and low levels of virion were enriched and extracted using the in-tube protocol, whereby extraction proceeded with 95 °C incubations at either 5- or 1 min. **Figure 4-8** demonstrates that a reduced lysis dwell time of only 1 min showed successful in-tube RNA isolation from clinical samples. A 2-way ANOVA comparing C_t values indicated RNA yields were statistically similar after 5- and 1 min incubations across all sample concentrations ($\alpha = 0.05$, p-value = 0.2968). Thus, all µCD lysis reactions had a duration of only 1 min.

4.3.4. Characterization of a Rotational Microdevice for Viral Enrichment and Enzymatic Extraction. The µCD was designed with a view toward increased throughput and includes six identical domains for parallel, multiplexed sample preparation (**Fig. 4-9A and B**). Within a single

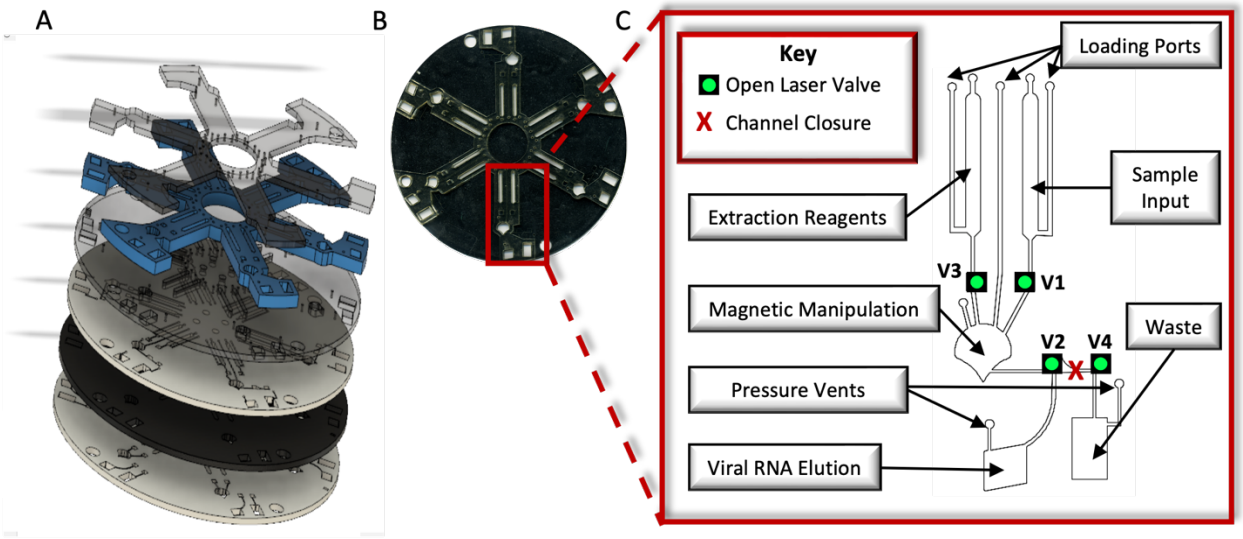

Figure 4-9. Sample preparation µCD architecture. (A) Exploded depiction of the 5-layer polymeric disc and capping layer to enable increased chamber volumes, affixed to the disc by PSA and capped with PeT. (B, C) Top view of µCD and one labeled domain depicting sample chambers, fluidic channels, pressure vents, laser valves, and reagent loading ports. Adapted from Turiello et al. 2022, *Lab Chip.*[13]

domain, NP enrichment and enzymatic lysis occur in the centrally located magnetic manipulation chamber. This "concave-shaped"[19] chamber features a distal vertex, designed to retain magnetic NPs during supernatant removal and, ultimately, RNA elution (**Fig. 4-9C**). Chambers closer to the center of rotation (COR) are designed for aqueous patient samples and extraction reagents; these are loaded through overhead ports designed to interface with pipette tips and feed the liquid into the device through the bottom of the chamber as air is displaced through pressure vents. The magnetic manipulation chamber is designed to house magnetically-actuated NPs, with a vertex to sequester them between steps in response to centrifugal force, so that waste and eluate can be removed toward the periphery of the disc.

The sequential unit operations begin when the liquid sample, suspended NPs, and the enzymatic extraction cocktail are loaded into the sample input, magnetic manipulation, and extraction reagents chambers, respectively (**Fig. 4-10**). Comprehensive virion capture during NP

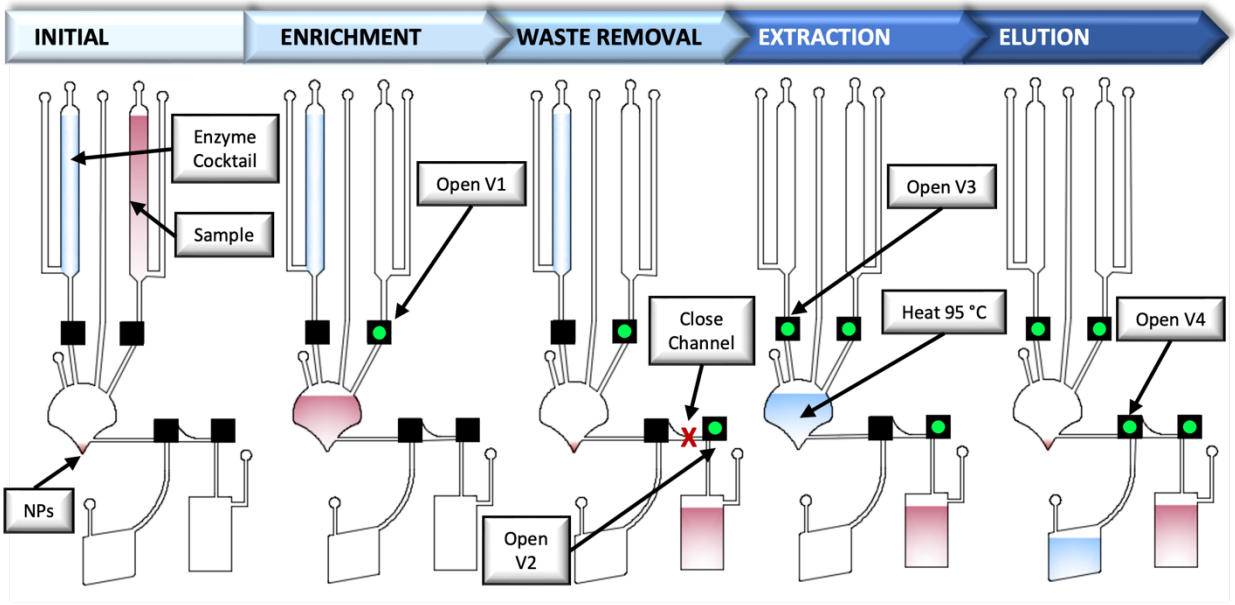

Figure 4-10. AutoCAD rendering demonstrating sequential unit operations performed with the µCD. Operations include reagent and sample loading, enrichment, waste removal, extraction, and viral RNA elution. Adapted from Turiello et al. 2022, *Lab Chip.*[13]

enrichment of the sample was facilitated through bRMF-induced back-and-forth NP "sweeping". The sample/NP mixture was subjected to the bRMF for 5 min, the same interval determined to provide enrichment in-tube (**Fig. 4-4**). NPs, now with adsorbed virions, are centrifugally pelleted into the chamber vertex to maximize retention for supernatant removal to the waste chamber. NPs are resuspended via introduction of the enzymatic lysis cocktail to the magnetic manipulation chamber. Lysis of adsorbed virions was enhanced via the bRMF to increase turbulence and promote more frequent interactions between trapped virions and lysis enzymes than possible under purely diffusive conditions. The cocktail was heated for 1 min at 95 °C, as prescribed by earlier results. Finally, NPs were centrifugally pelleted, and the eluate was rotationally driven into the viral RNA elution chamber, from which it could be collected and amplified with no further purification required..

The reliability of the µCD method was dependent on reproducible performance of the sequential unit operations in the requisite order. Furthermore, the carryover of the matrix into the RNA eluate confers detrimental effects on the performance of downstream real-time RT-PCR.[29] To evaluate the µCD architecture and determine whether this type of inhibition is likely to occur in our system, dye studies were completed to colorimetrically characterize the matrix presence in the on-disc eluate. Here, aqueous blue and yellow dye solutions were used to represent the sample and extraction cocktail, respectively. **Figure 4-11** shows digital scans demonstrating that the dyes were moved throughout each domain according to the assay workflow, with all valve openings and channel closures reproducibly operating as expected. Quantification of matrix prevalence in the eluate was enabled by collecting empirical measurements of the hue, the circular variable that represents a color within the visible portion of the electromagnetic spectrum.[24] The hue of the yellow dye in the eluate chamber after the completion of the assay workflow (0.175 ± 0.003) was statistically significantly higher than that

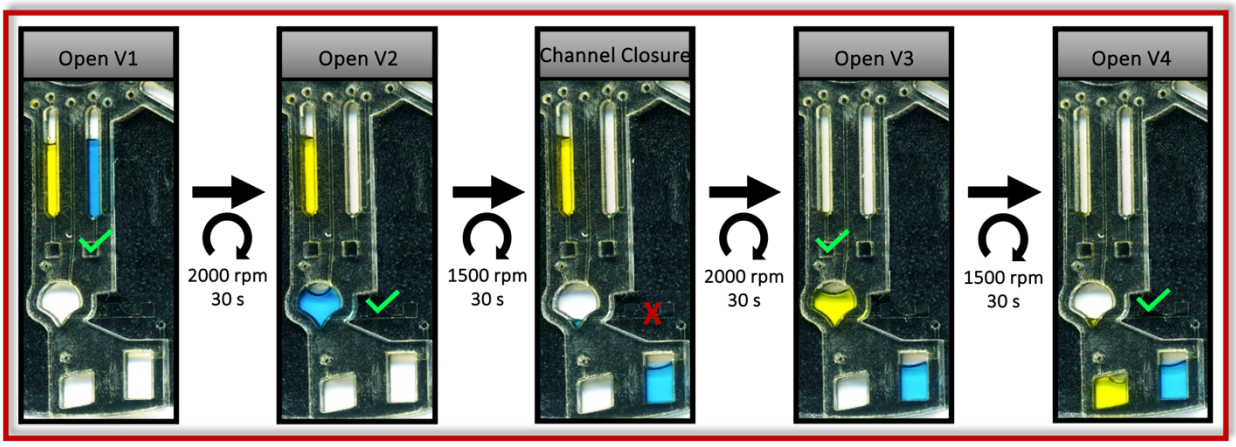

Figure 4-11. Representative dye study demonstrating fluidic control. One representative µCD domain depicting the progress of a dye study (n = 6). Aqueous blue and yellow dye solutions represent the sample and extraction cocktail, respectively. Adapted from Turiello et al. 2022, *Lab Chip.*[13]

of pure yellow dye (0.147 ± 0.004), according to an unpaired t test for means (α = 0.05, two-tailed p-value <0.0001). This upward shift in hue was attributed to contamination with the blue dye (hue = 0.571 ± 0.002), which reflects the carryover of the matrix into the viral RNA eluate (**Fig. 4-12A**). Mixing between fractions was not unexpected; the magnetic manipulation chamber geometry was designed to retain NPs in the vertex extending radially outward below the elution channel for maximized RNA recovery, as discussed above.[19] Simultaneous capture of fluid in this vertex, and ultimately carryover into the eluate, was unavoidable. To characterize the extent of matrix carryover, hue measurements taken from the µCD eluate fraction were compared to dye mixtures of known composition. Specifically, colorimetric analysis of serially diluted dye standards (blue in yellow) demonstrated a strong linear correlation between increases in the hue and in the prevalence of the blue dye (R^2 = 0.996) (**Fig. 4-12B**). This relationship was used to calculate that the final eluate is comprised of 6.58 ± 0.72% blue dye, or crude sample matrix. However, NPs were not included in this dye study; I anticipate that the prevalence of sample

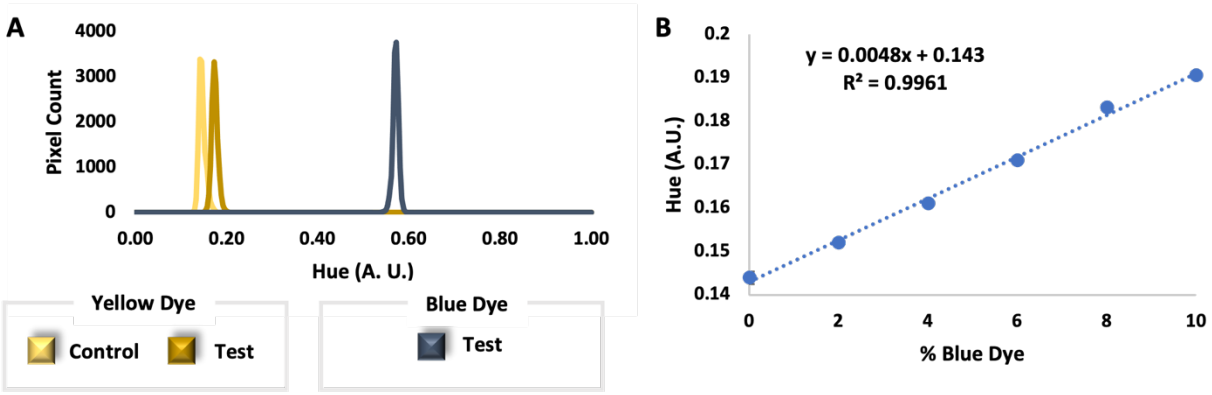

Figure 4-12. Quantification of residual matrix by the µCD. (A) Line graph depicting the hue of blue and yellow representative dyes following the µCD protocol, compared to control dye solutions. The increased hue measured from the yellow dye after the assay represents the carryover of the blue dye (sample matrix) into the final eluate (yellow fraction). (B) Calibration curve of the hue against the percentage of blue dye mixed with yellow solution used to calculate the magnitude of sample carryover into the final eluate observed during the µCD assay. Adapted from Turiello et al. 2022, *Lab Chip.*[13]

matrix in viral RNA eluates would be much lower. During preparation of real samples, NPs would occupy the chamber vertex during supernatant flow to waste, sterically excluding fluid. Therefore, I concluded that on-disc viral RNA eluates would contain only minimal matrix, which would likely not inhibit PCR.

4.3.5. Integration of SARS-CoV-2 Reference Material and Clinical Samples. Experimental results from replicate dye studies indicated effectual architectural features and reliable fluidic control. Furthermore, in-tube studies indicated that the RNA preparation workflow produced comparable results to a gold standard method. To demonstrate successful µCD adaptation, SARS-CoV-2 reference material was serially diluted and prepared in parallel using the proposed method in-tube and with the µCD. As previously discussed, this reference material was selected because it features an extractable viral protein coat encapsulating the RNA, and thus may serve as a full-process control. C_t values obtained from in-tube and µCD extractions were compared to those from the 2019-nCoV Positive Control plasmid, diluted to equivalent concentrations (**Fig. 4-13**). It was hypothesized that samples prepared by both methods would produce equivalent C_t values and likewise be similar to cDNA plasmid positive controls, indicating successful automation with the µCD and good

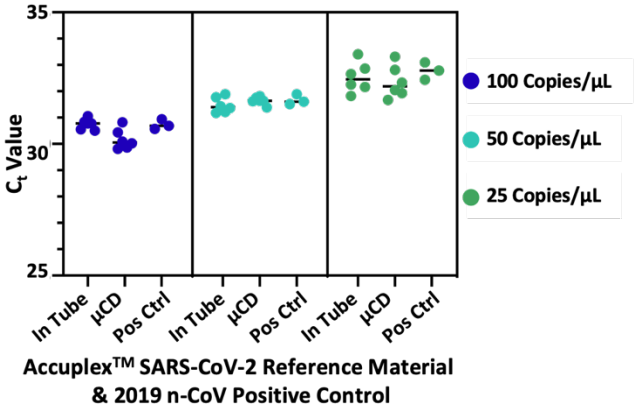

Figure 4-13. Sensitivity testing with SARS-CoV-2 reference material. Full-process SARS-CoV-2 control was extracted in duplicate neat and diluted in water with the in-tube and µCD methods. Resultant Ct value comparisons suggest statistically significant differences at 100 copies/µL, but not at 50 and 25 copies/µL. Adapted from Turiello et al. 2022, *Lab Chip.*[13]

extraction efficiency, respectively. According to one-way ANOVA tests to analyze the equivalence of means, for samples prepared at 50 and 25 copies/µL, the null hypothesis could not be rejected (α = 0.05, p-values = 0.3306 and 0.5281, respectively), suggesting C_t values were statistically similar. Thus, at these concentrations, RNA isolation performs comparably in-tube and in the µCD, producing similar RNA yields. Furthermore, statistical similarity between extracted RNA C_t values with that of the plasmid positive control, which does not require enrichment or extraction, suggests highly efficient rnaGEM extraction both in-tube and on-disc. Conversely, analysis of 100 copies/µL samples indicated a statistically significant difference between the three conditions (α = 0.05, p-value <0.0001). Upon closer examination using a Tukey's test, more variation exists between the prepared samples and the plasmid positive control than between the two preparation methods. The mean C_t values between the in-tube and on-disc methods were 3.711 and 3.134 units different from that of the plasmid positive control, respectively. For contrast, a comparison of the C_t values obtained from in-tube and µCD preparation reveals a mean difference of only 0.577 units, indicating adaptation to the µCD was not detrimental to the sample preparation chemistry. Here, it was demonstrated that, with full-process controls, sample preparation by the µCD produces amplification-ready RNA comparable to that by the in-tube method.

Next, to evaluate the method's capacity for the preparation of clinical samples, positive samples were prepared via the µCD workflow. Real-time RT-PCR amplification of RNA isolated from VTM samples neat and diluted (1:2, 1:4) was successful for all samples prepared using both the in-tube and µCD methods. Notably, eluates with different dilution factors exhibit similar C_t values between methods, a phenomenon observed previously, and one that has been attributed

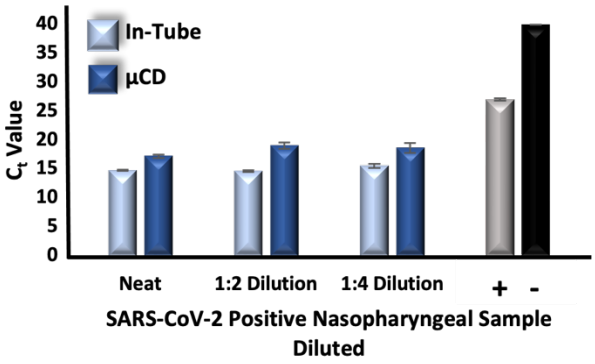

Figure 4-14. Device compatibility with clinical samples. Nasopharyngeal swabs were extracted neat and diluted in water using both methods. Resultant eluates produced higher Ct values with the µCD method. Adapted from Turiello et al. 2022, *Lab Chip.*[13]

to the viral saturation of NPs at high viral titers and that does not prevent SARS-CoV-2 identification.[13] Still, resultant C_t values indicated larger differences between the eluates generated across methods using real clinical samples compared to those observed from reference material and positive controls (**Fig. 4-14**). On average, C_t values resulting from amplification of µCD isolates were 3.266 units higher than those prepared in-tube. I suspect these results diverge from those generated when comparing the full-process control as a direct result of the presence of a residual matrix. Recall that, with the µCD method, the carryover of some matrix is expected.

4.3.6. Performance with Multiple Sample Matrices. To this point, dilutions of full-process controls and VTM from nasopharyngeal swabs were prepared in water. I considered whether this may have contributed to the higher C_t values and sought to investigate this further by instead diluting the samples in matrices negative for SARS-CoV-2. This way, the matrix would ostensibly remain consistent, while the input concentration of controls? changed. To control for the concentration, undiluted full-process SeraCare controls (100 copies/µL) were again processed in-tube and with the µCD (**Fig. 4-15**). In parallel, samples were diluted in the nasopharyngeal VTM matrix, prepared by both methods, and amplified via real-time RT-PCR (**Fig. 4-15**). Unpaired t tests indicate a statistical difference between replicate C_t values at concentrations of 100, 50, and

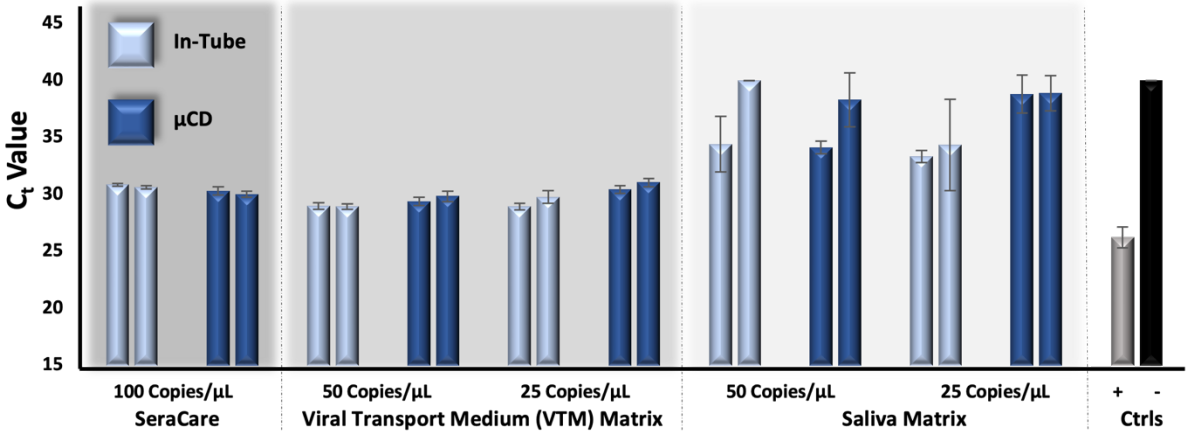

Figure 4-15. Method performance with multiple sample matrices. Full-process SARS-CoV-2 control was extracted in duplicate by the in-tube and µCD methods neat and diluted in two different matrices: (1) a negative clinical nasopharyngeal sample suspended in VTM and (2) fresh saliva. Statistical differences were observed between resultant Ct values across all concentrations and conditions analyzed; notably, average Ct value differences were less than 1 unit with VTM samples prepared by either method. Adapted from Turiello et al. 2022, *Lab Chip.*[13]

25 copies/µL ($\alpha = 0.05$, p-values = 0.0086, 0.0158, and 0.0026, respectively). Interestingly, the average C_t value difference between conditions at all concentrations was less than 1 unit (~0.9122), which is much less variable than those of samples diluted in water (**Fig. 4-13**). I hypothesize the increased success with samples diluted in VTM can be attributed to the stabilizing properties of the medium;[30] furthermore, studies have demonstrated diminished stability for other coronavirus strains suspended in water.[31] I next evaluated the capacity for the µCD to process saliva, which has recently garnered much attention as an alternative sampling type for SARS-CoV-2 detection, given its noninvasive collection.[32] I hypothesized the increased viscosity and complexity of saliva may pose analytical challenges. This was observed when samples prepared in saliva demonstrated higher C_t values, and thus diminished amplification sensitivity, compared to the VTM-diluted samples (**Fig. 4-15**). For example, at 25 copies/µL,

average C_t values for samples prepared in VTM were ~30.05, while those prepared in saliva were ~36.35. Additionally, the disparity in performance between in-tube and μCD preparation was more pronounced in the analysis of saliva compared to that of VTM (**Fig. 4-15**). Considering the 25 copies/μL samples, amplification of μCD extracts from VTM exhibited diminished sensitivity of only ~1.38 C_t units relative to RNA prepared in-tube; analogous samples diluted in saliva showed a larger difference.

4.3.7. Investigation Toward On-Disc Reagent Storage by Vacufuge Dehydration. The work described in this chapter was positioned to align with a downstream detection technology, enabling the development of a sample-to-answer PON microfluidic system for viral preparation and detection. Of course, a true PON method requires careful consideration of on-board reagent storage and ideally does not require cold-chain transport.[33] While the enrichment and extraction chemistries described herein maintain their stability at room temperature for some time, any associated amplification chemistry would not, unless dehydrated. Thus, early studies were completed to enable long-term reagent storage on a microdevice.

Two different chemistries designed for dehydration and storage by the manufacturer were compared for their functionality following a 60 min vacufuge protocol. The kit chemistries, referred to hereafter as 'Lo-Rox' and 'Lyo-Ready,' were rehydrated with either extracted SeraCare full process controls or CDC plasmid diluted in nuclease-free water, theoretically permitting enrichment of the amplification reactions since the bulk volume was made up with sample. **Figure 4-16** demonstrates preliminary results from the vacufuge experiment, comparing the amplification performance of each mix. Overall, the Lo-Rox chemistry resulted in failure to amplify

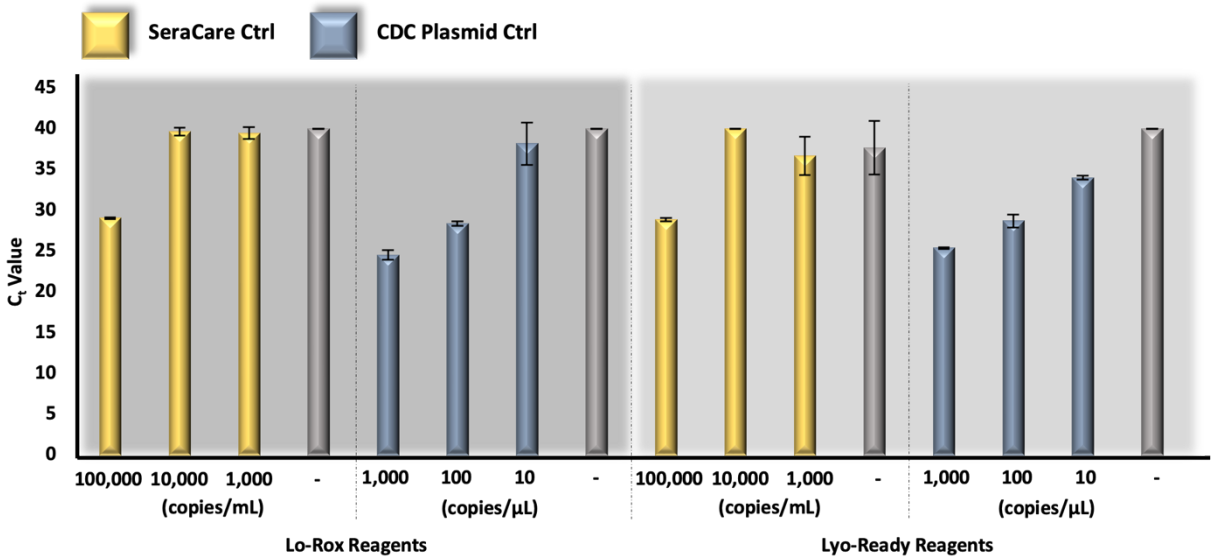

Figure 4-16. Comparison of alternative chemistries in preparation for long-term storage. Full process SARS-CoV-2 controls extracted and amplified alongside CDC plasmid positive controls by two separate reaction chemistries, both dried down via vacufuge for a total of 60 min. Lyo-ready reagents perform better overall.

a total of 6 replicates and the Lyo-Ready mix only failed to amplify 4 replicates, indicating enhanced performance by the Lyo-Ready mix. Interestingly, the majority of detection failures by both chemistries occurred with SeraCare positive controls, perhaps demonstrating that the functionality of the reverse transcriptase may have been affected by the vacufuge process. Recall that the CDC plasmid controls are already reverse transcribed into cDNA, whereas the SeraCare positive controls release an RNA template upon lysis of the constructed viral envelope. Therefore, an unevenly distributed failure rate between the two positive controls, and shared by the two chemistries, points to the diminished efficiency of the enzyme responsible for transcribing RNA into cDNA. Still, these results were largely stochastic, and similar results may also be observed if the extraction method was not successful across the SeraCare positive control samples. Moving forward, SeraCare samples were re-extracted and amplified in triplicate alongside plasmid-based positive controls using the dehydrated Lyo-Ready reagents alone. **Figure 4-17** shows enhanced

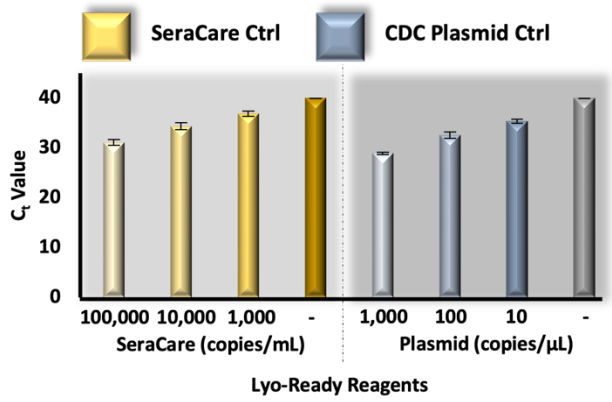

Figure 4-17. Vacufuge analysis of Lyo-Ready reagents. Full process SARS-CoV-2 control amplified in triplicate alongside CDC plasmid positive controls by the Lyo-Ready chemistry, dried down via vacufuge.

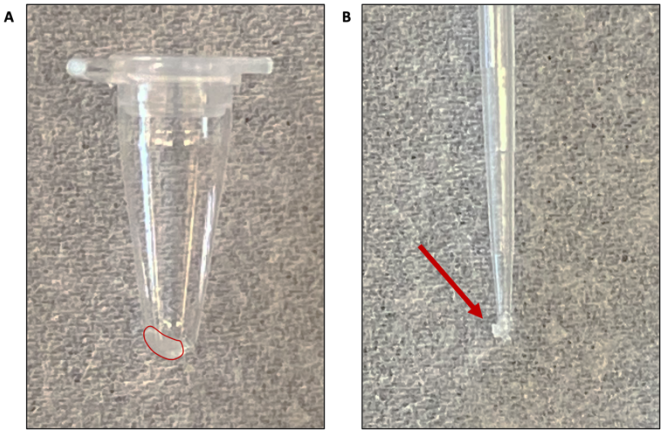

Figure 4-18. Vacufuged Lyo-Ready reagents. Photographs of Lyo-Ready reagents, vacufuged for a total of 60 min. (A) in-tube, as outlined in red, and (B) removed via pipette tip, introducing a potential manufacturing issue.

performance overall: all samples amplify as expected with minimal deviation between replicates and C_t values trend according to the dilution factor. Thus, it is suspected that previously observed stochasticity may be attributed to the RNA extraction for that particular batch of samples and/or the diminished functionality of the reverse transcriptase in the Lo-Rox kit.

Despite the experimental success with Lyo-Ready reagents, it's important to note that neither mix dried to a powder following the 60 min vacufuge protocol; instead, the aqueous reagents were transformed into a glutinous pellet at the bottom of the amplification tube (**Fig. 4-18A**). From a reagent storage perspective, this may be ideal, as it permits reagents to adhere to a particular 'zone' within the device that can be targeted for laser-induced fluorescence detection in the case of RT-PCR. However, rendering a 'sticky' pellet is not ideal from a manufacturing perspective, whereby the pellet must be somehow removed from the tube it has been vacufuged into in order to transfer it into a

requisite amplification chamber. **Figure 4-18B** demonstrates the attempted removal of the glutinous pellet using a 10μL pipette tip; one can imagine the sampling variability that must be accounted for should this be the approach. Alternatively, the reagents may be dehydrated onto a surface that is more easily removed following the dehydration process and placed into the microdevice. The selection of that surface must be biocompatible to ensure the stability of analytes and reagents, heat-resistant to withstand thermal cycling, and not inhibitory to amplification or exhibiting of autofluorescence that might interfere with excitation or detection signals.

Cyclic olefin copolymer (COC) is a commonly used polymer for microfluidic device fabrication that is known to be low cost, biocompatible, and detection-friendly in terms of autofluorescence.[34, 35] With a view toward enhancing manufacturability in terms of reagent storage, two COC substrates were tested for their ability to adhere the dehydrated reagent pellet, while also not inhibiting amplification or fluorescent signal during RT-PCR. As before, the Lyo-Ready reagents were used for amplification and the results from amplicons derived from reactions containing each COC punch were compared against the results from fresh 'liquid' reagents, and those dried with no COC. **Figure 4-19** shows the results from this study, which indicate that the samples prepared with COC showed enhanced sensitivity overall, but with more variability between C_t values, when compared with the

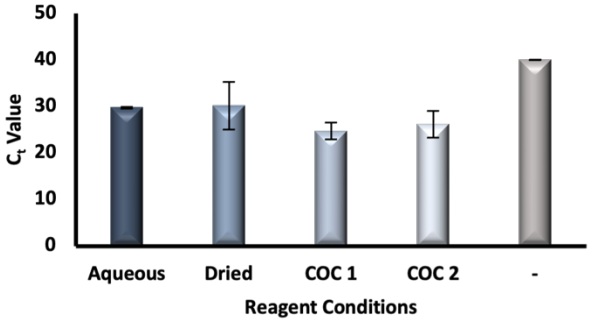

Figure 4-19. Testing COC substrates for compatibility with RT-PCR. CDC plasmid positive controls amplified by the Lyo-Ready chemistry in various conditions. COC substrates demonstrate enhanced sensitivity, compared to their aqueous and dried counterparts.

aqueous reagents. This is not inherently surprising, as the reaction mix was designed by the manufacturer to perform optimally in its dried form. Unfortunately, the tubes containing 'Dried' reagents were crushed by the instrument, and therefore no conclusions can be drawn about their comparative performance. Generally, the value of a method for dried down reagent storage is demonstrated, with preliminary data suggesting deposition on COC for amplification may alleviate the issues involving manufacturability.

4.3.8. Opportunities for Population Surveillance via Pooling. In considering the implementation of PON technologies for virion testing specifically, surveillance testing via pooling multiple patient samples has been of great interest. For context, as the COVID-19 pandemic spread rapidly throughout the world, commercial nucleic acid preparation kits, required to isolate genetic material from the virus, became supply-chain limited. Likewise, laboratory infrastructure was overwhelmed by the influx of multiple tests to ultimately inform on strategic shutdown initiatives. Largescale pooling initiatives provided agencies with the opportunity to surveil the population, while also reducing the analytical bottlenecks that come with screening several individuals. One such strategy, proposed by the United States Department of Human Health and Safety (DHHS) for surveillance in asymptomatic or low disease prevalence populations involves pooling samples from up to 20 individuals in a single test. In one analysis, 1191 samples required only 267 tests to detect 23 positive individuals.[36, 37] This chapter (section?) describes a sample preparation method for the sensitive and rapid detection of SARS-CoV-2 RNA that would be situated for use at the PON and has the potential to enrich analytes from a large volume of sample via nanoparticle enrichment and enzymatic extraction. Thus, the preparation method described is ideally situated

to provide value to largescale pooling efforts; however, the microfluidic interface is less than ideal, as it only permits up to 50 µL of sample volume.

The coupled enrichment and extraction approach was executed with a semi-automated platform that permitted the use of larger sample volumes to permit largescale pooling. This methodology is illustrated in **Figure 4-20**, where enrichment and removal of contributing matrices occurs manually and the remaining processes are completed via PDQeX technology. While this process is described in more detail elsewhere,[13] the method involves the use of an instrument that completes a single-temperature heating step to induce vial enzymatic lysis, RNA extraction, and the elimination of RNases. Additionally, the system enables the physical

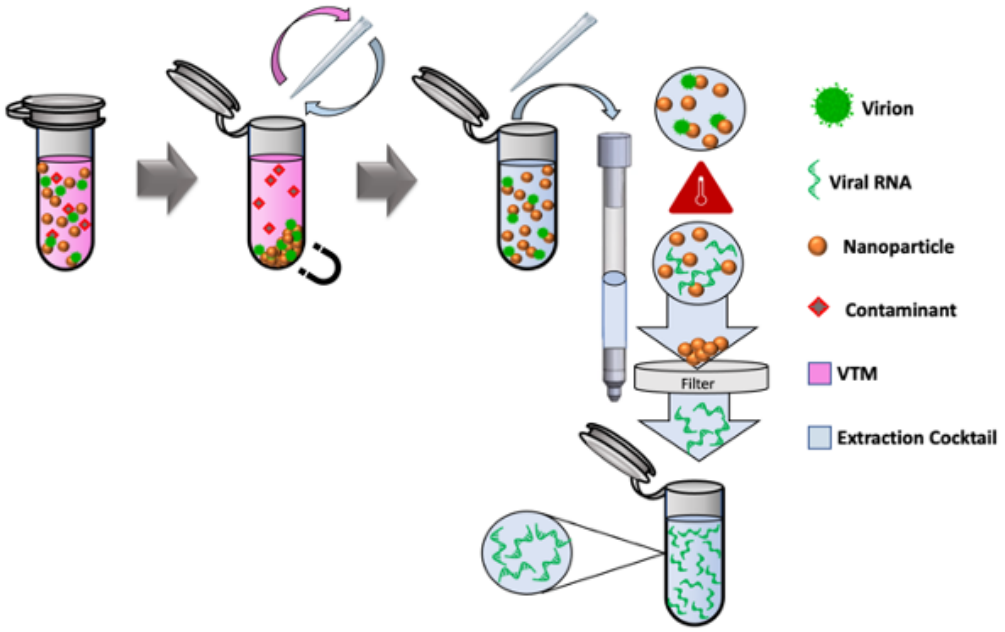

Figure 4-20. Adaptation of the extraction protocol to PDQeX method. (A) Following in-tube viral preconcentration, the capture particle suspension in rnaGEM cocktail was transferred to a PDQeX tube. Incubation induced the inner walls of the tube to shrink and the heat-burst valve below the sample reservoir to be actuated, forcing the purified RNA solution through an on-board filter and into a final collection tube.

separation of the capture particles from the eluate via the constriction of the sample tube's inner heat-shrink layer and actuation of a heat burst valve below the sample reservoir. This action forces fluid through an on-board filter and into a collection tube while retaining the capture particles.

To demonstrate proof-of-feasibility, analogous with DHHS initiatives, sample pooling up to dilutions of 1:20 were prepared and tested using this semi-automated sample preparation approach. Notably, sample volumes were able to be increased 10x in comparison to the microfluidic system described earlier in this chapter. That is, a total of 500 µL of pooled samples were used for analysis. **Figure 4-21** shows the C_t values associated with samples tested neat and diluted 1:5, 1:10, and 1:20 in negative patient samples to maintain matrix effects across dilutions.

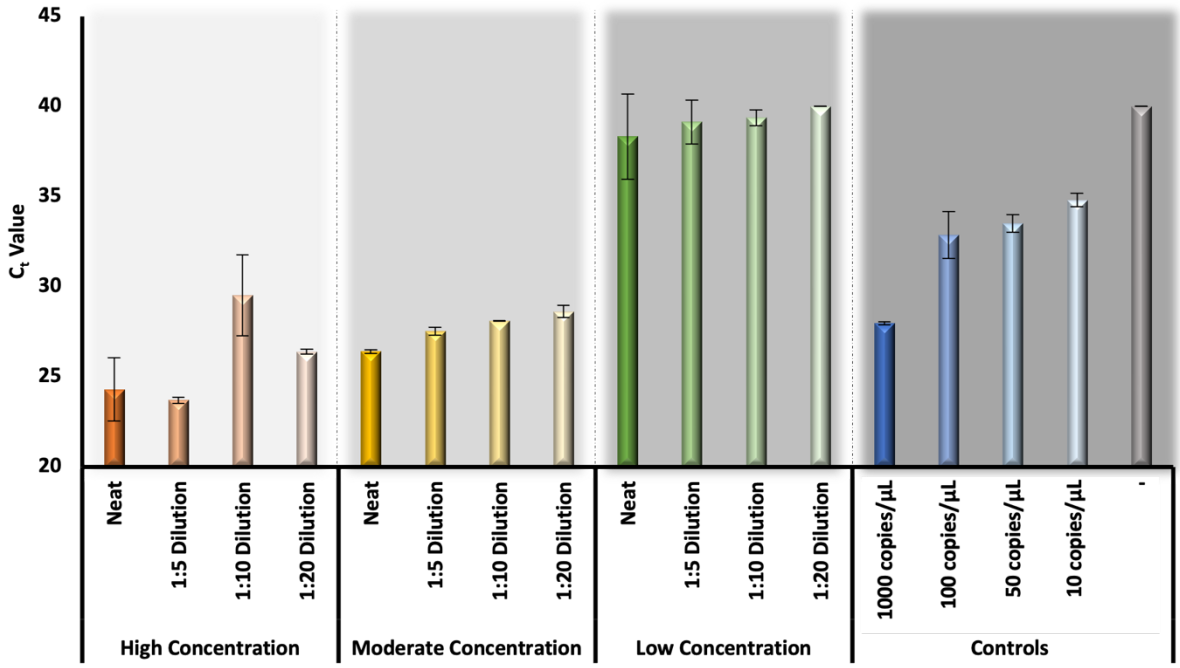

Figure 4-21. SARS-CoV-2 sample pooling using a semi-automated enrichment and extraction method. Nasopharyngeal swabs diluted in VTM from SARS-CoV-2 patients, prepared in 500 µL sample volumes. Samples were prepared using the modified PDQeX protocol with manual enrichment via Nanotrap particles. Resulting eluates were amplified alongside CDC plasmid positive controls, showing detection with CDC chemistry.

While moderate concentration samples perform as expected, that is, scaling dilution with C_t value, the results for the high concentration samples may demonstrate stochasticity as a result of the matrix effects. For reference, the matrices between samples were highly variable. Low concentration samples were largely approaching the negative threshold. Of note, a series of standards at various concentrations were tested in parallel and the reference results suggest that the lowest concentration sample is likely below 10 copies/μL. Further studies were completed by Marshall et al. demonstrating sensitivity with this method for pooling of up to 100 samples in one reaction tube.[21]

4.4. Conclusions

The most pervasive method for the testing and diagnosis of SARS-CoV-2 has proven to be amplification and detection by RT-PCR, due largely to its sensitivity and inherent specificity. Unfortunately, this method requires careful consideration of the sample preparation process to maintain that specificity, especially as it relates to population surveillance of the virus by sample pooling. I report multiple methods for the preparation of SARS-CoV-2 samples, slated for detection by RT-PCR. Both methods described leverage a workflow whereby viral enrichment and RNA extraction are coupled. Enrichment is based upon affinity-based Nanotrap particles that may be magnetically actuated for preconcentration of the virus itself and removal of any associated sample matrix (e.g., saliva, nasopharyngeal swab eluate, etc.). RNA extraction employs a neutral protease to simultaneously remove any implicit RNases and cleave cell-membrane proteins to release SARS-CoV-2 RNA; importantly, extraction occurs in a buffer compatible with downstream RT-PCR and does not require further purification steps that may lead to DNA loss. Here, the

methods are coupled in fully- and semi-automated modes, geared toward the preparation of samples with volumes <50 µL[14] and >50 µL[13], respectively. The preponderance of work described in this chapter focuses on the fully-automated method; however, the application of the larger volume method for sample pooling is discussed briefly.

The fully-automated method involves a rotationally driven system for SARS-CoV-2 sample preparation in under 15 min. The µCD is capable of processing up to six samples in parallel. Each domain can accommodate as much as 50 µL of input, which serves to ease the difficulty in bridging the macro- to microinterface, a persistent obstacle encountered in the development of microfluidic diagnostics.[38] Beyond the manual addition of clinical sample and reagents, all fluidic steps were automated to minimize user intervention, ease assay automation, and limit analyst exposure to viral pathogens. Integration of this method was facilitated by both the durability of the affinity-bait NPs and the versatility of the lysis chemistry.[8,13] Incorporation of enrichment enabled the removal of the virion from a matrix, likely to contain sample constituents that would negatively impact detection. The automation of this process on the µCD necessitated the design of an infrastructure capable of removing residual supernatant matrix without the use of an internal filter to sequester virion-containing NPs. To permit this, I used rotational force to our advantage, driving NPs to the vertex[19] of the requisite chamber for retention during supernatant flow to waste. I used dye studies to confirm that only a small amount of residual matrix remains in the final RNA eluate. Experimentally optimized enrichment parameters were paired with a one-step enzymatic extraction method to permit rapid provision of PCR-ready RNA. In-tube, the workflow demonstrated comparable performance to a gold-standard analytical technique, producing statistically similar C_t values with clinical samples at various concentrations diluted in

both water and saliva. Thus, our approach exhibits applicability to clinically relevant matrices. Using the μCD method for preparation, I reliably detected SARS-CoV-2 downstream with full-process controls and positive nasopharyngeal swabs suspended in VTM; in some cases, a comparison of C_t values indicated no statistical difference between eluates produced by the in-tube and μCD methods. Viral RNA was also successfully detected from saliva samples prepared by the μCD method, emphasizing the method's ability to handle sample matrices commonly encountered in clinical diagnostics.

With a view toward the integration of a downstream detection technology that would enable the development of a sample-to-answer PON microfluidic system for viral preparation and detection, on-board reagent storage strategies were explored. More specifically, amplification mixes were tested for their detection functionality following drying by vacufugation to mitigate the need for cold-chain transport. These preliminary studies indicate that, in addition to housing preparation reagents on-board that are known to be stable at room temperature, the amplification and detection reagents can also be dried down for integration with a microdevice while maintaining the sensitivity and selectivity for viral targets. Finally, as described earlier, sample pooling via a semi-automated method was tested for its ability to handle 'pools' of samples with a total volume up to 500 μL. Preliminary work toward surveillance monitoring demonstrates the application of the preparation mode for pools as dilute as 1:20 and acted as the foundation for a publication that successfully detected virion from pools with up to 100 patients.[21]

4.5. Acknowledgements

Special thanks to the National Institutes of Health (NIH) and the organizers of the Rapid Acceleration of Diagnostics (RADx) initiative for the financial support of this work. Acknowledgements to MicroGEM International, PLC for their collaborative efforts and supply of reagents.

4.6. References

(1) Guan, W.; Ni, Z.; Hu, Y.; Liang, W.; Ou, C.; He, J.; Liu, L.; Shan, H.; Lei, C.; Hui, D. S. C.; Du, B.; Li, L.; Zeng, G.; Yuen, K.-Y.; Chen, R.; Tang, C.; Wang, T.; Chen, P.; Xiang, J.; Li, S.; Wang, J.; Liang, Z.; Peng, Y.; Wei, L.; Liu, Y.; Hu, Y.; Peng, P.; Wang, J.; Liu, J.; Chen, Z.; Li, G.; Zheng, Z.; Qiu, S.; Luo, J.; Ye, C.; Zhu, S.; Zhong, N. Clinical Characteristics of Coronavirus Disease 2019 in China. *N Engl J Med* **2020**, *382* (18), 1708–1720. https://doi.org/10.1056/NEJMoa2002032.

(2) Uhteg, K.; Jarrett, J.; Richards, M.; Howard, C.; Morehead, E.; Geahr, M.; Gluck, L.; Hanlon, A.; Ellis, B.; Kaur, H.; Simner, P.; Carroll, K. C.; Mostafa, H. H. Comparing the Analytical Performance of Three SARS-CoV-2 Molecular Diagnostic Assays. *Journal of Clinical Virology* **2020**, *127*, 104384. https://doi.org/10.1016/j.jcv.2020.104384.

(3) Ali, N.; Rampazzo, R. de C. P.; Costa, A. D. T.; Krieger, M. A. Current Nucleic Acid Extraction Methods and Their Implications to Point-of-Care Diagnostics. *BioMed Research International* **2017**, *2017*, 1–13. https://doi.org/10.1155/2017/9306564.

(4) Esbin, M. N.; Whitney, O. N.; Chong, S.; Maurer, A.; Darzacq, X.; Tjian, R. Overcoming the Bottleneck to Widespread Testing: A Rapid Review of Nucleic Acid Testing Approaches for COVID-19 Detection. *RNA* **2020**, *26* (7), 771–783. https://doi.org/10.1261/rna.076232.120.

(5) Katevatis, C.; Fan, A.; Klapperich, C. M. Low Concentration DNA Extraction and Recovery Using a Silica Solid Phase. *PLoS ONE* **2017**, *12* (5), e0176848. https://doi.org/10.1371/journal.pone.0176848.

(6) Mina, M. J.; Parker, R.; Larremore, D. B. Rethinking Covid-19 Test Sensitivity — A Strategy for Containment. *N Engl J Med* **2020**, NEJMp2025631. https://doi.org/10.1056/NEJMp2025631.

(7) Hall, R. J.; Wang, J.; Todd, A. K.; Bissielo, A. B.; Yen, S.; Strydom, H.; Moore, N. E.; Ren, X.; Huang, Q. S.; Carter, P. E.; Peacey, M. Evaluation of Rapid and Simple Techniques for the Enrichment of Viruses Prior to Metagenomic Virus Discovery. *Journal of Virological Methods* **2014**, *195*, 194–204. https://doi.org/10.1016/j.jviromet.2013.08.035.

(8) Shafagati, N.; Narayanan, A.; Baer, A.; Fite, K.; Pinkham, C.; Bailey, C.; Kashanchi, F.; Lepene, B.; Kehn-Hall, K. The Use of NanoTrap Particles as a Sample Enrichment Method to Enhance the Detection of Rift Valley Fever Virus. *PLoS Negl Trop Dis* **2013**, *7* (7), e2296. https://doi.org/10.1371/journal.pntd.0002296.

(9) Barclay, R. A.; Akhrymuk, I.; Patnaik, A.; Callahan, V.; Lehman, C.; Andersen, P.; Barbero, R.; Barksdale, S.; Dunlap, R.; Goldfarb, D.; Jones-Roe, T.; Kelly, R.; Kim, B.; Miao, S.; Munns, A.; Munns, D.; Patel, S.; Porter, E.; Ramsey, R.; Sahoo, S.; Swahn, O.; Warsh, J.; Kehn-Hall, K.; Lepene, B. Hydrogel Particles Improve Detection of SARS-CoV-2 RNA from Multiple Sample Types. *Sci Rep* **2020**, *10* (1), 22425. https://doi.org/10.1038/s41598-020-78771-8.

(10) Maddu, N. Functions of Saliva. In *Saliva and Salivary Diagnostics*; Gokul, S., Ed.; IntechOpen, 2019. https://doi.org/10.5772/intechopen.84709.

(11) Schrader, C.; Schielke, A.; Ellerbroek, L.; Johne, R. PCR Inhibitors - Occurrence, Properties and Removal. *J Appl Microbiol* **2012**, *113* (5), 1014–1026. https://doi.org/10.1111/j.1365-2672.2012.05384.x.

(12) Luchini, A.; Geho, D. H.; Bishop, B.; Tran, D.; Xia, C.; Dufour, R. L.; Jones, C. D.; Espina, V.; Patanarut, A.; Zhou, W.; Ross, M. M.; Tessitore, A.; Petricoin, E. F.; Liotta, L. A. Smart Hydrogel Particles: Biomarker Harvesting: One-Step Affinity Purification, Size Exclusion, and Protection against Degradation. *Nano Lett.* **2008**, *8* (1), 350–361. https://doi.org/10.1021/nl072174l.

(13) Dignan, L. M.; Turiello, R.; Layne, T. R.; O'Connell, K. C.; Hickey, J.; Chapman, J.; Poulter, M. D.; Landers, J. P. An Ultrafast SARS-CoV-2 Virus Enrichment and Extraction Method Compatible with Multiple Modalities for RNA Detection. *Analytica Chimica Acta* **2021**, *1180*, 338846. https://doi.org/10.1016/j.aca.2021.338846.

(14) Turiello, R.; Dignan, L. M.; Thompson, B.; Poulter, M.; Hickey, J.; Chapman, J.; Landers, J. P. Centrifugal Microfluidic Method for Enrichment and Enzymatic Extraction of Severe Acute Respiratory Syndrome Coronavirus 2 RNA. *Anal. Chem.* **2022**, *94* (7), 3287–3295. https://doi.org/10.1021/acs.analchem.1c05215.

(15) Coolbear, T.; Eames, C. W.; Casey, Y.; Daniel, R. M.; Morgan, H. W. Screening of Strains Identified as Extremely Thermophilic Bacilli for Extracellular Proteolytic Activity and General Properties of the Proteinases from Two of the Strains. *Journal of Applied Bacteriology* **1991**, *71* (3), 252–264. https://doi.org/10.1111/j.1365-2672.1991.tb04456.x.

(16) Moss, D.; Harbison, S.-A.; Saul, D. J. An Easily Automated, Closed-Tube Forensic DNA Extraction Procedure Using a Thermostable Proteinase. *International Journal of Legal Medicine* **2003**, *117* (6), 340–349. https://doi.org/10.1007/s00414-003-0400-9.

(17) Strohmeier, O.; Keller, M.; Schwemmer, F.; Zehnle, S.; Mark, D.; von Stetten, F.; Zengerle, R.; Paust, N. Centrifugal Microfluidic Platforms: Advanced Unit Operations and Applications. *Chem. Soc. Rev.* **2015**, *44* (17), 6187–6229. https://doi.org/10.1039/C4CS00371C.

(18) Tian, F.; Liu, C.; Deng, J.; Han, Z.; Zhang, L.; Chen, Q.; Sun, J. A Fully Automated Centrifugal Microfluidic System for Sample-to-Answer Viral Nucleic Acid Testing. *Sci. China Chem.* **2020**, *63* (10), 1498–1506. https://doi.org/10.1007/s11426-020-9800-6.

(19) Dignan, L. M.; Woolf, M. S.; Tomley, C. J.; Nauman, A. Q.; Landers, J. P. Multiplexed Centrifugal Microfluidic System for Dynamic Solid-Phase Purification of Polynucleic Acids Direct from Buccal Swabs. *Anal. Chem.* **2021**, *93* (19), 7300–7309. https://doi.org/10.1021/acs.analchem.1c00842.

(20) Woolf, M. S.; Dignan, L. M.; Lewis, H. M.; Tomley, C. J.; Nauman, A. Q.; Landers, J. P. Optically-Controlled Closable Microvalves for Polymeric Centrifugal Microfluidic Devices. *Lab Chip* **2020**, *20* (8), 1426–1440. https://doi.org/10.1039/C9LC01187K.

(21) Marshall, J. S.; Turiello, R.; Cunha, L. L.; Frazier, E. V.; Hickey, J.; Chapman, J.; Poulter, M. D.; Fehling, H. L.; Landers, J. P. Rapid SARS-CoV-2 Virus Enrichment and RNA Extraction for Efficient Diagnostic Screening of Pooled Nasopharyngeal or Saliva Samples for Dilutions Up to 1:100. *Diagnostics* **2022**, *12* (6), 1398. https://doi.org/10.3390/diagnostics12061398.

(22) Thompson, B. L.; Ouyang, Y.; Duarte, G. R. M.; Carrilho, E.; Krauss, S. T.; Landers, J. P. Inexpensive, Rapid Prototyping of Microfluidic Devices Using Overhead Transparencies and

a Laser Print, Cut and Laminate Fabrication Method. *Nat Protoc* **2015**, *10* (6), 875–886. https://doi.org/10.1038/nprot.2015.051.

(23) Garcia-Cordero, J. L.; Kurzbuch, D.; Benito-Lopez, F.; Diamond, D.; Lee, L. P.; Ricco, A. J. Optically Addressable Single-Use Microfluidic Valves by Laser Printer Lithography. *Lab Chip* **2010**, *10* (20), 2680. https://doi.org/10.1039/c004980h.

(24) Woolf, M. S.; Dignan, L. M.; Scott, A. T.; Landers, J. P. Digital Postprocessing and Image Segmentation for Objective Analysis of Colorimetric Reactions. *Nat Protoc* **2021**, *16* (1), 218–238. https://doi.org/10.1038/s41596-020-00413-0.

(25) Freire-Paspuel, B.; Garcia-Bereguiain, M. A. Analytical Sensitivity and Clinical Performance of a Triplex RT-qPCR Assay Using CDC N1, N2, and RP Targets for SARS-CoV-2 Diagnosis. *International Journal of Infectious Diseases* **2021**, *102*, 14–16. https://doi.org/10.1016/j.ijid.2020.10.047.

(26) Xu, W.; Xu, N.; Zhang, M.; Wang, Y.; Ling, G.; Yuan, Y.; Zhang, P. Nanotraps Based on Multifunctional Materials for Trapping and Enrichment. *Acta Biomaterialia* **2021**, S1742706121005808. https://doi.org/10.1016/j.actbio.2021.08.047.

(27) Lounsbury, J. A.; Coult, N.; Miranian, D. C.; Cronk, S. M.; Haverstick, D. M.; Kinnon, P.; Saul, D. J.; Landers, J. P. An Enzyme-Based DNA Preparation Method for Application to Forensic Biological Samples and Degraded Stains. *Forensic Science International: Genetics* **2012**, *6* (5), 607–615. https://doi.org/10.1016/j.fsigen.2012.01.011.

(28) Bullard, J.; Dust, K.; Funk, D.; Strong, J. E.; Alexander, D.; Garnett, L.; Boodman, C.; Bello, A.; Hedley, A.; Schiffman, Z.; Doan, K.; Bastien, N.; Li, Y.; Van Caeseele, P. G.; Poliquin, G.

Predicting Infectious Severe Acute Respiratory Syndrome Coronavirus 2 From Diagnostic Samples. *Clinical Infectious Diseases* **2020**, ciaa638. https://doi.org/10.1093/cid/ciaa638.

(29) Kirkland, P. D.; Frost, M. J. The Impact of Viral Transport Media on PCR Assay Results for the Detection of Nucleic Acid from SARS-CoV-2. *Pathology* **2020**, *52* (7), 811–814. https://doi.org/10.1016/j.pathol.2020.09.013.

(30) Perchetti, G. A.; Huang, M.-L.; Peddu, V.; Jerome, K. R.; Greninger, A. L. Stability of SARS-CoV-2 in Phosphate-Buffered Saline for Molecular Detection. *J Clin Microbiol* **2020**, *58* (8). https://doi.org/10.1128/JCM.01094-20.

(31) Carraturo, F.; Del Giudice, C.; Morelli, M.; Cerullo, V.; Libralato, G.; Galdiero, E.; Guida, M. Persistence of SARS-CoV-2 in the Environment and COVID-19 Transmission Risk from Environmental Matrices and Surfaces. *Environmental Pollution* **2020**, *265*, 115010. https://doi.org/10.1016/j.envpol.2020.115010.

(32) Ceron, J.; Lamy, E.; Martinez-Subiela, S.; Lopez-Jornet, P.; Capela-Silva, F.; Eckersall, P.; Tvarijonaviciute, A. Use of Saliva for Diagnosis and Monitoring the SARS-CoV-2: A General Perspective. *JCM* **2020**, *9* (5), 1491. https://doi.org/10.3390/jcm9051491.

(33) Deng, J.; Jiang, X. Advances in Reagents Storage and Release in Self-Contained Point-of-Care Devices. *Adv Materials Technologies* **2019**, *4* (6), 1800625. https://doi.org/10.1002/admt.201800625.

(34) Bruijns, B.; Veciana, A.; Tiggelaar, R.; Gardeniers, H. Cyclic Olefin Copolymer Microfluidic Devices for Forensic Applications. *Biosensors* **2019**, *9* (3), 85. https://doi.org/10.3390/bios9030085.

(35) Rodrigues, R. G.; Condelipes, P. G. M.; Rosa, R. R.; Chu, V.; Conde, J. P. Scalable Processing of Cyclic Olefin Copolymer (COC) Microfluidic Biochips. *Micromachines* **2023**, *14* (10), 1837. https://doi.org/10.3390/mi14101837.

(36) Lohse, S.; Pfuhl, T.; Berkó-Göttel, B.; Rissland, J.; Geißler, T.; Gärtner, B.; Becker, S. L.; Schneitler, S.; Smola, S. Pooling of Samples for Testing for SARS-CoV-2 in Asymptomatic People. *The Lancet Infectious Diseases* **2020**, *20* (11), 1231–1232. https://doi.org/10.1016/S1473-3099(20)30362-5.

(37) *Report to Congress COVID-19 Strategic Testing Plan*; 2020. https://www.democrats.senate.gov/imo/media/doc/COVID%20National%20Diagnostics%20Strategy%2005%2024%202020%20v%20FINAL.pdf.

(38) Fredrickson, C. K.; Fan, Z. H. Macro-to-Micro Interfaces for Microfluidic Devices. *Lab Chip* **2004**, *4* (6), 526. https://doi.org/10.1039/b410720a.

Chapter 5. Perspectives Regarding Microfluidic Technologies Aimed at Forensic Implementation, Final Remarks, and A Vision For the Future.

Publication(s) included in Chapter 5:

- **Turiello, R.**; Nouwairi, R.; Landers, J. P. Taking the Microfluidic Approach to Nucleic Acid Analysis in Forensics: Review and Perspectives. *Forensic Science International: Genetics*, 2022, 63. doi: 10.1016/j.fsigen.2022.102824

5.1. Conclusions

The microfluidic technologies developed as part of this dissertation were focused on enhancing nucleic acid (NA) sample preparation workflows for laboratory automation and improved recovery of genetic material for both forensic and clinical applications. The motivation to concentrate specifically on NA preparation as opposed to downstream analytical steps was because the success of the sample enrichment, extraction, and/or epigenetic conversion is outcome determinative, regardless of the application. Likewise, each of the aforementioned NA preparation methods are conventionally labor-intensive and time-consuming, making automation difficult from start-to-finish and generally challenging for laboratories to adopt. Furthermore, adapting each workflow to a microfluidic scheme permits not only streamlined sample preparation, but also the coupling of multiple preparation processes that would otherwise require hours at the bench.

As the preponderance of the work featured in this dissertation was focused on microfluidic technologies aimed to enhance a forensic genetics workflow, **Chapter 1** serves as a

review and perspective in this area.[1] An abridged history of the convergence of microfluidic technology and forensic practice is presented, as it relates to DNA-based human identification (HID). A brief summary detailing many of the recent microfluidic approaches to discrete portions of the forensic genetics workflow is provided, as well as descriptions and comparisons of the few sample-to-answer systems that have been commercialized to date. For additional context, the unique advantages and practical limitations of microfluidic technologies slated for the forensic genetics marketplace are provided. Finally, the chapter narrows to focus specifically on the limited implementation of forensic epigenetic analysis in criminal casework, especially considering the magnitude of related research publications.

Chapter 2 described the development of a microfluidic disc for dynamic solid phase bisulfite conversion (dSP-BSC) aimed for epigenetic-based human chronological age prediction.[2] The disc was designed to facilitate the deamination of unmethylated cytosines to uracil, beginning with sulphonation and hydrolytic deamination via incubation with ammonium bisulfite in a *conversion chamber*, to produce 5,6-dihydrouracil-6-sulphonate. The partially-converted material was then bound to silica particles to undergo purification and a final desulphonation step in a *magnetic manipulation chamber*, designed specifically to partition the sample from magnetic beads during each unit operation and as reagents are released in sequence. The device was evaluated for its comparative performance to the conventional workflow with regard to DNA recovery and conversion efficiency by targeted real-time polymerase chain reaction (RT-PCR) and high resolution melting (HRM), respectively. While limited in scope from a genomic perspective, the relative differences in C_t and T_m values as reaction conditions were altered in a stepwise fashion did follow expected trends; for example, shortened sulphonation and deamination

incubation time scaled appropriately with melting temperatures as GC content was preserved. Ultimately, the entire conversion workflow duration was reduced by ~40%, an estimation not including the time saved with automation on the microfluidic platform. While DNA recovery on the device showed comparable results to the conventional method overall, recovery was increased when testing the microfluidic conditions in-tube. Thus, it was surmised that the fluid lost, either due to evaporation or to the surrounding heat-sensitive adhesive (HSA) between disc layers, contributed to some loss of DNA in the system. Still, performance was determined to be comparable to the gold-standard workflow in terms of recovery and conversion efficiency.

To further reduce the amount of DNA lost during the epigenetic sample preparation workflow, **Chapter 3** focused on the use of an enzymatic method for DNA extraction to be incorporated upstream of microfluidic conversion. Compared to the standard mode of DNA extraction that utilizes proteinase K/sodium dodecyl sulfate (SDS), enzymatic lysis by the neutral protease *Bacillus* sp. strain EA1 is a one-step extraction method that eliminates the need for purification by silica. Initial studies concentrated on characterizing exactly how much DNA was lost with purification, and retained by the EA1 extraction method. To this end, pre-purified DNA standards with non-methylated and methylated genomes were “extracted” by either method and results from parallel reactions each indicated that an average of 26% of DNA was lost to purification. Integration of EA1 extraction upstream of epigenetic conversion was completed with K-562 prepared cells and venous blood from anonymous donors at UVA hospital; preliminary studies indicated that the non-purified eluate originating from EA1 extraction was indeed compatible with downstream conversion followed by targeted RT-PCR, HRM, and pyrosequencing with age-associated targets. The method also demonstrated effective lysis and downstream

testing following an extraction protocol as short as 15 s. As part of this work, a microfluidic architecture was proposed to enable integrated extraction and conversion, permitting direct-from-swab enzymatic lysis followed by the precise metering of ~2.039 μL of eluate for epigenetic conversion by bisulfite. Preliminary characterization of the microfluidic extraction method was completed with FLOQSwabs containing 10 μL of blood; RT-PCR and HRM results confirmed functionality of the microfluidic approach in terms of DNA recovery and conversion efficiency. While the pyrosequencing of samples prepared using the device does result in sequencing reads, one of three replicates was flagged, indicating there may be some inhibition related to disc materials that requires further optimization.

Utilizing similar microfluidic design features as those proposed in **Chapters 2 – 3**, **Chapter 4** presents a method for the sample preparation of severe acute respiratory syndrome coronavirus 2 (SARS-CoV-2) aimed for diagnostic testing via downstream RT-PCR.[3,4,5] The work described therein was developed in response to the 2020 global pandemic and with support from the National Institutes of Health (NIH) Rapid Acceleration of Diagnostics (RADx) initiative to enhance viral surveillance and containment efforts. Initial studies, not fully detailed in this dissertation but described elsewhere,[6] worked to characterize the coupling of affinity-capture nanoparticle enrichment and EA1-based enzymatic lysis of the viral envelope. This workflow was meant to effectively enhance diagnostic sensitivity via virus preconcentration, matrix removal, and eliminate the need for silica-based purification, which is known to result in nucleic acid (NA) loss. In particular, **Chapter 4** of this dissertation seeks to characterize the enrichment method in terms of optimal incubation time and nanoparticle percent contribution with aqueous samples constructed from patient nasopharyngeal (NP) swabs diluted in viral transport medium (VTM)

and saliva collections. To automate the entire workflow, a rotationally-driven microfluidic disc is proposed and validated for functionality by colorimetric dye studies. The fully integrated microfluidic workflow performance is compared with the benchtop approach using reference standards, NP swabs suspended in VTM, and patient samples diluted in a saliva matrix. The full workflow required a total of 50 μL of sample per replicate and permitted the parallel preparation of up to 6 samples in under 15 min. Additional work tested the method by measuring amplification with a chemistry designed toward a sample-to-answer COVID diagnostic, and results indicated the potential for the method to be used for surveillance testing via sample pooling.

5.2. Ongoing Studies, Future Work, and Persistent Challenges.

Below, ongoing studies and future work are described, specifically as it relates to the forensic epigenetic technology disclosed in this dissertation. Briefly, ongoing studies are focused on the validation of the method for coupled sample preparation, described in **Chapter 3**. These would ideally include additional work to more thoroughly characterize the performance of the integrated extraction and conversion method, with a focus on the quantity and quality of genomic DNA following preparation and the resultant bisulfite conversion efficiency. Future work will shift to the development of a sample-to-answer epigenetic system leveraging microfluidic cycle sequencing. Persistent challenges related to pyrosequencing optimization and the use of a potentially inhibitory reagent are described as well.

5.2.1. Ongoing and Future Work Toward an Integrated Method for Epigenetic Sample Preparation and Beyond. As discussed, **Chapters 2 – 3** were focused on the development of microfluidic tools for epigenetic sample preparation with the goal of automating the entire process and making it more amenable to input forensically-relevant concentrations of genetic material. Once again, these processes included DNA extraction by a neutral protease and bisulfite conversion. Contrary to their order in the analytical workflow, the development of a conversion method was completed first. **Chapter 3** focused predominantly on verifying the extraction chemistry was compatible with downstream conversion by ammonium bisulfite, with very preliminary studies involving the coupling of both processes onto the microfluidic system. Work to further develop, characterize, and validate the entire microfluidic process is ongoing.

In addition to the typical elements associated with validation of a microfluidic method, like demonstration of analytical range and sensitivity, studies to examine the effect of using this method upstream of human chronological age prediction are required. For context, recent work comparing the accuracy of age prediction using different amounts of input DNA have demonstrated increased error in age predication (mean absolute error, MAE) with less than ~2 ng of DNA in the amplification reaction, a very small amount for the application.[7,8] While promising, this input amount is still not comparable to other highly sensitivity forensic genetics methods capable of produced results from only picograms on input material.[8] We can extrapolate that accurate predictions require the recovery of as much input DNA as possible. Using conventional methods for extraction and conversion result in a significant and highly variable loss of genetic material; therefore, recouping the losses by eliminating the need for purification, whereby an estimated ~26% of DNA may be lost (**Chapter 3**), and by reducing conversion incubation

parameters to abasic site-related strand scission (**Chapter 2**), should enhance prediction accuracies. In summary, ongoing work will estimate the total time saved and the increase in recovered DNA after coupling these processes onto a microfluidic platform.

Future work should focus on shifting from a targeted genetic approach to device validation to one that provides a more comprehensive, (epi)*genomic* view of experimental outcomes. In brief, the targeted approach taken to examine the aforementioned technology, specifically as it relates to the bisulfite conversion method described in **Chapter 2**, may not be considered ideal since it only provides insight into a limited number of age-associated targets that are ostensibly *enriched* by amplification. That is, a targeted approach does not indicate the extent of DNA fragmentation or conversion efficiency across differentially methylated regions of the genome. Of course, if the application is for RT-PCR and HRM-based age prediction at ~2 loci, as reported by Hamano et al., validating the method using a targeted approach is acceptable, as it is only necessary to determine how those loci are effected by preparation with the microdevice.[9] However, if this method of sample preparation is to be considered compatible with epigenetically-based age predication assays that leverage pyrosequencing and next generation sequencing (NGS), a more global estimation of the quality and quantity of bisulfite-converted DNA is necessary. Therefore, future work would include the use of a multi-target assay, such as the "QBico Tool" developed by Athina Vidaki,[10] to more thoroughly evaluate bisulfite conversion efficiency and degradation. The Vidaki assay uses multiplex PCR and comparative analysis with standards in parallel to assess bisulfite-treated genomic DNA for quality, quantity, and conversion efficiency.[10]

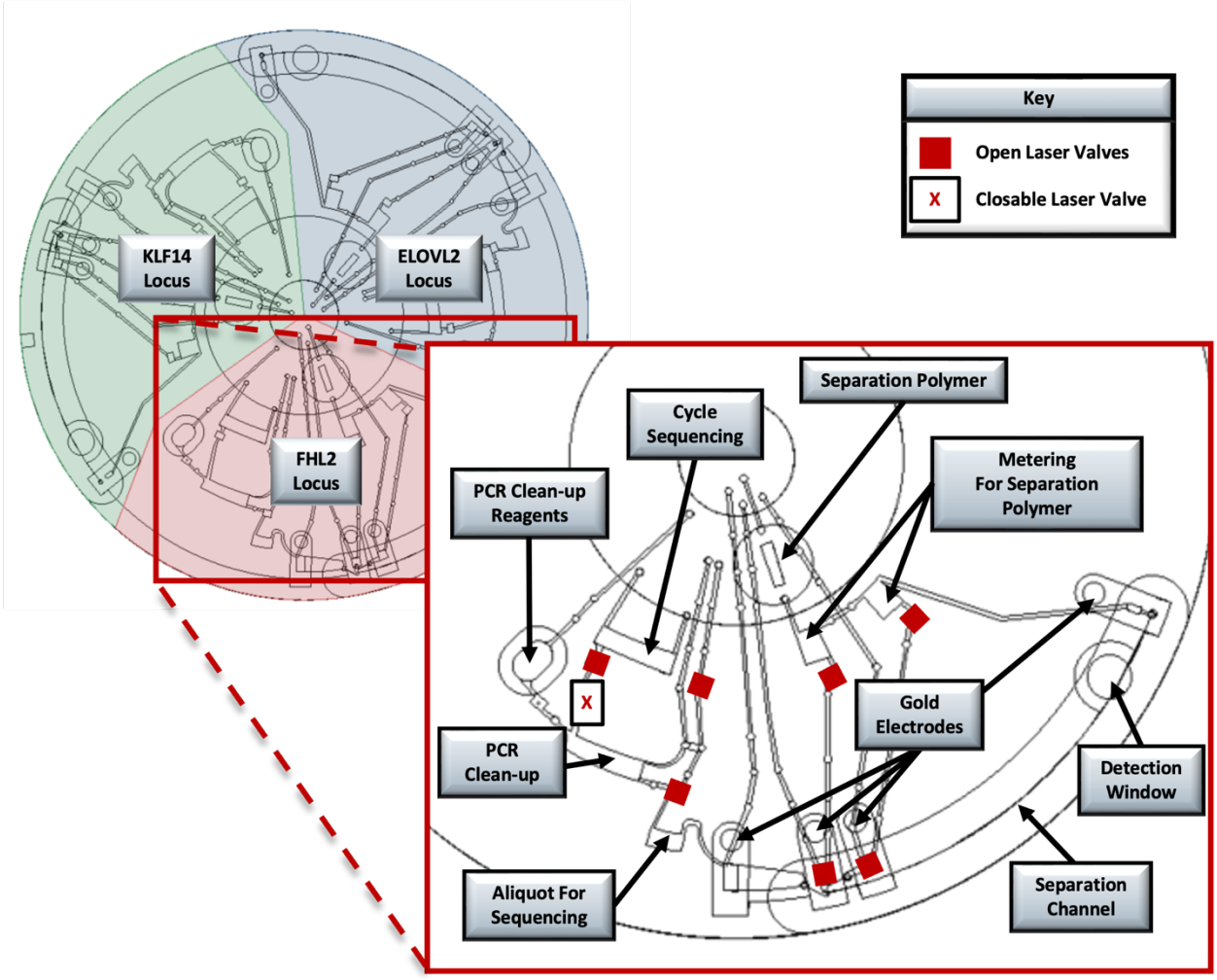

Figure 5-1. Microfluidic Disc for Downstream Age Detection by Sanger Sequencing. AutoCAD rendering with highlighted domains designated for separation of three age-related targets and a close-up of the microfluidic architecture in one domain. Design includes the reagent chambers for PCR clean-up, and separation polymer; reaction chambers for cycle sequencing, PCR clean-up, and sequencing; and metering chambers for sample amplicons and separation polymer. Accessory pieces include a central adaptor for integration with the mechatronic system, gold electrodes flanking the channel, and the COC separation channel with an integrated cross-T design.

Looking to the future and beyond epigenetic sample preparation alone, the creation of an integrated sample-to-answer method for forensic epigenetic analysis would increase ease of analysis in the lab and at the point-of-need. The proposed design for a rotationally-driven disc for multiplexed age-prediction is depicted in **Figure 5-1**. The microdevice unit operations would include template preparation by cycle sequencing (i.e., sanger sequencing amplification), post-

PCR clean-up, and electrophoretic separation and detection. The architecture described would house three separate domains, each capable of performing the fully-integrated aforementioned workflow; that is, each disc will be capable of running Sanger sequencing for three targets and in three individual separation channels. The purpose of domain sequestration is to enable target multiplexing from one donor sample with the age-associated targets ELOVL2, FHL2, and KLF14.[11] This way, multiple linear regression analysis of the data produced by one microdevice could provide enough genetic information for a predictive measure of human chronological age. This disc would leverage the mechatronic system, termed the "FaSTR System," first developed by the Landers Group for forensic analysis of short tandem repeats (STRs) (**Fig. 5-2**).[12] This associated instrument will facilitate the pumping of fluid rotationally through a series of channels and vented chambers for thermal cycling, incubations, and injection-based separations. As with the methods described in this dissertation (**Chapters 2 – 4**), accurate and precise on-disc fluidic control and integration should be tested with dye studies and subsequent objective image analysis via digital postprocessing using imaging software, such as Fiji ImageJ Freeware.[13] Additional optimization would include testing the separation and detection architecture to ensure adequate injection and separation

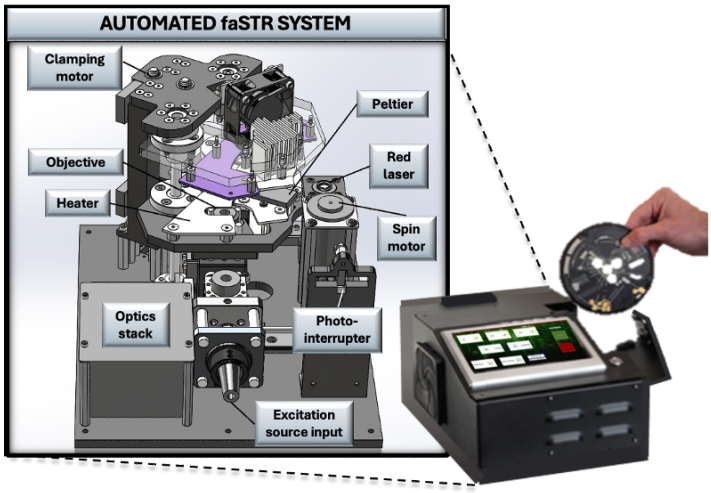

Figure 5-2 Schematic of the FaSTR System. The mechatronic system includes architecture for device rotation, laser valving, thermal cycling, and separation and detection of STRs for forensic identification in under 45 minutes. The full system is complete with a touchscreen featuring a graphical-user interface (GUI) for ease of analysis. Figure adapted from Tsuei Scott.[12]

parameters, focused laser excitation, fluorescence detection, and single-base pair resolution. For sample-to-answer epigenetic analysis, this disc would require integration with the sample preparation disc detailed in **Chapter 3**.

5.2.2. Persistent Challenges.

5.2.2.1. Pyrosequencing Assay Optimization. Human age approximation via interrogation of methylation status at select CpGs is most often accomplished using pyrosequencing assays.[14] Pyrosequencing is a sequencing-by-synthesis method whereby DNA elongation is catalyzed by DNA polymerase as deoxynucleotide triphosphates (dNTPs) are introduced and pyrophosphate (PPi) is released and converted to adenosine triphosphate (ATP) by sulfurylase. To generate a light for interpretation by the instrument's software, ATP powers the oxidation of luciferin by luciferase to ultimately produce a fluorescent signal each time a dNTP is incorporated in a predetermined order.[15] While the method is limited in its ability to multiplex large numbers of samples and CpGs in a single run compared with other NGS tools, it is cost-effective and ideal for limited locus analysis applications like age estimation. However, similar to other methylation-specific detection modes, careful consideration must be paid to assay design to ensure specificity, sensitivity, and maintained signal across the locus, especially as it relates to bisulfite-treated DNA. In fact, it has been reported that sequencing efficiency drops after 140 base pairs (bps), as enzyme concentrations and efficiencies dilute with each cycle of base addition.[16] While limited data related to pyrosequencing is presented as part of the dissertation work, optimization of multiple assays are in progress for additional validation and age approximation. Initial efforts focused on implementing an assay to interrogate the ELOVL2 region, described by Zbieć-Piekarska et al. in

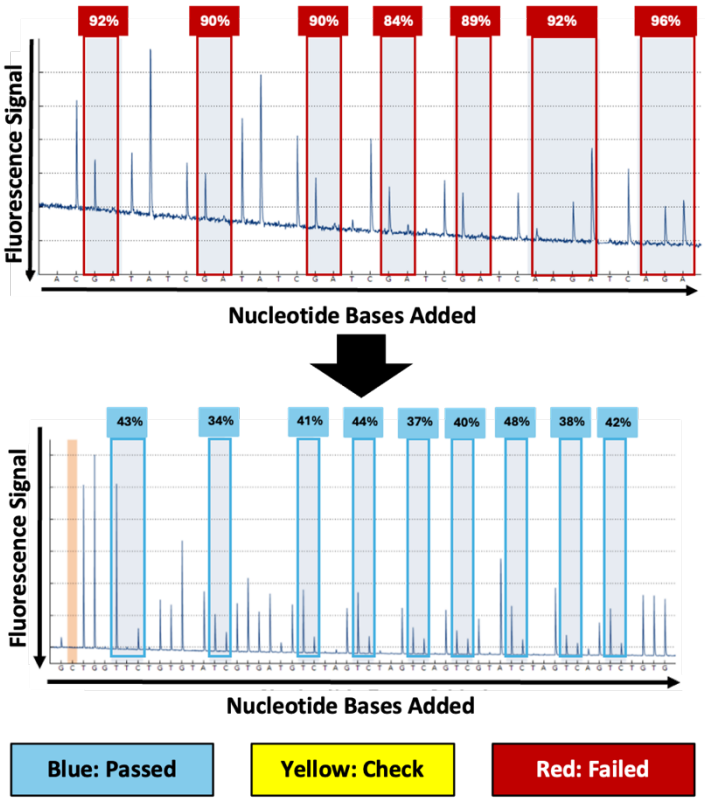

Figure 5-3. Pyrosequencing Signal Optimization. Enhanced performance following assay optimization and vibrational noise reduction through the incorporation of a granite slab.

2015.[11] Unfortunately, due to the complexity of the region and CpGs of interest, the amplicon length far exceeded the 140 bps required for efficient pyrosequencing, leading to red flagged allele calls and indicating signal decline across the locus. Of note, this assay was first developed to work on a different generation pyrosequencing instrument. Several studies were completed in an effort to enhance pyrosequencing results with this assay, including a titration of the amplification primers, primer annealing studies to minimize bisulfite-related PCR bias, a reduction of the streptavidin bead volume per reaction, and a titration of sequencing primers. Through collaborative efforts with Qiagen, the assay was improved by the addition of a third amplification primer, which included biotinylated sequences designed to amplify both methylated and unmethylated transcripts. However, results remained stochastic overall, even with the additional optimization repeated for the redesigned assay (i.e., primer titrations, annealing temperature optimization, etc.). It was not until the instrument was stabilized on a granite slab to minimize vibrational noise that signal was improved enough to be considered "passed" by the instrument and across the locus (**Figure 5-3**). A similar finding related to vibrational noise-related

pyrosequencing failure was reported by Konrad et al. in 2022.[17] Konrad described that 73% of analyses "failed" prior to the placement of PyroMark Q48 instruments on weighing tables that minimized vibrational disruption and resulted in successful and reproducible pyrosequencing in 88% of samples tested.[17] Kampmann et al., who also modeled their age assay and prediction model on the Zbieć-Piekarska method,[11] described that 218 of 960 sequencing runs were flagged by the PyroMark Q48 software.[18] In response, the authors opted to ignore the quality assessment, instead electing to use their own manual analysis for quality control, resulting in the inclusion of 957 of 960 runs.[18] In this dissertation, the ELOVL2 assay described by Kampmann was leveraged for the sequencing described in **Chapter 3.** While the testing was successful overall, the Q48 quality assessment did flag some of the data that showed clearly resolved peaks at the loci of interest. Additional work to test the upstream sample preparation method with the entire aging panel is underway.[18]

5.2.2.2. Indications of Fluid Loss and Inhibition Related to the Heat-Sensitive Adhesive used for Polymeric Disc Fabrication. The microfluidic devices described in this dissertation were composed of layered polymeric materials, chiefly polyethylene terephthalate (PeT), that were thermally bonded together via a heat-sensitive/activated adhesive (HSA/HAA). For bonding, disc layers containing all architectural features including all chambers and channels, were aligned, placed inside of an envelope composed of brass shimstock, and laminated together using a commercial-off-the-shelf laminator by passing the envelope through the laminator twice.[19] The bonding temperature was routinely monitored via external thermocouple and typically approached between 180°C to 183°C. Following lamination, the device was placed in an oven and

under weights at 40°C for no less than one hour before accessory components were added. With this protocol, the fabricated discs appeared as a monolithic structure with successfully connected channels and chambers, as intended.

Functionality in terms of fluid retention and flow was confirmed with dye studies and with the addition of reagents; however, the targeted application of heat via a Peltier to microdevice chambers resulted in the visual deformation of the disc in this region. This phenomenon was observed for heated incubations greater than 75°C, especially when the hold duration was greater than 30 s, which was required for the enzymatic extraction described in **Chapter 3**. Furthermore, following the heated incubation and deformation, the full volume of fluid was not retained and the area directly surrounding the chamber often appeared darker, as if saturated with some amount of liquid. The amount of fluid loss experienced with the longest heated incubation, according to the bisulfite conversion reaction, is characterized by colorimetric dye studies in **Chapter 2** (**Fig. 2-16 and 2-17**). These results indicate that some amount of delamination is occurring with heated incubations on-disc. According to the product information sheet provided by the manufacturer, the heat-activated adhesive transfer tape used for thermal bonding is composed of a polyester resin and a cross-linker that can be activated *at temperatures less than 100 ℃*, with an optimal application temperature around 162°C.[20] Thus, fluid loss is likely occurring through re-activation of the adhesive material and subsequent delamination.

In addition to the fluid loss following the heated re-activation of adhesive material between layers, there is concern of the potential for HSA-related acidification of aqueous reagents on the discs. While the exact formulation of the particular HSA is proprietary, polyester resins are typically composed of various unsaturated acids, such as fumaric acid, maleic anhydride, or

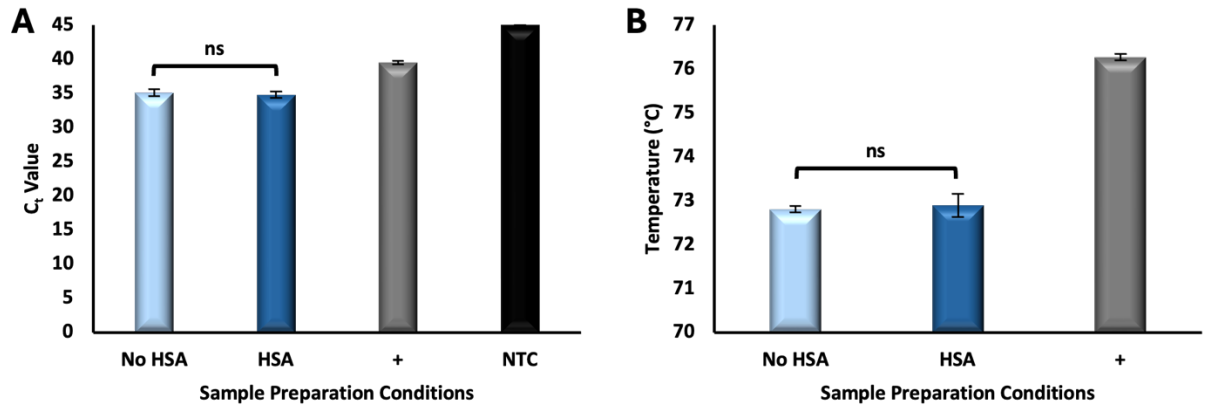

Figure 5-4. Performance Following Conversion with HSA. Heat-sensitive adhesive was incubated in 4 mm punches during the sulphonation and deamination incubations associated with bisulfite conversion. RT-PCR (A) and HRM (B) results show no resultant statistical differences between conditions, indicating that HSA-related acidification doesn't interfere with the reaction at this stage.

phthalic or terephthalic acid. Dignan completed a colorimetric evaluation of a pH solution that had been heated on a microfluidic disc composed of the same HSA; her findings suggested that hue distributions widened considerably following only 1 min of heating in the presence of HSA at 95°C, indicating rapid acidification (unpublished work). These experiments confirmed the release of protons into solution following delamination of the material from on-disc heating. Concerning the applications described in **Chapter 2 and 3**, samples spiked with HSA punches during the sulphonation and deamination step showed no inhibition via RT-PCR and HRM (**Fig. 5-4A and B**). Average C_t and T_m values showed no statistical differences between replicates tested by either condition (unpaired t-tests, $\alpha = 0.05$, p-values = 0.233 and 0.415, respectively). However, irregular pyrosequencing data was observed between the two conditions, indicating that samples processed in the presence of HSA might result in more flagged alleles by the Q48 quality assessment mechanism. Still, for the reasons described in section 5.2.2.1 of this chapter,

additional research should be completed to ensure this is not also an effect of adverse instrument vibration.

5.3. Considering Technological Developments Slated for Forensic Implementation.

Considering much of the work detailed in this dissertation was focused on the development of a microfluidic tool for forensic genetic integration, the remaining focus of this chapter is on the future implementation of microfluidic tools for forensic use. In the following sub-sections, I consider the trade-offs associated with microfluidic integration into the forensic genetics workflow, describing the intricate forensic climate and commenting on the limited implementation of these tools to-date. I posit that microfluidic technologies would have a higher impact potential if they were developed to solve new problems or facilitate the use of emerging techniques that have not yet been utilized widely beyond proof-of-principle research. Multiple opportunities for microfluidic integration within HID and criminal investigation are proposed to increase laboratory efficiency and expand the capacity of forensic science services in the future. Furthermore, the potential for the integration of the existing commercial systems for Rapid DNA analysis and expedited HID are discussed.

5.3.1. Trade-offs and the Forensic Landscape. When considering the unique advantages of deployment of microfluidic devices for Rapid DNA typing, one should be cognizant of the practical limitations that must be overcome and contextualize them within the broader forensic genetics community. Collectively, the forensic culture contributes to a nuanced marketplace that is not easily distilled down to a simple case of supply and demand. It is clear that this particular

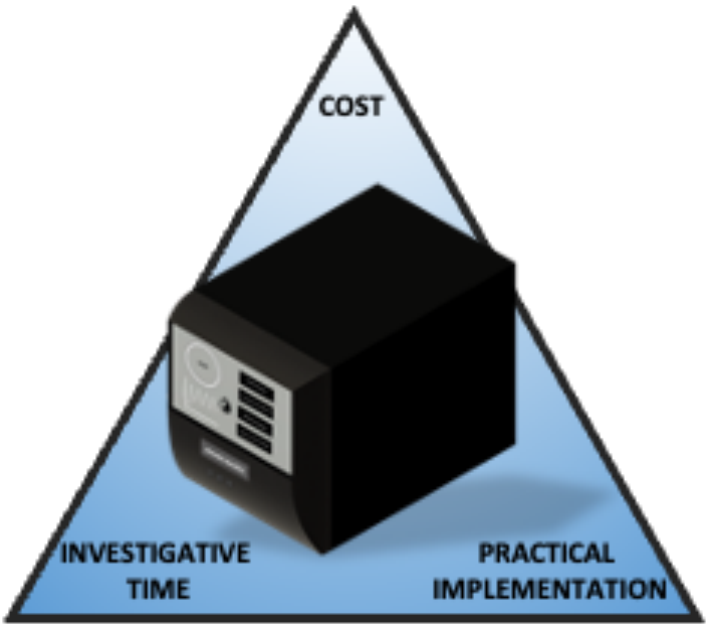

Figure 5-5. Trade off-triangle. Related to the implementation of microfluidic technology for forensic human identification. Adapted from Turiello et al. 2023[1]

landscape is complex and multifaceted, and layered with considerations pertinent to the case-working laboratories, critical to their oversight bodies, and important to the communities they serve. These considerations restrict microfluidic tools from being deployed in the same manner across all labs, or even among members or units within one organization. Here I discuss some of the factors and hurdles that I believe have contributed to the limited implementation of these tools in practice. For clarity and case study purposes, the focus is primarily on the commercially-available tools for sample-to-answer Rapid DNA analysis. Additionally, this discussion is contextualized around public crime laboratories, which can be collectively regarded as being overburdened, underfunded, and existing within an adversarial judicial system designed to scrutinize every fact in the pursuit of a fair trial.[21] The implementation of new technology in these types of bureaucratic organizations requires a careful consideration of the trade-offs and realistic expectations, narrowing the menu of potential opportunities to those that are more conservative. For Rapid DNA technology in particular, these trade-offs predominantly involve cost, practical use at the scene, and investigative time (**Fig. 5-5**).

5.3.1.1. Cost. On its face, currently available microfluidic DNA technology is more expensive and limited in throughput relative to traditional analytical workflows. For example, when calculating reagent cost per sample, the ANDE 6C Rapid DNA Identification System is ~$250 (assuming 5-sample analysis), almost 10x the cost relative to conventional analysis.[22] Additionally, the instrument only supports the processing of a maximum of five samples simultaneously. While there is no direct comparison for end-to-end throughput using the traditional methods, it is noteworthy that the QIAcube HT (QIAGEN) biorobot automates sample preparation for up to 96 samples and the 3500xL Genetic Analyzer (Thermo Fisher Scientific) has the capacity to perform CE on as many as 384 samples in one run. Unlike the ANDE 6C, however, it would be hard to imagine the QIAcube or the 3500xL to be considered '2-man luggable', a prerequisite for Rapid DNA technologies developed as a result of the 2010 Rapid DNA Initiative. In addition to the steep per sample cost, purchase of the ANDE 6C can run as high as $250,000.[23] Up-front costs aside, recall that no analyst intervention is required for reference samples, and is only necessary for more complex inputs at the interpretation stage. Thus, with laboratory overhead considerations, the cost of analysis could be considered justifiable. From a societal perspective, it has been argued that the 'added value' can be correlated to the outcome of criminal investigations, courtroom rulings, and the corresponding ability to reduce crime.[24] Unfortunately, factors like crime reduction and courtroom outcomes are not easily quantified, and may take years to come to fruition for a true assessment of the added value versus cost of a new technology, especially considering most forensic laboratories are crowd-funded by tax dollars appropriated for forensic services. This government-defined budget is reevaluated and renewed annually on the basis of perceived need, crime clearance rates, and budgetary restrictions. With a true added value

difficult to quantify and with limited availability of resources, even the most forward-thinking and adaptable crime laboratories might not be willing or able to justify the start-up costs associated with a new technology that, at least initially, is more expensive and can be considered less capable than existing strategies.

5.3.1.2. Practical Implementation. The commercially-available instruments are constrained by lower sensitivity, absence of pre-PCR quantitation, and the inability to handle some complex samples. These factors alone don't restrict use at the crime scene, but from a quality assurance/quality control perspective, it becomes difficult to ensure standard performance across a variety of case scenarios. The precedent for forensic HID via laboratory-based DNA analysis is that standardization is key to successful prosecution. Public laboratories must abide by the rules and regulations developed by numerous accreditation bodies, each with their own guiding principles, to ensure quality DNA profiles are being generated and recorded in STR databases for use in criminal proceedings. From a legal perspective, the regulations and procedures surrounding DNA typing should be unapologetically stringent, given the weight with which DNA evidence is considered. However, in practice, all case scenarios cannot be weighed equally, and there must be some flexibility; in fact, forensic quality management systems are designed to facilitate continuous improvement.[25] The complicating factor here is 'expectation': the scientific requirements for implementation of new technology in the field should be flexible to allow for progress, but standards for the admissibility of evidence necessitate established, widely-accepted, and strict protocols. The result of this conflict is a legal struggle to find common ground whenever a new technology enters the forensic workflow (e.g., admissibility hearings)

ultimately setting a new precedent for use cases. With so many unanswered questions involving universal compatibility with crime scene samples and the labyrinth that is providing expert testimony on the results generated from systems featuring proprietary technology, laboratory personnel may be hesitant to use Rapid DNA tools at the PON in their current form. Furthermore, agencies may be mandated to conserve raw sample and/or DNA extract to enable analysis in the future or by an independent laboratory on behalf of the defendant, discouraging the use of analytical methods beyond those deemed conventional.

5.3.1.3. Investigative Time. For public safety reasons, instruments capable of the rapid return of genetic information are extremely beneficial to investigative efforts, whereby the first few days of an investigation are critical. Findings from an exploratory study of the National Incident-Based Report System (NIBRS) reported data confirming that, from a statistical perspective, murders are solved quickly or not at all, with a significant drop in the percentage of cleared cases after one week.[26] Thus, the success of any forensic endeavor is not only a function of robust scientific analysis, but also the turn-around time of the analysis.[27] This creates the trade-off: while an investigative lead may be generated early, there is the possibility of limitation-based false negative generation and sample loss.[28] For technology implementation, a cost-benefit analysis should be conducted by an interdisciplinary team including the investigators and trained laboratory professionals to determine whether or not Rapid technology should be deployed in a given case. This requires parties to agree on the expedited processing of a sample based upon the urgency (e.g., 'red ball' cases) and a deep understanding and acceptance of the technological limitations of their system, including compatibility with certain tissues and/or touch

contributions, false negative rates, and the availability of reference samples to do comparative analysis in lieu of database searching.[29] In a perfect scenario, this type of concerted effort would be as simple as a discussion; however, in reality, investigations take place in a bureaucratic system, divided into discrete units and further complicated by dense and layered chains of command.

5.3.2. Opportunities in a broader application of microfluidics to forensic analysis. The application of microfluidic technology for use in industry, medicine, life sciences, and academia is experiencing rapid growth as the investment in research over decades converges with development of strategies for commercialization and standardization. Continued success requires learning from the factors that contributed to the early stifling of microdevice translation from academia to commercial use, including those discussed in **Chapter 1**. Those developing new microfluidic methods should be cognizant of whether they are creating better technology to supplant existing methodologies, or creating innovative solutions for unmet needs in emerging or niche applications. With the majority of existing microfluidic technologies, customers are forced to consider trade-offs that often do not favor the of purchasing new technology that only provides incremental improvements over the existing infrastructure.[30] With the goal of providing solutions for emerging forensic applications that may otherwise be overlooked as a result of analyst time/training or start-up costs, there are some unique opportunities for microfluidic integration into serological practices, microbiome analysis, and forensic DNA phenotyping.

5.3.2.1. Forensic Serology. In the majority of forensic biology workflows, NA work is preceded by serological analysis, where evidence is sampled and tested for the presence of body fluids,

most commonly blood, semen and saliva. This provides contextual information for cases, including event timelines and scene reconstruction, and directs analysts to those probative items likely to contain genetic material. Whether they are considered presumptive or confirmatory, most tests share the criticisms that they are time-consuming to perform, destructive to evidence materials, and lacking in sensitivity and/or specificity.[31] In response, research focused on the use of the transcriptome for body fluid identification (BFID) has emerged as a means of distinguishing deposits via differentially expressed RNAs, including messenger RNAs (mRNAs), microRNAs (miRNAs), and circular RNAs (circRNAs).[32] The regulatory transcripts may be differentiated by massively parallel sequencing (MPS), but are most commonly identified with assays including reverse transcription endpoint or quantitative real-time PCR (RT-qPCR), with RT-qPCR providing more sensitivity and greater dynamic range.[33,34] While these panels are robust, highly predictive, and capable of multiplexed analysis, case working laboratories have not universally adapted RNA-based BFID, likely as a result of the increased cost and lack of standardized methods compared with microscopic, colorimetric, and/or immunological methods.[35] Ideally, tests for BFID should be rapid, simple to implement into the existing workflow, nondestructive to the sample, and amenable to analysis from multiple substrates.[32]

A microfluidic method for RT-qPCR-based BFID would enable streamlined tissue determination that is comparably more appropriate for forensic use. The theoretical cost, sensitivity, and speed advantages provided with a microfluidic approach to amplification at scale was previously discussed in **Chapter 1**. With a multicolor detection system and integrated extraction, which have both been previously demonstrated in several microdevices, the system becomes capable of simultaneous identification of multiple body fluids, and is suitable for facile

implementation in the laboratory or at the PON.[36,37] Furthermore, on-board co-extraction of DNA and RNA during the sample preparation process would provide a DNA lysate for further purification, eliminating the need for the consumption of multiple swab cuttings for NA analysis. Ultimately, a microfluidic system to provide automated, transcriptomic BFID would minimize analyst intervention, streamline analysis, possibly increase sensitivity compared with conventional methods, and require the sacrifice of fewer evidence cuttings to serological and genetic identification. Development of systems capable of sample-to-answer BFID are already underway.[38]

5.3.2.2. Microbiome analysis. Human microbiome analysis, or the study of the host microorganisms that colonize the human body and associated environments, has been of great interest to the forensic community in recent years for its numerous potential applications.[39] Briefly, the identification and/or quantification of human microbiota has been described as having utility for HID, BFID, post-mortem interval (PMI) estimation, time since deposition approximation of forensically-relevant stains, and pinpointing geographic locations.[40] Beyond application, microbiome analysis could be of great use to investigative efforts given that NA sequences are distinct from human sequences and thus, less prone to analyst contamination. Yet, currently employed research methods make use of either sequencing or RT-PCR for detection, putting the burden of work on the forensic laboratory and limiting integration into forensic practices. Beyond this complication, the detection and analysis of microbial evidence for these purposes is restricted to research-based investigation at this point, as there are currently no standard operating procedures (SOP).[41] A microfluidic approach to microbiome analysis for forensic purposes would

increase the investigative bandwidth without greatly impacting analyst workloads. Practically, both sequencing and RT-PCR have been thoroughly characterized for a number of different applications, and their use here could both minimize analyst intervention and streamline data analysis. The fact that SOPs have not yet been developed for this application is beneficial: methods may be tested in parallel with interfacing systems to set the precedent for analysis.

5.3.2.3. Forensic DNA Phenotyping. The current approach to HID of unknown persons in forensic case working laboratories is comparative in nature. That is, either resultant STR profiles are compared to references generated from victim/suspect standards or they are entered into databases like CODIS for identification. Unfortunately, this approach may not always lead to a 'match', leaving countless unidentified human remains and suspects unknown each year. In lieu of comparison, forensic DNA phenotyping has emerged as a way of providing investigators with phenotypic information to act as a biological witness and provide investigative leads.[42] Research efforts have resulted in robust prediction mechanisms to discern biogeographical ancestry and human colorimetric traits (i.e., hair, skin, and eye color) from single-nucleotide polymorphisms (SNPs).[43] Likewise, prediction of human chronological age, and even dietary and lifestyle information, may be derived from tracking epigenetic alterations.[44] Today, many of these tools have been thoroughly validated and even commercialized for use by private and public entities alike; however, the widespread use of these techniques has been limited in forensic practice compared with STR typing. Microfluidic approaches to the determination of externally visible characteristics (EVCs) may make these workflows more accessible to overburdened HID labs that would otherwise be unable to increase their capacity via conventional instrumentation.

5.4. Future Considerations.

The incorporation of microfluidic methods for NA analysis into the forensic HID toolbox has been limited thus far. To-date, few research-based devices have been supported and manufactured for commercial use, and sample-to-answer Rapid DNA systems are not universally used for PON identifications. Explanations for this are complex, and vary among invested parties, from the forensic laboratories themselves and the organizations they operate within, to law makers and commercial entities. Furthermore, not all laboratories handle identical communities; for example, forensic HID labs may be designated as public or private and serving vastly different populations, dictating their oversight and corresponding restrictions in terms of Rapid DNA usage. For those in smaller jurisdictions, countries with amenable regulations, or investigative offices willing to forgo database comparison, the ability and incentive to utilize a microfluidic tool may only be delayed as a result of the associated costs and/or the development of a clearly defined set of use cases or decision factor analysis methods.[29] In the U.S., the implementation of the Rapid DNA Act of 2017[45] can be viewed in two ways: (1) a vehicle for limiting the use of microfluidic tools for HID to only process reference samples from buccal collections, or (2) a set of guiding principles that engages the investigative community with the capabilities associated with current microfluidic HID technology. These sentiments are not mutually exclusive, but the tone and impressions set by each lab and commercial vendor may be based on their interpretation of this Act and the commentaries that followed.[46,47,48,49]

From the author's perspective, it is clear that microfluidic systems for HID do not simply incorporate miniaturized analytical processes that perfectly mimic existing strategies. Thus,

sample-to-answer HID systems should be differentiated from benchtop programs in terms of use cases, electrophoretic output, and ability to handle all sample types. Rapid DNA systems have proven quite useful for buccal reference and arrestee samples and provided a mode for rapid analysis at the PON that was sorely lacking from the marketplace prior to their inception. At the crime scene, a number of trade-offs should be carefully evaluated for specific use cases, specifically involving cost, practical implementation, or investigative time. Regarding the further development and commercialization of microfluidic-based tools for forensic NA analysis, a focus shift toward more innovative paths that further enrich investigative strategies is recommended. Moving forward, as these tools become more refined through continued discovery and validation, we urge those who have previously dismissed the technology to revisit the possibility that there will be suitable use cases. Beyond those systems commercially available, the introduction of rigorously tested, research-based investigative techniques (e.g. genetic BFID, phenotyping, etc.) may be most easily integrated into case working laboratories in an automated, microfluidic format.

5.5 References

(1) Turiello, R.; Nouwairi, R. L.; Landers, J. P. Taking the Microfluidic Approach to Nucleic Acid Analysis in Forensics: Review and Perspectives. *Forensic Science International: Genetics* **2023**, *63*, 102824. https://doi.org/10.1016/j.fsigen.2022.102824.

(2) Turiello, R.; Nouwairi, R. L.; Keller, J.; Cunha, L. L.; Dignan, L. M.; Landers, J. P. A Rotationally-Driven Dynamic Solid Phase Sodium Bisulfite Conversion Disc for Forensic Epigenetic Sample Preparation. *Lab Chip* **2024**, *24* (1), 97–112. https://doi.org/10.1039/D3LC00867C.

(3) Dignan, L. M.; Turiello, R.; Layne, T. R.; O'Connell, K. C.; Hickey, J.; Chapman, J.; Poulter, M. D.; Landers, J. P. An Ultrafast SARS-CoV-2 Virus Enrichment and Extraction Method Compatible with Multiple Modalities for RNA Detection. *Analytica Chimica Acta* **2021**, *1180*, 338846. https://doi.org/10.1016/j.aca.2021.338846.

(4) Turiello, R.; Dignan, L. M.; Thompson, B.; Poulter, M.; Hickey, J.; Chapman, J.; Landers, J. P. Centrifugal Microfluidic Method for Enrichment and Enzymatic Extraction of Severe Acute Respiratory Syndrome Coronavirus 2 RNA. *Anal. Chem.* **2022**, *94* (7), 3287–3295. https://doi.org/10.1021/acs.analchem.1c05215.

(5) Marshall, J. S.; Turiello, R.; Cunha, L. L.; Frazier, E. V.; Hickey, J.; Chapman, J.; Poulter, M. D.; Fehling, H. L.; Landers, J. P. Rapid SARS-CoV-2 Virus Enrichment and RNA Extraction for Efficient Diagnostic Screening of Pooled Nasopharyngeal or Saliva Samples for Dilutions Up to 1:100. *Diagnostics* **2022**, *12* (6), 1398. https://doi.org/10.3390/diagnostics12061398.

(6) Dignan, L. M. Microfluidic Integration of Multi-Step Bioanalytical Assays. PhD Dissertation, University of Virginia, Charlottesville, VA 22904, 2022. https://libraetd.lib.virginia.edu/public_view/3b5919687.

(7) Naue, J.; Hoefsloot, H. C. J.; Kloosterman, A. D.; Verschure, P. J. Forensic DNA Methylation Profiling from Minimal Traces: How Low Can We Go? *Forensic Science International: Genetics* **2018**, *33*, 17–23. https://doi.org/10.1016/j.fsigen.2017.11.004.

(8) Aliferi, A.; Ballard, D.; Gallidabino, M. D.; Thurtle, H.; Barron, L.; Syndercombe Court, D. DNA Methylation-Based Age Prediction Using Massively Parallel Sequencing Data and Multiple Machine Learning Models. *Forensic Science International: Genetics* **2018**, *37*, 215–226. https://doi.org/10.1016/j.fsigen.2018.09.003.

(9) Hamano, Y.; Manabe, S.; Morimoto, C.; Fujimoto, S.; Ozeki, M.; Tamaki, K. Forensic Age Prediction for Dead or Living Samples by Use of Methylation-Sensitive High Resolution Melting. *Legal Medicine* **2016**, *21*, 5–10. https://doi.org/10.1016/j.legalmed.2016.05.001.

(10) Vidaki, A. Method for Determining Global Bisulfite Conversion Efficiency. US20220372574A1, November 24, 2022. https://patents.google.com/patent/US20220372574A1/en?q=(vidaki)&inventor=athina&oq=athina+vidaki.

(11) Zbieć-Piekarska, R.; Spólnicka, M.; Kupiec, T.; Parys-Proszek, A.; Makowska, Ż.; Pałeczka, A.; Kucharczyk, K.; Płoski, R.; Branicki, W. Development of a Forensically Useful Age Prediction Method Based on DNA Methylation Analysis. *Forensic Science International: Genetics* **2015**, *17*, 173–179. https://doi.org/10.1016/j.fsigen.2015.05.001.

(12) Scott, A. C. Novel Analytical Systems for Rapid Forensic Nucleic Acid Detection, University of Virginia, 2020. https://doi.org/10.18130/V3-6VFN-W188.

(13) Woolf, M. S.; Dignan, L. M.; Scott, A. T.; Landers, J. P. Digital Postprocessing and Image Segmentation for Objective Analysis of Colorimetric Reactions. *Nat Protoc* **2021**, *16* (1), 218–238. https://doi.org/10.1038/s41596-020-00413-0.

(14) Eipel, M.; Mayer, F.; Arent, T.; Ferreira, M. R. P.; Birkhofer, C.; Gerstenmaier, U.; Costa, I. G.; Ritz-Timme, S.; Wagner, W. Epigenetic Age Predictions Based on Buccal Swabs Are More Precise in Combination with Cell Type-Specific DNA Methylation Signatures. *Aging* **2016**, *8* (5), 1034–1048. https://doi.org/10.18632/aging.100972.

(15) De Benedictis, P.; De Battisti, C. Demonstration of Lyssavirus Nucleic Acids by Pyrosequencing. In *Current Laboratory Techniques in Rabies Diagnosis, Research and*

Prevention; Elsevier, 2014; pp 205–217. https://doi.org/10.1016/B978-0-12-800014-4.00020-2.

(16) Ghemrawi, M.; Tejero, N. F.; Duncan, G.; McCord, B. Pyrosequencing: Current Forensic Methodology and Future Applications—a Review. *Electrophoresis* **2023**, *44* (1–2), 298–312. https://doi.org/10.1002/elps.202200177.

(17) Konrad, H.; Schäfer, L.; Sturm, H.; Hördt, L.; Bajanowski, T.; Poetsch, M. Vibration as a Pitfall in Pyrosequencing Analyses. *Int J Legal Med* **2022**, *136* (1), 103–105. https://doi.org/10.1007/s00414-021-02716-7.

(18) Kampmann, M.-L.; Fleckhaus, J.; Børsting, C.; Jurtikova, H.; Piters, A.; Papin, J.; Gauthier, Q.; Ghemrawi, M.; Doutremepuich, C.; McCord, B.; Schneider, P. M.; Drabek, J.; Morling, N. Collaborative Exercise: Analysis of Age Estimation Using a QIAGEN Protocol and the PyroMark Q48 Platform. *Forensic Sciences Research* **2024**, *9* (1), owad055. https://doi.org/10.1093/fsr/owad055.

(19) Thompson, B. L.; Ouyang, Y.; Duarte, G. R. M.; Carrilho, E.; Krauss, S. T.; Landers, J. P. Inexpensive, Rapid Prototyping of Microfluidic Devices Using Overhead Transparencies and a Laser Print, Cut and Laminate Fabrication Method. *Nat Protoc* **2015**, *10* (6), 875–886. https://doi.org/10.1038/nprot.2015.051.

(20) Product Information Sheet ARCare 7970-39, 2021. https://www.adhesivesresearch.com/wp-content/uploads/2020/06/Electronics-Solutions.pdf.

(21) Maguire, C.; Houck, M. M.; Williams, R.; Speaker, P. J. Efficiency and the Cost-Effective Delivery of Forensic Science Services: Insourcing, Outsourcing, and Privatization. *Forensic*

Science Policy & Management: An International Journal **2012**, *3* (2), 62–69. https://doi.org/10.1080/19409044.2012.734546.

(22) Ragazzo, M.; Melchiorri, S.; Manzo, L.; Errichiello, V.; Puleri, G.; Nicastro, F.; Giardina, E. Comparative Analysis of ANDE 6C Rapid DNA Analysis System and Traditional Methods. *Genes* **2020**, *11* (5), 582. https://doi.org/10.3390/genes11050582.

(23) Dolan, M. 'Rapid DNA' Promises Breakthroughs in Solving Crimes. So Why Does It Face a Backlash? *Los Angeles Times*. September 25, 2019. https://www.latimes.com/california/story/2019-09-24/rapid-dna-forensics-crime-police.

(24) van Asten, A. C. On the Added Value of Forensic Science and Grand Innovation Challenges for the Forensic Community. *Science & Justice* **2014**, *54* (2), 170–179. https://doi.org/10.1016/j.scijus.2013.09.003.

(25) Brown, S.; Willis, S. Complexity in Forensic Science. *Forensic Science Policy & Management: An International Journal* **2010**, *1* (4), 192–198. https://doi.org/10.1080/19409041003698454.

(26) Addington, L. A. Hot vs. Cold Cases: Examining Time to Clearance for Homicides Using NIBRS Data. *Justice Research and Policy* **2007**, *9* (2), 87–112. https://doi.org/10.3818/JRP.9.2.2007.87.

(27) Kobus, H.; Houck, M.; Speaker, P.; Riley, R.; Witt, T. Managing Performance in the Forensic Sciences: Expectations in Light of Limited Budgets. *Forensic Science Policy & Management: An International Journal* **2011**, *2* (1), 36–43. https://doi.org/10.1080/19409044.2011.564271.

(28) Mapes, A. A.; Kloosterman, A. D.; Poot, C. J. de; van Marion, V. Objective Data on DNA Success Rates Can Aid the Selection Process of Crime Samples for Analysis by Rapid Mobile DNA Technologies. *Forensic Science International* **2016**, *264*, 28–33. https://doi.org/10.1016/j.forsciint.2016.03.020.

(29) Mapes, A. A.; Stoel, R. D.; de Poot, C. J.; Vergeer, P.; Huyck, M. Decision Support for Using Mobile Rapid DNA Analysis at the Crime Scene. *Science & Justice* **2019**, *59* (1), 29–45. https://doi.org/10.1016/j.scijus.2018.05.003.

(30) Volpatti, L. R.; Yetisen, A. K. Commercialization of Microfluidic Devices. *Trends in Biotechnology* **2014**, *32* (7), 347–350. https://doi.org/10.1016/j.tibtech.2014.04.010.

(31) Lewis, C. A.; Layne, T. R.; Seashols-Williams, S. J. Detection of microRNAs in DNA Extractions for Forensic Biological Source Identification. *J Forensic Sci* **2019**, *64* (6), 1823–1830. https://doi.org/10.1111/1556-4029.14070.

(32) Lynch, C.; Fleming, R. RNA Based Approaches for Body Fluid Identification in Forensic Science. *WIREs Forensic Sci* **2021**, *3* (4). https://doi.org/10.1002/wfs2.1407.

(33) Sijen, T. Molecular Approaches for Forensic Cell Type Identification: On mRNA, miRNA, DNA Methylation and Microbial Markers. *Forensic Science International: Genetics* **2015**, *18*, 21–32. https://doi.org/10.1016/j.fsigen.2014.11.015.

(34) Juusola, J.; Ballantyne, J. mRNA Profiling for Body Fluid Identification by Multiplex Quantitative RT-PCR. *J Forensic Sci* **2007**, *0* (0), 070917231752009-??? https://doi.org/10.1111/j.1556-4029.2007.00550.x.

(35) Ingold, S.; Dørum, G.; Hanson, E.; Berti, A.; Branicki, W.; Brito, P.; Elsmore, P.; Gettings, K. B.; Giangasparo, F.; Gross, T. E.; Hansen, S.; Hanssen, E. N.; Kampmann, M.-L.; Kayser, M.;

Laurent, F.-X.; Morling, N.; Mosquera-Miguel, A.; Parson, W.; Phillips, C.; Porto, M. J.; Pośpiech, E.; Roeder, A. D.; Schneider, P. M.; Schulze Johann, K.; Steffen, C. R.; Syndercombe-Court, D.; Trautmann, M.; van den Berge, M.; van der Gaag, K. J.; Vannier, J.; Verdoliva, V.; Vidaki, A.; Xavier, C.; Ballantyne, J.; Haas, C. Body Fluid Identification Using a Targeted mRNA Massively Parallel Sequencing Approach – Results of a EUROFORGEN/EDNAP Collaborative Exercise. *Forensic Science International: Genetics* **2018**, *34*, 105–115. https://doi.org/10.1016/j.fsigen.2018.01.002.

(36) Gorgannezhad, L.; Stratton, H.; Nguyen, N.-T. Microfluidic-Based Nucleic Acid Amplification Systems in Microbiology. *Micromachines* **2019**, *10* (6), 408. https://doi.org/10.3390/mi10060408.

(37) Yin, J.; Suo, Y.; Zou, Z.; Sun, J.; Zhang, S.; Wang, B.; Xu, Y.; Darland, D.; Zhao, J. X.; Mu, Y. Integrated Microfluidic Systems with Sample Preparation and Nucleic Acid Amplification. *Lab Chip* **2019**, *19* (17), 2769–2785. https://doi.org/10.1039/C9LC00389D.

(38) Layne, T. R.; Nouwairi, R. L.; Fleming, R.; Blair, H.; Landers, J. P. Rapid Microchip Electrophoretic Separation of Novel Tran-Scriptomic Body Fluid Markers for Forensic Fluid Profiling. *Micromachines*.

(39) García, M. G.; Pérez-Cárceles, M. D.; Osuna, E.; Legaz, I. Impact of the Human Microbiome in Forensic Sciences: A Systematic Review. *Appl Environ Microbiol* **2020**, *86* (22), e01451-20. https://doi.org/10.1128/AEM.01451-20.

(40) Clarke, T. H.; Gomez, A.; Singh, H.; Nelson, K. E.; Brinkac, L. M. Integrating the Microbiome as a Resource in the Forensics Toolkit. *Forensic Science International: Genetics* **2017**, *30*, 141–147. https://doi.org/10.1016/j.fsigen.2017.06.008.

(41) Zhang, J.; Liu, W.; Simayijiang, H.; Hu, P.; Yan, J. Application of Microbiome in Forensics. *Genomics, Proteomics & Bioinformatics* **2022**, S1672022922000961. https://doi.org/10.1016/j.gpb.2022.07.007.

(42) Kayser, M. Forensic DNA Phenotyping: Predicting Human Appearance from Crime Scene Material for Investigative Purposes. *Forensic Science International: Genetics* **2015**, *18*, 33–48. https://doi.org/10.1016/j.fsigen.2015.02.003.

(43) Schneider, P. M.; Prainsack, B.; Kayser, M. The Use of Forensic DNA Phenotyping in Predicting Appearance and Biogeographic Ancestry. *Deutsches Aerzteblatt Online* **2019**. https://doi.org/10.3238/arztebl.2019.0873.

(44) Vidaki, A.; Kayser, M. From Forensic Epigenetics to Forensic Epigenomics: Broadening DNA Investigative Intelligence. *Genome Biol* **2017**, *18* (1), 238. https://doi.org/10.1186/s13059-017-1373-1.

(45) James F. Sensenbrenner Jr. *Rapid DNA Act of 2017*; 2017. https://www.congress.gov/bill/115th-congress/house-bill/510.

(46) Romsos, E. L.; French, J. L.; Smith, M.; Figarelli, V.; Harran, F.; Vandegrift, G.; Moreno, L. I.; Callaghan, T. F.; Brocato, J.; Vaidyanathan, J.; Pedroso, J. C.; Amy, A.; Stoiloff, S.; Morillo, V. H.; Czetyrko, K.; Johnson, E. D.; Tagyos, J.; Murray, A.; Vallone, P. M. Results of the 2018 Rapid DNA Maturity Assessment. *J Forensic Sci* **2020**, *65* (3), 953–959. https://doi.org/10.1111/1556-4029.14267.

(47) *Scientific Working Group on DNA Analysis Methods Position Statement on Rapid DNA Analysis*; Scientific Working Group DNA Analysis Methods (SWGDAM), 2017. https://docs.wixstatic.com/ugd/4344b0_f84df0465a2243218757fac1a1ccffea.pdf.

(48) *ASCLD Position Statement*; American Society of Crime Laboratory Directors (ASCLD), 2017. https://www.ascld.org/wp-content/uploads/2017/11/ASCLD-Position-Statement-RAPID-DNA.pdf.

(49) *NDAA Position Statement on Use of Rapid DNA Technology*; National District Attorneys Association, 2018. https://dps.alaska.gov/getmedia/fb933229-8e52-4cf8-8fe0-cb72d5e039e3/NDAA-Statement-on-Use-of-Rapid-DNA-Technology-2018.pdf.